In vivo pathology markers in tauopathies: prognostic and diagnostic implications

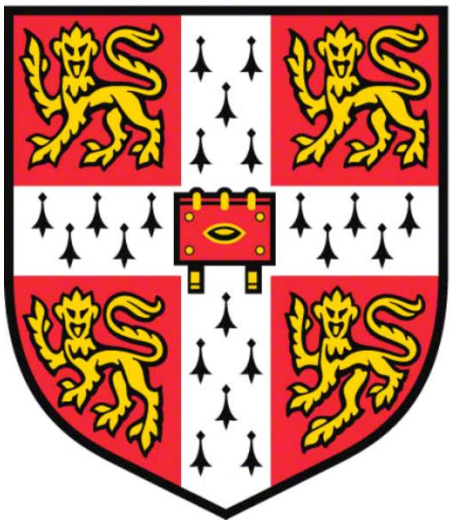

Maura Malpetti

Sidney Sussex College

University of Cambridge

This thesis is submitted for the degree of Doctor of Philosophy

September 2020

Declaration

This thesis is the result of my own work and includes nothing which is the outcome of work done in collaboration except as declared in the Preface and specified in the text. It is not substantially the same as any that I have submitted, or, is being concurrently submitted for a degree or diploma or other qualification at the University of Cambridge or any other University or similar institution except as declared in the Preface and specified in the text. I further state that no substantial part of my thesis has already been submitted, or, is being concurrently submitted for any such degree, diploma or other qualification at the University of Cambridge or any other University or similar institution except as declared in the Preface and specified in the text.

The word count of 51,000 does not exceed the prescribed word limit for the relevant Degree Committee.

Abstract

***In vivo* pathology markers in tauopathies: prognostic and diagnostic implications**

Maura Malpetti

The neurodegenerative tauopathies include Alzheimer's disease, frontotemporal dementia (half due to tauopathy), and progressive supranuclear palsy (PSP). In addition to abnormal accumulation of tau protein, they are each characterised by neuroinflammation, with increasing evidence that the neuroinflammation plays a role in the onset and progression of these diseases, rather than simply being a response to neuronal injury. PET and MRI allow the *in vivo* visualisation and quantification of markers of neuropathology and neurodegeneration. However, the value of these *in vivo* measures at different stages of disease, and their value for predicting the clinical progression in patients, remains undetermined.

In my thesis, I examine the prognostic value of multimodal *in vivo* PET imaging for predicting longitudinal clinical and cognitive decline in Alzheimer's disease, frontotemporal dementia and PSP. I use the PET ligand [^{11}C]PK11195 PET as a marker of microglial activation, and [^{18}F]AV-1451 PET to quantify tau pathology (or in the case of frontotemporal dementia, tau and/or TDP-43 pathology), with structural 3T MRI as an index of atrophy.

In patients with Alzheimer's dementia (n=12) and its prodrome, mild cognitive impairment with amyloid positivity (n=14), I applied latent growth curve models (LGCMs), multiple linear regression and Bayesian regression analyses to test the prognostic value of PET and MRI, alone and in combination, to predict cognitive decline over three years. Tau burden and microglial activation in temporo-parietal cortical regions were identified as significant predictors of cognitive decline, over and above baseline atrophy.

In frontotemporal dementia, I undertook three complementary analyses. First, in pre-symptomatic carriers of genetic mutations associated with frontotemporal dementia (i.e. in MAPT, GRN, or C9orf72 gene), I applied LGCMs to test for associations between cross-sectional and longitudinal changes in atrophy, apathy and cognition. I compared gene mutation carriers (n=304) to non-carrier relatives as controls (n=296). My results suggest that apathy occurs early in disease progression and worsens over time in those considered to be still

asymptomatic carriers. Worsening of apathy over time was associated with early brain changes in frontal and cingulate cortex, and predicted subsequent deterioration of cognitive performance. Second, in a case series of post-symptomatic frontotemporal dementia mutation carriers (n=7), I assessed [^{11}C]PK11195 and [^{18}F]AV-1451 PET uptake, and discuss their association with clinical phenotype. The genetic cases each showed neuroinflammation in frontotemporal regions, and [^{11}C]PK11195 distribution reflected clinical symptoms in each patient. Last, in a larger group of genetic and sporadic frontotemporal dementia cases (n=30), I applied a linear mixed effects model and regression analyses to test the prognostic value of [^{11}C]PK11195, structural MRI and apathy assessment on cognitive decline up to 4 years of follow-up. Across the frontotemporal dementia spectrum, *in vivo* atrophy and neuroinflammation markers in frontal regions, and apathy severity at baseline, were associated with faster cognitive decline.

Finally, I examined the prognostic value of MRI and PET markers in PSP (n=17), as a model of primary non- Alzheimer's tauopathy. First, I studied the *in vivo* association between tau accumulation and neuroinflammation, finding that they co-localise in subcortical and cortical regions, previously described as affected by PSP-related neuropathology. Next, I applied linear mixed effects and regression models to test the prognostic value of baseline PET markers for microglial activation and tau pathology, and atrophy-related MRI measures on clinical progression over time. Inflammation in subcortical regions was strongly associated with cross-sectional clinical severity and faster clinical worsening, similar to [^{18}F]AV-1451 binding in the same regions. However, atrophy measures were not related to clinical progression over time.

Together these studies demonstrate that inflammation occurs in Alzheimer's disease, frontotemporal dementia and PSP. Inflammation as measured by [^{11}C]PK11195 PET in regions known to be affected pathologically in the disease can predict cognitive decline and clinical progression over time, independent of tau burden and atrophy. In frontotemporal dementia, apathy and structural brain changes also resulted to be predictive of clinical changes in pre- and post-symptomatic patients. This work provides evidence supporting future trials of immune-mediated strategies, with the aim of modifying the course of disease, which might be coupled with improved stratification or individualised treatment approaches based on cognitive and imaging assessment at baseline. I suggest these therapeutic approaches would be more effective if given early in the disease course.

Preface

A large group of researchers and clinicians as part of the NIMROD study and the multicentre GENFI initiative have contributed to data collection. At the beginning of each experimental chapter I report a preface to state contributions to each study.

The material in Chapter 3 has been published as:

> **Malpetti M**, Kievit RA, Passamonti L, Jones PS, Tsvetanov KA, Rittman T, et al. Microglial activation and tau burden predict cognitive decline in Alzheimer's disease. *Brain* 2020; 143: 1588–1602 - doi: 10.1093/brain/awaa088

The material in Chapter 4 has been published as:

> **Malpetti M**, Jones PS, Tsvetanov KA, Rittman T, van Swieten JC, Borroni B, et al. Apathy in presymptomatic genetic frontotemporal dementia predicts cognitive decline and is driven by structural brain changes. *Alzheimer's Dement* 2020: 1–15 - doi: 10.1002/alz.12252

The material in Chapter 5 has been published as:

> **Malpetti M**, Rittman T, Jones PS, Cope TE, Passamonti L, Bevan-Jones WR, et al. In vivo PET imaging of neuroinflammation in familial frontotemporal dementia. *J Neurol Neurosurg Psychiatry* 2020 – doi: 10.1136/jnnp-2020-323698

The material in Chapter 7 has been published as:

> **Malpetti M**, Passamonti L, Rittman T, Jones PS, Rodríguez PV, Bevan-Jones WR, et al. Neuroinflammation and tau co-localize in vivo in progressive supranuclear palsy. *Ann Neurol* 2020: 1–11 - doi: 10.1002/ana.25911

The material in Chapter 8 has been submitted to a scientific journal and is under peer-review.

Acknowledgements

Although in Science it is not always easy to get a good sample size for our studies, these 3 years of PhD and life recruited an unexpectedly large sample of people who helped me on this beautiful voyage. For the first two people I want to thank, I think it is particularly difficult to find the right words to express my gratitude. My two supervisors have been the best co-captains that I could ask for. I am immensely grateful to Prof. James Rowe for having nurtured my confidence as a scientist, and more importantly as a person, since the first time we met during my interview three years ago. His daily support and guidance through the most difficult methodological and emotional storms of these travels have been essential to strengthen my enthusiasm for and belief in scientific research; his deep caring for patients as much as our lab members has been truly inspirational. I am equally immensely grateful to Prof. John O'Brien, who never misses an opportunity to show and share the most human and empathetic nature that everyone would love to find in an outstanding PI, academic, and medical doctor, which he demonstrates to be in his research and clinical practice every day. His scientific advice and kindness contributed to always make me feel truly supported in this adventure.

All present and ex lab members, colleagues and other students from the same department or other corners of the University of Cambridge have contributed to make my PhD path much straighter, more colourful and easier than how I could have ended up drawing it by myself. I will not mention all names, but each of them well knows which colour they made appear on my horizon, even on the most rainy days. Special thanks are reserved for Mr. Simon Jones, who has been an endless resource of technical knowledge, a never-tired collaborator, and an infallible compass through all my imaging doubts; Dr. Luca Passamonti, whose enthusiasm, critical thinking and patience have been fortunate lifeboats in so many moments of my PhD, sharing the spirit from our motherland in our daily teamwork; and Dr. Tim Rittman, for the support on the complete spectrum from clinic to hard-core research, and for celebrating every successful conference talk or analysis with motivational cheers. I also want to really thank Dr. Kamen Tsvetanov, who made me feel welcome on the island of complex imaging analysis methods since the beginning, always treating me as a peer and encouraging every single of my little steps; and Prof. Rogier Kievit who had the magical ability to make the most difficult statistical approaches accessible to me through his enthusiastic talks, and all his answers to my endless doubts. Equally special thanks goes to Dr. Negin Holland, Dr. Sanne Kaalund, and Dr.

Rong Ye, who with different expertise and shared being at-the-ready played a key role in allowing me to navigate the theoretical and practical tides of PSP; and to Dr. Leonardo Iaccarino, who still remains one of the best encyclopaedias for culinary and scientific knowledge, even from overseas. A particular thanks also goes to Merete Bergmann and Dr. Bea Kiddle; the NIMROD, GENFI, and CCPP teams; PET/CT and WBIC teams; medical doctors, nurses, research assistants and funding bodies, especially the Cambridge Trust and Sidney Sussex College, whose invaluable support and constant assistance made every bit of science in this thesis possible.

There are three other precious people I would never get tired to tell that I am and will always be infinitely thankful to: my parents and my sister, who gave me the strength to set sail towards my life goals and dreams, being at the same time my safety net in front of any difficulties and my harbour where I always return to, sharing joys and pains, the excitement and emotions of our daily adventures. I will be always grateful to them for having taught me how commitment, passion and caring can shorten any distance and ease any climb. I also truly thank the lifelong and new friends who have navigated the same waters, for long or short distances, sharing moments, ideas and true feelings; and a surprising traveling companion that has become the favourite guiding star, even in the most cloudy days. They all have contributed to make me the person and researcher I am.

Last but not least, there are people that I cannot really find the words to describe my gratitude and esteem for. These are the participants and their families that constantly volunteer to take part in our research studies - sharing our hopes and aims to improve the quality of life and to find a cure for those who live with dementia and related conditions. They are the most important oars to continue our mission in clinical research.

Abbreviations

ACE-R	Addenbrooke's Cognitive Examination - Revised
ANOVA	Analysis of variance
BPND	Non-displaceable binding potential
bvFTD	Behavioural variant frontotemporal dementia
C9orf72	Chromosome 9 open reading frame 72
CAT12	Computational Anatomy Toolbox
CBD	Corticobasal degeneration
CBI-R	Cambridge behavioural inventory - revised
CFI	Comparative fit index
CSF	Cerebrospinal fluid
CT	Computer tomography
DeNDRoN	Dementias and Neurodegeneration specialty of the UK Clinical Research Network
EYO	Years to the expected symptom onset
FAB	Frontal assessment battery
FTD	Frontotemporal dementia
FTDRS	Frontotemporal dementia rating scale
FTLD	Frontotemporal lobar degeneration
FUS	Fused in sarcoma protein
GENFI	Genetic Frontotemporal Dementia Initiative
GRN	Progranulin
LGCM	Latent growth curve model
LMEM	Linear mixed-effects model
MAO	Monoamine oxidase
MAPT	Microtubule associated protein tau
MBq	Megabecquerel
MCI	Mild cognitive impairment
MCI+	Amyloid-positive patients with mild cognitive impairment
MEM	Mixed-effects model
MMSE	Mini mental state examination
MNI	Montreal Neurosciences Institute
MPRAGE	Magnetization-prepared rapid acquisition gradient-echo
MRI	Magnetic resonance imaging
nfvPPA	Non-fluent variant of primary progressive aphasia
NIMROD	Neuroimaging of Inflammation in Memory and Related Other Disorders
PCA	Principal component analysis
PET	Positron emission tomography
PPA	Primary progressive aphasia

PSP	Progressive supranuclear palsy
PSP-RS	PSP rating scale
RMSEA	Root-mean-square error of approximation
ROI	Region of interest
SEM	Structural equation modelling
SPM	Statistical parametric mapping
SRMR	Standardized root mean-square residual
svPPA	Semantic variant of primary progressive aphasia
TBK-1	TANK-binding kinase 1
TDP-43	Transactive response DNA binding protein 43
TREM2	Triggering receptor expressed on myeloid cells 2
TSPO	18-kDa translocator protein
WBIC	Wolfson Brain Imaging Centre
χ^2	Chi-square test

Table of contents

Chapter 1 | Introduction 1
1.1. Overview 2
1.2. Tauopathies 5
1.2.1. Alzheimer's dementia 5
1.2.2. Frontotemporal dementia 6
1.2.3. Progressive supranuclear palsy 7
1.3. Commonalities across tauopathies 8
1.3.1. Pre-symptomatic and prodromal phases 8
1.3.2. Transdiagnostic symptoms 10
1.4. Three pathological hallmarks of tauopathies 12
1.4.1. Tau pathology 12
1.4.2. Inflammation 14
1.4.3. Neuronal loss 16
1.5. *In vivo* imaging markers of neuropathology in tauopathies 16
1.5.1. PET imaging for tau pathology: [^{18}F]AV-1451 PET 17
1.5.2. PET imaging for neuroinflammation: [^{11}C]PK11195 PET 20
1.5.3. Structural MRI as marker of neuronal loss 21
1.6. Challenge of prognosis in tauopathies 23
1.7. Aims and hypotheses of my thesis 25
Chapter 2 | Study cohorts and methods 29
2.1. Introduction 30
2.2. NIMROD study 30
2.2.1. Introduction 30
2.2.2. Participants 31
2.2.3. Design 32
2.2.4. Cognitive and behavioural measures 33
2.2.5. Neuroimaging acquisition and processing 33
2.3. GENFI study 35
2.3.1. Introduction 35
2.3.2. Participants 35
2.3.3. Design 37

2.3.4. Cognitive and behavioural measures 37
2.3.5. Neuroimaging acquisition and processing 38
2.4. Longitudinal models 39
2.4.1. Latent Growth Curve Model (LGCM) 40
2.4.2. Mixed-effects model 44
2.5. Power calculation 46
2.6. Conclusions 46
Chapter 3 | Prognostic markers of cognitive decline in Alzheimer's disease 49
3.1. Introduction 50
3.2. Methods 53
3.2.1. Participants 53
3.2.2. Imaging data acquisition and pre-processing 54
3.2.3. Statistical analyses 56
3.3. Results 60
3.3.1. Descriptive statistics 60
3.3.2. Principal component analysis 62
3.3.3. Annual rate of cognitive decline 63
3.3.4. One-step prediction LGCM with predictors 65
3.3.5. Two-step prediction: linear regression 66
3.3.6. Two-step Bayesian prediction 73
3.4. Discussion 75
3.5. Conclusions 80
3.6. Supplementary materials of Chapter 3 81
Chapter 4 | Apathy, cognition and brain changes in pre-symptomatic genetic frontotemporal dementia 83
4.1. Introduction 84
4.2. Material and Methods 85
4.2.1. Participants 85
4.2.2. Imaging data acquisition and pre-processing 86
4.2.3. Statistical analyses 87
4.3. Results 89
4.3.1. Descriptive statistics 89
4.3.2. LGCM on longitudinal apathy scores 90
4.3.3. LGCM on longitudinal cognition 91
4.3.4. LGCMs on longitudinal grey-matter brain volumes 93

4.3.5. Bivariate LGCMs on apathy scores and grey-matter brain volumes 95
4.4. Discussion 98
4.5. Conclusions 102
Chapter 5 | *In vivo* pathological markers in familial frontotemporal dementia 103
5.1. Introduction 104
5.2. Methods 105
5.2.1. Participants 105
5.2.2. Imaging data acquisition and pre-processing 106
5.2.3. Statistical analyses 106
5.3. Results 107
5.3.1. Descriptive statistics 107
5.3.2. Visual evaluation of voxel-wise PET maps and association with clinical symptoms 108
5.3.3. Hierarchical cluster analysis 113
5.4. Discussion 114
5.5. Conclusions 116
5.6. Supplementary materials of Chapter 5 117
Chapter 6 | Prognostic imaging markers of cognitive decline in frontotemporal dementia 123
6.1. Introduction 124
6.2. Methods 126
6.2.1. Participants 126
6.2.2. Imaging data acquisition and pre-processing 126
6.2.3. Statistical analyses 128
6.3. Results 130
6.3.1. Descriptive statistics 130
6.3.2. Linear mixed effects model on longitudinal cognitive scores 130
6.3.3. Predictive value of grey-matter volumes and neuroinflammation levels 131
6.3.4. Inter-modality imaging correlations 132
6.3.5. Predictive value of baseline cognition and apathy 132
6.4. Discussion 133
6.5. Conclusions 136
Chapter 7 | Neuroinflammation and tau co-localise *in vivo* in progressive supranuclear palsy 137
7.1. Introduction 138
7.2. Methods 139

7.2.1. Participants 139
7.2.2. Imaging data acquisition and pre-processing 140
7.2.3. Statistical Analyses 141
7.3. Results 143
7.3.1. Descriptive statistics 143
7.3.2. Regional [^{11}C]PK11195 and [^{18}F]AV-1451 BP_{ND} in PSP 144
7.3.3. Principal component analysis 146
7.3.4. Inter-modality correlations 148
7.4. Discussion 150
7.5. Conclusions 154
7.6. Supplementary materials of Chapter 7 155
Chapter 8 | Prognostic markers of clinical decline in progressive supranuclear palsy 157
8.1. Introduction 158
8.2. Methods 159
8.2.1. Participants 159
8.2.2. Imaging data acquisition and pre-processing 159
8.2.3. Statistical Analyses 160
8.3. Results 161
8.3.1. Descriptive statistics 161
8.3.2. Principal component analysis 163
8.3.3. Linear mixed effects model on longitudinal PSP-RS 165
8.3.4. Single-modality linear regressions 165
8.3.5. Inter-modality correlations between predictive imaging components 167
8.4. Discussion 168
8.5. Conclusions 171
8.6. Supplementary materials of Chapter 8 172
Chapter 9 | General discussion 173
9.1. Summary of the results 174
9.2. Neuroinflammation and prognosis 175
9.3. Tau pathology markers: ongoing challenges 178
9.4. Structural MRI vs. PET imaging in predicting tauopathies' clinical progression 180
9.5. Utility of *in vivo* neuroimaging measures for cognitive prognosis 182
9.6. Apathy as early marker in frontotemporal dementia 183
9.7. Disease-specific biomarkers for differential therapy and stratification 185
9.8. General limitations 186

9.8.1. Modest sample size 186
9.8.2. Longitudinal data collection 187
9.8.3. *Post mortem* pathological confirmation 188
9.8.4. PET methodological limitations 189
9.9. Future directions 190
9.10. Conclusions 193
References 195
List of tables 235
List of figures 237

Chapter 1 | Introduction

1.1. Overview

Epidemiological studies estimate that over 47 million people are affected by dementia (Livingston *et al.*, 2017), which arises from several neurodegenerative diseases. In the general population, Alzheimer's disease is the most common cause of dementia, followed by vascular dementia, a-synucleinopathies and frontotemporal lobar degeneration. These diseases are all characterised by a progressive loss of physiological structure and function of brain cells, with synaptic dysfunction and neuronal death. Despite differences in the pathology of dementias, they have shared or analogous pathogenic mechanisms, such as the accumulation of pathologic intra-cellular and extracellular misfolded proteins in the brain (Taylor *et al.*, 2002; Kovacs *et al.*, 2010; Jucker and Walker, 2013). These directly and indirectly affect neuronal function and survival, with clinical symptoms as a relatively late stage manifestation of a pathological disease process starting decades earlier (Bateman *et al.*, 2012; Jack *et al.*, 2013; Rohrer *et al.*, 2015). However, the relation between clinical phenotype and molecular pathology is complex. For example, similar clinical manifestations can be caused by different genetic mutations, and different molecular pathological processes, while a given pathological subtype can lead to different clinical syndromes. Neuropathological studies have also shown that most elderly dementia patients have a mixed pathology, which can include not only tau and amyloid pathology, but also Lewy body disease, vascular pathology, limbic age-related TDP-43 encephalopathy, and other aging-related changes (Jellinger and Attems, 2010; Jellinger, 2020). In particular, in elderly people with dementia cerebrovascular disease is a common neuropathological finding, coupled with Alzheimer's disease (Toledo *et al.*, 2013), a-synucleinopathies (Jellinger and Attems, 2008; Schwartz *et al.*, 2012) or frontotemporal lobar degeneration (De Reuck *et al.*, 2012).

Despite this complex clinico-pathological framework, *post mortem* studies have led to a classification of neurodegenerative diseases according to the predominant misfolded and accumulated protein (Kovacs *et al.*, 2010). However, *in vivo ante mortem* identification of specific neurodegenerative processes underpinning the clinical manifestation is important for clinical practice and for research. For this purpose, neuroimaging techniques enable the identification of *in vivo* disease-specific structural, functional and molecular brain alterations, which are an index of neurodegenerative processes and underlie clinical manifestations (Shimizu *et al.*, 2018). Structural Magnetic Resonance Imaging (MRI) can be used to assess cerebral atrophy and structural connectivity at high resolution, providing measures of structural

alterations and neuronal loss in dementia (Harper *et al.*, 2016; Koikkalainen *et al.*, 2016; Agosta *et al.*, 2017). On the other hand, molecular imaging techniques, such as Positron Emission Tomography (PET) with specific radioligands, can assess pathophysiological and biochemical changes at the molecular level, i.e. the burden, regional distribution and severity of ß-amyloid (Quigley *et al.*, 2011), tau pathology (Hall *et al.*, 2017), and of activated microglia (Stefaniak and O'Brien, 2015), as summarised in Chandra et al. (Chandra *et al.*, 2019). PET imaging of tau pathology and microglial activation has been increasingly applied in dementia to identify early molecular changes at group and single-subject levels (Stefaniak and O'Brien, 2015; Villemagne and Okamura, 2016; Dupont *et al.*, 2017; Hall *et al.*, 2017; Saint-Aubert *et al.*, 2017). Previous findings with MRI and PET in dementia suggest that *in vivo* imaging measures can help with early and differential diagnoses, providing evidence for clinicopathological correlations. However, their role and utility as prognostic tools in dementia remains undetermined.

In this chapter, I describe the main clinical spectrum associated with Alzheimer's disease and two non-Alzheimer's tau-related disorders included in later studies, specifically Progressive Supranuclear Palsy (PSP) and frontotemporal dementia. Overall, I will refer to these disorders as tauopathies. However, note that only half of frontotemporal dementia cases are driven by tauopathy, the other half by TDP-43-associated pathology. In Chapter 5, I distinguish the Tau and non-Tau forms of frontotemporal dementia based on genetics.

I describe the main shared clinical features and neuropathology processes (i.e. tau pathology and inflammation), beyond the main clinical syndromes. Next, I introduce the utility of structural MRI and PET imaging as tools to visualise and measure *in vivo* neuropathological changes in patients, and how these techniques have provided critical insights on clinicopathological correlations in these disorders. Finally, I conclude highlighting the literature gaps on the use of these imaging methods as prognostic tools in dementia, to then describe aims and hypotheses of my thesis.

For my thesis, I will focus in particular on three main clinical syndromes associated with tau pathology: (i) Alzheimer's dementia, caused by Alzheimer's disease; (ii) frontotemporal dementia; and (iii) the PSP "Richardson's syndrome" clinical phenotype which is associated with PSP pathology in ~95% of cases. In **Figure 1**, I report a simplified representation of the

clinicopathological spectrum associated with these three diseases and the related terms to refer to clinical syndromes and pathology that I will use accordingly in this thesis.

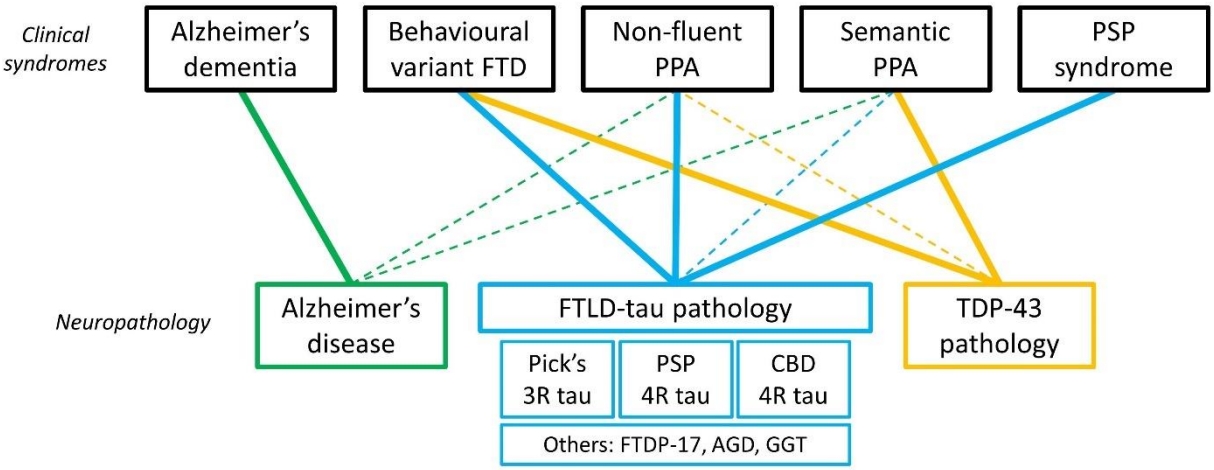

Figure 1. *Representation of the association between clinical syndromes (top) and neuropathology (bottom boxes) in tauopathies included in my thesis. Thick solid lines represent the predominant clinicopathological correlation for each disease, while slim dashed lines represent less common clinicopathological associations. Abbreviations: FTD=frontotemporal dementia; PPA= primary progressive aphasia; PSP=progressive supranuclear palsy; FTLD=frontotemporal lobar degeneration; TDP-43= transactive response DNA binding protein of 43 kD; CBD=corticobasal degeneration; FTDP-17=Frontotemporal dementia with parkinsonism-17; AGD=Argyrophilic grain disease; GGT=Globular glial tauopathy.*

In addition to Alzheimer's dementia, frontotemporal dementia and PSP, a neurodegernative tauopathy can be clinically manifested in other syndromes that are not included in this thesis. These other syndromes were not part of our PET cohorts. An example is corticobasal syndrome (CBS), which manifests as a combination of asymmetric rigidity, apraxia, dystonia, alien limb, and cognitive impairment. This syndrome is often caused by corticobasal degeneration, a rare tauopathy characterised by diffuse astrocytic plaques and ballooned neurons (Irwin et al 2016), while a minority of CBS cases are underpinned by Alzheimer's pathology (Alexander *et al.*, 2014). This choice was made based on the multimodal nature of the study and low prevalence of this syndrome. In Cambridge, patients with CBS have been recruited in cross-sectional epidemiological and MRI studies, but only recently they have been included in multi-tracer PET imaging (SENDeR) and longitudinal studies (PROSPECT).

1.2. Tauopathies

Tauopathies are a group of neurodegenerative diseases characterised by abnormal accumulation and deposition of neuronal and glial inclusions of tau protein. They can be divided into primary and secondary tauopathies, based on the presence or absence of other concomitant proteinopathies (Irwin, 2016). The classification of tauopathies also depends on the specific morphology and distribution of dysfunctional tau protein, and the ratio between different tau isoforms (Josephs, 2017), as described in section *"1.4.1. Tau pathology".* Tau isoform ratio (i.e. tau 4R and 3R isoforms) and conformation (i.e. straight vs. paired helical filaments) also divide tauopathies into Alzheimer's tauopathy and non-Alzheimer's tauopathies.

In my thesis, primary tauopathies refer to tau-related frontotemporal lobar degeneration pathologies, including Pick's disease and PSP pathology. They can be clinically manifested in different phenotypes, from frontotemporal dementia and progressive primary aphasia variants to parkinsonian syndromes, such as PSP. Secondary or non-primary tauopathies are neurodegenerative diseases that are characterised not only by tau pathology, but also by other abnormal proteins (i.e. β-amyloid). Alzheimer's disease, for example, can be considered a secondary tauopathy because of the co-existence of neurofibrillary tau pathology and β-amyloid plaques, and that it can be caused by mutations in genes that regulate amyloid but not tau protein.

1.2.1. Alzheimer's dementia

Alzheimer's disease, described by Alois Alzheimer in 1907 (Alzheimer, 1907), is the most common cause of dementia, accounting for 50-60% of cases at autopsy (Querfurth and LaFerla, 2010), with 1275 new diagnosed cases per year per 100,000 people aged over 65 years (Hirtz *et al.,* 2007). The incidence doubles every 5 years after 65 years of age, affecting about 5-10% of the population over 65, and up to 40% of people older than 85 years (Hebert *et al.,* 2003). The typical clinical presentation, referred to as the "amnestic variant" of Alzheimer's dementia, presents at first as a marked amnestic syndrome related to hippocampal alterations, and is characterised by early and insidious episodic memory deficits. A reduction in autonomy and the ability to carry out daily activities are also key features for the clinical diagnosis of Alzheimer's dementia (McKhann *et al.,* 2011). The clinical progression in later stages of the disease involves all cognitive domains (i.e. attention, language and visuo-spatial functions).

In this context, the term "Mild Cognitive Impairment" (MCI) has been used to extend the clinical spectrum of Alzheimer's disease to its earliest clinical manifestation in cases who may progress to a clinical diagnosis of Alzheimer's dementia. Patients with MCI are characterised by low performance in one or more cognitive domains, but these do not substantially interfere with daily functioning and activities (Knopman and Petersen, 2014). A clinical diagnosis of MCI does not require pathological validation, however, positivity of Alzheimer's disease specific biomarkers (i.e. tau and ß-amyloid levels at CSF or PET examinations) are required for the diagnosis of MCI due to Alzheimer's pathology; as MCI can indeed also be a clinical manifestation of other non-Alzheimer's underlying pathologies (Albert *et al.,* 2011; Ganguli *et al.,* 2011). New blood-based biomarkers, with pTau181 or pTau217 have been proposed, but the validity and accuracy of these biomarkers remain under evaluation.

1.2.2. Frontotemporal dementia

The complexity of the interaction between neuropathology, genetics and clinical manifestations is of particularly crucial importance in frontotemporal dementia syndromes. In addition to tau protein, other proteins are pivotal pathological underpinnings in frontotemporal dementia: TDP-43 in approximately half of cases, and the tumour-associated protein fused in sarcoma (FUS) in 2-5% of cases (Josephs *et al.,* 2011*a*). In addition, although the majority of frontotemporal dementia cases are sporadic, a fifth are familial and associated with genetic mutations, especially in microtubule-associated protein tau (MAPT) gene, progranulin (GRN) and gene and chromosome 9 open reading frame 72 (C9orf72) hexanucleotide expansion repeat (Rohrer *et al.,* 2009*a*). The first is typically related to tau pathology, while GRN and C9orf72 mutations are associated with TDP-43 pathology (Josephs *et al.,* 2011*a*; Seelaar *et al.,* 2011).

The heterogeneous pathological spectrum of frontotemporal dementia is associated with three main clinical syndromes: the behavioural variant of frontotemporal dementia (bvFTD), the non-fluent variant of Primary Progressive Aphasia (nfvPPA) and the semantic variant of Primary Progressive Aphasia (svPPA). All these variants are characterised by an insidious onset (Seelaar *et al.,* 2011). BvFTD is the most common of these subtypes, and is characterised by progressive personality and behaviour changes and cognitive decline (Piguet *et al.,* 2011; Rascovsky *et al.,* 2011). Apathy, disinhibition, socially inappropriate and stereotyped behaviour, loss of empathy and social engagement, poor planning skills and hyperorality are the most common symptoms

in patients with bvFTD, who typically have limited insight into their condition and show also cognitive deficits, especially in executive function (Rascovsky *et al.*, 2011). The other frontotemporal dementia subtypes are variants of primary progressive aphasia, which is a term to define several clinical phenotypes associated with progressive language impairment (Gorno-Tempini *et al.*, 2011). The nfvPPA (or progressive non fluent aphasia) syndrome is characterised by disrupted, slow and poor speech with agrammatism and speech apraxia signs. In contrast, svPPA (or semantic dementia) syndrome is characterised by fluent and grammatically correct speech but impaired semantic memory, which leads to deficits in objects/concepts knowledge, naming, and recognition. Although different clinical syndromes are characterised by distinct prevalent symptoms, such as relative episodic memory impairments in bvFTD (Hornberger and Piguet, 2012), and language deficits in PPA (Gorno-Tempini *et al.*, 2004), severe deficits in executive function have been reported across all clinical frontotemporal dementia syndromes, and in the pre-symptomatic phase of genetic frontotemporal dementia (Geschwind *et al.*, 2001; Rohrer *et al.*, 2015; Staffaroni *et al.*, 2020).

In frontotemporal dementia spectrum, apathy is one of the most prevalent and early cross-diagnostic symptoms (Johnson and Kumfor, 2018). In these patients, apathy is associated with the severity of executive function impairment (Zamboni *et al.*, 2008; Eslinger *et al.*, 2012), including deficits in working memory, decision making, selective/sustained attention, planning, processing speed, inhibitory processes and mental/cognitive flexibility (Hornberger *et al.*, 2008; Zamboni *et al.*, 2008; Eslinger *et al.*, 2012; Stopford *et al.*, 2012; O'Callaghan *et al.*, 2013). Executive dysfunction, like apathy, is a diagnostic criterion for bvFTD (Rascovsky *et al.*, 2011) and shares several anatomical correlates with apathy (see (Ducharme *et al.*, 2018) for a review). Recent studies have also highlighted the negative impact of apathy on survival in patients with frontotemporal dementia. The prognostic importance of apathy suggests that effective therapeutic strategies might ultimately influence patient outcomes and prognosis.

1.2.3. Progressive supranuclear palsy

PSP is a neurodegenerative disorder characterised by the neuro-glial accumulation of aggregated tau protein, particularly in the basal ganglia, diencephalon, and brainstem (Dickson *et al.*, 2007). The classical clinical phenotype of PSP is the sporadic Richardson's syndrome, which was first described by Drs Steele, Richardson and Olszewski in 1964 (Steele *et al.*, 1964). This clinical syndrome is characterised mainly by vertical supranuclear gaze palsy, akinetic-

rigidity, postural instability, and falls (Williams *et al.*, 2005; Höglinger *et al.*, 2017) and is associated with PSP pathology at *post mortem* examination in most cases (Litvan *et al.*, 2003; Bensimon *et al.*, 2009; Gazzina *et al.*, 2019). PSP Richardson's syndrome is also associated with behavioural and cognitive impairments (Burrell *et al.*, 2014; Kim *et al.*, 2014; Rittman *et al.*, 2016; Lansdall *et al.*, 2017; Peterson *et al.*, 2019). Specifically, behavioural symptoms include personality changes, obsessive behaviours, apathy and impulsivity but also loss of empathy, social cognition and insight (O'Keeffe *et al.*, 2007; Ghosh *et al.*, 2009, 2012; Kobylecki *et al.*, 2015; Höglinger *et al.*, 2017; Lansdall *et al.*, 2017). Common cognitive deficits in PSP patients involve frontal, executive and language domains (Burrell *et al.*, 2014; Kim *et al.*, 2014; Kobylecki *et al.*, 2015; Rittman *et al.*, 2016; Peterson *et al.*, 2019). Atypical clinical presentations of PSP are recognised by the latest diagnostic criteria and include PSP parkinsonism, PSP akinesia with gait failure, PSP progressive nonfluent aphasia, PSP corticobasal syndrome, and a more rare PSP clinical presentation similar to bvFTD (Höglinger *et al.*, 2017).

1.3. Commonalities across tauopathies

Although tauopathies can be divided into labelled clinical syndromes, based on established clinical and diagnostic criteria, they share several clinical features and symptoms. In particular, they are all characterised by heterogeneous clinicopathological correlations, an insidious onset, an inexorable disease progression, a progressive clinical decline, and a functional disability within a few years from the clinical diagnosis.

1.3.1. Pre-symptomatic and prodromal phases

In recent decades, the concept of tauopathies in neurodegenerative diseases has been evolving, and the related literature has contributed to the definition and the extension of two linked concepts: (i) a pre-symptomatic phase and (ii) a prodromal phase.

From previous genetic studies, it has been shown that tauopathies have a long pre-clinical phase, where neuropathology starts and progresses, but without reaching the threshold causing clinical symptoms and manifestations. Previous studies in subjects with an autosomal dominant mutation associated with Alzheimer's disease or frontotemporal dementia have investigated the pre-symptomatic phase in these diseases, showing early sub-clinical and brain changes in

individuals at risk for dementia years and decades before the dementia onset (Geschwind *et al.*, 2001; Jack *et al.*, 2013; Tan *et al.*, 2014; Schuster *et al.*, 2015; Greaves and Rohrer, 2019). Autosomal dominant mutations are ideal to investigate clinicopathological trajectories and potential early biomarkers because of their high penetrance within families and the possibility to estimate the time from dementia onset at individual level. This has allowed the description of cognitive and brain alterations and investigations of potential early biomarkers mainly in Alzheimer's disease (Jack and Holtzman, 2013; Tan *et al.*, 2014) and more recently also in frontotemporal dementia (Greaves and Rohrer, 2019). In PSP, genome-wide association studies have found that specific MAPT polymorphisms are associated with higher risk of this disease (Höglinger *et al.*, 2011; Chen *et al.*, 2019). However, autosomal dominant mutations (i.e. in MAPT gene) associated with PSP have been reported in very rare cases (Boxer *et al.*, 2017), as PSP is predominantly a sporadic disease. Thus, although the pre-symptomatic phase of PSP could last for years before symptom onset, as in Alzheimer's disease and frontotemporal dementia, it can only be identified incidentally at *post mortem* examination in clinically normal subjects with histological evidence of PSP pathology. Indeed, previous *post mortem* studies reported evidence of PSP pathology in 2-4% of healthy aging population (Kovacs *et al.*, 2013; Dugger *et al.*, 2014).

Clinical syndromes associated with degenerative tauopathies progress from the pre-clinical stage to the full manifestation of the disease, *via* a mild impairment stage. A pre-dementia and prodromal phase has been described in many neurodegenerative conditions, including Alzheimer's disease and frontotemporal dementia, which contributed to an increase of clinical referrals and diagnoses at earlier disease stages (Petersen *et al.*, 2009). This phase, when it is possible to identify early clinical and neurological signs before the patient fully reach as a clinical condition of functional impairment, in dementia is often referred to as mild cognitive impairment (MCI). MCI patients can be classified into two phenotypes according to the clinical signs that they present: amnestic MCI, defined by prevalent memory impairment, and non-amnestic MCI, characterised by prevalent deficits in other cognitive domains (Petersen *et al.*, 2009; Dugger *et al.*, 2015). The amnestic MCI cases may have a higher chance of developing Alzheimer's dementia, while non-amnestic MCI is more likely followed by a clinical diagnosis of frontotemporal dementia or dementia with Lewy bodies (Petersen *et al.*, 2009; Ferman *et al.*, 2013; Peters *et al.*, 2014). However, previous studies identified multiple concomitant pathologies underlying the two MCI phenotypes, with a propensity for increased neurofibrillary

tangles in amnestic patients and of Lewy bodies evidence in non-amnestic, but without a clear cut distinction of single pathologies and their unique contribution to one phenotype or another (Petersen and Negash, 2008; Dugger *et al.,* 2015). In PSP, a prodromal phase has also been described, but historically this was not operationalised in diagnostic criteria. In this context, the stage after the pre-symptomatic phase is defined as the *suggestive* phase, and it is characterised by a few clinical symptoms that raise a suspicion of PSP pathology and no other causes, but without fully meeting the clinical criteria for a diagnosis of PSP. The suggestive PSP is often followed by a fully symptomatic phase, where the patients meet the full criteria for one of the clinical variants of PSP (Boxer *et al.,* 2017). However, as for MCI and dementia, also the definition of suggestive PSP brings some degree of uncertainty on whether the patient will progress to a fully met diagnosis of PSP.

1.3.2. Transdiagnostic symptoms

In the complex and multidimensional framework of degenerative tauopathies, characterised by heterogeneous clinicopathological correlations, clinicians and researchers have been working together to clarify the boundaries between different diagnostic groups, and prescribe disease-specific criteria for patients' classification. Despite the undoubted utility of the established diagnostic criteria in both clinical management and research, there is a recognition that common symptoms sit across different clinical syndromes, which we can refer to as "transdiagnostic symptoms" (Husain, 2017). Indeed, in addition to syndrome-specific features, different clinical phenotypes associated with tau pathology are also characterised by common and relevant symptoms.

A distinction has often been made between "movement disorders" and "cognitive disorders" in neurodegenerative diseases. However, this classification has become more and more recognised as an artificial distinction given the growing evidence of both motor and cognitive symptoms that are shared across neurodegenerative disorders. For example, people with PSP have both difficulties with movement and cognition, while people with Alzheimer's disease can present motor coordination deficits (i.e. apraxia, akinesia), and frontotemporal dementia can be associated with parkinsonism and motor neurone disease (Rowe, 2019). Previous studies suggest that movement deficits, such as akinesia and rigidity, are present in over half of frontotemporal dementia cases (Coyle-Gilchrist *et al.*, 2016; Irwin *et al.*, 2016). In particular, the boundaries between movement disorders and dementia are indistinct in nfvPPA with

frequent progression to movement deficits resembling PSP or corticobasal syndromes (Murley *et al.,* 2020*a*). Similarly, although PSP is predominantly associated with movements disorders, previous studies suggest that up to 70% of the cases with PSP develop dementia (Daniel *et al.*, 1995; Coyle-Gilchrist *et al.*, 2016), however with more sensitive testing having revealed frontal dysfunction as a central and defining feature of the disease (Kaat *et al.,* 2007; Stamelou *et al.*, 2015; Rittman *et al.,* 2016; Höglinger *et al.*, 2017)

In different tauopathies we can also find an overlap in cognitive deficits. Cognitive evaluation in these patients identifies impaired episodic memory as a prominent deficit in patients with amnestic Alzheimer's disease, as well as executive dysfunction in bvFTD and PSP patients, while language deficits are defined as cognitive hallmarks for primary progressive aphasia variants (i.e. agrammatism in nfvPPA and semantic deficits in svPPA). However, episodic memory can also be impaired in frontotemporal dementia and PSP (Hornberger and Piguet, 2012; Burrell *et al.,* 2014), language deficits can be present in patients with Alzheimer's disease (Taler and Phillips, 2008), bvFTD (Hardy *et al.,* 2015) and PSP (Peterson *et al.,* 2019), and severe deficits in executive function have been widely described across all these clinical syndromes (Geschwind *et al.,* 2001; Hornberger *et al.,* 2008; Gerstenecker *et al.,* 2013; Guarino *et al.,* 2019; Staffaroni *et al.*, 2020).

In addition to cognitive and movement deficits, clinical syndromes associated with Alzheimer's disease or FTLD-tau also share behavioural and neuropsychiatric symptoms. Behaviour changes are a key feature of bvFTD (Rascovsky *et al.,* 2011) but are also reported in primary progressive aphasia (Rohrer and Warren, 2010), Alzheimer's disease (Lyketsos *et al.,* 2002; Fernández *et al.,* 2010), and can be a presenting feature of PSP (Gerstenecker *et al.,* 2013). One of the most important and disabling neuropsychiatric symptoms that are present in most of the cases across all these three diseases is apathy. In addition to bvFTD, previous studies reported presence of significant apathy severity in primary progressive aphasia variants and PSP (Mendez *et al.*, 2008; Rohrer and Warren, 2010; Coyle-Gilchrist *et al.*, 2016; Lansdall *et al.*, 2017, Murley *et al.*, 2020*a*). Apathy is also the most frequent neuropsychiatric symptom in patients with Alzheimer's dementia (Lyketsos *et al.,* 2002; Zhao *et al.,* 2016), and this is associated with caregiver distress, lower quality of life and increased mortality rate of patients (Nobis and Husain, 2018). In Alzheimer's research, previous evidence suggested that apathy may emerge early in the preclinical phase of the disease progression and is common in pre-

symptomatic carriers of autosomal dominant mutations related to Alzheimer's disease (Ringman *et al.*, 2015). Although few studies investigate the prevalence apathy and its influence on disease progression in Alzheimer's disease, frontotemporal dementia and PSP (Rohrer and Warren, 2010; Gerstenecker *et al.*, 2013, O'Connor *et al.*, 2016*b*; Zhao *et al.*, 2016; Lansdall *et al.*, 2017; Nobis and Husain, 2018; Lansdall *et al.*, 2019, Murley *et al.*, 2020*b*), there are no studies on apathy in the pre-clinical phase of frontotemporal dementia, and the causative relationship between apathy progression and cognitive impairment in these patients remain unclear.

1.4. Three pathological hallmarks of tauopathies

Tauopathies are characterised by abnormal accumulation of tau protein, and can be associated with other concomitant proteinopathies, such as ß-amyloid in Alzheimer's disease. However, in addition to tau pathology, these diseases are also commonly characterized by neuroinflammatory responses, which include microglial activation, astrocytic responses and increases in inflammatory molecules (Pasqualetti *et al.*, 2015; Ransohoff, 2016; Bright *et al.*, 2019). Both tau pathology and neuroinflammation contribute to disease progression and neuronal cell loss, which is one of the major pathological hallmarks of tauopathies.

In this section, I will describe three main pathological features observed across all tauopathies: tau aggregates, neuroinflammation and neuronal loss.

1.4.1. Tau pathology

Tau protein is normally expressed in neurons and performs a vital function binding and stabilising microtubules, which are part of the cellular cytoskeleton and maintain cell structure and facilitate intracellular transport (Lee *et al.*, 2011; Yoshiyama *et al.*, 2013). The tau protein is encoded by the MAPT gene on chromosome 17q21, and can be transcribed into six isoforms with different splicing, including or excluding exons 2, 3 and 10 (Goedert *et al.*, 1989). Tau isoforms containing exon 10 result in tau protein with four microtubule-binding repeats (tau 4R isoforms), while tau isoforms without exon 10 constitute tau protein with three microtubule-binding repeats (tau 3R isoforms). Healthy brains are characterised by an equal ratio of 3R and 4R tau (Hong *et al.*, 1998). In normal conditions, tau phosphorylation is an important process for the correct function of this protein, however, its abnormal and excessive

hyperphosphorylation results in abnormal accumulation of intraneuronal tau inclusions (i.e. pre-tangles, neurofibrillary tangles, neuropil threads), which leads to microtubules' disassembly and cellular impairment (Goedert and Spillantini, 2006; Spires-Jones and Hyman, 2014). The accumulation of tau pathology, associated with other disease-specific pathological factors, contributes to neuron loss, degeneration of neurites and synapses, resulting in pathology-related atrophy patterns (Serrano-Pozo *et al.,* 2011; Spires-Jones and Hyman, 2014).

Abnormal hyperphosphorylation, aggregation and propagation of tau protein have been described as a fundamental etiopathogenic mechanism in several neurodegenerative diseases. Abnormal tau inclusions associated with Alzheimer's disease are composed by paired helical filaments of 4R and 3R tau isoforms (Querfurth and LaFerla, 2010; Irwin, 2016), and constitute neurofibrillary tangles. Tangle deposition progresses from the entorhinal cortex to hippocampus, associative cortical regions, mainly in temporal and parietal lobes, and to primary sensory areas only in the latest stage of the disease (Braak and Braak, 1991). In this disease, tau aggregation is a primary factor in neuropathological staging, playing a key role in synaptic dysfunction and neuronal loss, and as such directly correlates with clinical severity (Iqbal *et al.,* 2005; Nelson *et al.,* 2012; Murray *et al.,* 2014).

In contrast to secondary tauopathies like Alzheimer's disease, in primary tauopathies the intraneuronal and astrocytic pathological tau aggregates are considered the principal hallmark. The aggregation of misfolded and hyper-phosphorylated tau protein, first to oligomers and then fibrillary tangles, is central to the PSP pathophysiology (Hauw *et al.,* 1994; Williams *et al.,* 2007; Dickson *et al.,* 2010; Kovacs, 2015), especially with tau isoforms that have 4 repeats of the microtubule-binding domain (Clavaguera *et al.,* 2015). In PSP tau aggregates are present in the form of straight filaments, and have been found mainly in basal ganglia, brain stem and cerebellum (Burrell *et al.,* 2014; Kovacs *et al.,* 2020). In this disease, characteristic fibrillary tau inclusions are also present in astrocytes, which are referred to as "tufted astrocytes" (Dickson *et al.,* 2007). In PSP patients, tau pathology promotes neuronal loss and gliosis, and also correlates with the clinical presentation (Murray *et al.,* 2014). Equally, intraneuronal tau tangle accumulations have also been reported as an important pathological substrate in frontotemporal dementia, with a different prevalence according to the clinical syndrome (Chare *et al.,* 2014). Tau pathology is the most common underlying substrate in bvFTD and nfvPPA, but only a secondary factor in svPPA. Variations in the MAPT gene have been found associated

with tau pathology in both frontotemporal dementia and PSP, due to an autosomal dominant monogenetic mutation (Ghetti *et al.*, 2015; Forrest *et al.*, 2018), or as a genetic risk factor (Höglinger *et al.*, 2011; Chen *et al.*, 2019).

1.4.2. Inflammation

Turning to the second main hallmark in tauopathies, there is growing evidence supporting neuroinflammation as a key process in Alzheimer's disease and frontotemporal lobar degeneration. This evidence comes from *post mortem* examinations, genome-wide association studies, animal models and epidemiologic evidence on anti-inflammatory use. Neuroinflammation involves a cascade of physiological responses mainly led by innate immune glial cells (i.e. microglia and astrocytes), which react to potentially harmful processes or factors, such as infections, autoimmunity, toxins, and trigger pro-inflammatory responses to modify the nervous microenvironment. In normal conditions neuroinflammation plays a protective role, removing pathogens, damaged cells and toxic aggregates to return the tissue homeostasis, but an excessive and chronic inflammatory response can lead to neurotoxic effects through the release of inflammatory mediators (e.g. pro-inflammatory cytokines) that promote an abnormal activation of microglia and astroglia (Glass *et al.*, 2010). This uncontrolled and prolonged overexpression then can lead to impaired neuronal repair processes, and malfunction of neurons and synapses, resulting in neurodegeneration (González *et al.*, 2014; Ransohoff, 2016; Vogels *et al.*, 2019). The interaction between neuroinflammation and other pathological hallmarks (i.e. amyloid and tau pathology) has been suggested as an important factor for disease progression in neurodegenerative conditions. Multiple cell types can have immune functions; however, microglia are the main macrophages, and of particular interest for their role in healthy and neurodegenerating brains.

In Alzheimer's disease, several lines of evidence indicate inflammation as a key pathological process. In particular, genome-wide association studies have identified several risk variants associated with Alzheimer's disease related to specific microglial proteins and immune response pathways (i.e. TREM2, CD33, CR1) (Verheijen and Sleegers, 2018; McQuade and Blurton-Jones, 2019). Epidemiology studies consistently show that long term anti-inflammatory use decreases the risk of Alzheimer's disease (McGeer *et al.*, 1996). Furthermore, *post mortem* examinations and animal studies, and more recently *in vivo* human biomarker data, have described an association between neuroinflammation and other pathological processes

associated with Alzheimer's disease. In particular, microglial activation has been reported to surround ß-amyloid plaques and hyperphosphorylated tau in early stage Alzheimer's disease, becoming largely considered the third neuropathological process in neurodegeneration (Heneka *et al.,* 2015; Pasqualetti *et al.,* 2015; Calsolaro and Edison, 2016; Vogels *et al.,* 2019). A growing literature also supports the driving role of neuroinflammation in tau spreading and neurodegeneration (Yoshiyama *et al.,* 2007; Asai *et al.,* 2015, Fan *et al.,* 2015*a*; Maphis *et al.,* 2015). Specifically, activated microglia have been suggested to trigger the spread of tau pathology across all the cortical regions (Maphis *et al.,* 2015; Perea *et al.,* 2018).

Growing evidence indicates a significant occurrence of activated microglia, inflammatory cytokine expression and their association with tau aggregation in frontotemporal dementia and PSP (Pasqualetti *et al.,* 2015; Bright *et al.,* 2019). In frontotemporal dementia, neuroinflammation may represent an early etiopathogenic event, rather than a consequence of neurodegeneration. This evidence comes from *post mortem* identification of microglial activation (Lant *et al.,* 2014; Sakae *et al.,* 2019; Woollacott *et al.,* 2020), genome wide association studies implicating inflammatory pathways in the etiology of frontotemporal dementia disorders (Ferrari *et al.,* 2014; Broce *et al.,* 2018; Pottier *et al.,* 2019), and from animal models where inflammatory responses were observed before aggregation of tau (Yoshiyama *et al.,* 2007). In PSP, activated microglia have been found surrounding neurofibrillary tangles even in the earlies stages (Ishizawa and Dickson, 2001; Fernández-Botrán *et al.,* 2011). In this disease, the notion of a 'toxic' alliance between neuroinflammation and tau-mediated neurodegeneration is supported by studies showing that genetic variants linked to inflammatory pathways concur, with specific tau-haplotypes (e.g. MAPT), to the risk for PSP (Höglinger *et al.,* 2011; Respondek *et al.,* 2018).

Overall, in these conditions, neuroinflammation and other pathological substrates may have a synergistic effect on neuronal degeneration. Indeed, chronic microglial activation may influence disease processes interacting differently with specific neuropathological proteins and releasing neurotoxic molecules. This process may contribute to neurodegeneration and influence dementia progression.

1.4.3. Neuronal loss

Although the pathogenesis of tauopathies is not yet fully understood, tau pathology accumulation and inflammatory responses may be part of the initial triggers in a cascade of events ending with neuronal loss and atrophy. Atrophy affects disease-related specific regions at the early stage and involves more and more brain regions as disease progresses. In tauopathies, volume loss reflects cell death due to apoptosis and necrosis, but also loss of neuronal innervations and synapses (Chi *et al.,* 2018). In Alzheimer's disease, neuronal loss involves multiple brain regions. In the early stage this is detectable in the entorhinal cortex, especially in pyramidal projection neurons (layer 2), the cholinergic nucleus basalis of Meynert and the locus coeruleus (Arendt *et al.,* 2015), and in the later phase this expands to cortical regions, especially in cingulate cortex, temporal and parietal lobes (Serrano-Pozo *et al.,* 2011).

In frontotemporal dementia, tau and TDP-43 protein aggregates are mainly associated with neuronal and synapse loss in the superficial cortical laminae (layers 2-3) in frontal and temporal lobes (Schofield *et al.,* 2003; Kersaitis *et al.,* 2004), even in the early stage of the disease. Cell loss in deeper layers has been reported , referring to von Economo neurons, which is evident in early stage of bvFTD (Seeley *et al.,* 2006; Seeley, 2008).

In patients with PSP Richardson's syndrome, pathological examinations have identified marked neuronal loss in midbrain, the cerebellar dentate nucleus and basal ganglia, and mild atrophy in prefrontal cortex, supramarginal gyrus, and thalamus (Tsuboi *et al.,* 2003; Dickson *et al.,* 2010; Schofield *et al.,* 2011). Evidence for loss of dopaminergic neurons in substantia nigra and loss of pigmented neurons in locus coeruleus have also been reported (Dickson *et al.,* 2010; Kaalund *et al.,* 2020).

1.5. *In vivo* imaging markers of neuropathology in tauopathies

In order to improve our understanding of pathological processes in neurodegenerative diseases, different neuroimaging techniques have been developed to *in vivo* molecular biological processes and visualise structural brain changes. One way of measuring structural brain changes underlying dementia is by using structural MRI, while for molecular processes, PET imaging is the most used approach, which employs molecules labelled with radioactive isotopes (i.e. Carbon-11 and Fluorine-18), called radioligands, to target specific molecular processes of

interest, such as protein accumulation and neuroinflammation. Both structural MRI and PET are well established as research tools and partially also in clinical practice.

In the following section, I review the background to PET imaging with radioligands for tau/TDP-43 pathology and neuroinflammation, and to structural MRI as a measure of atrophy and neurodegeneration. I will briefly describe the main application of these techniques in each of the tauopathies considered in my projects, leaving a deeper description of imaging literature for each disease in the introduction part of each experimental chapter (Chapters 3-8).

1.5.1. PET imaging for tau pathology: [^{18}F]AV-1451 PET

In recent years, several PET tracers have been developed to measure *in vivo* tau pathology quantity and distribution, such as FDDNP, THK and PBB compounds families (Laforce *et al.,* 2018). Although some concerns have also been raised regarding the specificity of these ligands to non-Alzheimer's tau pathology (Saint-Aubert *et al.,* 2017), the most widely used and studied tau-sensitive radioligand so far is [^{18}F]AV-1451 (also known as T807). Studies have reported that [^{18}F]AV-1451 PET accurately measures tau accumulation, with higher affinity for paired helical filaments of tau than β-amyloid or α-synuclein (Xia *et al.,* 2013*a*; Marquié *et al.,* 2015; Lowe *et al.,* 2016), and has low retention in the white matter. In the Neuroimaging of Inflammation in Memory and Related Other Disorders (NIMROD) study, [^{18}F]AV-1451 has been chosen as the PET marker for tau pathology because previous evidence supported its use in neurodegenerative disease. In particular, [^{18}F]AV-1451 was significantly better than other tau tracers available at the time, such as FDDNP which also binds amyloid, and THK which was severely confounded by monoamine oxidase (MAO) cross binding. [^{18}F]AV-1451 was the most specific on data available at the time the study was begun. Today, other tracers such as [^{18}F]PI-2620 might be considered, as they have higher affinity for PSP tauopathy while retaining sensitivity to Alzheimer's disease (Brendel *et al.,* 2020; Mormino *et al.,* 2020).

Most [^{18}F]AV-1451 PET studies have been focused on MCI and Alzheimer's dementia (see for a review (Hall *et al.,* 2017)), showing tau accumulation in the entorhinal cortex in MCI and the temporo-parietal cortices in Alzheimer's dementia patients. In these patients, [^{18}F]AV-1451 uptake correlated with Braak staging of neurofibrillary tau (Schöll *et al.,* 2016; Schwarz *et al.,* 2016), cognitive impairment (Brier *et al.,* 2016, Cho *et al.,* 2016*b*; Johnson *et al.,* 2016; Ossenkoppele *et al.,* 2016; Pontecorvo *et al.,* 2017) and *post mortem* patterns of Alzheimer's

disease pathology (Sander *et al.*, 2016; Lowe *et al.*, 2020; Soleimani-Meigooni *et al.*, 2020). In Alzheimer's disease spectrum, [^{18}F]AV-1451is also associated with cortical atrophy and hypometabolism (Bischof *et al.*, 2016; Iaccarino *et al.*, 2018, 2020; Ossenkoppele *et al.*, 2019; Timmers *et al.*, 2019; Joie *et al.*, 2020).

Although [^{18}F]AV-1451 shows strong *in vivo* and *post mortem* binding to tau pathology in Alzheimer's disease, it displays a variable affinity in healthy aging and non-Alzheimer's tauopathies (Marquié *et al.*, 2015; Lowe *et al.*, 2016; Sander *et al.*, 2016; Soleimani-Meigooni *et al.*, 2020). It binds to nonspecific sites, which is referred as "off-target" binding sites, including neuromelanin (Marquié *et al.*, 2015), monoamine oxidase (Vermeiren *et al.*, 2018)) and choroid plexus (Lowe *et al.*, 2016). However, previous *post mortem* data (Passamonti *et al.*, 2017) have shown that off-target binding to neuromelanin cannot be the cause for [^{18}F]AV-1451 binding in the striatum or the cortex, as these regions do not accumulate neuromelanin (Hansen *et al.*, 2016). In the basal ganglia MAO-A is significantly expressed, and this has been proposed as an alternative off-target binding site of [^{18}F]AV-1451 (Vermeiren *et al.*, 2018). MAO-B has also been found to be expressed in reactive astrocytes and activated microglia (Saura *et al.*, 1994; Vermeiren *et al.*, 2018), which raises the critical issue of whether [^{18}F]AV-1451 binding relates not only to tau pathology but also neuroinflammation. However, this hypothesis was not supported by data in a carrier of a MAPT genetic mutation in which high neuroinflammation PET binding in frontotemporal regions was found despite a lack of significant [^{18}F]AV-1451 binding (Bevan-Jones *et al.*, 2019). Finally, although [^{18}F]AV-1451 binding in the choroid plexus has been described as molecular off-target binding in healthy aging, histological analyses have challenged this hypothesis, reporting tangle-like structures in epithelial cells of this region (Ikonomovic *et al.*, 2016).

The affinity of [^{18}F]AV-1451 to the 4R tau in non-Alzheimer's tauopathies is lower than its affinity to 3/4-repeat tau pathology related to Alzheimer's disease (Marquié *et al.*, 2015; Sander *et al.*, 2016). However, this ligand reveals the distribution of tau pathology in cases due to MAPT mutations, which are associated with tau pathology (Bevan Jones *et al.*, 2016; Smith *et al.*, 2016; Spina *et al.*, 2017). In PSP patients, increased [^{18}F]AV-1451 binding has been shown in sub-cortical rather than cortical regions, consistent with previous neuropathological evidence (Cho *et al.*, 2017; Passamonti *et al.*, 2017; Schonhaut *et al.*, 2017; Smith *et al.*, 2017, Whitwell *et al.*, 2017*b*). This evidence supports the use of [^{18}F]AV-1451 PET to quantify and localise tau pathology in tauopathies with clear and known pathologic substrates, such as PSP. Our previous

study (Passamonti *et al.*, 2017) also showed that it is possible to discriminate the neuroanatomical pattern of [^{18}F]AV-1451 binding in PSP from the one seen in patients with Alzheimer's disease using machine-learning approaches and multivariate pattern analyses. This corroborates the use of [^{18}F]AV-1451 PET as a marker of disease-specific pathological changes.

In addition to non-Alzheimer's tauopathies, [^{18}F]AV-1451 also showed characteristic binding in cases with bvFTD related to C9orf72 mutation and in patients with svPPA, which are caused by TDP-43 rather than tau pathology (Bevan-Jones *et al.,* 2018*b*, *a*; Josephs *et al.,* 2018; Makaretz *et al.,* 2018, Cho *et al.,* 2019*b*; Tsai *et al.,* 2019). In semantic dementia, [^{18}F]AV-1451 binds regions affected by TDP-43 pathology and where neuronal monoamine oxidase or neuromelanin are unlikely to be present (Bevan-Jones *et al.,* 2018*b*). Similarly, C9orf72 mutation, which is associated with TDP-43 pathology, increases [^{18}F]AV-1451 binding in frontotemporal cortex of patients compared to healthy controls (Bevan-Jones *et al.,* 2018*a*). This suggests that the [^{18}F]AV-1451 ligand is not specific to tau pathology, but also binds abnormal protein aggregation related to TDP-43 pathology (although not to TDP-43 itself) (Bevan-Jones *et al.*, 2018*b*; Makaretz *et al.*, 2018). Looking at frontotemporal dementia clinical variants, [^{18}F]AV-1451 patterns in nfvPPA and svPPA patients allows good separation between these two conditions, showing high uptake in frontal regions for nfvPPA and in temporal regions for svPPA (Josephs *et al.*, 2018; Tsai *et al.,* 2019). In nfvPPA, different [^{18}F]AV-1451 patterns reflect differences in specific symptoms manifestations. For example, elevated uptake was found in inferior frontal gyrus in patients with agrammatic aphasia (Utianski *et al.,* 2018b), and in motor cortices for patients with apraxia of speech (Utianski *et al.,* 2018a). In svPPA, elevated [^{18}F]AV-1451 uptake has been found mainly in the anteromedial temporal lobe, but also in basal frontal regions and insula (Bevan-Jones *et al.*, 2018*b*; Josephs *et al.,* 2018; Makaretz *et al.,* 2018, Cho *et al.,* 2019*b*; Tsai *et al.,* 2019). In bvFTD, the results are variable, and elevated frontotemporal [^{18}F]AV-1451 uptake is reported in 50% of the patients. This may be due to the pathological heterogeneity that characterises these patients (Tsai *et al.,* 2019).

Considering previous findings, [^{18}F]AV-1451 PET can be used to quantify and localise tau pathology burden in neurodegenerative diseases with clear and known pathologic substrates. Otherwise, in conditions with unknown pathology, [^{18}F]AV-1451 PET is able to localise pathological molecules and discriminate Alzheimer's disease and non-Alzheimer's cases, but not to identify the specific type of pathological molecules involved. Further evaluation and

awareness of its limitations are necessary for correct interpretations of the research results and clinical applications.

1.5.2. PET imaging for neuroinflammation: [^{11}C]PK11195 PET

Considering the growing literature suggesting a central role of neuroinflammation in neurodegeneration, quantification and *in vivo* measurement of microglial activation have become critical to clarify pathophysiology and disease progression in patients with dementia. In this context, most of the neuroimaging studies about neuroinflammation in dementia patients have been focused on the measure of microglial activation with PET imaging. In recent years, several PET radioligands have been developed targeting the 18-kDa translocator protein (TSPO), a mitochondrial membrane protein which is overexpressed in activated microglia (Scarf and Kassiou, 2011). The PET ligand [^{11}C]PK11195 was the first TSPO radioligand to be widely used in neurodegenerative disease to visualise microglial activation.

In Alzheimer's disease, results with [^{11}C]PK11195 have been variable (see (Chandra *et al.*, 2019) for a review), however this variability may arise from small samples and the lack of standardised methods for the previous *in vivo* studies. Overall, this ligand for TSPO has shown strong binding in temporo-parietal regions and cingulate cortex in Alzheimer's disease patients (Stefaniak and O'Brien, 2015) – regions in which neuroinflammation is negatively associated with cognitive performance in MCI and Alzheimer's dementia (Edison *et al.*, 2008; Yokokura *et al.*, 2011, Fan *et al.*, 2015*a*, Passamonti *et al.*, 2018*b*, 2019).

Only few PET studies have assessed neuroinflammation in patients with non-Alzheimer's dementias. PET studies with [^{11}C]PK11195 have shown increased neuroinflammation in frontotemporal regions in patients with sporadic frontotemporal dementia (Cagnin *et al.*, 2004; Bevan-Jones *et al.*, 2020), and have reported evidence that neuroinflammation may precede the development of the full frontotemporal dementia syndrome in carriers of MAPT mutations (Bevan-Jones *et al.*, 2019). A *post mortem* study reported higher microglial activation of frontal subcortical white matter in patients with frontotemporal dementia compared to patients with Alzheimer's disease (Lant *et al.*, 2014). In the same study, considering patients in the frontotemporal dementia spectrum, cases with MAPT mutation presented higher microglial activation in temporal subcortical white matter than other frontotemporal dementia cases (Lant *et al.*, 2014). A few studies have also explored neuroinflammation in patients with corticobasal

syndrome (Gerhard *et al.*, 2004) and PSP (Gerhard *et al.*, 2006, Passamonti *et al.*, 2018*b*). Especially, in PSP compared to controls, [^{11}C]PK11195 PET binding was increased in the basal ganglia, striatum, midbrain, frontal lobe, and the cerebellum (Gerhard *et al.*, 2006, Passamonti *et al.*, 2018*b*). In these patients, microglial activation in the pallidum, midbrain, and pons correlated with the PSP rating scale (PSP-RS), a measure of disease severity (Passamonti *et al.*, 2018*b*).

Although at present [11C]PK11195 PET remains the most used and relevant method to study microglial activation in neurodegenerative diseases, its application is not without limitations. TSPO expression in the neuroinflammation cascade is complex. In addition to activated microglial, overexpressed TSPO can be found in astrocytes and vascular smooth muscle cells (Gui *et al.,* 2020). However, previous evidence showed that [^{11}C]PK11195 binds selectively for activated microglia over other cells, like astrocytes, and also the quiescent microglia (Banati, 2002). This supports the utility of this tracer for the visualisation and measure of activated microglia. Several second-generation PET radioligands for TSPO have been developed since [^{11}C]PK11195 (e.g. [^{11}C]PBR28 and [^{18}F]DPA-714), which are characterised by higher signal-noise ratio and lower lipophilicity than the latter. However, these tracers' binding affinity is influenced by a single-nucleotide polymorphism (rs6971), which causes heterogeneity in PET data (Dupont *et al.,* 2017). For this reason, the use of second-generation tracers requires genetic analyses, while it is well established that [^{11}C]PK11195 does not necessitate this assessment because this tracer is not strongly affected by this genetic polymorphism. However, a small difference in [^{11}C]PK11195 binding in the central nervous system remains a possibility (Fujita *et al.,* 2017). Although there are some limits associated with [^{11}C]PK11195, the second generation TSPO radioligands are also characterised by similar issues and require more invasive modelling of the PET data. Thus, [^{11}C]PK11195 remains the most robust radioligand to visualise neuroinflammation in neurodegenerative diseases, and the one chosen in the NIMROD study.

1.5.3. Structural MRI as marker of neuronal loss

MRI is a standard imaging technique to measure different aspects of structural and functional neuronal changes in neurodegenerative disease. For the purposes of my thesis, I describe structural MRI as a modality that enables the visualization of the disease specific patterns of neurodegeneration and atrophy. Atrophy measures by structural MRI correlate with

neuropathology disease severity and distribution, and have been suggested as a surrogate *in vivo* marker of neuropathology (Kantarci and Jack, 2004; Whitwell *et al.,* 2008). In my thesis, I focus on grey matter atrophy, rather than white matter degeneration and structural connectivity damages.

In Alzheimer's disease, the typical atrophy pattern identified with structural MRI involved predominantly temporal and parietal lobes, including medial temporal and parietal regions (Singh *et al.,* 2006; Dickerson *et al.,* 2009). Structural MRI markers, including hippocampal atrophy and enlarged ventricles, have been reported as reliable markers to differentiate patients at different stages on the Alzheimer's disease spectrum and from age-matched healthy controls (Nestor *et al.,* 2008; Chou *et al.,* 2009; Whitwell, 2018). In addition, MRI measures of medial temporal lobe volumes correlate with disease severity, and are reported as a predictive marker of future conversion from MCI to Alzheimer's disease (Frisoni *et al.,* 2010; Leung *et al.,* 2013; Jack *et al.,* 2015).

In frontotemporal dementia, volumetric MRI measures are validated biomarkers to investigate neuronal loss patterns in different clinical phenotypes (Gordon *et al.,* 2016). In bvFTD, previous MRI studies reported significant early atrophy across bilateral frontal paralimbic and insular cortices, to then involve bilateral frontal and temporal lobes, the cingulate cortex and subcortical structures (Rosen *et al.,* 2002; Schroeter *et al.,* 2007; Seeley *et al.,* 2008; Whitwell *et al.,* 2009; Pan *et al.,* 2012). In contrast, the classical manifestation of svPPA is associated with severe atrophy primarily in the left anterior temporal lobe but also in orbitofrontal, insula and anterior cingulate regions (Rosen *et al.,* 2002; Gorno-Tempini *et al.,* 2004, Rohrer *et al.,* 2009*b*; Rogalski *et al.,* 2011). In nfvPPA previous MRI studies showed limited atrophy in the left inferior frontal gyrus and insula cortices (Gorno-Tempini *et al.,* 2004, Rohrer *et al.,* 2009*b*; Rogalski *et al.,* 2011). In addition, within each frontotemporal dementia phenotype, different genetic mutations have been found associated with different atrophy patterns (Rohrer *et al.,* 2010; Mahoney *et al.,* 2012, Whitwell *et al.,* 2012*a*; Cash *et al.,* 2018). Specifically, in familial frontotemporal dementia atrophy involves common regions across genetic variants (mutations in MAPT, GRN or C9orf72 gene) which include the insula, orbitofrontal lobe, and anterior cingulate. However, in carriers of a MAPT mutation, atrophy primarily also involves anterior and medial temporal regions; in GRN mutation cases, atrophy is also found in dorsolateral and ventromedial prefrontal cortices, lateral temporal and parietal regions, and precuneus; while in

C9orf72 mutation carriers, atrophy also involves posterior regions and cerebellum (Cash *et al.*, 2018). Structural MRI studies in frontotemporal dementia suggested that executive dysfunction and apathy in these patients share several anatomical correlates in terms of atrophy (see (Ducharme *et al.*, 2018) for a review). Apathy severity, similar to executive dysfunction, correlates with widespread atrophy in frontotemporal areas, including the dorsolateral, ventromedial and orbital prefrontal cortex and anterior cingulate cortex (Rosen *et al.*, 2005; Zamboni *et al.*, 2008; Lansdall *et al.*, 2017, Murley *et al.*, 2020*a*) (see(Ducharme *et al.*, 2018, Passamonti *et al.*, 2018*a*)).

In PSP, structural MRI has been widely used, in terms of visual evaluation of clinical scans and of quantitative measures at group level. Atrophy in the midbrain and other subcortical regions, including caudate nucleus, putamen, globus pallidus, and thalamus, is typically reported from structural MRI studies with PSP patients (Whitwell *et al.*, 2017*a*). The visual assessment of midbrain atrophy and morphological markers is part of clinical practice, such as the assessment of the presence of the "hummingbird" sign due to atrophy of the dorsal midbrain (Mueller *et al.*, 2018), the "Mickey Mouse" sign that presents as rectangular midbrain peduncles (Massey *et al.*, 2012), and the "morning glory" sign representing the concavity of the midbrain tegmentum margin (Adachi *et al.*, 2004). In addition to subcortical regions, PSP-Richardson's syndrome is also associated with atrophy in frontal cortical regions (Cordato *et al.*, 2002; Brenneis *et al.*, 2004). The degree of cortical vs. subcortical atrophy differentiates Richardson's syndrome from cortical and other subcortical phenotypes (Jabbari *et al.*, 2020*a*).

1.6. Challenge of prognosis in tauopathies

Tauopathies are heterogeneous at genetic, biochemical, morphological and clinical levels. In addition to clinical and pathological commonalities between Alzheimer's disease, frontotemporal dementia and PSP, these diseases also share the lack of effective disease modifying treatments and the unsolved question on which may be the most sensitive prognostic biomarkers.

Several experimental animal models of tauopathies have been employed to investigate the role of pathological processes at different stages of these diseases and to explore potential treatments (Dujardin *et al.*, 2015). Despite the utility of these preclinical models, there is urgent need for validated tools and biomarkers to track *in vivo* human pathogenesis, which could improve our

understanding of pathological processes and disease progression in living patients. This will be crucial to enhance patient stratification and to empower future clinical trials. Disease modifying treatments have not yet been successfully developed for patients with tauopathies, who are supported solely with symptomatic therapies. Previous disease modulating trials in Alzheimer's disease and PSP have failed (Coughlin and Irwin, 2017). Most of the current clinical trials have focused on Alzheimer's disease or PSP, while in frontotemporal dementia the low specificity of clinical diagnoses makes the challenge even harder.

In this context, a challenge is to identify *in vivo* human pathological markers related to clinical variations and progression, which could contribute to the development of new targeted therapies. The application of MRI and PET in human diseases has led to the *in vivo* quantification of neurodegeneration and neuropathology markers. Previous findings on structural changes, protein-specific pathology, and neuroinflammation in dementia suggest that *in vivo* imaging tools can provide evidence for early diagnosis and a better understanding about the relation between neuropathology and clinical phenotypes. As such, neuroimaging has contributed to the clarification of the complexity and heterogeneity of clinicopathological spectrums. Although previous findings support the use of MRI and PET imaging in the diagnosis and monitoring of disease progression, the prognostic value of these *in vivo* measures and their combined effect in predicting clinical and cognitive decline in tauopathies remains undetermined.

Understanding and anticipating different trajectories and courses in these disorders is crucial for a better stratification and a more accurate prediction of outcomes in research and clinical trials. Specifically, new treatments should be considering cohorts with different decline rates, separating patients with stable course from patients with high risk of complications and rapid decline. Furthermore, in the complex clinicopathological framework of neurogenerative diseases, the better characterisation of the factors predicting decline in large cohorts and individual patients will help to develop enhanced prognostic and outcome measures for clinical trials targeting more than one pathological process. This emerges as particularly relevant in disorders like Alzheimer's disease, frontotemporal dementia and PSP, where multiple pathological processes are involved, but tau pathology and neuroinflammation play a central role.

In frontotemporal dementia, which has weaker clinico-pathology correlations than in amnestic Alzheimer's dementia and PSP Richardson's syndrome, a better understanding of the causes and consequences of a cross-syndromic symptom like apathy and its role in the clinical progression is vital to develop effective treatment strategies, including preventive strategies in the context of genetic risk of frontotemporal dementia. Specifically, apathy may precede other neuropsychiatric features, accelerate cognitive and functional decline and increase dementia conversion rates. Thus, apathy may represent a modifiable factor to slow or prevent dementia progression.

In the following experimental chapters (Chapters 3-8), I will describe in detail previous studies that employed neuroimaging markers to investigate longitudinal clinical progression in these disorders, highlighting the questions the current research projects aim to address. Overall, previous work has assessed the correlations between longitudinal imaging markers and clinical changes, while only few studies have explored the predictive value of cross-sectional imaging markers for subsequent clinical progression. In addition, most of these studies employed neuroimaging modalities in isolation rather than exploiting the mechanistic and prognostic value that is offered by a multi-modal approach, that combines different neuroimaging markers and/or clinical measures.

1.7. Aims and hypotheses of my thesis

Although previous findings support the utility and application of structural PET and MRI as *in vivo* markers of neuropathology and neurodegeneration, their prognostic values for clinical changes remains under-investigated. The overarching aim of my thesis is to determine the predictive value of *in vivo* structural MRI and PET markers of pathology on longitudinal clinical and cognitive decline in three major tauopathies: Alzheimer's disease, frontotemporal dementia, and PSP. In frontotemporal dementia, in addition to imaging, I also investigate the prognostic value of apathy, one of the most common and early symptoms across all frontotemporal dementia syndromes that may represent an early sign of brain changes and a modifiable factor in the pre-symptomatic stage of this condition.

I set the following three objectives

1) to determine the prognostic value of structural MRI and PET markers for tau pathology and neuroinflammation in Alzheimer's disease;

2) to test the predictive value of imaging and behavioural measures for cognitive decline in frontotemporal dementia;
3) to determine the predictive value of *in vivo* pathology neuroimaging markers in PSP, as a model of non-Alzheimer's primary tauopathy.

My projects used data from two main datasets: the Neuroimaging of Inflammation in Memory and Related Other Disorders (NIMROD) study and the Genetic Frontotemporal Dementia Initiative (GENFI) study (see Chapter 2 for details). These two studies both have longitudinal measures of clinical repeated assessment. They both use neuroimaging to identify the specific brain changes underlying clinical manifestations. However, the two cohorts are different in many aspects. The NIMROD study was undertaken locally in Cambridge, the participants have been visited by the same clinicians and researchers, and the imaging scans acquired with the same protocol and techniques. The main advantage of this database is the multimodal imaging approach applied on different diagnostic groups, which led to the collection of both MRI and PET data with different tracers in patients with distinct clinical syndromes. However, the local and multimodal nature of this project did not permit cohorts with large sample size. In contrast, the multicentre nature of GENFI initiative enabled the recruitment of over 1000 participants, with longitudinal MRI visits in addition to repeated clinical assessments. Beyond the large sample size, another strength of this dataset is the focus on genetic cases with frontotemporal dementia, which allows us to study the pre-symptomatic phase of this disease with patients' relatives that carry the same gene mutation. In contrast to NIMROD, however, the GENFI study does not include PET imaging but only MRI, which is not able to inform about the pathological accumulation of junk proteins and inflammation processes.

In **Chapter 2**, I describe the main cohorts and statistical models I used to answer these research questions, which were divided into the following six experimental chapters (Chapters 3-8).

In each of the following experimental chapters, I report a detailed literature review with studies of interest for the formulation of my research questions and hypothesis in each investigated disease.

In **Chapter 3**, I examine the independent and combined predictive effects of baseline neuroimaging biomarkers for tau pathology ([^{18}F]AV-1451 PET), neuroinflammation

([^{11}C]PK11195 PET) and brain atrophy (structural MRI) on longitudinal cognitive changes in the clinical spectrum of Alzheimer's disease. I begin with this disorder, due to its clinical and pathological homogeneity as compared with e.g. frontotemporal dementia, and as the PET ligands utilised here were developed in the context of Alzheimer's disease. Considering the previous literature, the main hypothesis is that the baseline PET markers for tau and neuroinflammation would be more informative than structural MRI on longitudinal cognitive deterioration in Alzheimer's disease.

In **Chapter 4**, I follow up on this issue in a second disorder, frontotemporal dementia, which is characterised by complex clinicopathological correlations. I start from testing for relationships between baseline and longitudinal changes in atrophy, apathy and cognition in pre-symptomatic carriers of a genetic mutation associated with frontotemporal dementia (i.e. in MAPT, GRN, or C9orf72 gene), compared to non-carrier relatives. The main hypothesis here is that apathy increases over time in pre-symptomatic carriers, anticipating cognitive decline that occurs years before the onset of dementia symptoms.

In **Chapter 5**, I investigate the *in vivo* pathology in a case series of frontotemporal dementia patients with a monogenetic dominant mutation in MAPT, GRN, or C9orf72 genes. I use [^{11}C]PK11195 and [^{18}F]AV-1451 ligands to respectively quantify *in vivo* neuroinflammation and tau or TDP-43 pathology, and to examine the association between their distribution across cortical and subcortical structures, and the clinical features of each case.

In **Chapter 6**, I move from a cross sectional correlation to a formal model of trajectory in a larger group of patients with frontotemporal dementia. I examine the predictive value of baseline neuroimaging biomarkers for neuroinflammation ([^{11}C]PK11195 PET) and grey-matter atrophy (structural MRI) on longitudinal cognitive decline, across all three major frontotemporal dementia clinical variants. I test the prognostic value of baseline apathy for the annual rate of cognitive decline. The hypothesis is that baseline imaging measures of both atrophy and neuroinflammation, but also apathy severity, are associated with annual rate of cognitive decline of these patients. Given the pathological heterogeneity in the frontotemporal dementia spectrum and the differential affinity of [^{18}F]AV-1451 PET for non-Alzheimer's tau and TDP-43 pathology, I did not include this ligand in the analyses of frontotemporal dementia.

In Chapter 7 and Chapter 8, I address the third objective, moving to the primary tauopathy PSP. First, in **Chapter 7**, I examine the *in vivo* relationship and co-localisation between neuroinflammation and tau protein aggregation in patients with PSP, as this has not been previously investigated in the literature. Then, in **Chapter 8**, I examine the prognostic value of *in vivo* measures of brain atrophy derived from structural MRI, activated microglia ([^{11}C]PK11195 PET) and tau pathology ([^{18}F]AV-1451 PET) to predict the annual rate of clinical progression in these patients. The main hypotheses are that (i) pathological tau accumulation and neuroinflammation are associated in specific regions, previously described as affected by PSP-related pathology, and that (ii) in these regions, baseline imaging markers for pathology and atrophy may be related to clinical progression over time.

Chapter 2 | Study cohorts and methods

2.1. Introduction

My thesis is based on two longitudinal datasets. The first has been collected within the context of the Neuroimaging of Inflammation in Memory and Related Other Disorders (NIMROD) study (Bevan-Jones *et al.*, 2017), the second under the Genetic Frontotemporal Dementia Initiative (GENFI) protocol. In this chapter, I briefly describe participants, design and imaging acquisition methods for both cohorts, and introduce two main statistical models to analyse longitudinal data that I applied in my projects. Imaging and statistical methods are further specified in the respective experimental chapters (Chapters 3-8) for each individual project.

2.2. NIMROD study

2.2.1. Introduction

The NIMROD study is a local project conducted at the University of Cambridge (Cambridge, UK) and led by Prof. James Rowe and Prof. John O'Brien, which aims to understand the role of inflammation and tau protein in the pathogenesis of dementia and neurodegenerative disorders. Patients were recruited from the counties of Cambridgeshire and bordering areas, through regional specialist clinics for cognitive disorder clinics in neurology, old age psychiatry, and related services at Cambridge University Hospital , other regional trusts, or the National Institute for Health Research Clinical Research Network Dementias and Neurodegeneration Speciality (DeNDRoN) and the Join Dementia Research platform. In this project, the clinical status and cognitive functioning of patients were tested annually over a period of three years. Following the baseline visit, participants underwent multimodal neuroimaging scans, including PET imaging with three different ligands, [^{11}C]PK11195 to trace microglial activation, [^{11}C]PiB for amyloid (only in MCI) and [^{18}F]AV-1451 for tau deposition, and MRI imaging to examine structural and functional impairments.

The study protocol and procedures (Bevan-Jones *et al.*, 2017) were approved by the East of England Cambridge Central Research Ethics Committee (reference: 13/EE/0104), and by the UK Administration of Radioactive Substances Advisory Committee (ARSAC).

2.2.2. Participants

All participants included were aged over 50 and had a proficient level of English. People with major psychiatric illness, systematic inflammatory medications, or who were unable to attend an MRI scan were excluded. In addition, patients had to be able to report the background clinic history and to have a reliable carer to complete some questionnaires. Given the long-term and intensive nature of the project, all patients had to score higher than 12 in the Mini-Mental State Examination (MMSE) or less than 2 in the Clinical Dementia Rating Scale (for patients with language/semantic deficits).

The specific inclusion criteria for each cohort included in this thesis were:

- controls: MMSE scores >26, absence of memory symptoms, signs of dementia, and any other medical illnesses;
- patients with MCI: MMSE >24, presence of memory impairment not ascribable to age and another diagnosis, nor Alzheimer's dementia (Albert *et al.,* 2011). Patients with MCI have been divided by biomarkers of Alzheimer's disease in MCI positive (MCI+) or negative;
- patients with Alzheimer's dementia: diagnostic criteria for probable Alzheimer's dementia of McKhann et al. (McKhann *et al.*, 2011);
- patients with frontotemporal dementia: clinical criteria for one of clinical syndromes defined by Rascovsky et al. (Rascovsky *et al.*, 2011) and Gorno-Tempini et al. (Gorno-Tempini *et al.,* 2011), namely bvFTD and PPA, which include svPPA, lvPPA and nfvPPA;
- patients with PSP: at the beginning of the NIMROD project, modified Litvan criteria (Litvan *et al.,* 1996), with falls criterion < 3 years, rather than 1 year (as suggested by the NNIPPS-PSP study group) have been considered. Then, they were re-classified by more recent diagnostic criteria (Höglinger *et al.,* 2017);

For my projects, I focused on these four patient cohorts: Alzheimer's dementia and MCI in Chapter 3, frontotemporal dementia cases in Chapters 5 and 6, and PSP in Chapters 7 and 8.

2.2.3. Design

Clinical, neurological and neuropsychological data were collected at the first clinical visit (baseline) and subsequently annually during a three-year follow-up period. In addition, patients and controls attended MRI and PET scans within 6 months from the first neuropsychological assessment (**Figure 2**). For PET imaging, MCI, Alzheimer's dementia, PSP and frontotemporal dementia groups had both dynamic [^{18}F]AV-1451 PET and [^{11}C]PK11195 PET, while to minimise radiation exposure to healthy people, control subjects were divided into two groups: one underwent [^{18}F]AV-1451 PET and another [^{11}C]PK11195 PET (**Table 1**). Patients with MCI also underwent [^{11}C]PiB PET to quantify the density of fibrillar ß-amyloid deposition for classification of amyloid status.

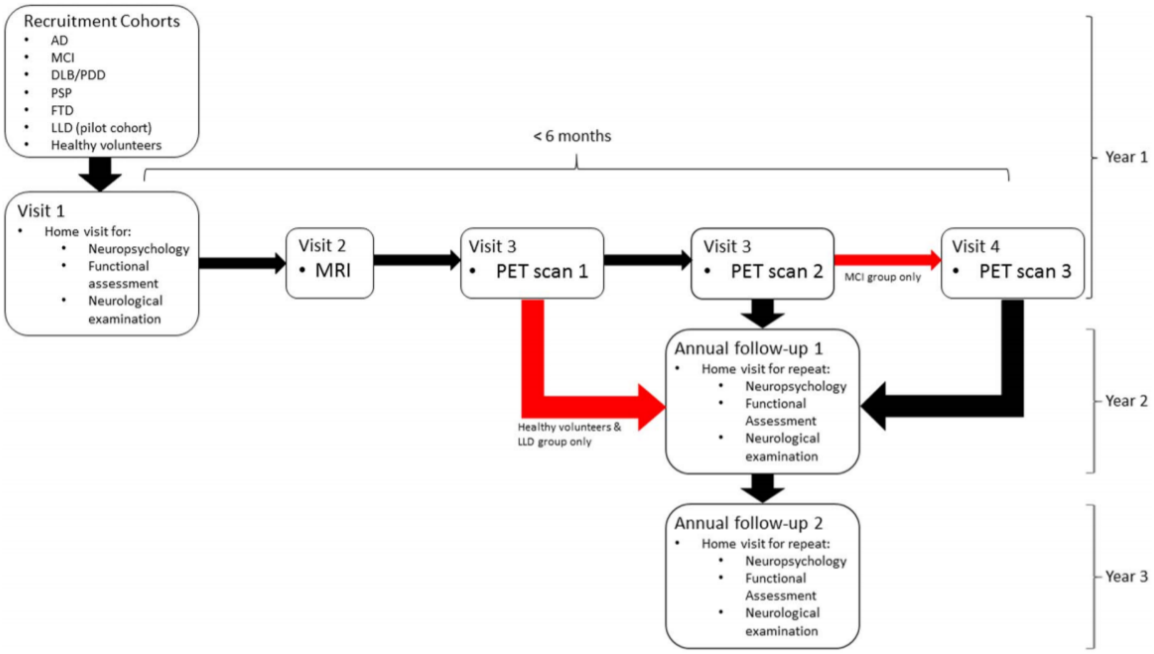

Figure 2. *NIMROD study design from Bevan-Jones et al. (2017)*

Table 1. *Neuroimaging methods applied in each group of patients with mild cognitive impairment (MCI), Alzheimer's dementia (AD), frontotemporal dementia (FTD), or progressive supranuclear palsy (PSP), and controls.*

	Controls	**MCI**	**AD**	**FTD**	**PSP**
MRI	x	x	x	x	x
[^{11}C]PiB PET	-	x	-	-	-
[^{18}F]AV-1451 PET	½ group	x	x	x	x
[^{11}C]PK11195 PET	½ group	x	x	x	x

2.2.4. Cognitive and behavioural measures

During the first visit, demographic information of all participants was collected, as well as their clinical background (i.e. neuropsychiatric features, family and medical history, medication and onset symptoms). Following this, clinical examination and cognitive, functional and neuropsychiatric assessments were the same at the baseline and during follow-up visits, including MMSE, Clinical Dementia Rating, Basic Activities of Daily Living, Cambridge Behavioural Inventory (Revised, CBI-R), the total score and sub-scores of Addenbrooke's Cognitive Examination (Revised, ACE-R), Frontal Assessment Battery (FAB), INECO frontal screening, Simple Reaction Time task, Pyramids and Palm Trees test, Rey Auditory Verbal Learning Test, Neuropsychiatric Inventory, Geriatric Depression Scale, and Hospital Anxiety and Depression Scale.

2.2.5. Neuroimaging acquisition and processing

All subjects underwent 3T MRI performed on a Siemens Magnetom Tim Trio or Verio scanner (Siemens Healthineers, Erlangen, Germany). Sequences included were structural high-resolution T1-weighted sequence, diffusion weighted imaging (DWI), T2 Fluid Attenuated Inversion Recovery (FLAIR), perfusion (arterial spin labelling) for blood flow, and resting state functional imaging. For my projects, I focused on the T1-weighted (magnetization-prepared rapid acquisition gradient-echo) MPRAGE images, acquired for each participant (repetition time = 2300 ms, echo time = 2.98 ms, field of view = 240 × 256mm^2, 176 slices of 1 mm thickness, flip angle = 9°). The T1-weighted images were segmented into grey matter, white matter and cerebrospinal fluid (CSF) with Statistical Parametric Mapping software (SPM12)

and used to determine regional grey matter, white matter and CSF volumes, and to calculate the total intracranial volume (grey matter + white matter + CSF) in each participant. Regional parcellation methods applied on T1 images to extract regional brain volumes are described in detail for each specific project-related chapter.

For PET scans, all three radioligands ([^{11}C]PiB, [^{18}F]AV-1451 and [^{11}C]PK11195) were prepared at the WBIC Radiopharmaceutical Chemistry laboratories. All three ligands were produced using the GE PETtrace cyclotron, a 16 MeV proton and 8 MeV deuteron accelerator. [^{11}C]PiB was prepared using the GE TRACER laboratory FX-C module, while [^{11}C] PK11195 using the 'Disposable' synthesis system or GE TRACER laboratory FX-C module. The production of [^{18}F]AV-1451 production was based on the synthetic methods developed by Avid Radiopharmaceuticals and modified to use the GE TracerLab FX-FN synthesiser, as reported in the protocol (Bevan-Jones *et al.*, 2017). PET scanning was undertaken on a GE Advance PET scanner (GE Healthcare, Waukesha, USA) at the Wolfson Brain Imaging Centre (WBIC) and a GE Discovery 690 PET/CT scanner at Addenbrooke's hospital. A 68Ge/68Ga transmission scan 15 minutes long was used for attenuation correction on the Advance, while a low dose computed tomography (CT) scan was used on the Discovery 690. The emission protocols were the same on both scanners. The emission protocols were: 90 minutes dynamic imaging following a 370 MBq [^{18}F]AV-1451 injection; 75 minutes of dynamic imaging starting concurrently with a 500 MBq [^{11}C]PK11195 injection; and 550 MBq [^{11}C]PiB injection followed by imaging from 40–70 min post-injection (see (Passamonti *et al.*, 2017, 2018*b*) for further details). All images were reconstructed with PROMIS 3D filtered back-projection (Kinahan and Rogers, 1989), with the Colsher filter apodised with a transaxial Hann filter cut-off at the Nyquist frequency. Corrections for dead time, randoms, normalisation, scatter, attenuation, and sensitivity were included in the image reconstruction process.

Across all NIMROD-related studies the same PET data pre-processing and regional parcellation methods were applied. For each subject, the aligned PET image series for each scan was rigidly co-registered to the T1-weighted MRI image. BP_{ND} was calculated in 83 cortical and subcortical regions of interest (ROIs) using a modified version of the Hammers atlas (www.brain-development.org), which includes brainstem parcellation and the cerebellar dentate nucleus. Prior to kinetic modelling, regional PET data were corrected for partial volume effects from cerebrospinal fluid by dividing by the mean regional grey-matter plus white-matter fraction

determined from SPM tissue probability maps smoothed to PET spatial resolution. For [^{11}C]PK11195, supervised cluster analysis was used to determine the reference tissue time-activity curve and non-displaceable binding potential (BP_{ND}) was calculated in each ROI using a simplified reference tissue model that includes correction for vascular binding (Yaqub *et al.*, 2012). For [^{18}F]AV-1451, BP_{ND} was assessed in each ROI with the simplified reference tissue model (Gunn *et al.,* 1997) using superior cerebellar cortex grey matter as the reference region.

2.3. GENFI study

2.3.1. Introduction

The GENFI study is an international multicentre project, led by Dr. Jonathan Rohrer at the University College London (London, UK), which aims to investigate longitudinal changes in pre- and post-symptomatic frontotemporal dementia and its associated disorders (including Motor Neuron Disease/Amyotrophic Lateral Sclerosis), and to identify biomarkers for early stages and progression of this disease. The GENFI cohort is composed by members of families with a known mutation in either MAPT, GRN or an expansion in C9orf72. This includes both those affected with the disorder and diagnosed with dementia, and at-risk members of families who are carrier of the same gene mutation. Non-carrier first-degree relatives are included as a control group. All participants undergo gene testing and are assessed longitudinally (annually) with a set of clinical, neuropsychiatric and cognitive assessments, MRI scans and biological analyses (i.e. blood and CSF), aiming for a 5-year follow up period.

2.3.2. Participants

Since 2012, the GENFI study has recruited over 1000 participants across 25 sites in Europe and Canada. All participants were aged over 18, gave informed consent or were recruited through a consultee process. Participants all had an identified close informant, who was willing and able to provide information, and complete questionnaires relating to their observation of the patient-participant's health and wellbeing. Participants were required to be fluent in the language of their country of assessment to be included in the study. For MRI scanning, participants with claustrophobia or contraindications related to MRI scan were excluded. Other exclusion criteria

included pregnancy, medical or psychiatric conditions that would interfere in completing assessments or impair the safety of the subject. No medications were deemed as exclusionary. Patients who were recruited in the study had (i) a clinical diagnosis within the frontotemporal dementia spectrum, fulfilling the consensus criteria for behavioural (Rascovsky *et al.*, 2011) or language (Gorno-Tempini *et al.*, 2011) variants or frontotemporal dementia associated with motor neuron disease (FTD-MND); and (ii) a positive genetic test for a mutation in MAPT, GRN, C9orf72 or other autosomal dominant cause of frontotemporal dementia, like TBK-1. Within patients' families, first-degree asymptomatic members were recruited as part the study either with or without a frontotemporal dementia related mutation. Relatives willing to participate in the study were not required to know their genetic status in order to take part. They underwent gene testing during the first research visit without discovering their genetic status as a result of taking part. As expected for first degree relatives, about half of these asymptomatic participants carry a gene mutation, and half not. Clinically unaffected relatives with the same dominant genetic mutation as their parent or sibling were classified as "pre-symptomatic mutation carriers", while asymptomatic relatives without frontotemporal dementia related gene mutations were classified as "non-carriers", and considered in the analyses as control group (**Figure 3**).

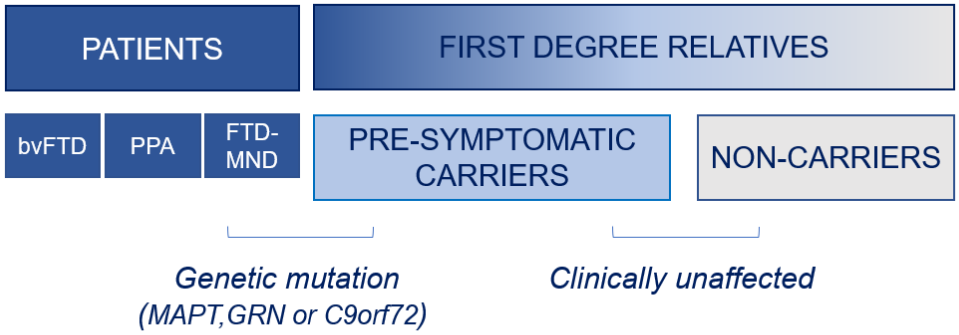

Figure 3. *Classification and general characteristics of participants recruited in the GENFI study.*

GENFI DataFreeze 4 was released in 2019, reporting 830 participants (176 affected carriers/patients, 329 pre-symptomatic mutation carriers, and 324 non-carriers) for a total of 1737 visits. For my project described in Chapter 4, I focused on apathy in pre-symptomatic mutation carriers, and 600 participants (304 pre-symptomatic mutation carriers, and 296 family members without mutations) were included accordingly in my analyses, excluding 53 cases without apathy scores in the first three visits.

2.3.3. Design

Written informed consent was obtained by each participant prior to any study-related procedure, according to local ethics approval obtained prior to beginning of the study. All participants underwent a baseline research visit which included the collection of demographic data, family and structured subject history, structured neurological examination, a functional and neuropsychiatric assessment, a neuropsychology assessment, an MRI scan, and bio-sample collection. According to protocol, all participants recruited were going to be annually followed-up, repeating all assessments carried out at baseline, i.e. the first visit. Each visit could take place across multiple days but all study measures for that time point (baseline or follow-up) needed to be completed within a 12-week window. Although a blood sample was collected for each visit, during the first visit only DNA was extracted for each asymptomatic participant, to determine whether they were pre-symptomatic carrier or non-carriers. Genetic results for at-risk subjects that were performed as part of the GENFI study were not released to the subject or to the clinicians involved in assessing the subjects.

2.3.4. Cognitive and behavioural measures

The current GENFI clinical assessment consists of a standardised history and examination, and includes scales measuring behaviour and function changes, such as the revised CBI-R, Frontotemporal dementia Rating Scale and Clinical Dementia Rating. A GENFI neuropsychological battery has been translated into each centre's language and consists of tests of executive function, working memory and attention, social cognition, naming and semantic knowledge, as well as tests of visuospatial skills and memory. The neuropsychological battery adopted since 2012 consists of the following tests: WMS-R Digit Span Forwards and Backwards, Trail Making Test A and B, Verbal Fluency – Category (animals), Verbal Fluency – Letter, Boston Naming Test (modified version: 30 items), Wechsler Adult Intelligence Scale–Revised (WAIS-R) Digit Symbol, WASI Block Design. In 2015, five new tests were added to the battery: Benson Figure Copy and Recall, Camel and Cactus Test (modified version), Free and Cued Selective Reminding Test (including Delayed Recall), D-KEFS Color-Word Interference Test and Mini-Social Cognition and Emotion Assessment.

For my project reported in Chapter 4, I focused on two specific tests: the Apathy subscale of the CBI-R (Wear *et al.*, 2008), as an index of apathy severity, and the WAIS-R Digit Symbol substitution task, which has been proven a sensitive marker for executive function related problems (Jaeger, 2018).

2.3.5. Neuroimaging acquisition and processing

All participants underwent standard MRI pre-screening according to local protocol and an MRI scan on a 3T MRI scanner (or 1.5T scanner where 3T scanning was not available) using the harmonized GENFI scan sequences. The GENFI 3T MR protocol (for Siemens, Philips and GE scanners) consists of volumetric T1, volumetric T2, resting state fMRI, diffusion tensor imaging and arterial spin labelling. The GENFI Trials Team handled the image quality control and inspection, and all cross-sectional images were reviewed within ten working days from receipt to identify any problems and indicate when it was necessary to re-run scan.

For my project reported in Chapter 4, I considered only T1-weighted MPRAGE images which were acquired at each site accommodating different manufacturers and field strengths. Grey-matter regional volumes were extracted from the subcortical segmentation and cortical parcellation labelled by the Desikan-Killiany Atlas (Desikan *et al.*, 2006) in Freesurfer 6.0 (http://surfer.nmr.mgh.harvard.edu/). Briefly, this process involves automated non-uniformity bias correction, removal of non-brain tissue (skull stripping), automated Talairach transformation, segmentation of the white matter and grey matter of subcortical structures, intensity normalization, identification of the boundary between the white and cortical grey matter. With the complete cortical model, the cortical parcellation can be applied to divide the cerebral cortex into units/ROIs. For cases with more than one scan, all available follow-up images were included in the processing with the longitudinal stream in Freesurfer, creating an unbiased within-subject template for case-specific segmentation (Reuter *et al.*, 2012). Notably, considering the multi-site and longitudinal nature of the GENFI project, Freesurfer morphometric procedures are particularly useful given that they have shown good test-retest reliability across scanner manufacturers and field strengths (Jovicich *et al.*, 2006; Reuter *et al.*, 2012). Raw and segmented data were visually inspected, and images with significant artefacts, or parcellation failure were excluded.

2.4. Longitudinal models

No single statistical procedure exists for longitudinal data analysis. Choosing which model and methodology is the most appropriate for a specific project depends on several factors, including which research questions we want to answer, and the project-specific data structure. Two traditional methods to study longitudinal changes that have been widely used are repeated-measures analysis of variance (rmANOVA) and multiple regression. However, these methods have several limitations for dealing with longitudinal data, and in their classic forms are able to analyse only mean-group changes over time, considering individual differences as error variance rather than a parameter of interest. While it is therefore possible to study homogeneous populations and inter-group variability with such methods, they are unsuitable to explore inter- and intra-individual differences at the same time and assess the heterogeneity of longitudinal trajectories in different subjects.

For my thesis, the most appropriate longitudinal model would be one able to capture not only the group statistics over time, but also to describe individual trajectories, and how those are governed by individual differences in key variables of interest. Another key aspect required by the nature of my research questions is the possibility to study predictors of individual differences, to investigate which factors and variables have an important impact on, or a predictive value for, the rate of change with time. Statistical models that are able to cover all these issues are referred to as "subject-specific models" (McNeish and Matta, 2018) and are more widely known as "growth curve models". These can be divided into two main families: the latent growth curve models (LGCMs) and the mixed-effects models (MEMs). The first class of models treats the repeated measures/visits as multivariate (wide data format) and is fitted within structural equation modelling (SEM) context and software. In contrast, the MEM approach considers the repeated measures as univariate (long data format) and is fitted with regression methods (McNeish and Matta, 2018). In practice, they share many strengths, and for many use cases yield similar or identical results. However, the choice of which modelling approach to apply is not only personal preference, but also led by crucial differences associated with model estimation and specification. As a result, LGCM is most useful for complex models with more than one dependent variable and one regressor, complex variance functions, multigroup model estimation with partial constraints, to assess global model fit, and to deal with random missing data. In contrast, MEM results to be more suited than LGCM for time

unstructured data and smaller sample sizes (McNeish and Matta, 2018). In the following sections I will briefly describe both.

2.4.1. Latent Growth Curve Model (LGCM)

The LGCM is carried out using SEM methodology. SEM allows researchers to test the global or local fit of a hypothesized model of change, to specify fixed and time-varying covariates/predictors, to extract a common trajectory from the data, or to define the estimation by groups, and to study the trajectories on several constructs simultaneously, and these constructs' relationship. The LGCM estimation commonly consists of two main phases: (i) a linear or curvilinear regression is fit across the repeated measures of each subject, and a growth curve shape which describes the change over time is identified; then, if so desired, (ii) the potential predictors of individual differences in intercepts/slopes are evaluated. In this way the growth model, as a collection of individual trajectories, is able to describe the individual differences in the changes over time – but also to report a growth curve at group level (Duncan and Duncan, 2009).

Across all subjects, the LGCM estimates (i) an intercept, which represents the initial level of the outcome measures; (ii) a slope, quantifying the rate of change and its shape (i.e. linear or nonlinear); (iii) a variance of the intercept and slope, capturing individual differences in baseline and change over time and (iv) the relation between intercept and slope, hence how the initial level influences the rate of change over time. For both intercept and slope, the model estimates a mean across all subjects in the sample and the variance between individuals. The parameters provide insight into average change (means) and individual difference surrounding that change (variances). In addition, the LGCM approach permits to extract an estimated value of both intercept and slope for each subject included in the analysis. As reported in **Figure 4**, the estimated coefficients can be visualised and interpreted plotting the repeated measures for the variable of interest (Y) across multiple time points. Here, the bold thick line represents the estimated change over time at group level, while the thin lines plot the longitudinal change in Y for each case (**Figure 4A**). For the standard parametrization of linear time (with loadings fixed at 0, 1, 2, etc.), the slope represents the rate of change in Y for a time unit, for example in this case from 1 to 2, from 2 to 3 etc, while the estimated intercept (indicated by the thick dot) is the initial mean value across all cases. The intercept and slope variances estimate the degree of individual differences around these group averages. The positivity or negativity of slope

estimated values influence the interpretation of the intercept-slope covariance term. The relationship between intercept and slope, if significant, can result in either a negative (**Figure 4A**) or a positive covariance term (**Figure 4B**). For example, in the former case, if the slope is positively defined, subjects with higher initial values show a slower annual rate of increase in Y, while those with low initial scores are characterised by a steeper increase in Y over time. In contrast, if the intercept-slope covariance term is negative and the slope is positively defined, subjects with higher initial values show a faster annual rate of increase in Y, while those with lowest initial scores show a less steep increase in Y over time. Graphs C and D in **Figure 4** represent how the data appear in case the variance term for either the intercept or the slope is not significant.

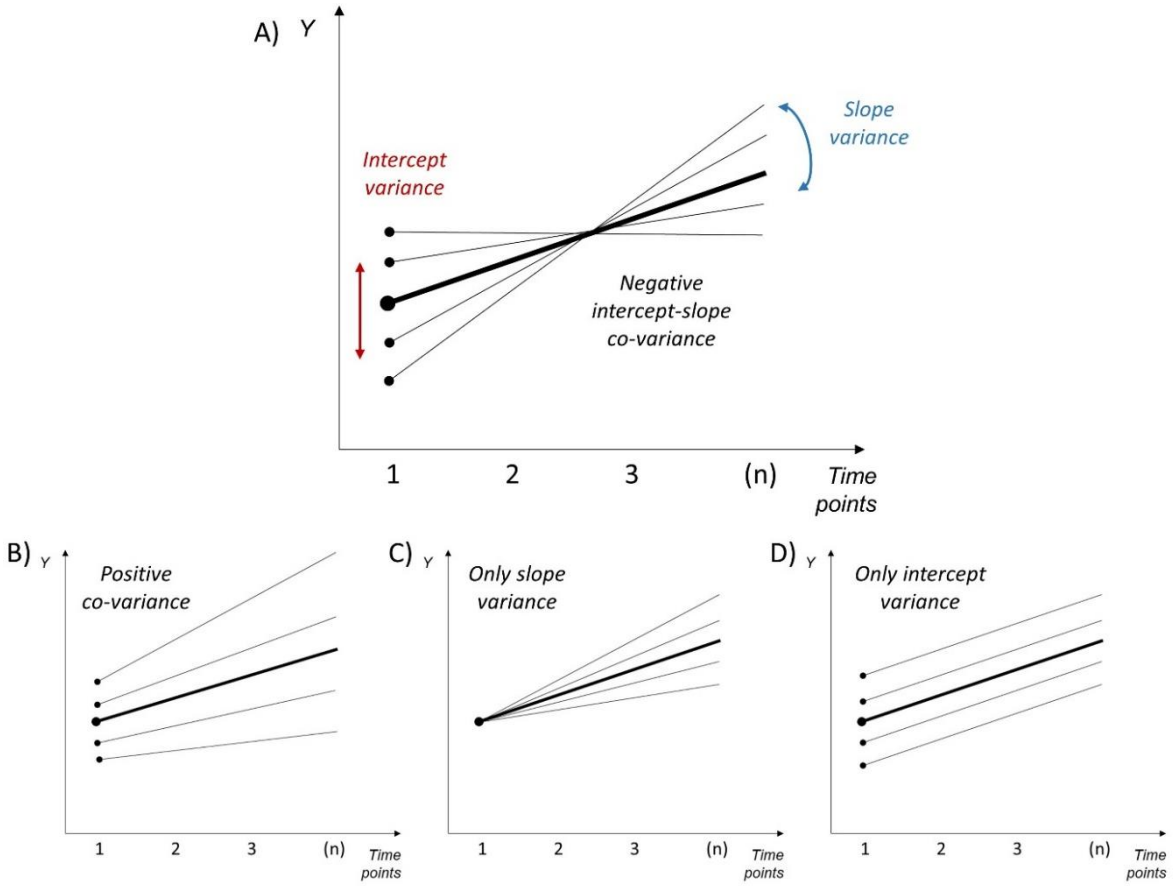

Figure 4. *Representation of four possible scenarios that can be identified by LGCM on variable Y measured over time (x axis): (A) positive average slope with significant between-subject variance, and negative covariance between intercept and slope; (B) positive average slope with significant between-subject variance, and positive covariance between intercept and slope; (C) positive average slope with significant between-subject variance, but non-significant intercept variance; (D) positive average slope but non-significant variance.*

In **Figure 5** a graphical representation with basic path model notation for a standard univariate linear LGCM to test the initial values (intercept – "i") and longitudinal changes (slope – "s") for an observed variable (Y) at multiple and equidistant time points (Y1, Y2, Y3…Yn) is reported. Circles indicate latent variables, rectangles indicate the observed measures, and triangles denote intercepts (1= population means on the parameters). Single-headed arrows indicate directed relationship and factor loadings, in red for intercept and in blue for slope, while undirected relationship (i.e. variances and covariances) are indicated by double-headed arrows. The factor loadings for intercept are represented by a series of 1 for each observed measure (i=~1*Y1+1*Y2+1*Y3…+1*Yn), while "0, 1, 2, 3, ….n-1" is a commonly used coding scheme to indicate factor loadings for a linear slope (s=~0*Y1+1*Y2+2*Y3…+(n-1)*Yn).

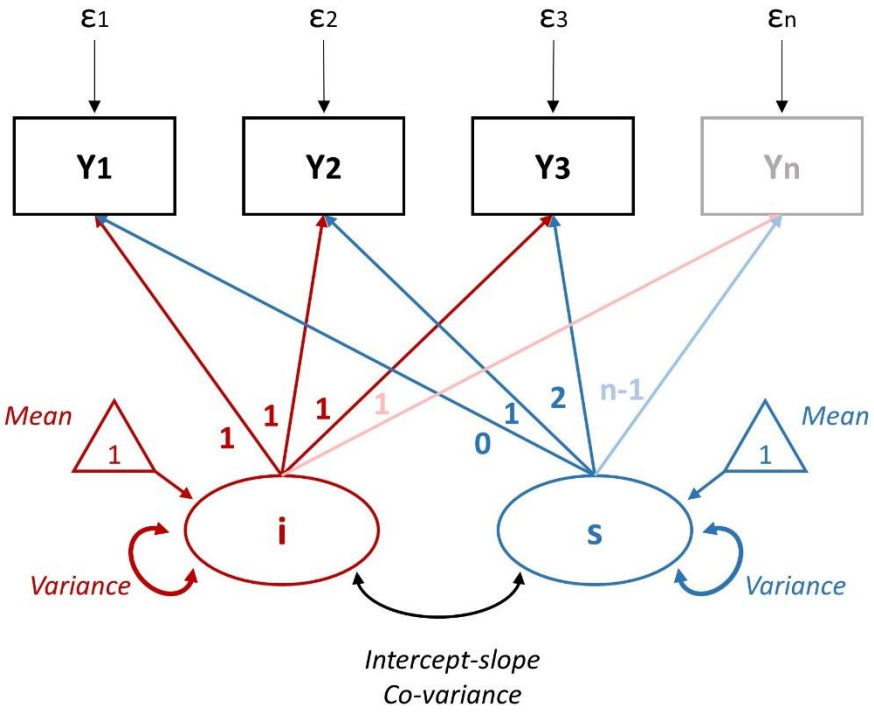

Figure 5. *Graphical representation of a standard univariate linear latent growth curve model and the estimated parameters.*

Predictors can be added to the model to assess their associations with intercept and/or slope. In multi-group LGCM, the model parameters can be allowed to vary or be set to be equal across all groups. Comparing the former case with the latter, constraining one or more parameter(s) at

a time, shows whether there is evidence for group differences on a given parameter or set of parameters.

To specify and fit a standard model, LGCM guidelines recommend a number of minimum requirements (Curran *et al.*, 2010; Newsom, 2015). First, at least three or more time points/repeated measures are needed to avoid empirical under-identification problems. This requirement refers to the overall design, indeed, a growth model can be fit with partially missing data (i.e., some subjects can have just one or two observations, while others three or more). Second, growth models typically require a minimum of 5 cases per parameter estimated, but also the total number of person-by-time observations is important for model convergence and estimation. Third, to apply the typical estimation method, called maximum likelihood estimation method (ML), continuous and multivariately normally distributed repeated measures are needed. However, there are alternative estimation methods that deal with continuous measures that are non-normally distributed, like the robust maximum likelihood (MLR). Overall, for my projects LGCM were estimated in the Lavaan software (Rosseel, 2012), the R package, using full information maximum likelihood with robust standard errors for missingness and non-normality. More details on project-specific model specifications are reported in Chapter 3 and 4.

As part of SEM, for LGCM it is possible to evaluate the overall model fit estimation through two classes of statistics: absolute model fit and relative model fit assessment measures. The absolute model fit measures are used to determine the disparity between the generated model given the available data, so how well the *a priori* model reflects the sample data; while the relative model fit measures are generated comparing the implied model with alternative or simpler models. This assessment is processed automatically in the Lavaan software, which returns the estimation of several fit indices for the specified model. Between these indices, it is advisable to consider more than one value to evaluate the model fit. For each model specified in my thesis, I reported the chi-square test (χ^2), which indexes deviation from the perfect model fit, an index which is sensitive to the sample size and tends to reject models applied in large cohorts (good fit: low values and $p > 0.05$) (Schermelleh-Engel *et al.*, 2003). For large sample size, like in the GENFI project (Chapter 4) I also report the ratio between chi-square and degrees of freedom (χ^2/df) as an alternative model fit index (acceptable fit: < 2, good fit: < 3) (Schermelleh-Engel et al., 2003). Then, I also considered two other main absolute model fit

indices: (1) the root-mean-square error of approximation (RMSEA, acceptable fit: < 0.08, good fit: < 0.05), which is a parsimony-adjusted index, and (2) the standardized root mean-square residual (SRMR, acceptable fit: 0.05–0.10, good fit: < 0.05), which measures the deviation between the implied and observed covariance matrices. A relative (or incremental) fit index was also considered: the comparative fit index (CFI, acceptable fit: 0.95–0.97, good fit: > 0.97), which compares the given model with a saturated baseline model (Schermelleh-Engel *et al.*, 2003). In addition, I also evaluated relative model assessments which measure the specific improvement in model fit between alternative models with and without covariates; or with and without grouping variables. This was mainly assessed by likelihood-ratio tests and $\chi 2$-difference tests.

2.4.2. Mixed-effects model

Similarly to LGCM, the MEM estimates a trajectory of a given observed variable over time, at group and individual levels. This approach estimates a mean trajectory across the population, accounting for the fact that different subjects undergo repeated measures over time. The term "mixed effects" refers to a model that includes both fixed- and random-effects in a predictive model. The mean intercept and slope parameters estimated across the entire sample are defined as "fixed effects". Generally, the fixed effects in a longitudinal model are the intercept, the predictor of interest (i.e. time) and any covariates. In contrast, to estimate the individual deviations from the population trajectory, the intercept and slope variance parameters are defined as "random effects" in the model. The random effects represent the individual-specific deviation from the group-estimated mean.

There are several software programs available to implement the MEM approach. For my thesis I fitted all models with the lme4 package (Bates et al., 2015) for R (R Core Team 2015). The implementation of a standard univariate linear MEM to estimate the changes in a dependent variable (Y) across repeated measures over multiple time points (time) starts from a null model (i), where only fixed effect on intercept (~ 1) and the error term are defined:

(i) $Y \sim 1 + \varepsilon$

The second step (ii) is including a fixed effect of the time variable (~ time) on the dependent variable (Y) to estimate a global slope across all subjects, which represent the average change in the dependent variable for unit of time across all repeated measures:

(ii) $Y \sim time + \varepsilon$

The third step (iii) is including the between-subject variations in the intercept estimation, including a random effect on individual intercept estimation (1|subjects), in addition to the global intercept (~ 1) and slope estimation (~ time):

(iii) $Y \sim time + (1|subjects) + \varepsilon$

Finally, to include the between-subject variations in the slope estimation (iv), we can include a random effect of the time on the individual slope estimation (time|subjects) in addition to the estimation of an average slope across the sample (~ time):

(iv) $Y \sim time + (time|subjects) + \varepsilon$

To this standard LMEM with fixed and random effects for both intercept and slope estimation, it is then possible to add covariates (v) as fixed effect terms:

(v) $Y \sim time + covariate + (time|subjects) + \varepsilon$

In summary, a random intercept model (iii) accounts for baseline-differences between subjects for a given dependent variable, but it assumes that the effect of time on the dependent variable is the same for all cases. In contrast, a random slope model (iv) accounts not only for subjects' differences in initial values but also for between-subject variations in the effect of time, estimating subject-specific slopes of the dependent variable.

In R software, there are two main methods to obtain a significance level for the specified models and estimated effects. First, for each model specified it is possible to get degree of freedom and p-value approximations using the lmerTest package, which gives an estimation for each effect specified. The second method permits to test whether each estimated parameter is significant,

comparing models with and without a specific specified term, using likelihood ratio tests (anova() function on fitted models). In other words, the comparison between two nested models defines whether adding a specific parameter to the simplest model significantly improves the model fit, and if the parameter estimation should be included in the model specification. When two models that differ for a fixed effect term are compared the maximum likelihood estimation should be used. In contrast, if the compared models differ in their random effects, the restricted maximum likelihood estimation is preferable (Bolker *et al.*, 2008; Harrison *et al.*, 2018).

2.5. Power calculation

I aimed to be sufficiently powered to detect moderate/strong associations between *in vivo* imaging markers, clinical severity or cognitive decline. With N=24, α =.05 (two-tailed), one has 80% power to detect a true correlation of ρ=0.54, as calculated with "pwr" R package. This is satisfied by analyses on GENFI data (Chapter 4) and partially by correlation analyses on NIMROD data for Alzheimer's disease and frontotemporal dementia cohorts (Chapter 3 and 6). An extensive literature on imaging suggests that groups sizes of 16-24 are often sufficient to detect changes associated with dementia in imaging studies, such as atrophy on MRI and increased binding on amyloid/tau PET imaging. For all cohorts and especially for the smaller sample sizes due to the rarity of conditions, such as genetic frontotemporal dementia and PSP, I limited the analyses to those that were feasible with strong hypothesis *a priori* and I corrected the results for multiple comparisons.

2.6. Conclusions

Similarities and differences between the two dementia-specific datasets used in my thesis, from the NIMROD study and the GENFI initiative, enable the investigation of the several objectives of my thesis, reported in Chapter 1. Specifically, the NIMROD dataset enables us to investigate the prognostic value of multimodal imaging data to determine the relative contributions of [^{11}C]PK11195 and [^{18}F]AV-1451 PET, as well as structural MRI in predicting decline in patients with Alzheimer's disease, frontotemporal dementia or PSP. On the other hand, GENFI data allows us to test the predictive value of structural MRI markers of atrophy on behavioural and cognitive changes in the pre-symptomatic phase of frontotemporal dementia.

The following experimental chapters focused on longitudinal NIMROD and GENFI cohorts to investigate clinical and cognitive changes over time in patients with several neurodegenerative diseases; and how these changes are predictable from baseline imaging and behavioural markers. The LGCM approach has been considered the gold standard in all my projects with time structured data (i.e. equidistant follow-up visits). When fitting all requirements was not possible for the nature of our data or the models did not converge, the MEM method was adopted. Specifically, to study cognitive decline and/or clinical progression over time in NIMROD cohorts of patients with frontotemporal dementia (Chapter 6) and PSP (Chapter 8), I applied the MEM method because of the limited sample size and large individual variance in time intervals between longitudinal visits.

Chapter 3 | Prognostic markers of cognitive decline in Alzheimer's disease

Preface: The contents of this chapter has been published in Malpetti et al. Microglial activation and tau burden predict cognitive decline in Alzheimer's disease. *Brain* 2020; 143: 1588–1602 - doi: 10.1093/brain/awaa088

A team of researchers and clinicians at the University of Cambridge have contributed to data collection. I performed all data analyses and drafted the text, with textual revision input from all co-authors. Simon Jones, Dr. Tim Fryer and Dr. Young Hong helped with MRI and PET pre-processing, Prof. Rogier Kievit and Dr. Kamen Tsvetanov with advice for the statistical methods.

Abstract: Tau pathology, neuroinflammation, and neurodegeneration are key aspects of Alzheimer's disease. In this chapter, I investigate how *baseline* assessments of *in vivo* tau pathology (measured by [^{18}F]AV-1451 PET), neuroinflammation (indexed via [^{11}C]PK11195 PET) and brain atrophy (derived from structural MRI) predicted *longitudinal* cognitive changes in patients with Alzheimer's dementia and amyloid positive MCI. I show that temporo-parietal tau pathology and anterior temporal neuroinflammation predict cognitive decline Alzheimer's disease spectrum. However, the MRI-derived atrophy component and demographic variables were excluded from the optimal predictive model of cognitive decline over 3 years of follow-up. This indicates the added prognostic value of PET biomarkers in symptomatic patients with Alzheimer's disease, over and above MRI measures of brain atrophy and demographic data. These findings also support the strategy for targeting tau and neuroinflammation in disease-modifying therapy against Alzheimer's disease.

3.1. Introduction

The pathological hallmarks of Alzheimer's disease are tau neurofibrillary tangles and amyloid-β plaques, but neuroinflammation has also emerged as a key process in Alzheimer's disease and other neurodegenerative disorders (Pasqualetti *et al.,* 2015; Ransohoff, 2016; Schain and Kreisl, 2017). The differential role of these pathologies in predicting clinical progression of Alzheimer's disease remains to be ascertained. This represents a critical step to develop new prognostic markers and test the effect of novel disease modifying therapies that target different pathologies in Alzheimer's disease. The aggregation of misfolded tau protein is associated with synaptic dysfunction and neuronal loss, and correlates with clinical severity in the Alzheimer's disease clinical spectrum (Nelson *et al.,* 2012; Spires-Jones and Hyman, 2014). A significant presence of amyloid-β plaques is also indicative of likely cognitive decline in mid- and later-life, although the association of both neurodegeneration and cognitive impairment has been found stronger with the distribution and burden of neurofibrillary tangles than it is for neuritic plaques (Nelson *et al.,* 2012; Spires-Jones and Hyman, 2014). Microglial activation and neuroinflammation represent a third key determinant in the etiopathogenesis of Alzheimer's disease and in its progression (Heneka *et al.,* 2015; Mhatre *et al.,* 2015; Calsolaro and Edison, 2016), independently or synergistically with tau and amyloid pathology.

Each of these processes can now be quantified and localised *in vivo* using brain imaging, such as PET imaging with radioligands targeting tau pathology, amyloid burden, and microglial activation (see Chandra *et al.,* 2019 for a review). The PET ligand [^{18}F]AV-1451 is sensitive to cortical tau accumulation in Alzheimer's disease, and has high affinity for the characteristic paired helical tau filaments (Xia *et al.,* 2013*a*; Marquié *et al.,* 2015; Lowe *et al.,* 2016). [^{18}F]AV-1451 PET studies have shown marked tau accumulation in the entorhinal cortex in patients with MCI which extends to temporo-parietal regions in Alzheimer's disease (Hall *et al.,* 2017). [^{18}F]AV-1451 bindings also correlates with Braak staging of neurofibrillary tau (Schöll *et al.,* 2016; Schwarz *et al.,* 2016), and *post mortem* patterns of Alzheimer's disease pathology (Sander *et al.,* 2016, Smith *et al.,* 2019*b*; Lowe *et al.,* 2020; Soleimani-Meigooni *et al.,* 2020). This is also in keeping with evidence that tau deposition is evident as a continuum from normal aging through MCI to Alzheimer's dementia (Schöll *et al.,* 2018), and correlates with cognitive impairment (Brier *et al.,* 2016, Cho *et al.,* 2016*b*; Johnson *et al.,* 2016; Ossenkoppele *et al.,* 2016; Pontecorvo *et al.,* 2017). In addition, PET imaging supported the

previous evidence on a stronger association of cognitive deficits with tau burden than with amyloid-β (Brier *et al.,* 2016; Johnson *et al.,* 2016).

The PET ligand [^{11}C]PK11195 is a well-established marker for microglial activation via its binding to the 18-kDa translocator protein (TSPO), a mitochondrial membrane protein which is overexpressed in activated microglia (Scarf and Kassiou, 2011). Results with this ligand in Alzheimer's disease have been variable (see (Chandra *et al.,* 2019) for a review), but this may due to small sample sizes and inconsistent methods between previous *in vivo* studies. [^{11}C]PK11195 has shown high binding in temporo-parietal regions and cingulate cortex in patients with Alzheimer's disease (Stefaniak and O'Brien, 2015), while neuroinflammation in these regions is inversely associated with cognitive performance in MCI and Alzheimer's dementia (Edison *et al.,* 2008, Fan *et al.,* 2015*a,* Passamonti *et al.,* 2018*b,* 2019). However, inflammation does not correlate well with amyloid burden (Yokokura *et al.,* 2011), suggesting an independent role of microglial activation in leading to cognitive deficits.

There are extensive data on atrophy in Alzheimer's disease, measured in terms of volume loss *in vivo* by MRI, at MCI and dementia stages of progressive Alzheimer's disease pathology. MRI measures, for example of medial temporal lobe volumes, correlates with disease severity, and are predictive of future conversion from MCI to Alzheimer's disease (Frisoni *et al.,* 2010; Leung *et al.,* 2013; Jack *et al.,* 2015). However, cell loss and atrophy are relatively late features in a cascade of pathology, and it is not clear how MRI compares with measures of molecular pathology as a prognostic marker, especially in view of marked age-related structural changes (Raz *et al.,* 2005; Walhovd *et al.,* 2011).

In this study, I test the ability of baseline *in vivo* measures of tau pathology, microglial activation, and brain atrophy to predict the rate of cognitive decline in patients with Alzheimer's disease pathology, ranging from MCI (with biomarker evidence of amyloid pathology) to clinically probable Alzheimer's disease (with dementia). The main hypothesis was that the PET biomarkers of tau pathology and neuroinflammation are strong predictors of cognitive impairment and decline, and that whereas MRI may be predictive in isolation, the prognostic information of MRI is better captured by direct PET measures of molecular pathology (Bejanin *et al.,* 2017; Mattsson *et al.,* 2019). This hypothesis builds on the evidence that tau burden relates to age-related cognitive decline (Schöll *et al.,* 2016; Aschenbrenner *et al.,* 2018; Maass

et al., 2018), and progression of dementia over 6 to 18 months in patients with Alzheimer's disease (Koychev *et al.,* 2017; Pontecorvo *et al.,* 2019). In contrast to past studies that have assessed the relationship between longitudinal PET markers and clinical changes in Alzheimer's disease (Fan *et al.,* 2015*b*, 2017; Chiotis *et al.,* 2018; Jack *et al.,* 2018; Southekal *et al.,* 2018, Cho *et al.,* 2019*a*), I study how a multi-modal and cross-sectional assessment of distinct pathologies is able to predict longitudinal decline in Alzheimer's disease, examining the individual or combined prognostic contribution of tau pathology, neuroinflammation, and brain atrophy in predicting cognitive decline.

The better characterisation of the factors predicting decline in Alzheimer's disease will help to develop enhanced prognostic and outcome measures for clinical trials targeting more than one pathology. Although previous findings support the use of MRI and PET imaging in the diagnosis and monitoring of disease progression, the prognostic value of these *in vivo* measures and their combined effect in predicting clinical decline in Alzheimer's disease remains undetermined. Previous studies which have evaluated the predictive values of neuroimaging markers in Alzheimer's disease have typically assessed different neuroimaging modalities in isolation rather than exploiting the mechanistic and prognostic values that is offered by multi-modal neuroimaging. I therefore assessed the independent and combined predictive effects of baseline neuroimaging biomarkers for tau pathology ([^{18}F]AV-1451 PET), neuroinflammation ([^{11}C]PK11195 PET) and brain atrophy (structural MRI) on longitudinal cognitive changes over a period of three years in the clinical spectrum of Alzheimer's disease. Given the published evidence of dominant involvement of temporal and parietal brain regions in early neurodegeneration, tau pathology, and neuroinflammation in Alzheimer's disease (Garibotto *et al.,* 2017; Jagust, 2018; Whitwell, 2018), I decided *a priori* to focus our analyses on these regions. Pathology may occur in frontal and occipital regions, but for typical amnestic phenotypes, I considered this to be of secondary importance. In the temporo- parietal regions there is a hierarchical evolution in tau pathology and atrophy from MCI to Alzheimer's dementia, recapitulating neuropathological staging and correlating with clinical severity (see review Jagust, 2018).

I predicted: 1) a significant association between baseline measures of each neuroimaging technique and longitudinal decline in cognition; 2) partially independent and additive effects of MRI and PET measures on cognitive decline, assessed with all modalities together in a single

multivariate model. Moreover, I predicted that the molecular markers of baseline tau and neuroinflammation PET would be more informative than structural MRI on longitudinal cognitive deterioration in Alzheimer's disease.

3.2. Methods

3.2.1. Participants

Twenty-six patients were recruited: twelve with a clinical diagnosis of probable Alzheimer's dementia and 14 with amnestic MCI and a positive amyloid PET scan as biomarker of Alzheimer's disease (Klunk *et al.,* 2004). Probable Alzheimer's dementia was diagnosed according to the National Institute on Aging-Alzheimer's Association guidelines (McKhann *et al.,* 2011) and confirmed in all patients during follow-up. Given the long-term and intensive nature of the longitudinal project, all patients at baseline had >12/30 on the MMSE to be eligible to the study. MCI patients had MMSE score > 24/30, and memory impairment not ascribable another diagnosis (Albert *et al.,* 2011). I also included 29 healthy controls with MMSE >26/30, absence of memory symptoms, no signs of dementia, or any other significant medical illnesses.

During the first visit, demographic information and medical history were collected. All participants underwent a baseline neuropsychological assessment, followed by an MRI scan and one, two or three PET scans depending on the group. The clinical examination and neuropsychological battery were repeated annually for three follow-up visits (see (Bevan-Jones *et al.*, 2017) for details). The revised Addenbrooke's Cognitive Examination (ACE-R) (Mioshi *et al.*, 2006) was used to assess the cognitive performance at each visit. All patients diagnosed with Alzheimer's dementia deteriorated significantly in the follow-up clinical visits compared to the study baseline. Six out of the 14 patients with MCI were clinically diagnosed as converting to Alzheimer's disease and/or presented MMSE ≤ 24/30 by the end of the study (3 years), and three further patients subsequently.

All participants gave informed consent according to the Declaration of Helsinki. The NIMROD protocol (Bevan-Jones *et al.*, 2017) was approved by the NIHR National Research Ethic Service Committee and East of England (Cambridge Central).

3.2.2. Imaging data acquisition and pre-processing

All subjects underwent 3T MRI performed on a Siemens Magnetom Tim Trio or Verio scanner (Siemens Healthineers, Erlangen, Germany). A T1-weighted MPRAGE image was acquired for each participant (repetition time = 2300 ms, echo time = 2.98 ms, field of view = 240 × 256mm^2, 176 slices of 1 mm thickness, flip angle = 9°). MCI and Alzheimer's dementia subjects had both dynamic [^{18}F]AV-1451 PET and [^{11}C]PK11195 PET, while, to minimise radiation exposure to healthy people, control subjects were divided into two groups: 14 underwent [^{18}F]AV-1451 PET, while another 15 underwent [^{11}C]PK11195 PET. PET scanning was undertaken on a GE Advance PET scanner (GE Healthcare, Waukesha, USA) and a GE Discovery 690 PET/CT (see Supplementary Table 1 for details). Patients with MCI also underwent 40-70 minutes post-injection [^{11}C]PiB PET to quantify the density of fibrillar Aβ deposits for classification of Aβ status. The emission protocols were: 90 minutes dynamic imaging following a 370 MBq [^{18}F]AV-1451 injection; 75 minutes of dynamic imaging starting concurrently with a 500 MBq [^{11}C]PK11195 injection; and 550 MBq [^{11}C]PiB injection followed by imaging from 40–70 min post-injection (see (Passamonti *et al.*, 2017, 2018*b*) for further details). All images were reconstructed with PROMIS 3D filtered back-projection (Kinahan and Rogers, 1989), with the Colsher filter apodised with a transaxial Hann filter cut-off at the Nyquist frequency. Corrections for dead time, randoms, normalisation, scatter, attenuation, and sensitivity were included in the image reconstruction process. [^{11}C]PiB scans were classified as positive if the average standardized uptake value ratio (SUVR) across the cortex using a cerebellar grey matter reference region was > 1.5 (Villemagne *et al.*, 2013). This threshold was chosen to minimize false positives (see Jack *et al.*, 2008; Villemagne *et al.*, 2011). Only MCI with positive Aβ status was included in this study, and combined with patients with Alzheimer's dementia on the basis that these two groups represent a continuum of the same clinical and pathological spectrum (Okello *et al.*, 2009*b*).

Structural imaging data were processed in SPM12. The T1-weighted images were segmented into grey matter, white matter and cerebrospinal fluid (CSF) and used to determine regional grey matter, white matter and CSF volumes, and to calculate brain volume (grey + white matter) and total intracranial volume (grey matter + white matter + CSF) in each participant. The grey and white matter segments from 33 subjects were used to create an unbiased template (11 controls, 11 patients with mild cognitive impairment and 11 patients with Alzheimer's dementia, matched for age and sex across the groups) using the DARTEL pipeline in SPM12.

The images from the remaining 22 participants were warped to the template to bring all participants into the same space. Segmented images were then warped to MNI space. The images were matched to the Hammers atlas [(Hammers *et al.*, 2003; Gousias *et al.*, 2008), modified to include brainstem parcellation and the cerebellar dentate nucleus in MNI152 2009c space] to perform a region of interest (ROI) analysis. The atlas comprised 83 cortical regions. The group template was warped to the ICBM MNI152 2009c template using 'Population to ICBM' function, applied to the Hammers atlas in DARTEL template space, followed by linear transformation to MNI space. These steps place the regions of interest in the same space as the individual normalised MRI images. Individual regional grey matter volumes were then extracted using the 'spm_summarise` function.

For each subject, the aligned PET image series for each scan was rigidly co-registered to the T1-weighted MRI image. Prior to kinetic modelling regional PET data were corrected for CSF contamination by dividing by the mean region grey plus white matter fraction determined from SPM tissue probability maps smoothed to PET spatial resolution. For [^{11}C]PK11195, supervised cluster analysis was used to determine the reference tissue time-activity curve and non-displaceable binding potential (BP_{ND}) was calculated in each ROI using a simplified reference tissue model that includes correction for vascular binding (Yaqub *et al.*, 2012). For [^{18}F]AV-1451, BP_{ND} was assessed in each ROI with the simplified reference tissue model (Gunn *et al.*, 1997) using superior cerebellar cortex grey matter as the reference region. For more details about the data pre-processing steps see Passamonti et al. (Passamonti *et al.*, 2017, 2018*b*).

The number of regions was reduced from 83 to 15 *a priori* regions of interest, by a) combining left and right regional values in bilateral regions (cf. (Passamonti *et al.*, 2017, 2018*b*)), and b) focusing on 15 bilateral temporo-parietal regions, related to Alzheimer's disease pathology (see Supplementary Table 2). Regional grey matter volumes were corrected for TIV. For both [^{11}C]PK11195 and [^{18}F]AV-1451, a volume-weighted mean of left and right regional BP_{ND} values was calculated for each bilateral ROI.

3.2.3. Statistical analyses

Descriptive statistics. Continuous variables (age, education, ACE-R) were compared between groups with an independent-samples t-test, and categorical variables (sex) with the Chi-square test. The effect size of each t-test comparison was computed to quantify differences between the two groups (Cohen's d > 0.8, valuable difference).

Principal components analysis (PCA). The standardised values determined for the 15 bilateral ROIs from each imaging dataset were included in three principal component analyses (PCAs), run separately for grey matter volumes, [^{11}C]PK11195 and [^{18}F]AV-1451 BP_{ND} values. This reduces dimensionality and the problem of multiple comparisons, identifying a limited number of components that best explain the data variance. I applied an orthogonal Varimax rotation to maximize interpretability and specificity of the resulting components. I retained components with eigenvalues >1. To test whether correction for CSF affected the PCA results, I applied the same analyses on [^{18}F]AV-1451 PET and [^{11}C]PK11195 regional data not corrected for CSF partial volume.

The individual component scores were corrected for the time interval in months between the baseline cognitive assessment and each scan. Median (mean and standard deviation) of the time interval between the baseline cognitive assessment and the imaging scans were: 1.0 (1.75±2.50) months for MRI, 7.5 (7.18±5.68) months for [^{18}F]AV-1451 PET and 2 (6.12±9.07) months for [^{11}C]PK11195 PET. The residuals extracted for each component were included in a multiple regression on cognitive decline as independent variables.

Latent Growth Curve Model for cognitive data. ACE-R scores at follow-up were annualised to the nearest whole year, using the absolute difference in scores between the baseline and the following visits, divided by the time interval in days between tests and multiplied by 365 (1 year), 730 (2 years) or 1095 (3 years). An LGCM was fitted on longitudinal annualised ACE-R scores across all subjects (n=55), to obtain the (i) intercept; (ii) slope, quantifying the rate of change and its form (i.e. linear or nonlinear); (iii) the relation between intercept and slope. A linear slope for the longitudinal ACE-R scores was estimated and used in further analyses. Addition of a non-linear (quadratic) term to the model did not improve the estimation of slope (see Supplementary Material). The estimated parameters are based on the individuals' trajectory, indicating average change and individual difference. Covariates can be added to the model to assess their associations with both intercept and slope. Three time points and 5-10

cases per parameter are required for a standard LGCM (Bentler and Chou, 1987; Newsom, 2015). LGCM was implemented in Lavaan software (Rosseel, 2012) using full information maximum likelihood estimation with robust standard errors for missingness and non-normality. I considered four indices of good model fit (Schermelleh-Engel *et al.*, 2003): 1) the chi-square test with the p-value (good fit: > 0.05), 2) the root-mean-square error of approximation (RMSEA, acceptable fit: < 0.08, good fit: < 0.05), 3) the comparative fit index (CFI, acceptable fit: 0.95–0.97, good fit: > 0.97), and 4) the standardized root mean-square residual (SRMR, acceptable fit: 0.05–0.10, good fit: < 0.05). From the model fitting, variables "intercept" and "slope" were created extracting the individual estimated values for each subject in the model. T-tests and analysis of variance tested for group differences in initial cognitive performance and annual change.

Hypothesising that the cognitive decline over 3 years follows a linear trajectory in aging and Alzheimer's disease, I compared the linear model of change with a quadratic model. To determine whether a quadratic function is appropriate, the models with and without the quadratic effect were compared with a likelihood ratio test.

One-step prediction procedure: Latent Growth Curve Models with predictors. Across all subjects, I tested the predictive value of each imaging method on cognitive decline, applying five LGCMs with each scan-specific component's values (corrected for months from the baseline) as predictor of cognitive intercept and slope. Models were tested separately for MRI (n=55), [^{11}C]PK11195 PET (n=41) and [^{18}F]AV-1451 PET (n=40). Then, in patients (n=26), the individual scores of all five imaging components were included as predictors in the LGCM on longitudinal ACE-R, estimating the combined predictive effect of imaging modalities.
The one step procedure is a simple approach to my research questions but brings estimation challenges with a modest sample size. Therefore, I next applied a two-step prediction procedure: 1) extracting individual slope values from the initial LGCM for cognitive data across all the population, and 2) including these values as dependent variable in linear regression models with brain imaging components as predictors. I present both frequentist and Bayesian analyses to ensure inferential robustness and allowing us to quantify evidence in favour of the null hypothesis.

Two-step frequentist prediction: linear regression models on LGCM parameters. First, across all subjects, the residual values of each scan-specific PCA component (corrected for months from the baseline) were included as single predictors in separated univariable linear regression models with the individual slope values extracted from the initial LGCM as dependent variable. The significance level was set at $p<0.01$ corrected for multiple comparisons (Bonferroni correction $\alpha=0.05/5$**)**. Next, the individual scores of the imaging methods' components were included as independent variables in a multivariable regression analysis on patients alone (N=26), who underwent all three imaging scans. This model was fit to examine the individual, as well as combined, ability to explain variance in cognitive decline using brain marker components as well as age, education, and sex as independent variables. The model used stepwise backward selection (entry criterion $\alpha=0.05$ and elimination criterion $\alpha=0.1$). A complementary post hoc 'exploratory' linear regression analysis included the interaction term between PET independent variables, to test whether their interaction was predictive of cognitive decline. In supplementary analyses, I applied a "reduced" multivariable linear regression analysis with slope as dependent variable and only the first component of each imaging method as predictors to test that the different number of components between MRI and PET did not affect the estimation. These supplementary analyses were performed with and without the interaction terms between tau and inflammation measures. Given the challenges of stepwise model selection, and the limitations of sample size to utilize more advanced methods (e.g. regularized model fitting), I ran the analysis using Bayesian methodology, to ensure inferential robustness of my findings and confidence in the null results.

Two-step Bayesian prediction: linear regression models on LGCM estimated parameters. I applied a Bayesian multiple regression analysis with brain components and demographic variables as predictors, and the estimated slope values as dependent variable. This approach was used to test whether there was evidence for the absence of independent variables' effect for those components excluded from the final models (as opposed to frequentist type II error). In the model comparisons, adopting a uniform prior over the models, I considered as final model the one with the highest Bayes Factor compared to the null model (BF_{10}). Then, I used a reduced Bayesian linear regression, mirroring the reduced model applied with the frequentist approach, which included only the first component of each imaging method as predictors of slope.

Two-step frequentist prediction procedure on patients only. I also applied a two-step prediction procedure to patient data only: 1) extracting individual slope values from the initial LGCM for cognitive data across the 26 patients, and 2) including these values as dependent variable in linear regression models with brain imaging components as predictors. I present both frequentist and Bayesian analyses to ensure inferential robustness and allowing us to quantify evidence in favour of the null hypothesis.

See **Figure 6** for a schematic representation of statistical analyses with one-step and two-step prediction procedures. All PCAs and regression models were performed in SPSS Statistics version 25 (IBM); all Bayesian analysis in JASP version 0.10.2 (JASP team) and all LCGMs used R version 3.6.1 (R Core Team).

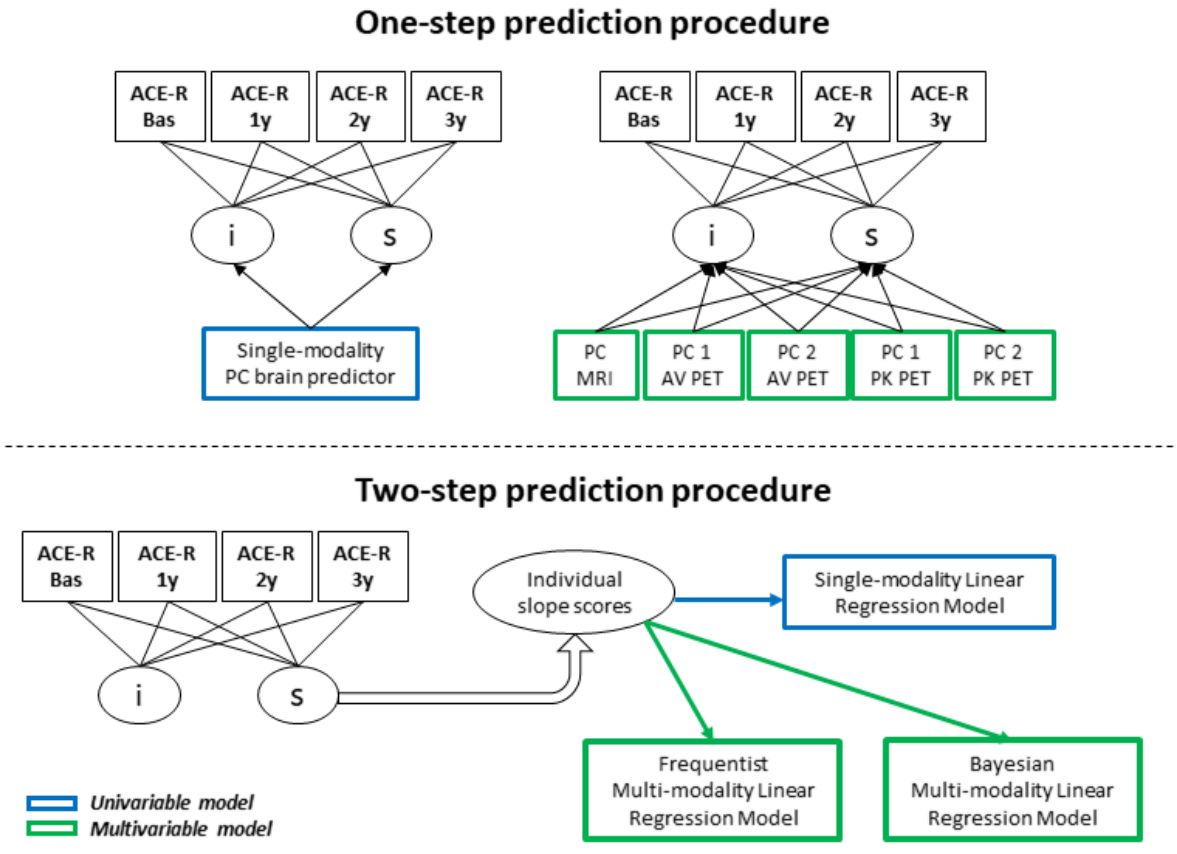

Figure 6. Schematic representation of statistical analyses for one-step and two-step prediction procedures. Abbreviation: ACE-R: Addenbrooke's Cognitive Examination – Revised; i: intercept; s: slope; PC: principal component; AV: [18F]AV-1451; PK: [11C]PK11195; Bas: baseline; y: years.

3.3. Results

3.3.1. Descriptive statistics

Significant differences between patient and control groups were found for education ($t(48.4)=2.4$, $p=0.02$, $d=0.64$) and ACE-R scores ($t(33.3)=8.6$, $p<0.001$, $d=2.37$). There were no significant group differences in age ($t(53)=-1.7$, $p=0.09$, $d=-0.47$) and sex ($\chi2(1)=0.17$, $p=0.68$) (**Table 2**). Individual ACE-R scores at baseline and at each follow-up are shown in **Figure 7**. See **Table 3** for demographics in patient and control subgroups.

Table 2. *Demographic and clinical characteristics for the patient and control groups.*

	Patients	**Healthy controls**	**Group difference**
N	26	29	
Sex (Female/Male)	12/14	15/14	$\chi2(1)=0.17$, $p=0.68$
Age (years - mean ± SD)	72.1±8.7	68.3±7.2	$t(53)=-1.7$, $p=0.09$, $d=-0.47$
Education (years - mean ± SD)	13.1±3.2	14.9±2.6	$t(48.4)=2.4$, $p=0.02$, $d=0.64$
ACE-R Baseline (mean ± SD)	77.8±9.1	94.4±4.0	$t(33.3)=8.6$, $p<0.001$, $d=2.37$ *
Disease Duration (years - mean ± SD)	3.6±2.1	-	

** denotes significant difference between patients and controls (p-value < 0.05) with effect size d > 0.8 for t-test. Abbreviations ACE-R: Addenbrooke's Cognitive Examination – Revised; SD: standard deviation; t(): t-test; p: p-value; d: Cohen's d*

***Table 3**. Demographic and clinical characteristics for the subsample of control and patient groups.*

	Controls AV PET	**Control PK PET**	**Group difference**	**MCI+**	**AD**	**Group difference**
N	**14**	15		**14**	**12**	
Disease Duration (years - mean ± SD)	-	-	-	3.8±2.3	3.4±1.8	t(24)=0.60; p=0.558
Sex (Female/Male)	7/7	8/7	$\chi2(1)=0.03$; p=0.858	7/7	5/7	$\chi2(1)=0.18$; p=0.671
Age (years - mean ± SD)	66.9±7.6	69.6±6.8	t(27)=-1.04; p=0.308	74.6±6.4	69.1±10.4	t(24)=1.64; p=0.115
Education (years - mean ± SD)	15.8±1.9	14.1±3.0	t(27)=1.77; p=0.09	12.3±2.8	14.0±3.5	t(24)=-1.39; p=0.176
ACE-R Baseline (mean ± SD)	95.4±3.1	95.5±4.5	t(27)=1.26; p=0.220	80.6±6.5	74.5±10.8	t(17.4)=1.70; p=0.107

Abbreviations AV: [^{18}F]AV-1451; PK: [^{11}C]PK11195; ACE-R: Addenbrooke's Cognitive Examination – Revised; SD: standard deviation; t(): t-test; p: p-value

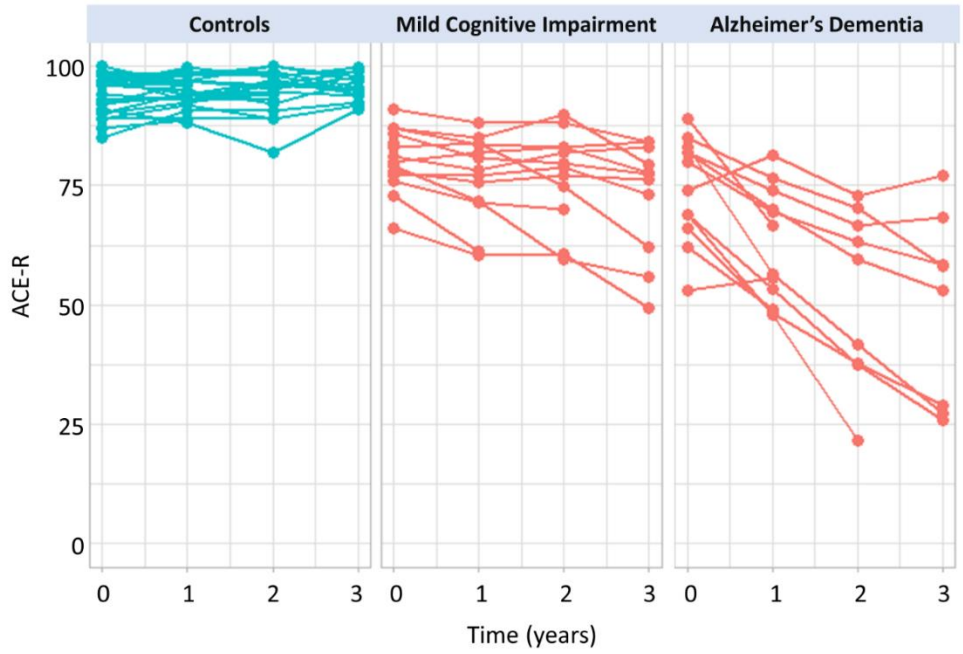

***Figure 7.** Longitudinal cognitive changes in patients and controls, as measured by revised Addenbrooke's Cognitive Examination (ACE-R). Points represent annualised ACE-R scores at baseline, 1-year, 2-years and 3-years follow-up for each subject in control (blue) and patient (red) groups.*

3.3.2. Principal component analysis

For grey-matter volumes, the PCA on the pre-selected 15 -Alzheimer's disease specific cortical regions identified only one component that encompassed all the temporo-parietal regions and explained 74% of the variance (**Figure 8**, left panel). Two principal components were detected for [^{18}F]AV-1451 BP_{ND} data, explaining 91% of the total variance (83% first component; 8% second component). The first component was loaded onto the posterior temporal and parietal regions, while the second component was weighted to the anterior temporal lobe, amygdala, insula and hippocampus (**Figure 8**, middle panel). For [^{11}C]PK11195 BP_{ND} data, two principal components were identified, and these explained together the 76% of data variance (56% for the first component; 20% for the second component). The first component involved anterior and medial temporal lobe, while the second component was mainly loaded onto the posterior temporo-parietal regions and insula (**Figure 8**, right panel). The loadings are shown in **Table 4**. Using PET data without CSF correction yielded qualitatively similar results.

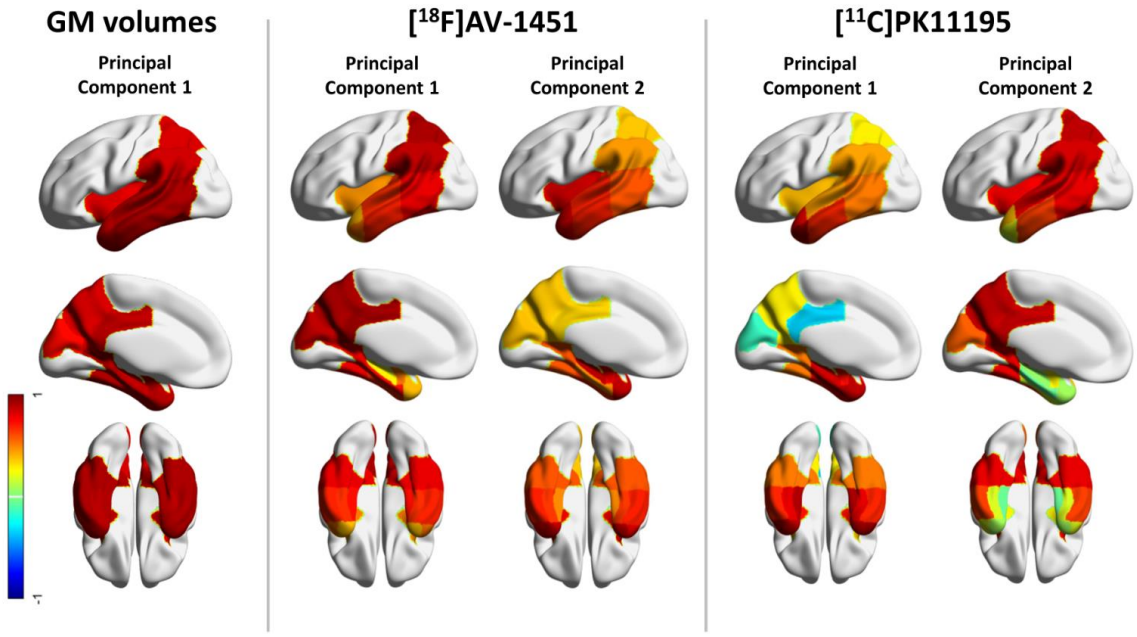

Figure 8. *Regional weights of the structural MRI component (left), and rotated regional weights of [^{18}F]AV-1451 components (middle) and the [^{11}C]PK11195 components (right). Components were identified applying three independent principal component analyses on 15 temporo-parietal regions. For structural MRI, regional grey matter (GM) volumes were included in the analysis, while for each PET tracer, the binding potential values in those regions were considered, separately for each modality. The colours represent the region-specific weights (range: from -1 to 1) on each component (**Table 4**).*

Table 4. *Regional weights of the structural MRI component (left), and rotated regional weights of [18F]AV-1451 components (middle) and the [11C]PK11195 components (right).*

GM volumes		[^{18}F]AV-1451			[^{11}C]PK11195		
Region	**Comp 1**	**Region**	**Comp 1**	**Comp 2**	**Region**	**Comp 1**	**Comp 2**
Posterior temporal lobe	0.910	Posterior cingulate gyrus	0.923	0.338	Anterior lateral temporal lobe	0.920	0.201
Middle and inferior temporal gyrus	0.909	Superior parietal gyrus	0.915	0.363	Parahippocampal gyri	0.906	-0.055
Parahippocampal gyri	0.903	Cuneus	0.872	0.380	Anterior medial temporal lobe	0.880	0.078
Amygdala	0.901	Inferiolateral parietal lobe	0.872	0.451	Hippocampus	0.835	0.057
Anterior medial temporal lobe	0.891	Posterior_temporal_lobe	0.791	0.587	Fusiform gyrus	0.796	0.187
Fusiform gyrus	0.884	Parahippocampal gyri	0.725	0.483	Superior anterior temporal gyrus	0.743	0.389
Superior posterior temporal gyrus	0.879	Fusiform gyrus	0.660	0.643	Amygdala	0.723	0.281
Anterior lateral temporal lobe	0.875	Hippocampus	0.274	0.891	Middle and inferior temporal gyrus	0.680	0.626
Hippocampus	0.869	Anterior medial temporal lobe	0.387	0.876	Superior parietal gyrus	0.282	0.879
Posterior cingulate gyrus	0.863	Superior anterior temporal gyrus	0.395	0.858	Posterior cingulate gyrus	-0.340	0.847
Inferiolateral parietal lobe	0.840	Insula	0.460	0.845	Inferiolateral parietal lobe	0.434	0.831
Superior parietal gyrus	0.821	Amygdala	0.508	0.791	Superior posterior temporal gyrus	0.438	0.804
Superior anterior temporal gyrus	0.812	Anterior lateral temporal lobe	0.530	0.768	Posterior temporal lobe	0.513	0.794
Insula	0.782	Middle and inferior temporal gyrus	0.687	0.694	Insula	0.385	0.755
Cuneus	0.735	Superior posterior temporal gyrus	0.662	0.688	Cuneus	-0.147	0.563

Abbreviations: GM=Grey Matter; Comp=Component.

Simple correlations between MRI and PET component scores across subjects were significant for the MRI component versus the first [^{11}C]PK11195 component (R=-0.459, p=0.003, significant after Bonferroni correction), but not the second [^{11}C]PK11195 component (R=-0.154, p=0.337). The MRI component was weakly associated with the first (R=-0.319, p=0.045, uncorrected) and the second (R=-0.329, p=0.038, uncorrected) [^{18}F]AV-1451 components. In patients, correlations between [^{18}F]AV-1451 and [^{11}C]PK11195 components were not significant, even uncorrected.

3.3.3. Annual rate of cognitive decline

The linear LGCM of longitudinal ACE-R scores fitted the data adequately ($\chi 2(8)=10.93$, p=0.206; RMSEA=0.09 [0.00 – 0.21], CFI=0.99, SRMR=0.04). Three out of the four model fit indices were 'acceptable' or 'good' by Schermelleh-Engel et al. guidelines (Schermelleh-Engel *et al.*, 2003), although the RMSEA (>0.08) was not. To exclude a large single source of misfit, I inspected the standardized residual matrix, and confirmed no single standardized residual greater than r=0.099. I therefore consider the overall model fit sufficient. The mean of the intercept was 86.40 (Standard Error (SE)=1.44, z-value=60.02, fully standardized estimate (Std Est) =8.28, p<0.001) and average cognition declined over time (slope, estimate (est)=-3.01, SE=0.80, z-value=-3.75, Std Est=-0.54, p<0.001). The intercept significantly co-varied with the slope (est=38.51, SE=9.24, z-value=4.17, Std Est (correlation)=0.67, p<0.001, such that individuals with higher (better) baseline performance showed less steep decline. As expected, patients significantly differed from controls in their intercept (t(31.8)=9.39, p<0.001) and slope

(t(25.9)=6.42, p<0.001) indicating a faster and more severe cognitive decline (**Figure 9**). Across three groups, ANOVA confirmed group differences in the intercept (F(2)=63.44, p<0.001; mean (SD) for: controls=94.18 (3.27); MCI+ patients=81.25 (6.17); Alzheimer's patients=73.60 (8.96)) and slope (F(2)=53.74, p<0.001; mean (SD) for: controls=0.40 (0.82); MCI+ patients=-3.56 (3.08); Alzheimer's patients=-10.62 (5.71)), with post-hoc confirmation of differences between each pair of groups (all p<0.005).

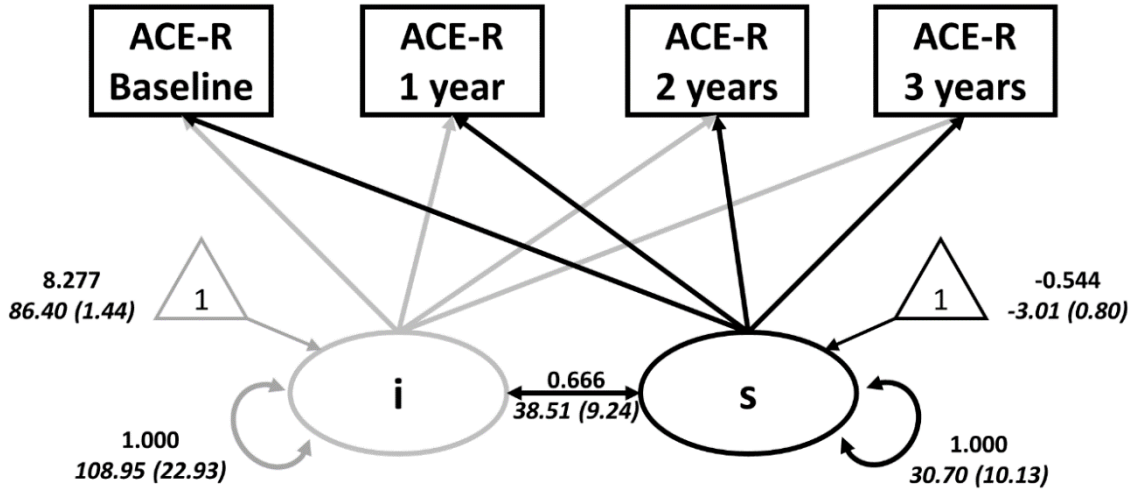

Figure 9. *Latent growth curve model to test the initial values (intercept – "i") and longitudinal changes (slope – "s") in scores of revised Addenbrooke's Cognitive Examination (ACE-R) across all sample. Circles indicate latent variables, rectangles indicate observed variables, and triangles denote intercepts (1= population means on the parameters). Thick single-headed arrows indicate regressions while thick double-headed arrows indicate variance and covariance (grey for intercept and black for slope). Values in Roman are standardized parameter estimates, and values in italics are unstandardized parameter estimates (with standard errors in parentheses). The annual rate of change was positively associated with performance at baseline (lower initial cognitive scores were associated with a higher annual rate of cognitive changes).*

The LGCM with the quadratic term on longitudinal ACE-R scores fitted the data adequately ($\chi2(4)=2.78$, p=0.595; RMSEA=0.00 [0.00 – 0.21], CFI=1.00, SRMR=0.014). However, comparing the model fit between the linear and the quadratic LGCM on ACE-R scores, the ANOVA test (anova() R function) did not find significant differences (Chisq Diff= 3.04, p=0.219) between the linear model (AIC=1249.2) and the quadratic one (AIC=1250.3). This means that adding the quadratic term does not improve the model of cognitive decline.

3.3.4. One-step prediction LGCM with predictors

The LGCM including MRI fitted the data adequately ($\chi2(10)=18.33$, p-value=0.05, RMSEA=0.13 [0.01-0.23], CFI=0.98, SRMR=0.03). Inspecting the standardized residual matrix, none was greater than r=0.105. Individual differences in the summary brain measure were strongly and positively associated with both slope (path Std Est=0.58, p<0.001) and intercept (path Std Est=0.67, p<0.001). This suggested that individuals with greater grey matter volumes showed better baseline performance, and slower longitudinal decline, than those with smaller volumes.

The LGCM of the posterior [^{18}F]AV-1451 component fitted the data adequately ($\chi2(10)=16.30$, p-value=0.09, RMSEA=0.12 [0.00-0.22], CFI=0.98, SRMR=0.03), and no single standardized residual was greater than r=0.101. Here too, both the slope (path Std Est=-0.62, p=0.001) and intercept (path Std Est=-0.53, p<0.001) were strongly governed by individual differences in the first component. In contrast, in the model with only the anterior [^{18}F]AV-1451 component ($\chi2(10)=21.75$, p-value=0.01, RMSEA=0.17 [0.07-0.27], CFI=0.96, SRMR=0.05), there was no association between the scores on the neural component and either the intercept (path Std Est=-0.12, p=0.431) or the slope (path Std Est=-0.39, p=0.057). In this model, no single standardized residual was greater than r=0.148.

Finally, the LGCM with the anterior [^{11}C]PK11195 component fitted the adequately ($\chi2(10)=16.32$, p-value=0.09, RMSEA=0.13 [0.00-0.23], CFI=0.97, SRMR=0.02), and no single standardized residual was greater than r=0.056. Individual differences in the [^{11}C]PK11195 component governed both slope (Std Est=-0.51, p=0.002) and intercept (Std Est=-0.43, p<0.001) correlated with the component #1. In the model with the posterior [^{11}C]PK11195 component as regressor, ($\chi2(10)=9.33$, p-value=0.50, RMSEA=0.00 [0.00-0.17], CFI=1.00, SRMR=0.03), the slope was significantly correlated with the component (Std Est=-0.45, p=0.009), but not the intercept (Std Est=-0.010, p=0.951). No single standardized residual was greater than r=0.108.

In patients, an LGCM including the components of all three imaging methods did not fit the data well ($\chi2(18)=34.76$, p-value=0.01, RMSEA=0.17 [0.08 – 0.26], CFI=0.92, SRMR=0.04), but no single standardized residual was greater than r=0.119. With this caveat, cognitive decline (slope) was predicted by baseline posterior [^{18}F]AV-1451 (path Std Est=-0.49, p=0.025)

and anterior [^{11}C]PK11195 (path Std Est=-0.40, p=0.017) components' scores, but not the posterior [^{11}C]PK11195, the MRI (path Std Est=0.10, p=0.52) or the anterior [^{18}F]AV-1451 (Std Est=-0.22, p=0.23) components.

3.3.5. Two-step prediction: linear regression

Across all subjects, the rate of cognitive decline (slope from LGCM) was significantly associated with: 1) the MRI weighting (Std Beta=0.61, p<0.001); 2) the posterior [^{18}F]AV-1451 (Std Beta=-0.60, p<0.001); 3) and anterior [^{11}C]PK11195 (Std Beta=-0.47, p=0.002). All these results survived Bonferroni's correction. Correlations of slope with the anterior [^{18}F]AV-1451 (Std Beta=-0.36, p=0.022), and the posterior [^{11}C]PK11195 (Std Beta=-0.39, p=0.012) did not survive correction for multiple comparisons (p<0.01). See **Figure 10** for a graphical representation of the significant associations between individual scores (x axis) of imaging-specific principal components and slope in ACE-R scores (y axis) extracted by LGCM. Model summary and coefficients for all univariable models with slope as dependent variable across the whole population are reported in **Table 5** (See

Table 6 for results from analysis of patients only). Strikingly, these parameter estimates remained effectively unchanged even when simultaneously including age, sex and education as covariates in the models (

Table **7).**

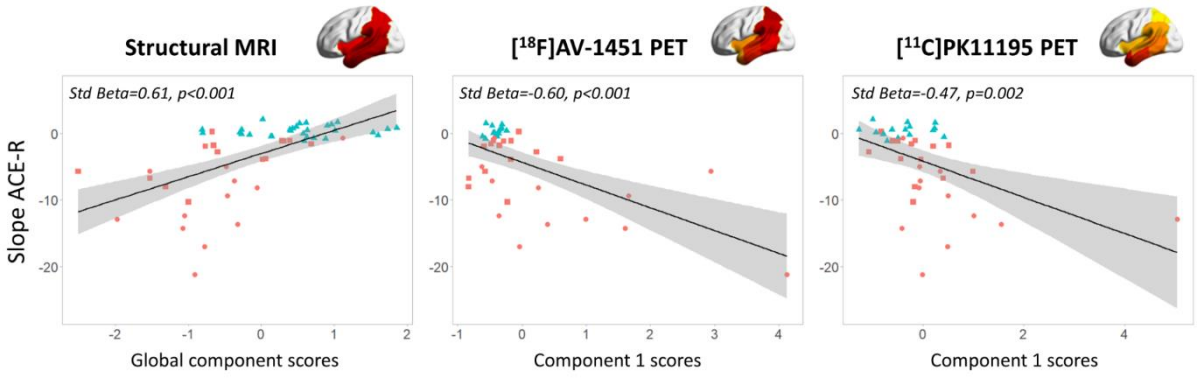

Figure 10. *Regression analyses with annual change in scores of revised Addenbrooke's Cognitive Examination (Slope ACE-R, y axis) and individual baseline scores for each modality-specific principal component (x axis): structural MRI (left panel), [18F]AV-1451 PET (middle panel), and [11C]PK11195 PET (right panel). Different colours represent different diagnostic groups (patients*

with Alzheimer's disease = red circles, patients with amyloid-positive mild cognitive impairment = red squares, controls = blue triangles). Abbreviations: Std=standard; p=p-value.

Table 5. *Results for the univariable regression models on slope across all population.*

Model		Estimate	Std Error	Std Beta	t value	p	Adj R^2 (std err)	F	p
MRI (N=55)	**(Intercept)**	-3.01	0.58		-5.23	0.000	0.358 (4.27)	31.18	<0.001*
	MRI component	3.48	0.63	0.61	5.58	0.000			
AV 1 (N=40)	**(Intercept)**	-4.31	0.73		-5.88	0.000	0.341 (4.64)	21.22	<0.001*
	AV component 1	-3.43	0.74	-0.60	-4.61	0.000			
AV 2 (N=40)	**(Intercept)**	-4.31	0.85		-5.05	0.000	0.108 (5.40)	5.72	0.022
	AV component 2	-2.08	0.87	-0.36	-2.39	0.022			
PK 1 (N=41)	**(Intercept)**	-4.15	0.80		-5.19	0.000	0.204 (5.13)	11.26	0.002*
	PK component 1	-2.72	0.81	-0.47	-3.36	0.002			
PK 2 (N=41)	**(Intercept)**	-4.15	0.84		-4.96	0.000	0.128 (5.36)	6.87	0.012
	PK component 2	-2.36	0.90	-0.39	-2.62	0.012			

*p=uncorrected p-values, *= Bonferroni corrected, significance threshold p<0.01. Abbreviations AV: [^{18}F]AV-1451; PK: [^{11}C]PK11195; Std: standard; Adj: adjusted*

Table 6. *Results for the univariable regression models on cognitive slope in patients.*

Model		Estimate	Std Error	Std Beta	t value	p	Adj R^2 (std err)	F	p
MRI (N=26)	**(Intercept)**	-5.02	1.25		-4.00	.001	0.167 (5.18)	6.02	0.022
	MRI component	3.08	1.26	0.45	2.45	.022			
AV 1 (N=26)	**(Intercept)**	-6.23	0.97		-6.43	.000	0.271 (4.84)	10.29	0.004
	AV component 1	-2.63	0.82	-0.55	-3.21	.004			
AV 2 (N=26)	**(Intercept)**	-6.56	1.13		-5.78	.000	0.007 (5.65)	1.18	0.289
	AV component 2	-1.08	0.99	-0.22	-1.09	.289			
PK 1 (N=26)	**(Intercept)**	-6.36	1.06		-6.01	.000	0.131 (5.29)	4.78	0.039
	PK component 1	-2.02	0.92	-0.41	-2.19	.039			
PK 2 (N=26)	**(Intercept)**	-6.54	1.06		-6.20	.000	0.116 (5.34)	4.27	0.05
	PK component 2	-2.11	1.02	-0.39	-2.07	.050			

Abbreviations AV: [^{18}F]AV-1451; PK: [^{11}C]PK11195; Std: standard; Adj: adjusted, p=uncorrected p-values

Across all subjects, the initial cognitive performance (intercept in LGCM on ACER scores) was significantly associated with: 1) the MRI component weighting (Std Beta=0.67, p<0.001); 2) the posterior [^{18}F]AV-1451 (Std Beta=-0.55, p<0.001); 3) and anterior [^{11}C]PK11195 (Std Beta=-0.46, p=0.003), surviving Bonferroni's correction. Non-significant correlations of slope were found with the anterior [^{18}F]AV-1451 (Std Beta=-0.15, p=0.35), and the posterior [^{11}C]PK11195 (Std Beta=-0.06 p=0.72). These results remained unchanged if including age, sex and education as covariates in the models (

Table **7)**.

Table 7*. Results for the univariable regression models on slope (left) and intercept (right) across all population with age, sex and education as covariates.*

		Dependent variable: cognitive slope					Dependent variable: cognitive intercept				
Model		**Est**	**Std Error**	**Std Beta**	**t value**	**p**	**Est**	**Std Error**	**Std Beta**	**t value**	**p**
MRI (N=55)	**(Intercept)**	-13.81	5.99		-2.31	0.025	55.06	10.59		5.20	<0.001
	MRI comp	4.03	0.65	0.70	6.19	**<0.001**	7.07	1.15	0.64	6.14	**<0.001**
	Age	0.18	0.07	0.27	2.45	0.018	0.25	0.13	0.20	1.97	0.055
	Sex	0.82	1.14	0.08	0.72	0.472	2.05	2.01	0.10	1.02	0.314
	Education	-0.13	0.20	-0.08	-0.67	0.505	0.92	0.35	0.27	2.59	0.012
AV 1 (N=40)	**(Intercept)**	-7.57	8.18		-0.93	0.361	67.95	11.94		5.69	<0.001
	AV comp 1	-3.67	0.81	-0.64	-4.56	**<0.001**	-7.19	1.17	-0.67	-6.12	**<0.001**
	Age	-0.04	0.09	-0.06	-0.39	0.699	-0.20	0.14	-0.16	-1.45	0.156
	Sex	0.97	1.54	0.09	0.63	0.533	3.77	2.24	0.18	1.68	0.102
	Education	0.38	0.26	0.21	1.49	0.144	2.00	0.37	0.57	5.33	<0.001
AV 2 (N=40)	**(Intercept)**	-18.95	9.18		-2.06	0.047	47.54	16.38		2.90	0.006
	AV comp 2	-2.26	0.90	-0.39	-2.51	**0.017**	-1.52	1.61	-0.14	-0.95	**0.351**
	Age	0.14	0.10	0.21	1.34	0.190	0.12	0.18	0.09	0.63	0.532
	Sex	1.55	1.82	0.14	0.85	0.402	3.68	3.25	0.17	1.13	0.265
	Education	0.30	0.30	0.16	1.02	0.316	1.88	0.53	0.54	3.53	0.001
PK 1 (N=41)	**(Intercept)**	-4.72	9.55		-0.49	0.624	71.26	16.81		4.24	<0.001
	PK comp 1	-2.65	0.93	-0.46	-2.86	**0.007**	-4.37	1.63	-0.42	-2.68	**0.011**
	Age	0.04	0.11	0.05	0.32	0.751	0.00	0.20	0.00	-0.01	0.995
	Sex	0.37	1.71	0.03	0.22	0.830	0.45	3.00	0.02	0.15	0.882
	Education	-0.16	0.28	-0.09	-0.59	0.561	0.90	0.49	0.27	1.83	0.076
PK 2 (N=41)	**(Intercept)**	-17.55	8.85		-1.98	0.055	51.04	16.37		3.12	0.004
	PK comp 2	-2.50	1.00	-0.41	-2.50	**0.017**	-2.17	1.85	-0.20	-1.17	**0.248**
	Age	0.13	0.11	0.18	1.21	0.232	0.18	0.20	0.14	0.92	0.362
	Sex	0.92	1.73	0.08	0.53	0.598	1.49	3.19	0.07	0.47	0.643
	Education	0.27	0.30	0.15	0.89	0.378	1.39	0.56	0.41	2.46	0.019

Abbreviations AV: [^{18}F]AV-1451; PK: [^{11}C]PK11195; Std: standard; p=uncorrected p-values

In patients, the final model of multiple regression on cognitive slope (adjusted R^2 = 0.418, Std Error= 4.18; p=0.001) included both [^{18}F]AV-1451 components (#1: Est=-2.57, Std Error=0.71, p=0.002; #2: Est=-1.64, Std Error=0.74, p=0.038), and the anterior [^{11}C]PK11195 (#1: Est=-1.92, Std Error=0.74, p=0.017) as predictors (**Figure 11** and **Table 9**). Of note age, education, sex, the MRI component, and the posterior [^{11}C]PK11195 component were excluded from the final model.

In patients, the final model of multiple regression on cognitive intercept (adjusted R^2 = 0.519, Std Error= 5.81; p<0.001) included the education variable (Est=1.02, Std Error=0.38, p=0.014), the MRI component (Est=3.61, Std Error=1.46, p=0.021) and the posterior [^{18}F]AV-1451 (Est=-3.99, Std Error=1.05, p=0.001) as predictors.

Model summary and coefficients for both the initial model (adjusted R^2 = 0.389, Std Error= 4.43; p=0.027), the full model with only brain predictors (adjusted R^2 = 0.474, Std Error= 4.12; p=0.002), and the final model are reported in **Table 8**. Either in the initial model with covariates or in the full model with only brain measures as predictors, the posterior [^{18}F]AV-1451 component and the anterior [11C]PK11195 component showed the highest estimated coefficients. The interaction between the imaging components in the final model was not significant (p > 0.05 uncorrected). In addition, the reduced multiple regression analysis, with the first component of each imaging method only, included the [^{18}F]AV-1451 component (Est=-2.42, Std Error=0.77, p=0.004) and the [^{11}C]PK11195 component (Est=-1.71, Std Error=0.80, p=0.042) in the final model (adjusted R^2 = 0.366, Std Error=4.52; p=0.002), while the MRI component was discarded. Again, the interaction between the imaging components was not significant (p > 0.05 uncorrected).

***Table 8**. Results for the multiple regression model in patients with Alzheimer's dementia and Mild Cognitive Impairment. For each of the three multiple regression models applied and described in the methods' section, the estimated coefficients are reported for the full/initial model and the final model, indicated by the stepwise backward elimination.*

Dependent variable	Model		Estimate	Std Error	Std Beta	t value	P	Adj R^2 (std err)	F	p
slope	Full	(Intercept)	-7.09	11.14		-0.64	0.533	0.389 (4.43)	2.99	0.027
		MRI component	0.85	1.39	0.12	0.62	0.547			
		AV component 1	-2.30	1.07	-0.48	-2.14	0.047*			
		AV component 2	-1.18	0.94	-0.24	-1.26	0.224			
		PK component 1	-1.59	1.10	-0.32	-1.45	0.164			
		PK component 2	-1.28	1.10	-0.24	-1.17	0.260			
		Age	0.00	0.15	0.01	0.03	0.980			
		Education	0.11	0.36	0.06	0.30	0.765			
		Sex	0.85	2.02	0.08	0.42	0.678			
	Full (only brain measures)	(Intercept)	-5.03	1.01		-4.99	0.000*	0.474 (4.12)	5.50	0.002
		MRI component	0.84	1.22	0.12	0.67	0.501			
		AV component 1	-2.20	0.74	-0.46	-2.96	0.008*			
		AV component 2	-1.07	0.82	-0.21	-1.31	0.205			
		PK component 1	-1.68	0.86	-0.39	-1.95	0.066			
		PK component 2	-1.25	0.87	-0.23	-1.43	0.168			
	Final	(Intercept)	-5.41	0.87		-6.19	0.000*	0.458 (4.18)	8.05	0.001
		AV component 1	-2.57	0.71	-0.54	-3.60	0.002*			
		AV component 2	-1.64	0.74	-0.33	-2.21	0.038*			
		PK component 1	-1.92	0.74	-0.39	-2.59	0.017*			

Abbreviations AV: [^{18}F]AV-1451; PK: [^{11}C]PK11195; Std: standard; Adj: adjusted
*Significance code: *= p<0.05*

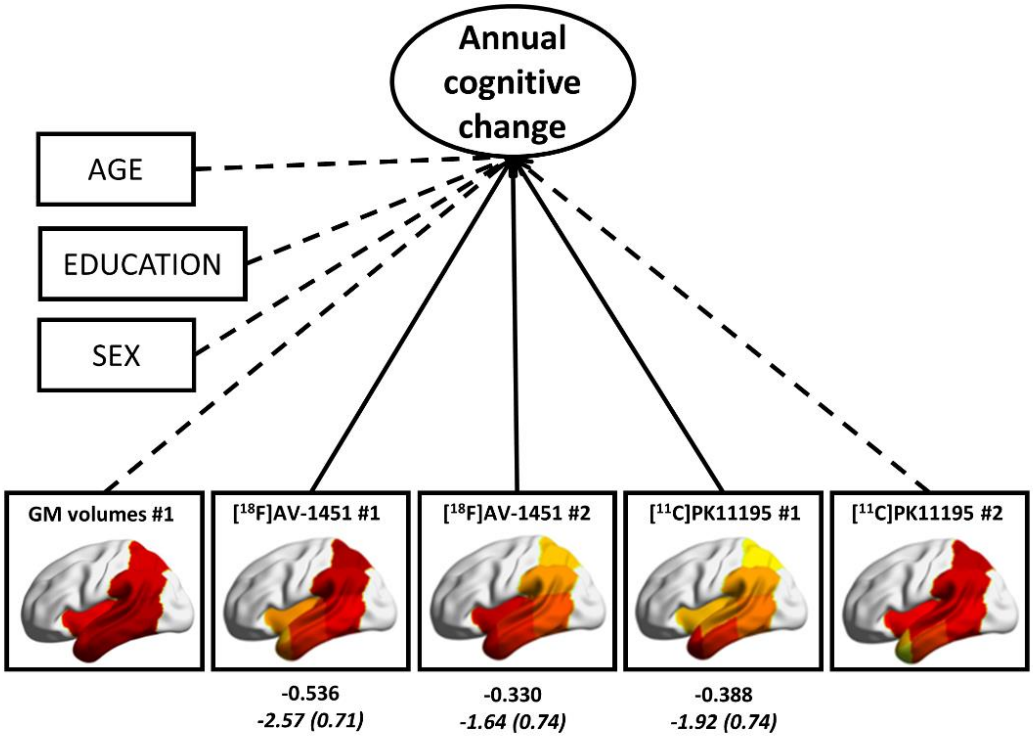

Figure 11. *Results of the multiple linear regression in patients, with cognitive slope (annual cognitive change) extracted by the Latent Growth Curve Model as dependent variable, and brain components' scores, age and education as independent variables. Solid arrows indicate significant coefficients of brain imaging measures indicated by the stepwise backward elimination, while dashed arrows indicate variables excluded by the final model. Values in Roman are standardized estimates, and values in italics are unstandardized beta estimates (standard errors in parentheses).*

Two-step frequentist prediction procedure on patients only. The cognitive LGCM on patients converged using robust maximum likelihood estimation and yielded adequate fit ($\chi2(8)=9.40$, p=0.310; RMSEA=0.08 [0.00 – 0.26], CFI=0.99, SRMR=0.07). The mean of the intercept was 77.52 (SE=1.73, z-value=44.93, Std Est =9.27, p<0.001) and average cognition declined over time (slope, estimate (est)=-6.87, SE=1.35, z-value=-5.09, Std Est=-1.09, p<0.001).

Across all patients, the rate of cognitive decline was associated with: 1) the MRI component (Std Beta=0.45, p=0.034); 2) the posterior [18F]AV-1451 (Std Beta=-0.53, p=0.005); 3) anterior [^{11}C]PK11195 (Std Beta=-0.40, p=0.041); and the posterior [^{11}C]PK11195 (Std Beta=-0.40, p=0.05). Running the regression model with all imaging components and demographic variables, the final model on cognitive slope selected by the backward selection (adjusted R^2 = 0.437, Std Error= 7.46; p=0.001) included both [^{18}F]AV-1451 components (#1: Est=-2.64, Std Error=0.77, p=0.002; #2: Est=-1.77, Std Error=0.81, p=0.039), and the anterior [^{11}C]PK11195 (#1: Est=-2.03, Std Error=0.80, p=0.019) as predictors. I estimated the comparable models

using Bayesian regression. The results were in accord with the backward selection method, with the best model including both [18F]AV-1451 components and the anterior [^{11}C]PK11195 component (BF10 = 32.85; R^2 = 0.504).

3.3.6. Two-step Bayesian prediction

With all brain components and demographic variables as candidate predictors of cognitive decline, model comparison using Bayes factors indicated that the best model included both [^{18}F]AV-1451 components (#1: Mean (SD) = -2.15 (0.65); #2: Mean (SD) = -1.37 (0.68)), and the anterior [^{11}C]PK11195 component (Mean (SD) = -1.61 (0.68)) as predictors (BF_{10} = 46.56; R^2 = 0.52). Hence, the best model in this statistical framework did not contain structural MRI data. See **Table 9** for details on the final model and **Table 10** for a list of models evaluated and the corresponding BF_{10}. The reduced Bayesian regression analysis with only the first component of each imaging method as predictor was in accord with the frequentist approach. The best model identified with BF_{10} criteria was the one with only the posterior [^{18}F]AV-1451 and the anterior [^{11}C]PK11195 components only as predictors of slope (BF_{10} = 20.81; R^2 = 0.42), but not the MRI component.

Table 9. *Results of the multivariable regression models on the regression slope in patients. For both frequentist (top) and Bayesian (bottom) the estimated coefficients for variables included in the final ("best") models are reported.*

Frequentist regression								
Final model (Stepwise Backward selection)	**Estimate**	**Std Error**	**Std Beta**	**t value**	**p**	**Adj R^2 (std err)**	**F**	**p**
(Intercept)	-5.41	0.87		-6.19	0.000	0.418	8.05	0.001
AV component 1	-2.57	0.71	-0.54	-3.60	0.002			
AV component 2	-1.64	0.74	-0.33	-2.21	0.038			
PK component 1	-1.92	0.74	-0.39	-2.59	0.017			
Bayesian regression								
Final model (Bayesian Factor based selection)	**Mean**	**Std Deviation**	**95% Credible interval**			**R^2**	**BF_{10}**	
			Lower	**Upper**				
(Intercept)	-6.82	0.82	-8.502	-5.129		0.523	46.56	
AV component 1	-2.15	0.65	-3.491	-0.802				
AV component 2	-1.37	0.68	-2.774	0.026				
PK component 1	-1.61	0.68	-3.001	-0.210				

Abbreviations AV: [^{18}F]AV-1451; PK: [^{11}C]PK11195; BF: Bayes factor; Std: standard; Adj: adjusted

Table 10. *Model comparison on the Bayesian multiple regression with cognitive slope as the dependent variable and brain imaging components and demographic variables as predictors. The models are ordered by the higher Bayes Factor (BF10) to the lowest. The table shows the ten most likely models, the null model, and the least likely model at the bottom. The Bayes Factor has been calculated for each model to the null model with respect to the null model. By convention, a BF>3 indicates positive evidence in favour of the alternate model, BF>10 strong evidence and BF>100 very strong evidence. The top three ranked models are therefore significantly 'better' prognostic models than any other model, including any model with MRI.*

Models	**P(M)**	**P(M|data)**	**BF $_{M}$**	**BF $_{10}$**	**R^2**
AV COMP1 + AV COMP2 + PK COMP1	0.004	0.033	8.744	46.560	0.523
AV COMP1 + PK COMP1 + PK COMP2	0.004	0.032	8.333	44.443	0.521
AV COMP1 + AV COMP2 + PK COMP1 + PK COMP2	0.004	0.030	7.804	41.705	0.569
MRI COMP + AV COMP1 + PK COMP1 + PK COMP2	0.004	0.018	4.680	25.31	0.543
MRI COMP + AV COMP1 + AV COMP2 + PK COMP1	0.004	0.016	4.112	22.289	0.536
MRI COMP + AV COMP1 + PK COMP2	0.004	0.016	4.031	21.856	0.481
AV COMP1 + PK COMP1	0.004	0.015	3.835	20.806	0.417
MRI COMP + AV COMP1	0.004	0.015	3.817	20.714	0.417
AV COMP1 + AV COMP2 + PK COMP1 + Sex	0.004	0.015	3.808	20.663	0.532
MRI COMP + AV COMP1 + AV COMP2 + PK COMP1 + PK COMP2	0.004	0.014	3.722	20.205	0.579
…					
Null model	0.004	7.120e -4	0.182	1	0
…					
AV COMP2 + Education + Sex	0.004	1.398e -4	0.036	0.196	0.082

Abbreviations AV: [^{18}F]AV-1451; PK: [^{11}C]PK11195; COMP: component; BF: Bayes factor

3.4. Discussion

This study demonstrates the independent and combined value of neuroimaging biomarkers for tau pathology ([^{18}F]AV-1451 PET), neuroinflammation ([^{11}C]PK11195 PET) and brain atrophy (structural MRI), in predicting longitudinal cognitive decline in patients with Alzheimer's disease. Baseline markers for tau pathology, neuroinflammation and atrophy in temporo-parietal regions individually predicted cognitive decline, across the spectrum of severity mild cognitive impairment to Alzheimer's dementia. But, in a multivariable model, cognitive decline was only associated with higher baseline tau pathology in posterior

temporo-parietal regions and increased neuroinflammation in the anterior temporal structures. Bayesian analysis confirmed the evidence against the predictive value of MRI atrophy over and above the PET markers of tau pathology and neuroinflammation.

I used PCA to derive the most parsimonious neuroanatomical patterns of pathology that explain most of the imaging variance across the cohort. It is highly efficient for reducing data dimensionality and the problem of multiple comparisons. The PCA indicated two sets of regions (i.e. components) of co-varying tau pathology and neuroinflammation, in anterior vs. posterior temporo-parietal regions. I focused on these regions because of their close association with Alzheimer's disease (Garibotto *et al.,* 2017; Jagust, 2018; Whitwell, 2018), but data are available on request for other, exploratory, analyses. In patients, the degree of neuroinflammation and tau pathology did not correlate in either anterior or posterior temporo-parietal cortex. Previous studies have considered the *in vivo* association between these two pathological processes in prodromal and early Alzheimer's disease. Significant associations between tau and neuroinflammation measures have been reported in fronto-temporal regions (Dani *et al.,* 2018), and parahippocampal cortex (Terada *et al.,* 2019). Using alternative ligands for tau and inflammation, [^{18}F]MK-6240 and [^{11}C]PBR28 respectively, positive correlations were found temporal, parietal and frontal cortex (Zou *et al.,* 2020). However, an earlier study failed to find significant correlations between tau and inflammation (Parbo *et al.,* 2018). Larger sample sizes may be needed to clarify the potential relationship, at different stages of disease.

The participants' weighting on atrophy, posterior [^{18}F]AV-1451 and anterior [^{11}C]PK11195 components were separately associated with more rapid cognitive decline. This result was confirmed by both the one- and two-step univariable prediction approaches. This corroborates the previously reported associations between cognitive deficits in Alzheimer's disease and the individual effects of tau pathology, neuroinflammation, and downstream cortical atrophy (Femminella *et al.,* 2016; Bejanin *et al.,* 2017; see Chandra *et al.,* 2019 and Melis *et al.,* 2019) for reviews). Although cross-sectional imaging studies with different PET ligands have reported single associations of cognitive performance with *in vivo* tau (Brier *et al.,* 2016, Cho *et al.,* 2016*b*; Johnson *et al.,* 2016; Ossenkoppele *et al.,* 2016; Pontecorvo *et al.,* 2017; Zou *et al.,* 2020), see Chandra *et al.,* 2019 for a review) and microglial activation (Edison *et al.,* 2008, Okello *et al.,* 2009*a,* Fan *et al.,* 2015*a,* Passamonti *et al.,* 2018*b,* 2019; Zou *et al.,* 2020); see Chandra *et al.,* 2019 for a review), less is known about their relationship to longitudinal cognitive decline. Previous PET studies in Alzheimer's dementia and MCI reported that

baseline [^{18}F]AV-1451 PET uptake correlates with cognitive decline over a period of six (Koychev *et al.,* 2017) or 18 months (Pontecorvo *et al.,* 2019). Conversely, microglial activation showed progression over 14-16 months (Fan *et al.,* 2015*b*, 2017), although the predictive value of baseline measures was not reported. Other studies using [^{11}C]-PBR28 to quantify neuroinflammation over a period of at least one year (median 2.7 years) in MCI and Alzheimer's disease reported increased microglial activation as a function of a significant worsening on the Clinical Dementia Rating scale (Kreisl *et al.,* 2016). Likewise, binding of [^{18}F]DPA-714, another TSPO PET ligand, is negatively associated with cognitive performance (Hamelin *et al.,* 2018).

Improving knowledge of how baseline measures of tau, neuroinflammation, and brain atrophy predict cognitive decline in Alzheimer's disease may inform future cost-effectiveness of studies in large and epidemiologically representative cohorts of patients. Although other studies have assessed the predictive value of different brain markers on longitudinal cognitive decline in Alzheimer's disease (see Chandra *et al.,* 2019 and Melis *et al.,* 2019 for reviews), this study compared the three biomarkers simultaneously (i.e. tau pathology, neuroinflammation, brain atrophy) in patients with amyloid-positive MCI and Alzheimer's dementia. Data in this study indicate the added value of PET imaging over and above MRI prognostic markers. Although brain atrophy in isolation is predictive for cognitive decline in Alzheimer's disease (Jack *et al.,* 2015), when models include tau burden, microglial activation and atrophy jointly, only PET was predictive. This critical result was confirmed by both frequentist and Bayesian analyses, with evidence against the added value of MRI data on predicting cognitive decline over and above PET assessments. This aligns with cross-sectional studies that report a stronger association of tau molecular imaging than structural MRI with cognitive performance in patients with Alzheimer's disease (Bejanin *et al.,* 2017; Mattsson *et al.,* 2019). More specifically, in patients with MCI and Alzheimer's dementia, Bejanin and colleagues reported an association between regional tau PET binding and cognitive impairment, which was partly mediated by grey matter volumes (Bejanin *et al.,* 2017). Cognition was equally explained by brain atrophy and tau pathology, but after accounting for grey-matter values, *in vivo* tau pathology remained correlated with cognitive performance (Bejanin *et al.,* 2017). Likewise, Mattson et al. (2019) found that both [^{18}F]AV-1451 PET and structural brain MRI are associated with cognition in Alzheimer's disease (spanning preclinical, prodromal, and dementia stages), although associations of tau PET indices were stronger than those for MRI

markers (Mattsson *et al.,* 2019). In this context, our results inform on the predictive value of molecular imaging and the corresponding pathophysiological processes on the cognitive decline across patients in the Alzheimer's disease spectrum. However, they may also build the basis for further studies focussing on individualised prediction in single cases, such as identifying thresholds that can identify those patients who will decline and at which rate in a defined time interval.

Our data suggest that posterior temporo-parietal [^{18}F]AV-1451 binding and anterior temporal [^{11}C]PK11195 binding are associated with cognitive decline. This may reflect a topographical differentiation in the relationship of neuroinflammation and tau pathology with cognitive impairment at the diagnosis and its progression. In our cohort, they do not interact in their association with cognitive decline, which suggests an additive and independent effect of the two pathological processes on clinical progression, rather than synergy. In patients with Alzheimer's disease, temporo-parietal cortical tau PET signal is consistent with Braak stage III and above, while in cognitively healthy older people, the signal is localised to entorhinal cortex and inferior temporal cortex (Cho *et al.,* 2016*a*; Johnson *et al.,* 2016; see Jagust, 2018 for a review). *Post mortem* studies have likewise reported tau deposition in the medial temporal cortex in healthy elderly people and Alzheimer's dementia (Jagust, 2018). Tau burden in the entorhinal, limbic, and temporal neocortex relates to cortical atrophy in patients with MCI and Alzheimer's disease, although not in cognitively normal controls (Timmers *et al.,* 2019). These findings suggest that tauopathy in the medial part of the temporal lobe may be an age-related norm, rather than indicative of Alzheimer's disease cognitive decline (Femminella *et al.,* 2018). For this reason, tau PET binding here may be a weaker predictor for cognitive decline than tau in the posterior temporo-parietal regions. From results of this study, we could speculate that microglial activation may have a marked impact on the global cognition deterioration since the first phases as localised in the anterior temporal pole, while tau pathology may impact on the global cognitive decline once it spreads to the posterior associative cortex. The co-occurrence with amyloid-β and neuroinflammation may induce the tau spreading from the medial temporal lobe to other cortical regions, which may be associated with downstream neurodegenerative processes and cognitive decline (Mhatre *et al.,* 2015; Jagust, 2018; Perea *et al.,* 2018). This suggests a driving role of neuroinflammation in tau spread and neurodegeneration in Alzheimer's disease (Yoshiyama *et al.,* 2007; Asai *et al.,* 2015; Maphis *et al.,* 2015), in which activated microglia facilitate tau spread (Maphis *et al.,* 2015; Perea et al. 2018). Inflammation

localised in medial temporal lobe may trigger tau pathology spreading from the same regions to posterior cortical areas. This may explain differences in tau and inflammation imaging patterns associated with cognitive decline. In addition, it is possible that the relationships between tau, neuroinflammation and cognitive progression is not constant, and that the PET biomarkers would have different prognostic relevance during pre-symptomatic, prodromal and dementia stages of Alzheimer's disease. Larger studies, or meta-analyses, would be required for adequate power to test such dynamic prognostic models. There are limitations to this study. TSPO expression in neuroinflammatory cascades is complex, and has been found not only in activated microglia but also in other cell types, like astrocytes and vascular smooth muscle cells (Gui *et al.*, 2020). However, [^{11}C]PK11195 is selective for activated microglia over quiescent microglia and reactive astrocytes (Banati, 2002), which favours its utility for imaging activated microglia. In this context, several second-generation PET radioligands for TSPO have been developed since [^{11}C]PK11195 (e.g. [^{11}C]PBR28 and [^{18}F]DPA-714), and used in human studies (Vivash and OBrien, 2016). They are characterised by higher signal-noise ratio and lower lipophilicity than [^{11}C]PK11195. However, they require genetic analysis to assess a single-nucleotide polymorphism (rs6971), which influences their binding affinity and causes heterogeneity in PET data (Dupont *et al.*, 2017). [^{11}C]PK11195 is less affected by this genetic polymorphism, especially between high and mixed affinity binders (Guo *et al.*, 2012; Kobayashi *et al.*, 2018) that represent ~90% of the Caucasian population (Owen *et al.*, 2012), although a small difference in [^{11}C]PK11195 binding in the central nervous system remains a possibility (Fujita *et al.*, 2017). Second, the cross-sectional nature of our imaging assessment does not enable a mediation analysis, or support inferences on the direction of causality between tau pathology, microglial activation progression and cognitive decline. However, both processes predict the rate of cognitive deterioration in Alzheimer's disease, suggesting their contribution in the acceleration of consequent decline. Third, the modest sample size of our cohort limited the applicability of the one-step prediction procedure with multiple predictors, which may lead to a more precise prediction than the two-step procedures. For the multivariable regression model the sample size was reduced to N=26 because of the exclusion of controls (who underwent [^{18}F]AV-1451 or [^{11}C]PK11195 PET, but not both, to limit radiation exposure). However, both frequentist and Bayesian multivariable approaches give similar results, aligning with those obtained by the one-step prediction. The convergence between the statistical models (i.e. LGCM with predictors, linear regression and Bayesian model) mitigates against sample-dependant biases on the estimation of the most parsimonious model**.** The

replication of these findings with larger and multicentre clinical cohorts will represent an important next step to establish the replicability and generalizability of the results. Fourth, the interval between cognitive assessment and imaging varied. However, I sought to mitigate this confound by including the interval in the statistical analyses, and note that the intervals were small compared with the three year follow up.

3.5. Conclusions

In conclusion, this study showed that PET markers of regional pathological processes are stronger predictors than atrophy, as measured by MRI, of clinical progression in patients with symptomatic Alzheimer's disease. The predictive models were convergent in identifying tau burden in posterior cortical regions and neuroinflammation in the anterior temporal lobe as imaging predictors of cognitive decline in the clinical spectrum of Alzheimer's disease. In contrast, atrophy predicted cognitive decline only if considered individually but not over and above the effects of tau burden and inflammation. These findings support the use of PET imaging of tau pathology and microglial activation for prognostication and patients' stratification in clinical trials.

3.6. Supplementary materials of Chapter 3

Supplementary Table 1. Counts and group comparisons between controls and patients who underwent ligand-specific PET scans on a GE Advance PET scanner (GE Healthcare, Waukesha, USA) and a GE Discovery 690 PET/CT. Chi-square tests resulted not significant for both tracers, indicating that subgroups of controls on different scanners for each ligand-specific PET were balanced with those of patients. In addition, to minimise differences in the data, the acquisition protocols (injected activity, scan duration) and image reconstruction strategies (frame durations, reconstruction algorithm) were matched between scanners. The transaxial reconstructed field of view (30 cm) and voxel dimension (2.34 mm) were invariant across scanners, as was the data analysis methodology. The use of scanners from the same manufacturer was also beneficial regarding the data corrections applied during image reconstruction.

[18F]AV-1451 PET				
		scanner PET		
		ADVANCE	**DISCOVERY**	**Total**
Group	**AD/MCI**	18	8	26
	Controls	8	6	14
Total		26	14	40
Group comparison		$\chi2(1)=0.58$; p=0.45		
[11C]PK11195 PET				
		scanner PET		
		ADVANCE	**DISCOVERY**	**Total**
Group	**AD/MCI**	18	8	26
	Controls	13	2	15
Total		31	10	41
Group comparison		$\chi2(1)=1.57$; p=0.21		

Supplementary Table 2. The fifteen Alzheimer's disease related cortical regions of interest, considered for principal component analyses. The name of each region is reported in the first column; while the second column gives the corresponding region numbers in the Hammers atlas.

Region	Numbers (R/L)
Hippocampus	1/2
Amygdala	3/4
Anterior medial temporal lobe	5/6
Anterior lateral temporal lobe	7/8
Parahippocampal gyri	9/10
Superior posterior temporal gyrus	11/12
Middle and inferior temporal gyrus	13/14
Fusiform gyrus	15/16
Insula	21/20
Posterior cingulate gyrus	27/26
Posterior temporal lobe	31/30
Inferiolateral parietal lobe	33/32
Superior parietal gyrus	63/62
Cuneus	67/66
Superior anterior temporal gyrus	83/82

Chapter 4 | Apathy, cognition and brain changes in pre-symptomatic genetic frontotemporal dementia

Preface: The contents of this chapter has been published in Malpetti et al. Apathy in presymptomatic genetic frontotemporal dementia predicts cognitive decline and is driven by structural brain changes. *Alzheimer's Dement* 2020: 1–15 - doi: 10.1002/alz.12252

A large group of researchers and clinicians as part of the multicentre GENFI initiative contributed to data collection and curation, including Dr. Timothy Rittman, Dr. John van Swieten, Dr. Barbara Borroni, Dr. Raquel Sanchez-Valle, Dr. Fermin Moreno, Dr. Robert Laforce, Dr. Caroline Graff, Dr. Matthis Synofzik, Dr. Daniela Galimberti, Dr. Mario Masellis, Dr. Carmela Tartaglia, Dr. Elizabeth Finge, Dr. Rik Vandenberghe, Dr. Alexandre de Mendonça, Dr. Fabrizio Tagliavini, Dr. Isabel Santana, Dr. Simon Ducharme, Dr. Chris Butler, Dr. Alex Gerhard, Dr. Johannes Levin, Dr. Adrian Danek, Dr. Markus Otto, Dr. Giovanni B. Frisoni, Dr. Roberta Ghidoni, Dr. Sandro Sorbi, Carolin Heller, Emily G. Todd, Dr. Martina Bocchetta, Dr. David M. Cash, Rhian S. Convery, Georgia Peakman, Dr. Katrina M. Moore, Dr. Jonathan D. Rohrer, Prof. James B. Rowe and all GENFI consortium collaborators. I performed the data analyses and wrote the text, with input from all co-authors. Simon Jones helped with imaging analyses; Prof. Rogier Kievit and Dr. Kamen Tsvetanov with methodological refinement.

Abstract: Apathy is a common feature of frontotemporal dementia that adversely affects patients' prognosis and survival. However, its role as an early marker and predictor of disease progression remains unclear. In this chapter, I test whether apathy develops in pre-symptomatic carriers of gene mutations approaching the onset of symptoms and predicts longitudinal cognitive decline. I also test whether pre-symptomatic apathy is associated with regional grey-matter atrophy. In genetic pre-symptomatic frontotemporal dementia cases, I found a significant increase in apathy scores over two years of follow-up and approaching the estimated age of onset. Lower baseline grey-matter volumes in frontal lobe and cingulate cortex were associated with more rapid progression of apathy over the following two years, which in turn predicted a

subsequent sub-clinical deterioration of cognitive performance, but not *vice versa*. This suggests that apathy may be a modifiable factor to protect cognitive function in those at risk of frontotemporal dementia.

4.1. Introduction

The clinical syndromes of frontotemporal dementia can be underpinned by different neuropathologies processes, such as 3R-Tauopahty, 4R-Tauopathy or TDP43 pathology. However, all variants present marked neuronal loss and common symptoms that may occur in early stages of disease progression. In particular, apathy is a common and disabling feature of frontotemporal dementia. It is part of the diagnostic criteria for behavioural variant of frontotemporal dementia (bvFTD) (Rascovsky *et al.,* 2011), and frequently occurs across all frontotemporal dementia variants (Mendez *et al.,* 2008; Rohrer and Warren, 2010; Coyle-Gilchrist *et al.,* 2016; Lansdall *et al.,* 2017). Apathy is a multifaceted construct that describes dysfunctional goal-directed behaviour, arising from affective, behavioural and cognitive impairments. Frontotemporal dementia has been associated with concurrent affective, behavioural, and cognitive apathy symptoms (Chow *et al.,* 2009), and worse prognosis in terms of survival (Lansdall *et al.,* 2019), disability (Kipps *et al.,* 2009, Josephs *et al.,* 2011*b*, O'Connor *et al.,* 2016*b*, 2017) and functional independence (Murley *et al.,* 2020*b*). Better understanding of the causes and consequences of apathy and its role in the clinical progression of frontotemporal dementia is vital to develop effective treatment strategies, including preventive strategies in the context of genetic risk of frontotemporal dementia.

Previous imaging studies have identified structural correlates and changes associated with apathy in frontotemporal dementia. The severity of apathy correlates with widespread atrophy in frontotemporal areas, including the dorsolateral, ventromedial and orbital prefrontal cortex and anterior cingulate cortex, insula and basal ganglia (Rosen *et al.,* 2005; Zamboni *et al.,* 2008; Eslinger *et al.,* 2012; Lansdall *et al.,* 2017, 2018; Ducharme *et al.,* 2018, Murley *et al.,* 2020*a*). Apathy has also been linked to impairments in executive function, through the diagnostic criteria (Rascovsky *et al.,* 2011), and shared anatomical correlates (Zamboni *et al.,* 2008; Eslinger *et al.,* 2012; Perri *et al.,* 2014). Severe deficits in executive function have been reported across all clinical frontotemporal dementia syndromes, with subtler impairments in the pre-symptomatic phase (Geschwind *et al.,* 2001; Rohrer *et al.,* 2015; Staffaroni *et al.,* 2020).

Executive function comprises many processes including selective attention, working memory, and planning. Although no single task can capture all these domains, common and well validated tasks that straddle cognitive domains, such as the Digit Symbol substitution task of the Wechsler Adult Intelligence Scale–Revised (WAIS-R), have proven sensitive markers for executive function related problems (Jaeger, 2018).

The causal relationship between apathy and executive function remains unclear: specifically, whether apathy predicts cognitive decline, or *vice versa*. This is especially relevant to the emergence of frontotemporal dementia symptoms in those at genetic risk. A third of patients with frontotemporal dementia present an autosomal dominant family history (Rohrer *et al.*, 2009*a*), with mutations of three main genes accounting for about a fifth of cases: MAPT, GRN, and C9orf72 (Rohrer *et al.*, 2009*a*; Greaves and Rohrer, 2019). I therefore examined longitudinal changes in apathy and their association with subclinical cognitive decline in pre-symptomatic gene carriers, in the international GENFI initiative (Rohrer *et al.*, 2015). I tested the hypothesis that apathy increases over time in pre-symptomatic carriers of frontotemporal dementia mutations, and is greater in older carriers and those closer to symptom onset. I examined the relationship between baseline and longitudinal changes in apathy and atrophy in pre-symptomatic gene carriers, versus non-carriers, and I tested the predictive value of apathy for executive function decline with latent curve modeling.

4.2. Material and Methods

4.2.1. Participants

From the GENFI study (Rohrer *et al.*, 2015), DataFreeze 4 (2019), 600 participants were included in this study: 304 pre-symptomatic mutation carriers (54 with mutation in MAPT, 142 in GRN, and 108 in C9orf72), and 296 family members without mutations (non-carrier control group). They all underwent the GENFI standardised assessment. During the first visit, demographic information of all participants was collected, and information regarding clinical background (neuropsychiatric features, family and medical history, medication and onset symptoms). The years to the expected symptom onset (EYO) for each subject was defined by the mean within each family of affected relatives (Rohrer *et al.*, 2015), while acknowledging that this is a weak predictor in GRN and C9orf72 families (Moore *et al.*, 2020). Participants underwent a clinical and cognitive assessment to evaluate the symptomatic status and the

cognitive performance at the baseline and annually for two years. This included structured clinical examination and ratings of behavioural and neuropsychiatric symptoms (i.e. depression) by clinicians (including sub-sections of the frontotemporal lobar degeneration clinical dementia rating scale; range 0-3). Behavioural symptoms were assessed using the revised Cambridge Behavioural Inventory (CBI-R). In GENFI study, which does not specifically focus on apathy, we have two relevant measures for my study: the clinician rating for apathy (range: 0-3) and CBI-R motivation/apathy subscale. In GENFI patients (N=168), they are highly associated (Independent Samples Kruskal-Wallis Test=68.3, $p<0.0001$). However, the clinician scale is insensitivity to pre-symptomatic states. Then, I used the apathy/motivation subscale of the revised Cambridge Behavioural Inventory (CBI-R) (Wear *et al.,* 2008), which has been employed in previous studies with frontotemporal dementia patients (Van Langenhove *et al.*, 2016, O'Connor *et al.,* 2016*b*; Lansdall *et al.*, 2017; O'Connor *et al.*, 2017). This subscale assesses patients' apathy severity through their carers' responses on loss of enthusiasm in personal interests, reduced interest in new things or maintaining social relationships, and indifference to family members. With my main focus on apathy, I excluded subjects without CBI-R scores across visits (N = 53) from the initial DataFreeze 4 (N = 653). I used the WAIS-R Digit Symbol test as a sensitive measure for executive function. For each test, I calculated z-scores based on control group data at the baseline.

4.2.2. Imaging data acquisition and pre-processing

In DataFreeze 4, 573 out of 600 participants included in this study had at least one volumetric T1-weighted MRI scan on 3T (or 1.5T scanners at sites where 3T scanning was not available) within two years of follow-up. Magnetization Prepared Rapid Gradient Echo (MPRAGE) images were acquired at each site accommodating different manufacturers and field strengths (Rohrer *et al.,* 2015). Grey-matter regional volumes were extracted from the subcortical segmentation and cortical parcellation labelled by the Desikan-Killiany Atlas in Freesurfer 6.0 (surfer.nmr.mgh.harvard.edu/). For cases with more than one scan, all available follow-up images were included in the processing with the longitudinal stream in Freesurfer, creating an unbiased within-subject template for case-specific segmentation (Reuter *et al.,* 2012). Regional volumes were combined into bilateral frontal, temporal (including amygdala and hippocampus), parietal and occipital lobes, insula cortex, cingulate cortex, subcortical central structures (basal ganglia and thalamus) and brainstem. Carriers' volumes were Z-scored with reference to non-carriers. Total intracranial volume was estimated as the sum of grey matter,

white matter, and cerebrospinal fluid segmentations using the Computational Anatomy Toolbox (CAT12 - http://www.neuro.uni-jena.de/cat/) within Statistical Parametric Mapping software (SPM12 - http://www.fil.ion.ucl.ac.uk/spm/). CAT12 also provides imaging quality ratings considering noise, motion, and spatial resolution. Raw and segmented data were visually inspected, and images with significant artefacts, or parcellation failure were excluded, asserting that all scans included in the analyses had CAT12 imaging quality ratings higher than 74/100 (mean: 84.2, standard deviation: 1.3, range: 74 to 87).

4.2.3. Statistical analyses

Descriptive statistics. Baseline age, education, EYO, CBI-R apathy scores, and Digit symbol scores were compared between groups with a two independent-samples t-test. Sex was compared between groups with Chi-square test. Within the two groups, for participants who presented scores > 0 at a depression severity clinical evaluation (0-3; N=38 non-carriers, N=43 pre-symptomatic carriers), I tested the baseline association between depression and apathy with the Independent Samples Kruskal-Wallis Test.

Latent Growth Curve Model (LGCM). Univariate LGCMs were fitted to the combined data from 3-waves of longitudinal behavioural/cognitive and imaging assessments, to test the relationships between apathy, cognition, and brain volumes. The LGCM provides insight into baseline scores, change and individual differences by estimating (i) an intercept, which represents the initial level of the outcome measures; (ii) a slope, quantifying the rate of change; (iii) a variance of the intercept and slope, capturing individual differences in baseline and change over time and (iv) the relation between intercept and slope, i.e. how the initial level is associated with the rate of change over time. Predictors can be added to the model to assess their effects (as an interaction) with intercept and/or slope. LGCM guidelines recommend ≥3 time points and ≥5 cases per parameter (Newsom, 2015). These requirements were met by our data and analyses. Our LGCM were estimated in the Lavaan software (Rosseel, 2012) using full information maximum likelihood with robust standard errors to deal for missingness and non-normality.

For each model, I considered three main model fit indices (Schermelleh-Engel *et al.*, 2003): (1) the root-mean-square error of approximation (RMSEA, acceptable fit: < 0.08, good fit: < 0.05), (2) the comparative fit index (CFI, acceptable fit: 0.95–0.97, good fit: > 0.97), and (3) the standardized root mean-square residual (SRMR, acceptable fit: 0.05–0.10, good fit: < 0.05). I

also report the model chi-square test (χ^2), noting this index is sensitive to the sample size and is liable to reject models of large cohorts (good fit: low values and $p > 0.05$) (Schermelleh-Engel *et al.*, 2003). I also report the ratio between chi-square and degrees of freedom (χ^2/df) as alternative model fit index (acceptable fit: < 2, good fit: < 3) (Schermelleh-Engel *et al.*, 2003).

LGCM of apathy and cognitive decline. In all models, the intercept was centred at baseline and a linear slope was tested. CBI-R apathy scores and Digit symbol scores at follow-up visits were annualised and recomputed at one and two years to adjust for small differences in intervals. EYO was included as a predictor of both intercept and slope, and the genetic status used to define groups. I applied four different LGCMs to behavioural and cognitive data: (1) on the longitudinal CBI-R apathy subscale scores; (2) as the previous with baseline Digit Symbol as predictor; (3) on the longitudinal Digit Symbol scores; (4) as the previous with baseline CBI-R apathy subscale scores as predictor.

First, a LGCM was fitted on the CBI-R apathy z-scores, estimating the parameters freely in a multigroup model defined by genetic diagnoses. This model was compared to one that was fitted by constraining the relevant parameters (e.g. the slope) to be equal between the two groups. To test the difference in fit between the group equality constrained model between pre-symptomatic carriers and non-carriers on the annual rate of change (slope), I used Akaike Information Criteria (AIC), which penalizes for model complexity. Second, baseline Digit Symbol scores were added to the model as predictor of both intercept and slope of apathy, to test the predictive value of baseline cognitive performance on longitudinal change in apathy. An analogous approach was applied to the longitudinal and annualised Digit Symbol z-scores: first, the initial LGCM with EYO as predictor of the intercept and slope was fitted in a multigroup model by freely estimating all parameters; second, I compared this free model with a model where I constrain key parameters to test for between-group differences; and lastly, baseline CBI-R apathy scores were added to the model as predictor variable on intercept and slope.

LGCM for structural brain changes. I applied eight independent univariate LGCMs to estimate longitudinal changes in grey-matter volumes of frontal, temporal, parietal and occipital lobes, insular cortex, cingulate cortex, subcortical central structures and brainstem. As for the behavioural and cognitive scores, all grey-matter values at follow-up visits were recomputed at one and two years to adjust for small differences in retest interval. In all models, the intercept

was centred at baseline and a linear slope was tested. EYO and TIV were included as predictors of both intercept and slope. Genetic status (pre-symptomatic carrier versus non-carrier) defined the groups. When change is homogeneous, or modelled in smaller subgroups, LGCM estimation may occasionally yield improper solutions (i.e. impossible values such as negative variances) which necessitate imposing constraints to achieve proper solutions. These will be noted when necessary. In pre-symptomatic carriers, I applied a bivariate LGCM model on longitudinal apathy scores and longitudinal grey-matter volumes in each of the brain regions that changed over time. With the bivariate LGCM it is possible to investigate the association between the annual rates of change (slopes) in the two variables considered, but also the associations between initial scores (intercepts) and the longitudinal changes.

4.3. Results

4.3.1. Descriptive statistics

Demographic and clinical characteristics at baseline are summarised in **Table 11**. Pre-symptomatic carriers had higher baseline apathy scores (p=0.015), and were slightly younger (p=0.044) than non-carriers. Descriptive statistics are reported in **Table 11**. At baseline, depression severity and CBI-R apathy scores were not significantly associated in either non-carriers (N=38, range depression scores: 0.5-3; Test(3)=4.134, p=0.247) or pre-symptomatic carriers (N=43, range depression scores: 0.5-2; Test(2)=1.129, p=0.569).

***Table 11**. Demographic and clinical characteristics at the baseline for pre-symptomatic gene carriers and non-carrier subjects. P values are the result of t-test or χ2 tests as appropriate.*

	Pre-symptomatic carriers	**Non-carriers**	**p-value**
N	304	296	
Age (years - mean ± SD)	44.5±12.1	46.6±14.0	0.044
Sex (Female/Male)	187/117	174/122	0.495
Education (years - mean ± SD)	14.3±3.4	13.9±3.6	0.108
Estimated Years from symptoms Onset (years - mean ± SD)	-14.0±12.1	-13.0±14.1	0.347
CBI-R Apathy Baseline (mean ± SD)	0.3±1.5	0.0±1.0	0.015
Digit Symbol Baseline (mean ± SD)	0.1±0.9	0.1±1.0	0.948

Abbreviations CBI: Cambridge Behavioural Inventory; SD: standard deviation

4.3.2. LGCM on longitudinal apathy scores

The LGCM on longitudinal CBI-R apathy scores fitted the data well ($\chi^2(11)=11.59$, p=0.395, $\chi^2/df=1.05$, RMSEA=0.025 [0.000 – 0.119], CFI=0.99, SRMR=0.082), after imposing a necessary constraint (slope variance and intercept-slope covariance to zero) in non-carriers. There was a significant increase in apathy scores over time in pre-symptomatic carriers (estimate est=0.511, standard error SE=0.177, z-value= 2.879, p=0.004), but not in non-carriers (est= 0.084, SE=0.081, z-value= 1.036, p=0.300) (**Figure 12**). Comparing the free *versus* constrained models, the groups differed significantly in the rate of change of apathy ($\Delta\chi^2$= 10.14, Δdf=1, p=0.0015). EYO was associated with initial values (intercept) of apathy in pre-symptomatic carriers (est=0.154, SE=0.70, z-value=2.192, p=0.028) and non-carriers (est= 0.109, SE=0.044, z-value= 2.468, p=0.014) (**Figure 13A** – left graph), reflecting its association with age in both groups. The effect of EYO on apathy slope in pre-symptomatic carriers was not significant (est= 0.170, SE=0.092, z-value= 1.834, p=0.067; **Figure 13A** – right graph). Including baseline Digit Symbol scores as predictor, the model fitted the data well ($\chi^2(13)=15.02$, p=0.306, $\chi^2/df=1.56$, RMSEA=0.040 [0.000 – 0.113], CFI=0.98,

SRMR=0.073). In pre-symptomatic carriers, baseline cognitive performance did not influence the rate of change in apathy (est=-0.133, SE=0.134, z-value=-0.988, std all=-0.140, p=0.323).

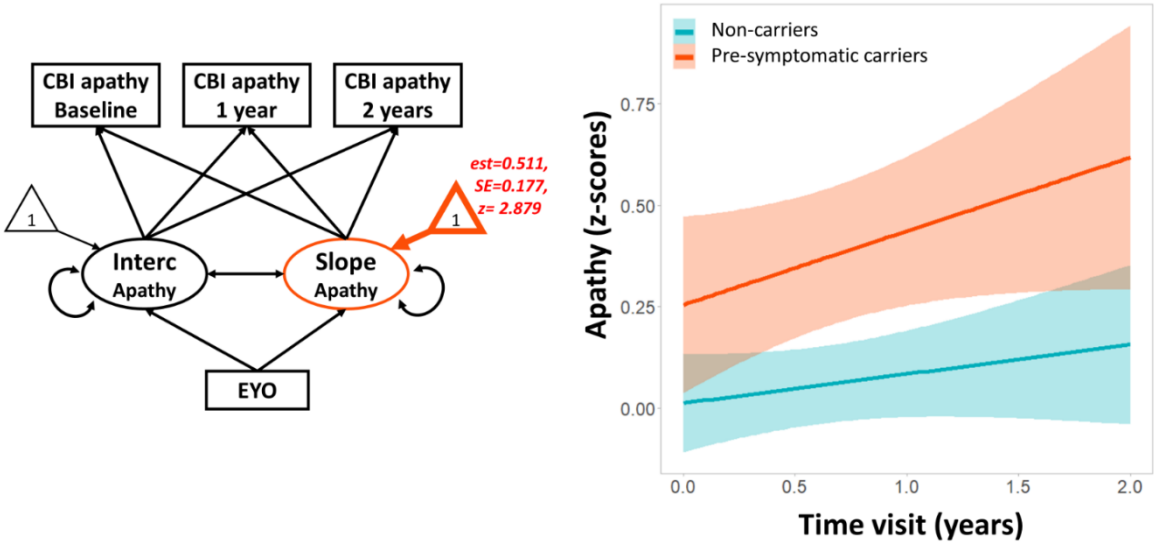

Figure 12. *Longitudinal increase in apathy scores over 2-year period in pre-symptomatic carriers (red) and non-carriers (blue). On the left, the latent growth curve model applied to test longitudinal changes in apathy levels, as assessed by the apathy sub-scale of the revised Cambridge Behavioural Inventory (CBI) over two years of follow-up, including the estimated years from onset (EYO) as covariate. Estimated regression values in pre-symptomatic group are reported in italics (est=estimate; SE=standard error; z=z-value). The graph on the right represents the raw data at group level for apathy scores (y axis) over 2-year follow-up visits (x axis). Individuals' data are not plotted, to protect anonymity.*

4.3.3. LGCM on longitudinal cognition

The LGCM on longitudinal Digit Symbol scores fitted the data adequately ($\chi^2(11)=24.39$, p=0.011, $\chi^2/df=2.22$, RMSEA=0.078 [0.036 – 0.120], CFI=0.97, SRMR=0.034), after constraining slope variance and intercept-slope covariance to zero in non-carriers. The rate of decline was significant in pre-symptomatic carriers (est=-0.077, SE=0.031, z-value=-2.487, p=0.013), but not in non-carriers (est= 0.002, SE=0.023, z-value= 0.107, p=0.915). Comparing the models confirmed that groups differed significantly in the rate of cognitive decline ($\Delta\chi^2$ = 3.912, $\Delta df=1$, p=0.04796). EYO was associated with initial values of executive performance in pre-symptomatic carriers (est=-0.303, SE=0.038, z-value=-7.885, p<0.001) and non-carriers (est= -0.279, SE=0.039, z-value= -7.150, p<0.001) groups (**Figure 13B** – left graph). EYO also modulated the rate of decline in pre-symptomatic carriers (est=-0.098, SE=0.024, z-value=-4.152, p<0.001). Including baseline CBI-R apathy scores as predictor, the model fitted the data

well ($\chi^2(13)=29.29$, p=0.006, $\chi^2/df=2.25$, RMSEA=0.076 [0.039 – 0.113], CFI=0.97, SRMR=0.030). The model identified a significant decline in pre-symptomatic carriers only (est=-0.064, SE=0.031, z-value=-2.095, p=0.036; **Figure 14**), with a significant effect of the baseline apathy severity on the rate of cognitive decline (est=-0.038, SE=0.014, z-value=-2.652, std all=-0.395, p=0.008), but not on the intercept (est=-0.053, SE=0.033, z-value=-1.594, std all=-0.102, p=0.111).

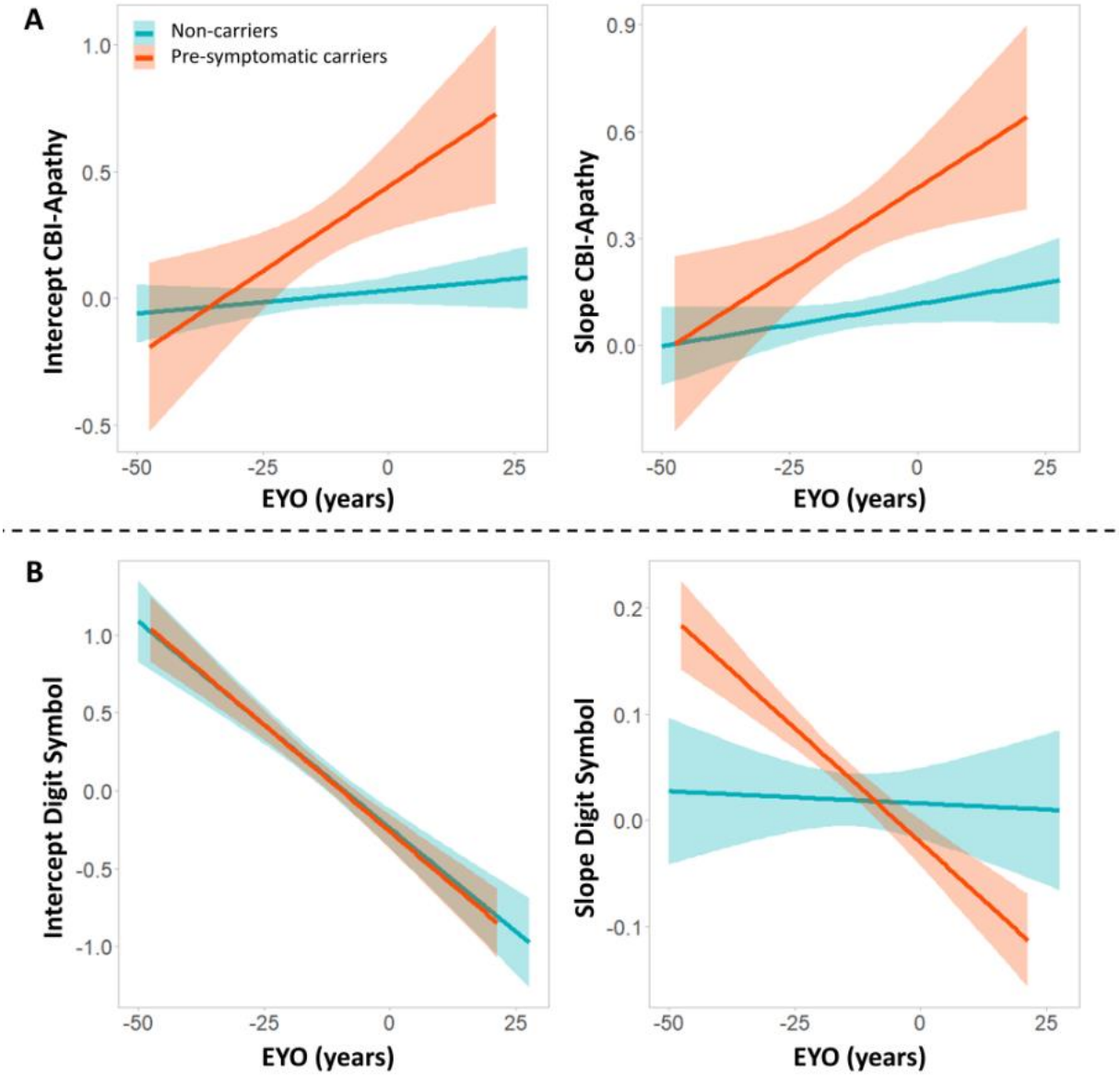

Figure 13. *Cross-sectional and longitudinal changes in apathy and executive function in pre-symptomatic carriers (red) and non-carriers (blue). Panel A: graphs represent the relationships of the estimated initial scores ("intercept" – left graph) and the annual rate of change ("slope" – right graph) in apathy scores with the estimated years from onset (EYO). Panel B: graphs represent the relationships of the estimated intercept (left graph) and slope (right graph) in executive function with estimated years to onset (EYO). Individuals' data are not plotted, to protect anonymity.*

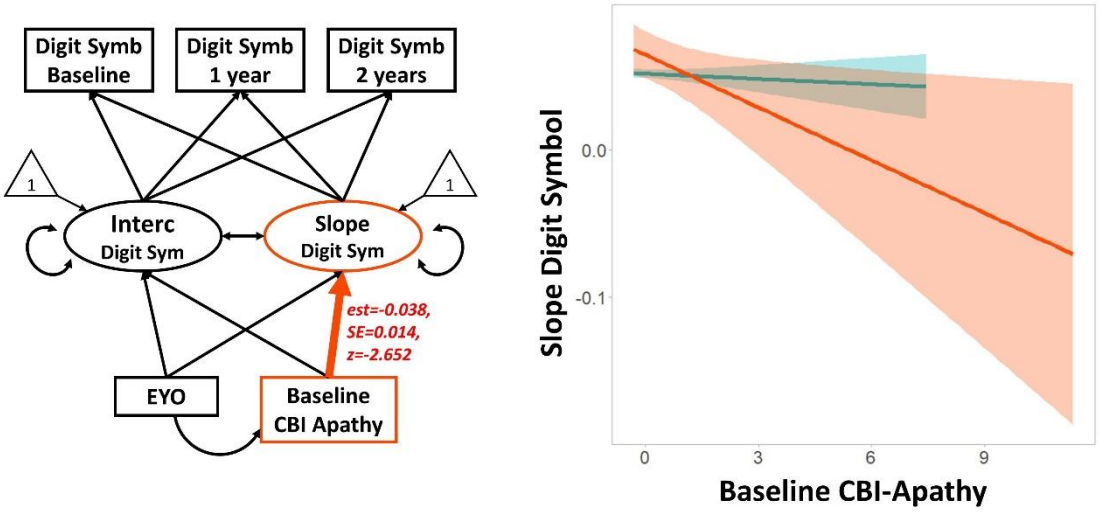

Figure 14. *Effect of baseline apathy on annual rate of change in executive function. On the left, the latent growth curve model applied to test the predictive value of baseline apathy levels, as assessed by the apathy sub-scale of the revised Cambridge Behavioural Inventory (CBI), for longitudinal cognitive decline, estimated from Digit Symbol (Digit Symb) test scores over two years of follow-up. The estimated years from onset (EYO) was included as covariate in the model. Estimated regression values in pre-symptomatic group are reported in italics (est=estimate; SE=standard error; z=z-value). The graph on the right represents the relationship between the estimated annual rate of change in executive function (y axis) and the baseline apathy scores (x axis). Individuals' data are not plotted, to protect anonymity.*

4.3.4. LGCMs on longitudinal grey-matter brain volumes

Model fit indices for LGCMs on brain volumes in cortical and subcortical regions, and the estimated slope for both pre-symptomatic carrier and non-carrier groups, are reported in **Table 12**. In summary, for non-carriers there were no significant structural changes in the regions of interest. In contrast, pre-symptomatic carriers showed progressive atrophy, which was significantly different from the non-carrier group, in frontal, temporal, and parietal lobes, cingulate cortex and in subcortical central structures, but not in occipital lobe and brainstem. Insular cortex showed longitudinal decline in the pre-symptomatic group, but this did not significantly differ from non-carriers' rate of change. In the model on parietal lobe values, the slope variance term was constrained to zero in non-carriers to make the model converge correctly. In **Table 13**, I also report an exploratory analysis including the gene mutations as grouping variable in the univariate LGCMs, to estimate longitudinal changes by gene.

Table 12. *Model fit indices and estimated slopes of Latent Growth Curve Models on longitudinal brain volumes in non-carriers (Non-Car) and in pre-symptomatic carriers (Pres-Car).*

	Frontal	**Temporal**	**Parietal**	**Occipital**	**Insula**	**Cingulate**	**Central Structures**	**Brainstem**
χ^2	24.82	17.01	21.14	15.38	8.56	16.68	18.20	16.21
χ^2/df	2.26	1.55	1.76	1.40	0.78	1.52	1.66	1.47
RMSEA	0.068 [0.03-0.10]	0.049 [0.00-0.09]	0.058 [0.00-0.098]	0.041 [0.00-0.09]	0.00 [0.00-0.06]	0.043 [0.00-0.08]	0.053 [0.00-0.10]	0.048 [0.00-0.09]
CFI	0.99	1.00	0.99	1.00	1.00	1.00	1.00	1.00
SRMR	0.013	0.013	0.011	0.013	0.009	0.005	0.004	0.014
Slope Non-Car (est, SE, z, p)	-0.015, 0.011, -1.381, p=0.167	-0.016, 0.011, -1.458, p=0.145	0.013, 0.009, 1.434, p=0.151	0.014, 0.013, 1.141, p=0.254	-0.006, 0.009, -0.676, p=0.499	-0.006, 0.006, -0.997, p=0.319	-0.010, 0.007, -1.340, p=0.180	0.020, 0.011, 1.802, p=0.071
Slope Pres-Car (est, SE, z, p)	**-0.069, 0.012, -5.907, p<0.001***	**-0.047, 0.011, -4.459, p<0.001***	**-0.025, 0.012, -2.148, p=0.032***	0.017, 0.012, 1.371, p=0.170	**-0.020, 0.009, -2.156, p=0.031***	**-0.031, 0.007, -4.584, p<0.001***	**-0.052, 0.007, -7.079, p<0.001***	0.017, 0.010, 1.713, p=0.087
$\Delta\chi^2$ models constraining the slope to equality between groups (p value)	**13.61 (0.0002)***	**4.52 (0.034)***	**6.04 (0.014)***	0.02 (0.877)	1.06 (0.302)	**8.17 (0.004)***	**28.39 (9.94e-08)***	0.06 (0.806)

Abbreviations: Non-Car=Non-Carriers; Pres-Car=Pre-symptomatic carriers; χ2=chi-square test; df=degrees of freedom; RMSEA=root-mean-square error of approximation; CFI=comparative fit index; SRMR=standardized root mean-square residual; est=estimate; SE=standard error; z=z-value; p=p value

Table 13. *Model fit indices and estimated slopes of Latent Growth Curve Models on longitudinal brain in pre-symptomatic carriers by gene groups.*

	Frontal	**Temporal**	**Parietal**	**Occipital**	**Insula**	**Cingulate**	**Central structures**	**Brainstem**
χ^2	24.13	29.49	39.18	63.70	24.79	20.71	52.74	51.48
χ^2**/df**	1.42	1.64	2.18	3.54	1.46	1.15	2.93	2.86
RMSEA	0.063 [0.00-0.12]	0.080 [0.02-0.13]	0.111 [0.06-0.16]	0.156 [0.12-0.20]	0.068 [0.00-0.12]	0.039 [0.00-0.10]	0.138 [0.096-0.18]	0.134 [0.09-0.18]
CFI	0.99	0.99	0.98	0.95	0.99	1.00	0.97	0.97
SRMR	0.029	0.015	0.018	0.029	0.012	0.008	0.011	0.023
Slope C9orf72 (est, SE, z, p)	**-0.071, 0.016, -4.574, p<0.001***	**-0.080, 0.014, -5.696, p<0.001***	-0.020, 0.019, -1.036, p=0.300	0.018, 0.024, 0.762, p=0.446	**-0.067, 0.016, -4.123, p<0.001***	**-0.043, 0.009, -4.750, p<0.001***	**-0.073, 0.011, -6.884, p<0.001***	0.005, 0.016, 0.331, p=0.741
Slope GRN (est, SE, z, p)	**-0.052, 0.016, -3.180, p=0.001***	-0.021, 0.014, -1.525, p=0.127	-0.022, 0.015, -1.469, p=0.142	0.029, 0.017, 1.756, p=0.079	0.009, 0.011, 0.812, p=0.417	**-0.028, 0.010, -2.931, p=0.003***	**-0.048, 0.011, -4.527, p<0.001***	0.021, 0.012, 1.744, p=0.081
Slope MAPT (est, SE, z, p)	**-0.113, 0.033, -3.458, p=0.001***	**-0.088, 0.026, -3.312, p=0.001***	**-0.069, 0.021, -3.225, p=0.001***	-0.024, 0.020, -1.183, p=0.237	-0.012, 0.026, -0.473. p=0.637	**-0.026, 0.014, -1.913, p=0.056**	-0.023, 0.018, -1.259, 0.208	0.021, 0.028, 0.756, p=0.450
$\Delta\chi^2$ models constraining the slope to equality between groups (p value)	2.95 (0.229)	**13.89 (0.00096)***	4.29 (0.117)	4.03 (0.135)	**12.74 (0.0017)***	1.35 (0.509)	4.49 (0.106)	0.49 (0.745)

Abbreviations: Non-Car=Non-Carriers; Pres-Car=Pre-symptomatic carriers; χ2=chi-square test; df=degrees of freedom; RMSEA=root-mean-square error of approximation; CFI=comparative fit index; SRMR=standardized root mean-square residual; est=estimate; SE=standard error; z=z-value; p=p value

4.3.5. Bivariate LGCMs on apathy scores and grey-matter brain volumes

In the previous models of brain changes, significant longitudinal changes in apathy and atrophy were identified in the pre-symptomatic group only. I therefore applied five new, bivariate, LGCMs of longitudinal apathy and atrophy of frontal, temporal and parietal lobes, cingulate cortex and the subcortical structures, constraining the covariance term between apathy intercept and slope to zero in all models to ensure proper solutions. I reported model fit indices and estimated covariance parameters for all brain regions in **Table 14**. In summary, the progression of apathy was associated with baseline grey-matter volumes in frontal lobe (est=-0.208, SE=0.100, z=-2.077, std est=-0.348, p=0.038) and cingulate cortex (est=-0.139, SE=0.058, z=-

2.085, std est=-0.237, p=0.037) (**Figure 15**). Comparing the bivariate LGCMs with and without constraining the estimation of covariance between brain volume intercept and progressive apathy to zero, freely estimating the association between brain structure and apathy change improved model fit for both frontal lobe ($\Delta\chi^2$ = 5.056, Δdf=1, p=0.025) and cingulate cortex ($\Delta\chi^2$ = 7.206, Δdf=1, p=0.007) grey-matter volumes. With reduced sample sizes in gene specific sub-groups, the LGCM method is not suitable for gene-specific analysis in this dataset. Larger future datasets in GENFI, or merged datasets between genetic frontotemporal dementia cohort studies, may enable gene-specific modelling.

Table 14. *Model fit indices and estimated covariance parameters of Bivariate Latent Growth Curve Models on longitudinal apathy scores (Ap) and longitudinal brain volumes (Br).*

	Frontal	**Temporal**	**Parietal**	**Cingulate**	**Central Structures**
χ^2	31.19	36.53	35.10	31.91	31.83
χ^2/df	1.73	2.03	1.95	1.77	1.68
RMSEA	0.066 [0.02-0.10]	0.079 [0.04-0.12]	0.075 [0.04-0.11]	0.069 [0.03-0.11]	0.068 [0.02-0.11]
CFI	0.98	0.97	0.97	0.98	0.98
SRMR	0.105	0.111	0.111	0.109	0.114
Intercept Ap ~~ Intercept Br (est, SE, z, p)	-0.067, 0.093, -0.723, p=0.469	0.025, 0.089, 0.280, p=0.780	0.023, 0.062, 0.368, p=0.713	0.037, 0.058, 0.647, p=0.518	0.027, 0.128, 0.210, p=0.834
Slope Ap ~~ Intercept Br (est, SE, z, p)	**-0.208, 0.100, -2.077, p=0.038***	-0.133, 0.080, -1.662, p=0.097	-0.121, 0.069, -1.735, p=0.083	**-0.139, 0.058, -2.085, p=0.037***	-0.090, 0.082, -1.094, p=0.274
Slope Br ~~ Intercept Ap (est, SE, z, p)	0.002, 0.048, 0.045, p=0.964	-0.018, 0.025, -0.716, p=0.474	0.011, 0.026, 0.424, p=0.672	-0.023, 0.018, -1.304, p=0.192	0.024, 0.030, 0.791, p=0.429
Slope Ap ~~ Slope Br (est, SE, z, p)	-0.003, 0.045, -0.070, p=0.944	0.007, 0.017, 0.447, p=0.655	-0.006, 0.023, -0.268, p=0.789	-0.016, 0.013, -1.176, p=0.240	-0.047, 0.033, -1.435, p=0.151

Abbreviations: Ap=apathy; Br=brain; χ2=chi-square test; df=degrees of freedom; RMSEA=root-mean-square error of approximation; CFI=comparative fit index; SRMR=standardized root mean-square residual; est=estimate; SE=standard error; z=z-value; std est=standard estimate; p=p value

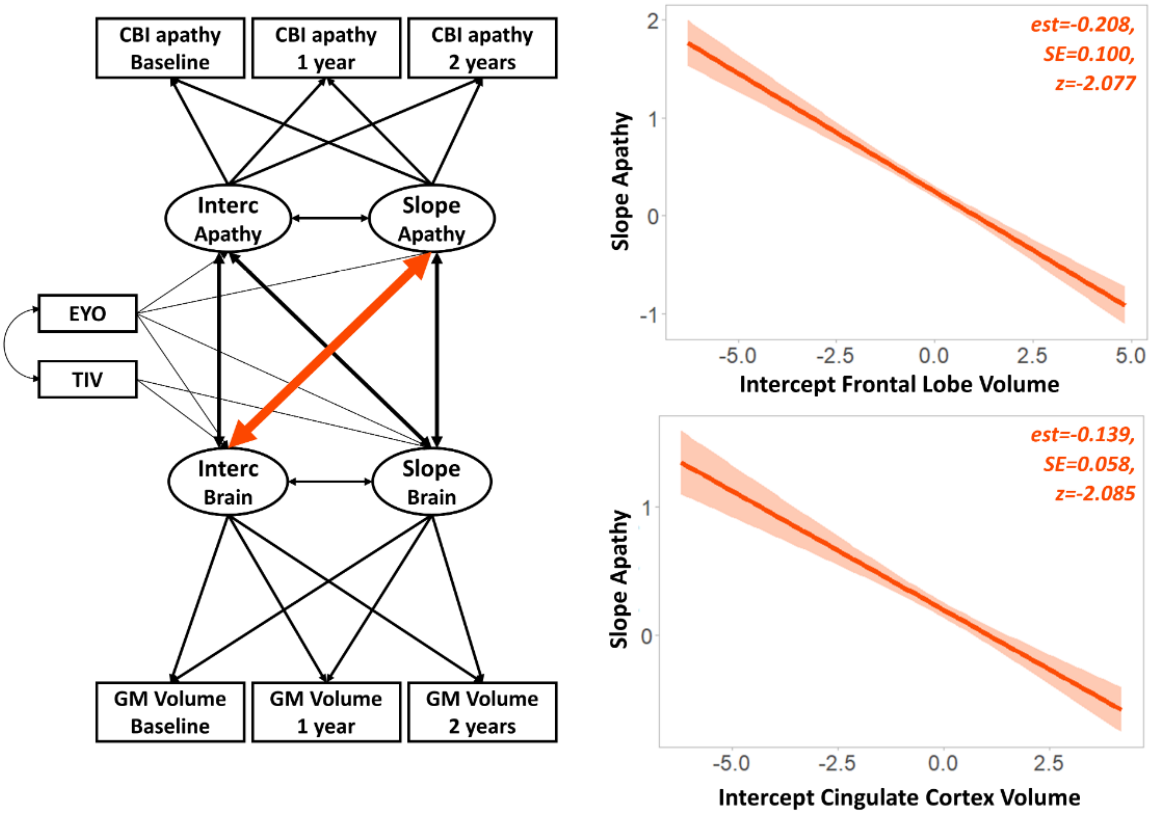

Figure 15. *Bivariate latent growth curve model. On the left, the bivariate latent growth curve model (LGCM) applied to test the relationship between longitudinal changes in apathy, as assessed by the apathy-subscale of the revised Cambridge Behavioural Inventory (CBI), and in grey-matter (GM) volumes over two years of follow-up. The graphs on the right represent the significant regressions identified by the bivariate LGCMs: annual rate of change in apathy scores (slope – y axis) was associated with baseline grey-matter volumes in frontal lobe (x axis – top graph) and cingulate cortex (x axis – bottom graph). Estimated regression values in pre-symptomatic group are reported in italics (est=estimate; SE=standard error; z=z-value). Individuals' data are not plotted, to protect anonymity.*

4.4. Discussion

In this study we found that apathy progresses significantly in presymptomatic carriers of mutations associated with FTD, and that individual differences in apathy at baseline predict the severity of progressive deterioration of performance on the Digit Symbol test over time. In presymptomatic carriers, the progression of apathy over 2 years is associated with atrophy of the frontal lobe and cingulate gyrus at baseline. In contrast, subclinical cognitive impairments, as assessed with low performance at Digit Symbol test, do not predict the worsening of apathy.

Apathy is one of the most prevalent symptoms in patients with frontotemporal dementia syndromes (Johnson and Kumfor, 2018), and is associated with negative outcomes, such as cognitive and functional decline, decreased quality of life, loss of independence and poorer survival (Zamboni *et al.,* 2008; Eslinger *et al.,* 2012; Perri *et al.,* 2014; Lansdall *et al.,* 2019, Murley *et al.,* 2020*b*). Here I examine the causal relationships between apathy and cognitive decline, through preditive modelling of longitudincal change. Moreover, I do so in the context of the long pre-symptomatic phase of frontotemporal dementia pathology, lasting many years before dementia onset (Rohrer *et al.,* 2015; Jiskoot *et al.,* 2016; Cash *et al.,* 2018, Jiskoot *et al.,* 2018*a,* 2019; Olney *et al.,* 2019; Panman *et al.,* 2019; Rittman *et al.,* 2019; Staffaroni *et al.,* 2020). Among ~300 carriers, subclinical apathy worsened over two years, and was more severe in older carriers. This effect was especially evident if timed with respect to the estimated year of onset of dementia. In contrast, their relatives without mutations did not show emergence of apathy. Carriers showed a similarly faster decline in executive function, before the critical functional threshold that underlines the diagnosis of dementia (Geschwind *et al.,* 2001; Rohrer *et al.,* 2015; Jiskoot *et al.,* 2016, 2018*b*; Olney *et al.,* 2019; Staffaroni *et al.,* 2020). The rate of cognitive decline was predicted by baseline apathy, but not *vice versa*, consistent with a causal effect of apathy on cognitive deterioration, over and above the presence of apathy as early manifestation of the mutations.

Among the gene carriers, baseline grey-matter volume of frontal lobe and cingulate cortex predicted the faster progression of apathy over two years. Apathy therefore represents an early neurobehavioral biomarker of brain changes related to frontotemporal dementia. Rohrer et al. (Rohrer *et al.,* 2015) reported cross-sectional atrophy in pre-symptomatic and symptomatic carriers of mutations in MAPT, GRN, or C9orf72. In relation to estimated year of onset of dementia, there was early volume loss of the insula and temporal lobe (~10 years before

expected symptoms onset), followed by the frontal lobe and subcortical structures (~5 years before expected onset), parietal and cingulate gyrus (around time of expected onset), and occipital lobe (~5 years after expected onset). However, cross-sectional studies are not reliable indicators of longitudinal change. In this larger and longitudinal sample of pre-symptomatic carriers, the cross-sectional and longitudinal data are concordant on the progression of apathy and atrophy, and their association.

I pooled the analyses over the pathogenic mutations of MAPT, GRN and C9orf72. Although MAPT mutation only is highly associated with tauopathy, while GRN and C9orf72 are typically related to TDP-43 pathology, in this study I included all three genetic variants. My aim was to determine the predictive value of structural MRI on apathy, and the prognostic value of the latter on cognitive decline in clinically unimpaired participants with one of these mutations, independently from the specific mutation they carried. This to determine the cross-diagnostic value of these tools to predict clinical progression in the pre-symptomatic phase of a spectrum characterised by complex clinico-pathology correlations like frontotemporal dementia. In addition, the sample size of the genetic subgroups was not sufficient for valid LCGM modelling of separate gene effects, and I could not use this method with only 304 pre-symptomatic carrier participants (54 with MAPT mutations, 142 with GRN mutations and 108 with C9orf72 mutations) to compare gene effects or explore gene-specific effects on the relationship between apathy, cognition and brain changes. There is evidence of genetic moderation of apathy in dementia, such as APOEe4 in Alzheimer's disease (Del Prete *et al.*, 2009), as well as C9orf72 and GRN mutations in frontotemporal dementia (Woollacott and Rohrer, 2016). For example, 88% of patients with C9orf72 expansions are reported to have severe apathy (Snowden *et al.*, 2012), often as a symptom at presentation (Mahoney *et al.*, 2012) (see for review (Takada and Sha, 2012)). Apathy has been reported in 69% of patients with GRN mutations (Le Ber *et al.*, 2008), but it may be less common with MAPT mutations (Piguet *et al.*, 2004; Snowden *et al.*, 2015; Woollacott and Rohrer, 2016). Although apathy is sometimes reported as more common than disinhibition (Snowden *et al.*, 2015), apathy and disinhibition are strongly positively associated (Murley *et al.*, 2020*a*).

There are several limitations to the study. Apathy is a multidimensional construct that is often considered in terms of affective, cognitive, and behavioural components, leading to reduced goal-directed behaviours. These apathy domains have been identified in patients with FTD,

and are associated with lesions or dysfunction involving the fronto-subcortical networks(Levy and Dubois, 2006; Ducharme *et al.*, 2018). We quantified apathy from the subscale of CBI-R, as it was the principal measure for apathy available in pre-symptomatic cases from the GENFI study. Although this has been successfully employed in previous studies on FTD, and more recently also in pre-symptomatic FTD(Tavares *et al.*, 2020), this questionnaire is not designed to tease apart the sub-components of apathy. In addition, as for other carer ratings scales, the emotional distress, personal background and awareness about the illness may bias the carer's evaluation. However, our results align with evidence in symptomatic FTD patients, showing an early association of apathy reported by patients' carers with frontal and cingulate grey-matter volume degeneration(Ducharme *et al.*, 2018, Passamonti *et al.*, 2018*a*). Similarly, in patients with syndromes of frontotemporal lobar degeneration including FTD, Lansdall et al. reported a significant association of carers' ratings for apathy with diffuse atrophy in fronto-striatum, cingulate and temporal regions(Lansdall *et al.*, 2017). Overall these findings suggest a clinicopathological association between apathy severity reported by carers, and neurodegeneration in key regions associated with motivation. The GENFI study did not include self-rated scales for apathy, which rely on insight and introspection abilities that may lack in patients with FTD. However, future studies on the pre-symptomatic phase of FTD may consider to also investigate longitudinal changes in self-rating apathy scores and multimodal apathy assessments (e.g., behavioural tests, computer tasks, patient and carer's ratings and questionnaires) to estimate separate domains of the multidimensional construct of apathy, and their associations with cognitive decline.

There are several limitations to the study. Apathy is a multidimensional construct that is often considered in terms of affective, cognitive, and behavioural components, leading to reduced goal-directed behaviours. These apathy domains have been identified in patients with FTD, and are associated with lesions or dysfunction involving the fronto-subcortical networks(Levy and Dubois, 2006; Ducharme *et al.*, 2018). We quantified apathy from the subscale of CBI-R, as it was the principal measure for apathy available in pre-symptomatic cases from the GENFI study. Although this has been successfully employed in previous studies on FTD, and more recently also in pre-symptomatic FTD (Tavares *et al.*, 2020), this questionnaire is not designed to tease apart the sub-components of apathy. In addition, as for other carer ratings scales, the emotional distress, personal background and awareness about the illness may bias the carer's evaluation. However, our results align with evidence in symptomatic frontotemporal dementia patients,

showing an early association of apathy reported by patients' carers with frontal and cingulate grey-matter volume degeneration (Ducharme *et al.*, 2018, Passamonti *et al.*, 2018*a*). Similarly, in patients with syndromes of frontotemporal lobar degeneration including frontotemporal dementia, Lansdall et al. reported a significant association of carers' ratings for apathy with diffuse atrophy in a fronto-striatal network, cingulate and temporal regions (Lansdall *et al.*, 2017). Overall these findings suggest a clinicopathological association between apathy severity reported by carers, and neurodegeneration in key regions associated with motivation. The GENFI study did not include self-rated scales for apathy, which rely on insight and introspection abilities that may lack in patients with FTD. However, future studies on the pre-symptomatic phase of FTD may consider to also investigate longitudinal changes in self-rating apathy scores and multimodal apathy assessments (e.g., behavioural tests, computer tasks, patient and carer's ratings and questionnaires) to estimate separate domains of the multidimensional construct of apathy, and their associations with cognitive decline. Executive dysfunction is common in all three genotypes (Snowden *et al.*, 2015). I quantified cognitive decline with WAIS-R Digit Symbol test, which is sensitive to executive function problems. This has high reliability (Matarazzo and Herman, 2008), but does not in itself allow one to dissociate the potential elements of executive cognition, such as selective attention, working memory, or planning. Another challenge in the quanitification of apathy and executive function is the potential overlap with other symptoms, such as depression and akinesia (Johnson and Kumfor, 2018). In our cohort, depression and apathy measures were not significantly associated, suggesting that CBI-R apathy subscale is not simply measuring depression. This aligns with previous evidence that supports the dissociation between apathy and depression in frontotemporal dementia and other neurodegenerative disease (Levy *et al.*, 1998; Starkstein *et al.*, 2005; Vicini Chilovi *et al.*, 2009; Hollocks *et al.*, 2015, Murley *et al.*, 2020*a*). While akinesia is common in symptomatic genetic frontotemporal dementia (Rowe, 2019), it is not common in presymptomatic cases and does not correlate with apathy measures in other cohorts (Murley *et al.*, 2020*a*). An open longitudinal study like GENFI will have incomplete longitudinal data. I therefore included only the first three waves of assessment, as minimum requirement in LGCM guidelines (Newsom, 2015). In years to come, it will be possible to examine a larger data sample and/or a longer follow-up period, including the role of apathy in the transition from pre-symptomatic to symptomatic phases of frontotemporal dementia.

4.5. Conclusions

My results demonstrate that apathy occurs early in disease progression of genetic frontotemporal dementia, reflecting early brain changes and predicting individual future clinical trajectory of executive function. The assessment of apathy could help with cohorts' stratification, according to their prognosis, and improve the power and design of future therapeutic trials. Apathy may also be a modifiable factor in its own right, by pharmacological (Padala *et al.,* 2018) or non-pharmacological interventions (Ventura *et al.,* 2019). As such, it becomes a potential target not only for symptomatic treatment but also to slow down or delay clinical decline in people at risk of frontotemporal dementia.

Chapter 5 | *In vivo* pathological markers in familial frontotemporal dementia

Preface: Parts of the contents of this chapter have been reported in a manuscript, which has been published in Malpetti et al. *In vivo* PET imaging for inflammation in familial frontotemporal dementia. *J Neurol Neurosurg Psychiatry*, 2020, doi:10.1136/jnnp-2020-323698.

A team of researchers and clinicians at the University of Cambridge have contributed to data collection. I performed all data analyses and drafted the text, with textual revision input from all co-authors. Simon Jones, Dr. Tim Fryer and Dr. Young Hong helped with MRI and PET pre-processing, Dr. Timothy Rittman with clinical revision of the cases.

Abstract: In this chapter, I describe the *in vivo* patterns of distribution of neuroinflammation and abnormal protein aggregation in seven cases of familial frontotemporal dementia with mutations in MAPT, GRN, and C9orf72 genes. Specifically, I investigate the association of the distribution of activated microglia, as measured by [^{11}C]PK11195 PET with individual clinical features. In the same patients, I also evaluated the distribution of [^{18}F]AV-1451 PET binding, which is sensitive to the presence of tau and TDP-43. Across all genes, [^{11}C]PK11195 PET showed increased binding with specific regional distribution corresponding to clinical symptoms. Patients with MAPT mutations had more homogeneous [^{18}F]AV-1451 binding than patients with mutations linked to TDP-43 protein aggregation (GRN and C9orf72). This case series suggests a crucial role for neuroinflammation in the pathophysiology and clinical presentation of familial frontotemporal dementia.

5.1. Introduction

Familial frontotemporal dementia is a prototypical and exemplar neurodegenerative disorder for the assessment of *in vivo* pathology. Indeed, there is a clear relationship between each monogenetic frontotemporal dementia disorder and the pathological accumulation of abnormal tau or TDP-43 protein. The pathological and clinical features of familial frontotemporal dementia closely resemble sporadic cases, but the mutations in specific genes allow researcher to infer the underlying pathology before *post mortem* examination. Around 20% of frontotemporal dementia cases have autosomal dominant aetiology (Bang *et al.,* 2015), most arising from mutations in one of three main genes - MAPT, GRN, and C9orf72 (Greaves and Rohrer, 2019). A genetic cause is more likely (i) if there is a positive family history and (ii) in behavioural variant of frontotemporal dementia (bvFTD) relative to other syndromes. In genetic and sporadic cases, the modification, misfolding and aggregation of tau or TDP-43 protein leads to characteristic neuropathology. However, new evidence has suggested that neuroinflammation may also be an early etiopathogenic event in frontotemporal dementia, rather than a mere consequence of neurodegeneration. This hypothesis is supported by genome-wide association studies that implicate immunological pathways in frontotemporal dementia (Broce *et al.,* 2018), and animals studies that identified inflammatory changes preceding tau accumulation (Yoshiyama *et al.*, 2007). In addition, positron emission tomography (PET) with the radioligand [^{11}C]PK11195 reveals *in vivo* neuroinflammation in frontotemporal regions in frontotemporal dementia (Cagnin *et al.,* 2004; Bevan-Jones *et al.,* 2020), even before the onset of symptoms in genetic cases (Bevan-Jones *et al.,* 2019). In pre-symptomatic frontotemporal dementia associated with a MAPT mutation, [^{11}C]PK11195 PET revealed increased levels of microglial activation, despite the lack of significant atrophy or binding of the [^{18}F]AV-1451 ligand (Bevan-Jones *et al.,* 2019). However, the presence and pattern of inflammation by genotype, and its relationship to phenotype and to tau/TDP-43 burden, remain under-investigated. The relationship between *in vivo* distribution of neuroinflammation and clinical symptoms in familiar cases of frontotemporal dementia has not been well investigated, and neither has been the *in vivo* relationship with protein aggregation.

Nowadays, multi-tracer PET imaging allows the quantification of *in vivo* neuroinflammation alongside pathological protein aggregation in several neurodegenerative disorders (Stefaniak and O'Brien, 2015; Hall *et al.,* 2017; Chandra *et al.,* 2019). PET studies with [^{11}C]PK11195 have shown increased neuroinflammation in frontotemporal regions in patients with sporadic

frontotemporal dementia (Cagnin *et al.*, 2004; Bevan-Jones *et al.*, 2020), and have reported evidence that neuroinflammation may precede the development of the full frontotemporal dementia syndrome in carriers of MAPT mutations (Bevan-Jones *et al.*, 2019). On the other hand, PET ligands designed to target the hyperphosphorylated tau protein have been used jointly in sporadic and familial frontotemporal dementia (Smith *et al.*, 2019*a*; Tsai *et al.*, 2019; Bevan-Jones *et al.*, 2020). For example, the ligand [^{18}F]AV-1451 reveals the distribution of tau pathology in cases due to MAPT mutations (Bevan Jones *et al.*, 2016; Smith *et al.*, 2016; Spina *et al.*, 2017). However, [^{18}F]AV-1451 also show characteristic binding in cases with bvFTD related to C9orf72 mutation and in patients with svPPA, which are related to TDP-43 pathology rather than tau pathology (Bevan-Jones *et al.*, 2018*b*, *a*). This suggests that the [^{18}F]AV-1451 ligand is not specific to tau pathology, but is also sensitive to the presence of TDP-43 pathology (although not binding to TDP-43 itself) (Bevan-Jones *et al.*, 2018*b*; Makaretz *et al.*, 2018).

In this multi-tracer PET study, I used [^{11}C]PK11195 and [^{18}F]AV-1451 ligand to respectively quantify *in vivo* neuroinflammation and tau or TDP-43 pathology in seven patients with familial frontotemporal dementia syndromes, caused by mutations in either MAPT, GRN, or C9orf72 gene. I tested the hypothesis that PET markers for microglial activation and junk proteins' aggregation may be informative on the disease stage at single subject level in patients with frontotemporal dementia. Specifically, I examined the distribution of neuroinflammation and tau/TDP-43 protein aggregation across cortical and subcortical structures and their relationship with clinical features in each case. I expected to find evidence of inflammation across all subjects, but with individual-specific associations between PET signal topography and clinical symptoms.

5.2. Methods

5.2.1. Participants

Seven patients with familial frontotemporal dementia were recruited from the Cambridge University Centre for frontotemporal dementia specialist NHS clinics: 2 with MAPT 10 + 16 gene mutation, 2 with GRN C388_391delCAGT p.(Gln130fs) and 3 with C9orf72 expansion. Six patients met diagnostic criteria for bvFTD (Rascovsky *et al.*, 2011) and one case met criteria for non-fluent variant of Primary Progressive Aphasia (nfvPPA) (Gorno-Tempini *et al.*, 2011). Six out of 7 patients were analysed together with other 25 sporadic frontotemporal dementia

cases as part of a previous study from our group (Bevan-Jones *et al.*, 2020), but the following analysis differs in several key respects including (i) separate comparison of each genetic case, versus controls, without principal component analysis (PCA) of the group data; (ii) voxel-wise analysis rather than only regional data All patients underwent a structured clinical, neuropsychological assessment and clinical diagnostic magnetic resonance imaging as part of their usual care. In addition, patients underwent a research protocol 3T MRI, [^{11}C]PK11195 PET and [^{18}F]AV-1451 PET and a standard battery of cognitive tests as part of the NIMROD study (Bevan-Jones *et al.*, 2017)).

Written informed consent was obtained from the participants, and approval for this study was obtained from the National Research Ethic Service's East of England Cambridge Central Committee.

5.2.2. Imaging data acquisition and pre-processing

Structural MRI, [^{11}C]PK11195 PET and [^{18}F]AV-1451 PET data were acquired and processed using previously described methods (Bevan-Jones *et al.*, 2017; Passamonti *et al.*, 2017, 2018*b*). Briefly, [^{11}C]PK11195 PET data were processed with reference to tissue defined by supervised cluster analysis to calculate the nondisplaceable binding potentials (BP_{ND}) at voxel-wise level and in 83 regions of interest (ROI) based on a modified version of Hammers atlas to include subcortical structures. For [^{18}F]AV-1451 PET, a simplified reference tissue model (superior cerebellar grey matter reference tissue) was used to obtain voxel-wise BP_{ND} maps and regional BP_{ND} values into the same 83 ROIs for [^{11}C]PK11195 PET. For both tracers, regional BP_{ND} was corrected for CSF partial volume effects.

5.2.3. Statistical analyses

To examine [^{11}C]PK11195 and [^{18}F]AV-1451 distribution at single subject level, I employed three approaches. First, I visually evaluated the voxel-wise PET maps for each patient, in relation to their symptoms, as commonly applied for qualitative assessment in clinical practice. Second, I calculated the voxel-wise z-scores maps for each patient *versus* a group of healthy controls, to identify the voxel peaks that are significantly increased in each case. The voxel-wise BP_{ND} maps were spatially normalised to MNI space and smoothed (6mm full width at half maximum). In view of substantial off-target subcortical [^{18}F]AV-1451 binding, I confine the

visual inspection of the binding and z-score maps to cortical regions. Finally, as secondary quantitative analysis, one-tailed Crawford tests for single-case analysis (Crawford and Garthwaite, 2007) were performed on CSF corrected regional values for each radioligand, to test significant differences at regional level between each case and controls. For the voxel-wise and regional comparisons between patients and controls, we included two age-, sex-matched groups of healthy elderly adults Supplementary Table 3, who underwent either [^{11}C]PK11195 PET (N=15) or [^{18}F]AV-1451 PET (N=15).

A hierarchical cluster analysis approach was used to determine whether the distribution of [^{11}C]PK11195 binding across all brain regions differs between patients and controls. The parcellated [^{11}C]PK11195 BP_{ND} values were converted into individual linear vectors by regions, which were nonparametrically correlated (Spearman's rho). The resulting correlation matrix was converted into a dissimilarity matrix. The latter was included in a hierarchical cluster analysis using the complete linkage (or furthest neighbour) method.

5.3. Results

5.3.1. Descriptive statistics

Demographic and clinical features are shown in **Table 15**.

Table 15. *Demographics, genetic and clinical features for each patient.*

PT	Gene	Diagnosis	Sex	Age at PET	Age at Diagnosis	Age at Onset	Disease duration at PET	Years of Education	ACE-R /100
A	MAPT	bvFTD	F	51	51	46	5.5	16	43
B	MAPT	bvFTD	F	61	60	52	9	16	44
C	GRN	bvFTD	F	71	70	66	4.8	10	33
D	GRN	nfvPPA	M	66	65	63	2.4	10	76
E	C9orf72	bvFTD	M	56	56	54	2.8	10	53
F	C9orf72	bvFTD	F	51	51	47	4.5	10	41
G	C9orf72	bvFTD	M	59	58	56	3	9	46

Abbreviations: PT=patient; bvFTD=behavioural variant frontotemporal dementia; nfvPPA=non-fluent primary progressive aphasia; F=Female; M=Male; ACE-R= Addenbrooke's Cognitive Examination Revised

5.3.2. Visual evaluation of voxel-wise PET maps and association with clinical symptoms

Individual BP_{ND} maps for [^{11}C]PK11195 and [^{18}F]AV-1451 are reported in **Figure 16**, while z maps for each patient as compared to controls for the two PET modalities are reported in **Figure 17**. Regional comparison results on [^{11}C]PK11195 and [^{18}F]AV-1451 are reported in Supplementary Table 4 and Supplementary Table 5, respectively.

MAPT mutations

Patient A was diagnosed with bvFTD aged 51, with progressive lack of insight and language, impairment of memory and judgement, loss of functional skills, apathy, and loss of semantic knowledge. She scored 43/100 on the revised Addenbrooke's Cognitive Examination (ACE-R), scoring 0/14 at the fluency test, 9/18 on the Frontal Assessment Battery (FAB), 2/30 on the on Frontotemporal Dementia Rating Scale (FTDRS), and 118/180 on the Cambridge Behavioural Inventory Revised (CBI-R). She had a family history of frontotemporal dementia, with her father carrying a symptomatic MAPT 10+16 mutation. [^{11}C]PK11195 binding was elevated in the medial and superior temporal lobes and temporal poles, the medial and posterior orbitofrontal cortex, the medial and dorsolateral prefrontal cortex, the cingulate gyrus, subcortical structures (i.e. globus pallidus, putamen and nucleus accumbens), and mildly in parietal regions. Elevated [^{18}F]AV-1451 binding overlapped with [^{11}C]PK11195 and it was spatially more extensive, involving extensively the frontal and temporal lobes, especially the anterior and medial temporal regions, the orbitofrontal cortex and the dorsolateral prefrontal cortex. The cingulate cortex and the inferior parietal lobe also showed increased [^{18}F]AV-1451. For some frontal regions and temporal regions, both [^{11}C]PK11195 and [^{18}F]AV-1451 binding were more elevated in the left hemisphere.

Patient B presented at 60 years of age with bvFTD, characterised by obsessional and compulsive behaviours, comprehension impairments, anomia, and a positive family history of dementia consistent with frontotemporal dementia. She scored 44/100 on ACE-R, 7/18 on FAB, 1/30 on FTDRS and 99/180 on CBI-R. PET scans showed increased [^{11}C]PK11195 binding mainly in the anterior and medial temporal regions, the fusiform gyri, and the middle-inferior frontal cortex. Secondarily, the dorsolateral and medial prefrontal cortex, the right parietal lobe and subcortical structures (i.e. putamen and nucleus accumbens) were also involved by

[^{11}C]PK11195 pattern. Similarly to Patient A, [^{18}F]AV-1451 binding pattern was overlapping with [^{11}C]PK11195 pattern, but visually more extensive than the latter. Increased [^{18}F]AV-1451 binding was evident across all frontal lobes, mainly in dorsolateral prefrontal cortex, middle frontal gyrus, anterior cingulate gyrus and orbitofrontal regions. Milder increased binding was also seen in medial temporal and parietal regions.

GRN mutations

Patient C presented bvFTD at age 70 with apathy, emotional incontinence and disinhibition, but no motor signs. She scored 33/100 on ACE-R, 3/30 on FTDRS, and 88/180 on CBI-R. [^{11}C]PK11195 binding was increased in the inferior temporal regions, orbitofrontal cortex and subcortical structures (i.e. putamen, globus pallidum and substantia nigra). Increased [^{11}C]PK11195 binding was also patchily seen in the medial prefrontal cortex and parietal lobes. [^{18}F]AV-1451 PET showed mildly increased binding in the left medial and inferior temporal regions. The voxel-wise map showed increased [^{18}F]AV-1451 levels in cerebellum, however this was not highlighted by the regional comparisons with controls.

Patient D presented progressive non-fluent aphasia at age 65 with additional mild behavioural changes including jocularity and hoarding of sweets. He was diagnosed with nfvPPA 18 months after his symptom onset. By the time of the PET scans, he had declined significantly with minimal speech, yes/no confusion and significant behavioural problems without motor involvement. He scored 76/100 on ACE-R, 9/18 on FAB, 12/30 on FTDRS, and 62/180 on CBI-R. There was no significant increased binding of [^{18}F]AV-1451 at regional level as compared to controls, with low intensity clusters seen in voxel-wise maps in the left inferior temporal lobe and the cerebellum. In contrast, the [^{11}C]PK11195 map showed more extensive increased binding in the temporal lobes (anterior, medial, inferior and fusiform regions), and in the prefrontal cortex, especially in the left inferior frontal gyrus.

C9orf72 mutations

Patient E presented bvFTD aged 56 years, with irritable behaviour, over-valued ideas and obsessions, a sweet tooth, semantic impairment, but no signs of motor neuron disease. He scored 53/100 on ACE-R, 6/18 on FAB, 9/30 on FTDRS, and 76/180 on CBI-R. On PET

imaging there was increased [^{11}C]PK11195 binding widely in the temporal and frontal lobes, especially involving the anterior medial and lateral temporal regions and the orbitofrontal cortex. Scattered foci of increased binding were seen in parietal lobes and cerebellum, however this was not significant at regional level in the comparisons with controls. There was increased [^{18}F]AV-1451 binding in the anterior lateral and medial temporal regions most notably in the left hemisphere, and in the superior and middle frontal cortex. Milder uptake was seen also in left parietal cortex.

Patient F presented bvFTD at age 51 with behavioural changes, abnormal beliefs, stereotypical and repetitive behaviours, but no features of motor neuron disease. She developed paranoid delusions, apathy, a sweet tooth with significant weight gain, and a moderate aphasia with non-fluent speech and anomia. She scored 41/100 on ACE-R, 7/18 on FAB, 3/30 on FTDRS, and 60/180 on CBI-R. Her pattern of [^{18}F]AV-1451 binding was low across the whole-brain, and only very mild excess binding in the lateral orbitofrontal regions. [^{11}C]PK11195 PET showed increased binding in frontotemporal and parietal regions, with peaks in the orbitofrontal cortex, the anterior temporal lobes, the middle frontal regions, and the left inferior frontal gyrus.

Patient G presented bvFTD at age 58 with a long history of psychiatric symptoms and an episode of psychotic depression at age 44 following bereavements. At age 56, he had a relapsing episode of depression with psychotic features and he was consequently treated with risperidone after which he developed a parkinsonian syndrome. His psychosis progressed and he developed disinhibited social behaviours and memory problems. There was a positive family history for motor neuron disease, although he had no signs or symptoms of motor neuron diseases. He scored 46/100 on ACE-R, 5/18 on FAB, 2/30 on FTDRS, and next of kin endorsed 140/180 items on CBI-R. [^{11}C]PK11195 PET showed scattered increases in binding in superior frontal and parietal regions, inferior temporal regions and cerebellum. There was no significant increased binding of [^{18}F]AV-1451 at regional level as compared to controls, while at voxel level, mildly increased [^{18}F]AV-1451 binding was seen in parietal-occipital regions, cingulate cortex, and cerebellum.

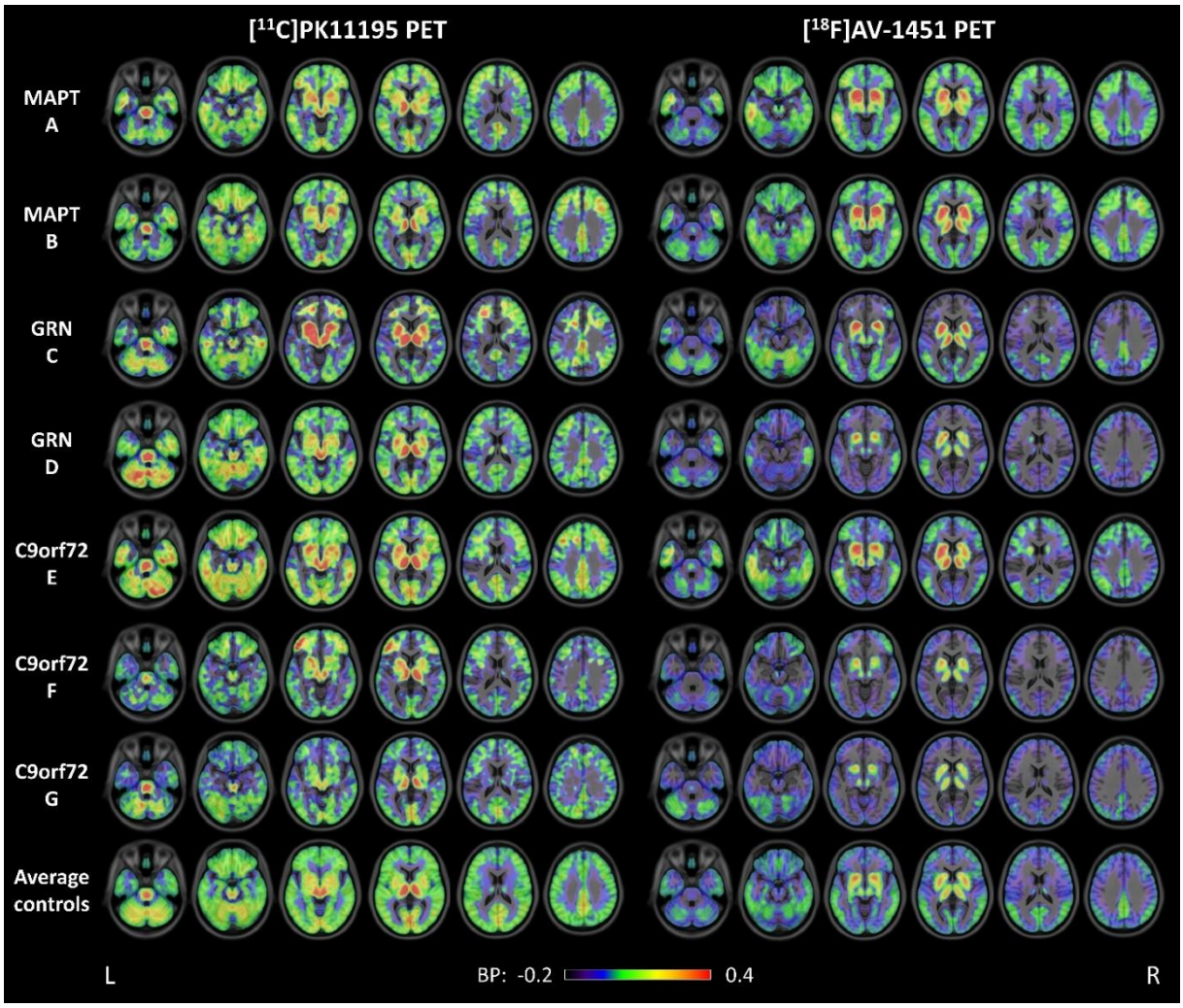

Figure 16. *Axial slices of the [^{11}C]PK11195 (left panel) and [^{18}F]AV-1451 (right panel) binding potential (BP_{ND}) maps for each patient (A-G). The last row represents the average BP_{ND} images across 15 controls. Patients A and B are MAPT mutation carriers; cases C and D are patients with GRN mutations; and patients E, F and G are C9orf72 mutation carriers. BP_{ND} scale bar runs along the bottom side of the figure and applies to both PET tracers. The maps were spatially normalised to MNI space and smoothed (6mm full width at half maximum), and the slices are reported in the neurological display convention (left on the left).*

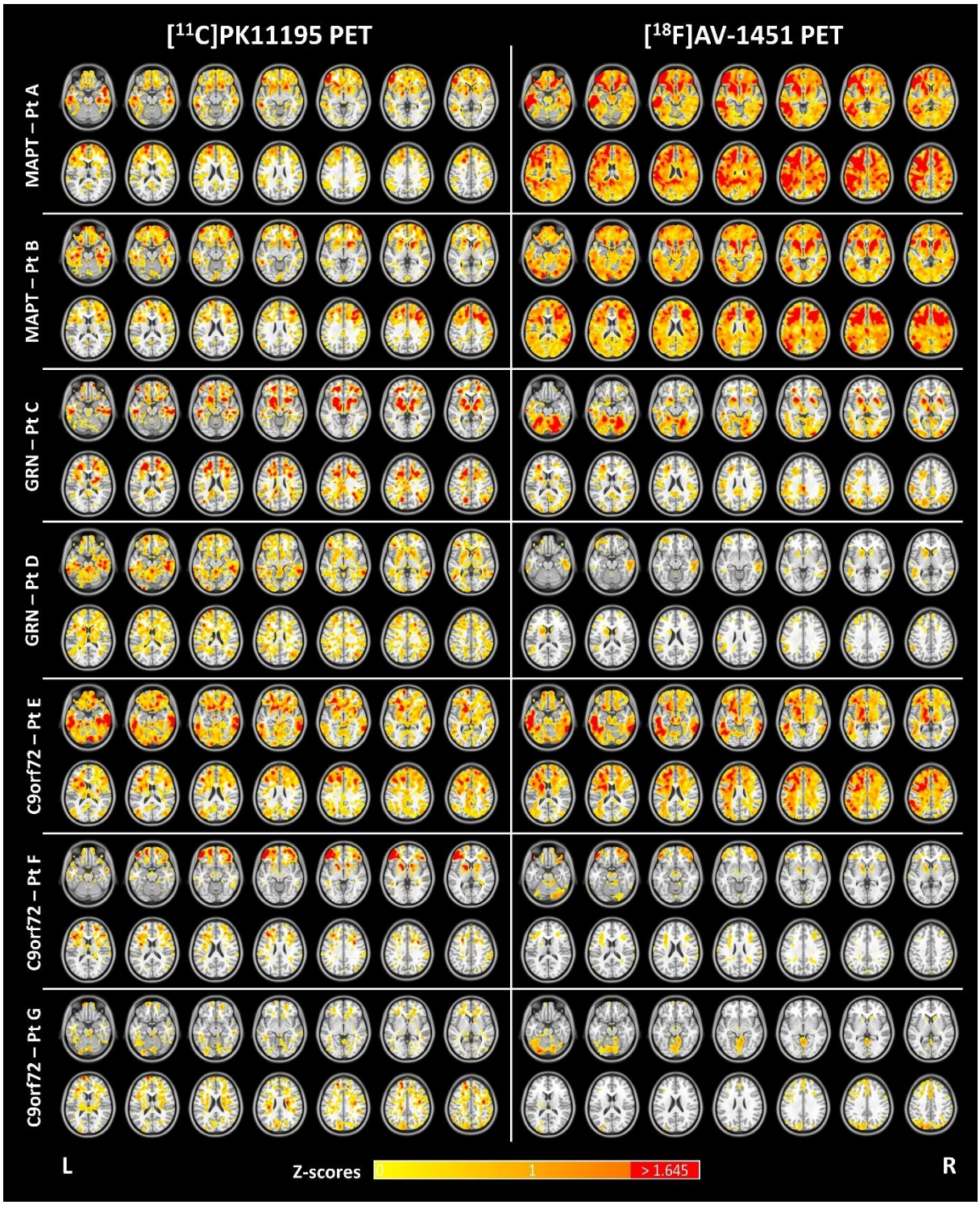

Figure 17*. Z-maps for [^{11}C]PK11195 (left panel) and [^{18}F]AV-1451 (right panel) binding potential (BP_{ND}) for each patient (A-G) as compared to 15 controls. Patients A and B are MAPT mutation carriers; cases C and D are patients with GRN mutations; and patients E, F and G are C9orf72 mutation carriers. Z-scale bar runs along the bottom side of the figure and applies to both PET tracers (z > 1.645 which corresponds to p<0.05 are reported in red). The slices are reported in the neurological display convention (left on the left) and aligned in MNI space.*

5.3.3. Hierarchical cluster analysis

In the hierarchical cluster analysis of the [^{11}C]PK11195 distribution, patients with MAPT mutation (patients A and B) were grouped together. Patients with GRN and C9orf72 mutations were divided into different clusters, but still separated from controls at an intermediate level branch in the dendrogram (**Figure 18**).

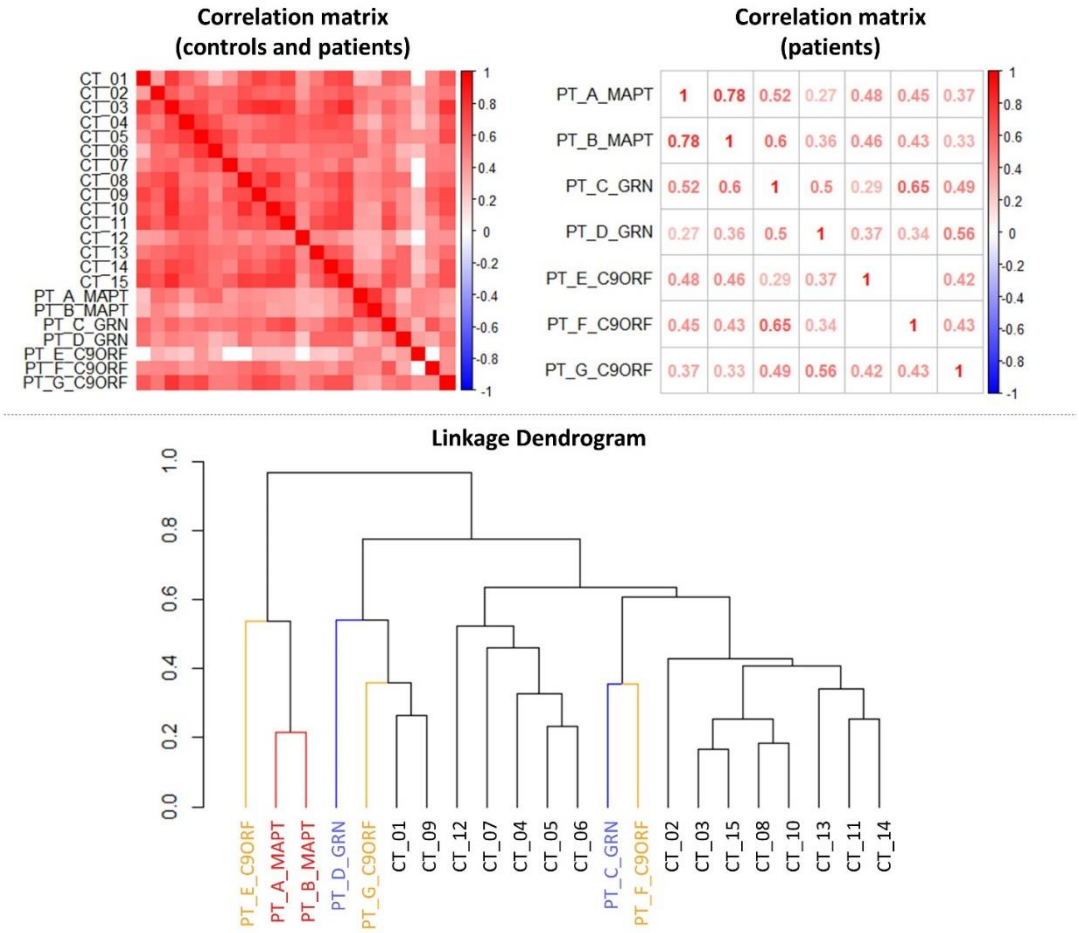

Figure 18. *Correlation matrices and linkage dendrogram obtained with [^{11}C]PK11195 binding potential regional values. Top-left panel: Spearman correlation matrix between all individuals ($p < 0.05$ FDR); the first 15 rows and columns represent controls while the other 7 rows and columns represent patients. Top-right panel: Spearman correlation matrix between patients, the numbers represents the strength of correlation (rho, $p < 0.05$ FDR). Bottom panel: the dendrogram produced by hierarchical cluster analysis. Patients with MAPT mutation are highlighted in red, patients with GRN mutation in blue and those with C9orf72 mutation in yellow.*

5.4. Discussion

I studied *in vivo* neuroinflammation and protein deposition in a series of cases with the three most common monogenetic forms of frontotemporal dementia (MAPT, GNR, C9orf72). The main results of this report are that: (i) familial frontotemporal dementia is consistently associated with neuroinflammation in frontotemporal regions across all genes; (ii) the distribution of neuroinflammation reflects clinical symptoms in each patient. Pathological differences that reflect the underlying tau or TDP-43 pathology and the associated clinical heterogeneity are captured by case-specific neuroinflammation patterns.

Across all familial frontotemporal dementia patients, [^{11}C]PK11195 binding provided a more evident and consistent signal than [^{18}F]AV-1451 PET. The distribution of neuroinflammation might reflect clinical heterogeneity. For example, in both MAPT patients, [^{11}C]PK11195 binding was elevated in frontostriatal regions in association with behavioural variant frontotemporal dementia, but Patient A's language impairments accompany increased binding in temporal regions. The GRN cases had different phenotypes for which the bvFTD in Patient C accompanied prominent orbitofrontal inflammation, but focal left inferior frontal inflammation in Patient D was associated with non-fluent aphasia. While inflammation in orbitofrontal regions may be associated with the neuropsychiatric symptomatology reported in the three C9orf72 cases, Patients E and F also presented language impairments, and increased inflammation in left inferior frontal gyrus and temporal regions. In these latter patients, who are expected to have TDP-43 pathology but not significant tauopathy, [^{18}F]AV-1451 binding was not intense or extensive compared to the distribution of neuroinflammation ([^{18}F]AV-1451 binding in the C9orf72 carriers was less marked than in semantic dementia, which typically has another form of TPD-43 pathology (Bevan-Jones *et al.*, 2018*a*)). These results suggest that [^{11}C]PK11195 may be more informative than [^{18}F]AV-1451 on single subject clinical manifestations and progression. [^{18}F]AV-1451 showed variable and less striking patterns in GRN and C9orf72 cases as compared to the results in MAPT cases. These findings, together with previous evidence, may discourage the use of the absolute binding quantification of this tracer to predict clinical outcomes across patients with different clinical and pathological sub-types, which lead to variable tracer affinity.

My findings align with previous evidence that support the importance of neuroinflammation in frontotemporal dementia (Bright *et al.*, 2019). I suggest that activated microglia play an

important role in defining clinical syndromes associated with genetic frontotemporal dementia related mutations. Previous *post mortem* evidence in frontotemporal dementia reported upregulated microglial activation in both tau and TDP-related pathologies (Lant *et al.*, 2014; Sakae *et al.*, 2019; Woollacott *et al.*, 2020). In patients with MAPT mutations, neuroinflammation may be triggered by the misfolding of mutant tau and contribute to its hyperphosphorylation and aggregation (Yoshiyama *et al.*, 2007; Bhaskar *et al.*, 2010; Bright *et al.*, 2019), while in C9orf72 and GRN cases, neuroinflammation could be triggered by dipeptide repeats or progranulin haploinsufficiency in advance of the large TDP-43 aggregates (Yin *et al.*, 2010; Bright *et al.*, 2019). However, further studies with pre-symptomatic cases at risk of familial frontotemporal dementia will be needed to reveal the temporal association between microglial activation and specific patterns of protein aggregation. Such studies will also be needed to confirm gene-specific inflammation patterns and the consistency of their association with specific clinical syndromes.

I present both regional and voxel-wise analyses. Voxel-wise maps at single subject level may reveal local intensities, while regional comparisons focus on consistent and diffuse increases in ligand binding. The ROI-based approach is more common in PET imaging, especially for group studies, and here incorporates partial volume correction which is controversial for voxel-wise analyses. However, averaging the tracer uptake over a region can mask the focal binding intensities within the region. Thus, the methods are complementary.

The case report approach is limited by its small size, which does not permit correlational analyses between PET imaging and clinical severity by genetic subgroups. However, small sample sizes can be informative about typicality of a feature in a population, when features are identified in the majority of cases sampled (Friston *et al.*, 1999). To empower the ROI-based comparisons between each patient and controls, I included separate groups of healthy adults who underwent either [^{11}C]PK11195 PET or [^{18}F]AV-1451 PET but not both. However, the control groups were older than patients on average, and the increased binding levels in symptomatic cases may therefore be underestimated. In addition, [^{11}C]PK11195 enables the visualisation of increased TSPO expression, which is a marker for microglial activation. However, neuroinflammatory cascade in neurodegenerative diseases is a complex process not confined to activated microglia (Ransohoff, 2016; Bright *et al.*, 2019). Further studies will be

needed to clarify other inflammatory processes associated with genetic frontotemporal dementia.

5.5. Conclusions

I report seven cases of familial frontotemporal dementia who were assessed for *in vivo* neuroinflammation and abnormal protein aggregation via multi-tracer PET imaging. The results support a key role for neuroinflammation and suggest that regional inflammation is a typical feature of genetic frontotemporal dementia, across the three most common monogenetic forms of frontotemporal dementia. Indeed, neuroinflammation was evident across all the monogenetic forms of frontotemporal dementia. The interaction between inflammatory processes and proteinopathies may be equally important in mediating some monogenetic but no all hereditary forms of frontotemporal dementia syndromes. As expected, [^{18}F]AV-1451 PET more reliably identified the patterns of abnormal protein accumulation in patients with MAPT mutations relatively to patients with GRN or C9orf72 mutations. Future studies with multi-tracer PET in pre-symptomatic carriers of different genetic mutations may provide further information to clarify the causality between pathological processes in genetic and sporadic frontotemporal dementia and to help develop early and targeted interventions.

5.6. Supplementary materials of Chapter 5

Supplementary Table 3. Demographics of the two age- and sex-matched control groups compared to each patient in radioligand-specific Crawford tests. Age, years of education, and ACE-R scores were compared between the two groups of controls with independent-samples t-tests, while sex was compared with the Chi-square test (reported p-values).

Group control	**N**	**Sex (F/M)**	**Age (mean ± SD)**	**Education (mean ± SD)**	**ACE-R (mean ± SD)**
[^{11}C]PK11195	15	8/7	68.8±5.5	14.4±2.8	93.3±4.4
[^{18}F]AV-1451	15	7/8	67.3±7.6	15.5±2.3	95.7±3.2
Difference controls (p-value)	**-**	**0.72**	0.56	0.26	0.11

Abbreviations: SD=standard deviation; F/M= female/male; ACE-R= Addenbrooke's Cognitive Examination Revised

Supplementary Table 4. Binding potential (BP) values and z-scores (Z) for brain regions with statistically significant increased [^{11}C]PK11195 binding potential in each patient (Pt) compared to controls at $p < 0.05$ uncorrected (tests surviving FDR correction are in bold). Mean and standard deviation (SD) values for controls are also reported).

Region		Controls		Pt A		Pt B		Pt C		Pt D		Pt E		Pt F		Pt G	
Name	#	Mean	SD	BP	Z	BP	Z	BP	Z	BP	Z	BP	Z	BP	Z	BP	Z
Hippocampus R	1	0.009	0.07	0.280	**3.81**	-	-	-	-	-	-	-	-	-	-	-	-
Hippocampus L	2	0.042	0.07	-	-	0.288	**3.75**	-	-	-	-	-	-	-	-	-	-
Amygdala R	3	0.014	0.07	0.371	**4.95**	0.210	2.72	-	-	-	-	0.221	2.87	-	-	-	-
Amygdala L	4	0.059	0.04	0.342	**6.35**	0.345	**6.40**	-	-	-	-	-	-	-	-	-	-
Anterior temporal lobe medial part R	5	0.040	0.06	0.230	**3.11**	-	-	-	-	-	-	0.351	**5.10**	0.192	2.50	-	-
Anterior temporal lobe medial part L	6	0.045	0.06	0.249	**3.14**	0.219	2.68	-	-	-	-	-	-	-	-	-	-
Anterior temporal lobe lateral part R	7	0.096	0.07	0.262	2.42	0.332	**3.46**	-	-	-	-	-	-	-	-	-	-
Anterior temporal lobe lateral part L	8	0.029	0.05	0.274	**4.70**	0.257	**4.38**	-	-	-	-	0.191	3.11	0.273	**4.70**	-	-
Parahippocampal and ambient gyri R	9	0.053	0.05	0.274	**4.08**	0.192	2.56	-	-	-	-	0.218	3.05	-	-	-	-
Parahippocampal and ambient gyri L	10	0.074	0.05	0.278	**3.79**	0.410	**6.23**	-	-	-	-	0.221	2.73	-	-	-	-
Middle and inferior temporal gyrus R	13	0.008	0.04	-	-	0.139	**3.32**	-	-	0.109	2.56	-	-	-	-	-	-
Middle and inferior temporal gyrus L	14	-0.020	0.03	0.136	**6.02**	0.078	**3.77**	0.076	**3.70**	-	-	0.082	**3.95**	0.096	**4.50**	-	-
Fusiform gyrus R	15	-0.006	0.02	0.109	**5.07**	0.204	**9.27**	0.049	2.41	0.191	**8.68**	0.162	**7.42**	0.088	**4.14**	-	-
Fusiform gyrus L	16	-0.013	0.05	0.162	**3.36**	0.239	**4.84**	-	-	0.102	2.21	0.368	**7.33**	-	-	0.111	2.37
Insula L	20	0.017	0.05	-	-	-	-	-	-	-	-	0.164	2.92	-	-	-	-
Middle frontal gyrus L	28	-0.048	0.06	-	-	-	-	-	-	-	-	-	-	0.086	2.28	-	-
Middle frontal gyrus R	29	-0.007	0.05	-	-	0.076	1.84	-	-	-	-	-	-	0.111	2.63	-	-
Nucleus accumbens L	36	0.111	0.07	-	-	0.331	**3.06**	-	-	-	-	-	-	-	-	-	-
Nucleus accumbens R	37	0.083	0.08	0.447	**4.84**	-	-	-	-	-	-	-	-	-	-	-	-
Putamen L	38	0.063	0.05	-	-	-	-	0.294	**4.85**	0.157	1.98	-	-	-	-	-	-
Putamen R	39	0.076	0.04	0.147	1.83	0.177	2.59	0.195	3.07	0.153	1.98	-	-	-	-	-	-
Pallidum L	42	0.029	0.10	0.274	2.40	-	-	0.246	2.13	-	-	-	-	0.274	2.40	-	-
Straight gyrus L	52	0.178	0.07	0.427	**3.55**	-	-	-	-	-	-	-	-	-	-	-	-
Straight gyrus R	53	0.159	0.09	0.439	**3.20**	-	-	-	-	-	-	-	-	-	-	-	-
Anterior orbital gyrus L	54	0.041	0.06	-	-	-	-	-	-	-	-	-	-	0.373	**5.27**	-	-
Anterior orbital gyrus R	55	0.069	0.06	-	-	-	-	-	-	-	-	-	-	0.267	**3.15**	0.229	2.56

Inferior frontal gyrus L	56	0.088	0.05	-	-	-	-	-	-	-	-	-	-	0.228	2.83	-	-
Inferior frontal gyrus R	57	0.122	0.06	-	-	0.249	2.31	-	-	-	-	-	-	0.234	2.03	-	-
Superior frontal gyrus L	58	0.068	0.05	-	-	-	-	-	-	-	-	-	-	-	-	0.185	2.48
Superior frontal gyrus R	59	0.043	0.06	-	-	-	-	-	-	-	-	-	-	-	-	0.172	2.11
Lingual gyrus L	64	0.150	0.07	-	-	-	-	-	-	-	-	-	-	-	-	0.293	2.10
Lingual gyrus R	65	0.109	0.06	-	-	-	-	-	-	-	-	-	-	-	-	0.231	1.96
Cuneus L	66	0.168	0.05	-	-	-	-	-	-	-	-	-	-	0.347	**3.74**	0.269	2.12
Cuneus R	67	0.123	0.05	-	-	-	-	-	-	-	-	-	-	-	-	0.226	1.88
Medial orbital gyrus L	68	0.119	0.06	0.246	1.97	-	-	-	-	-	-	-	-	0.365	**3.82**	-	-
Lateral orbital gyrus L	70	0.134	0.06	-	-	-	-	0.284	2.42	-	-	-	-	0.518	**6.22**	-	-
Lateral orbital gyrus R	71	0.134	0.06	-	-	-	-	-	-	-	-	-	-	0.520	**6.27**	-	-
Posterior orbital gyrus L	72	0.101	0.07	0.287	2.55	-	-	-	-	-	-	-	-	-	-	-	-
Posterior orbital gyrus R	73	0.135	0.06	-	-	-	-	-	-	-	-	-	-	0.272	2.32	-	-
Substantia nigra L	74	0.223	0.07	-	-	-	-	-	-	-	-	-	-	0.437	2.91	-	-
Substantia nigra R	75	0.148	0.07	-	-	-	-	0.601	**6.47**	-	-	-	-	-	-	-	-
Subgenual frontal cortex L	76	0.013	0.07	0.299	**4.13**	-	-	-	-	-	-	-	-	-	-	-	-
Subcallosal area L	78	0.174	0.12	-	-	-	-	-	-	-	-	0.431	2.10	-	-	-	-
Subcallosal area R	79	0.226	0.16	-	-	-	-	0.682	2.91	-	-	-	-	-	-	-	-
Presubgenual frontal cortex L	80	0.152	0.10	0.349	1.87	-	-	-	-	-	-	-	-	-	-	-	-
Presubgenual frontal cortex R	81	0.104	0.08	0.246	1.83	-	-	-	-	-	-	-	-	-	-	-	-
Superior temporal gyrus anterior part L	82	0.092	0.09	0.325	2.53	-	-	-	-	-	-	-	-	-	-	-	-
Superior temporal gyrus anterior part R	83	0.109	0.10	0.294	1.93	0.300	1.99	-	-	-	-	0.347	2.48	-	-	-	-

Supplementary Table 5. Binding potential (BP) values and z-scores (Z) for brain regions with statistically significant increased [^{18}F]AV1451 binding potential in each patient (Pt) compared to controls at $p < 0.05$ uncorrected (tests surviving FDR correction are in bold). Mean and standard deviation (SD) values for controls are also reported).

Region		Controls		Pt A		Pt B		Pt C		Pt D		Pt E		Pt F		Pt G	
Name	#	Mean	SD	BP	Z	BP	Z	BP	Z	BP	Z	BP	Z	BP	Z	BP	Z
Hippocampus L	2	0.073	0.08	-	-	-	-	0.339	3.12	-	-	-	-	-	-	-	-
Amygdala R	3	0.063	0.07	0.352	**4.11**	-	-	-	-	-	-	-	-	-	-	-	-
Amygdala L	4	0.051	0.08	0.243	**2.51**	-	-	-	-	-	-	-	-	-	-	-	-
Anterior temporal lobe medial part R	5	0.000	0.06	0.248	**4.39**	0.136	2.42	-	-	-	-	0.146	2.59	-	-	-	-
Anterior temporal lobe medial part L	6	0.005	0.06	0.373	**6.62**	-	-	0.108	1.86	-	-	0.272	**4.80**	-	-	-	-
Anterior temporal lobe lateral part R	7	0.054	0.08	0.348	**3.67**	0.235	2.27	-	-	-	-	0.217	2.03	-	-	-	-
Anterior temporal lobe lateral part L	8	0.039	0.08	0.420	**4.85**	0.212	2.20	-	-	-	-	0.318	**3.55**	-	-	-	-
Parahippocampal and ambient gyri R	9	0.027	0.06	0.290	**4.11**	0.162	2.11	-	-	-	-	-	-	-	-	-	-
Parahippocampal and ambient gyri L	10	0.043	0.06	0.265	**3.66**	0.187	2.37	0.175	2.17	-	-	-	-	-	-	-	-
Middle and inferior temporal gyrus R	13	0.012	0.06	0.162	**2.56**	0.168	2.68	-	-	-	-	0.118	1.82	-	-	-	-
Middle and inferior temporal gyrus L	14	0.006	0.05	0.289	**6.01**	0.132	2.67	0.149	3.04	-	-	0.280	**5.83**	-	-	-	-
Fusiform gyrus R	15	0.017	0.08	0.301	**3.63**	0.207	2.43	-	-	-	-	-	-	-	-	-	-
Fusiform gyrus L	16	0.030	0.06	0.339	**5.60**	-	-	-	-	-	-	0.271	**4.36**	-	-	-	-
Insula L	20	0.015	0.05	0.145	2.41	-	-	-	-	-	-	-	-	-	-	-	-
Lateral remainder of occipital lobe L	22	-0.038	0.06	-	-	0.093	2.04	-	-	-	-	-	-	-	-	-	-
Cingulate gyrus anterior part L	24	0.128	0.06	0.269	2.32	-	-	-	-	-	-	-	-	-	-	-	-
Cingulate gyrus anterior part R	25	0.093	0.05	-	-	0.188	1.84	-	-	-	-	-	-	-	-	-	-
Cingulate gyrus posterior part L	26	0.072	0.05	0.163	1.84	0.180	2.17	-	-	-	-	-	-	-	-	-	-
Cingulate gyrus posterior part R	27	0.048	0.05	0.150	1.91	-	-	-	-	-	-	-	-	-	-	-	-
Middle frontal gyrus L	28	-0.064	0.05	0.058	2.29	0.160	**4.22**	-	-	-	-	0.073	2.58	-	-	-	-
Middle frontal gyrus R	29	-0.021	0.06	-	-	0.196	3.57	-	-	-	-	-	-	-	-	-	-
Posterior temporal lobe L	30	-0.014	0.06	0.132	2.33	0.132	2.32	-	-	-	-	-	-	-	-	-	-
Posterior temporal lobe R	31	-0.009	0.05	0.087	1.95	0.113	2.48	-	-	-	-	-	-	-	-	-	-
Inferiolateral remainder of parietal lobe L	32	-0.012	0.07	0.130	2.16	0.164	2.69	-	-	-	-	-	-	-	-	-	-
Inferiolateral remainder of parietal lobe R	33	0.007	0.05	-	-	0.156	3.10	-	-	-	-	-	-	-	-	-	-
Caudate nucleus L	34	0.212	0.10	0.396	1.85	-	-	-	-	-	-	-	-	-	-	-	-
Caudate nucleus R	35	0.180	0.11	-	-	0.430	2.34	-	-	-	-	-	-	-	-	-	-
Nucleus accumbens L	36	0.159	0.07	0.618	**6.35**	0.303	1.99	0.432	3.78	-	-	-	-	-	-	-	-

Nucleus accumbens R	37	0.186	0.12	0.423	1.92	0.417	1.86	-	-	-	-	-	-	-	-	-	-
Putamen L	38	0.256	0.08	-	-	0.397	1.85	-	-	-	-	-	-	-	-	-	-
Thalamus L	40	0.230	0.06	0.343	1.84	-	-	0.389	2.59	-	-	-	-	-	-	-	-
Pallidum L	42	0.181	0.09	0.419	**2.64**	0.392	2.34	-	-	-	-	0.448	2.97	-	-	-	-
Pallidum R	43	0.208	0.13	-	-	0.468	2.03	-	-	-	-	-	-	-	-	-	-
Straight gyrus L	52	0.145	0.07	0.498	**4.72**	-	-	-	-	-	-	-	-	-	-	-	-
Straight gyrus R	53	0.128	0.07	0.378	**3.68**	-	-	-	-	-	-	-	-	-	-	-	-
Anterior orbital gyrus L	54	0.010	0.07	0.148	1.92	-	-	-	-	-	-	-	-	-	-	-	-
Anterior orbital gyrus R	55	0.011	0.06	0.149	2.18	-	-	-	-	-	-	-	-	0.222	3.34	-	-
Inferior frontal gyrus L	56	0.056	0.06	0.218	**2.87**	0.227	3.03	-	-	-	-	-	-	-	-	-	-
Inferior frontal gyrus R	57	0.091	0.07	-	-	0.267	2.70	-	-	-	-	-	-	-	-	-	-
Superior frontal gyrus L	58	0.042	0.05	0.198	**2.94**	0.154	2.11	-	-	-	-	0.172	2.46	-	-	-	-
Superior frontal gyrus R	59	0.036	0.07	-	-	0.232	2.95	-	-	-	-	-	-	-	-	-	-
Superior parietal gyrus L	62	0.006	0.06	-	-	0.152	2.48	-	-	-	-	-	-	-	-	-	-
Medial orbital gyrus L	68	0.079	0.07	0.297	**3.35**	-	-	-	-	-	-	-	-	-	-	-	-
Medial orbital gyrus R	69	0.083	0.08	0.244	2.11	0.255	2.25	-	-	-	-	-	-	-	-	-	-
Lateral orbital gyrus L	70	0.047	0.07	0.363	**4.50**	0.178	1.87	-	-	-	-	-	-	0.288	3.43	-	-
Lateral orbital gyrus R	71	0.045	0.07	0.193	1.99	-	-	-	-	-	-	-	-	0.341	3.97	-	-
Posterior orbital gyrus L	72	0.041	0.05	0.330	**5.26**	-	-	-	-	-	-	-	-	-	-	-	-
Posterior orbital gyrus R	73	0.067	0.08	0.299	**2.79**	-	-	-	-	-	-	-	-	-	-	-	-
Substantia nigra L	74	0.263	0.11	-	-	-	-	-	-	-	-	0.536	2.56	-	-	-	-
Substantia nigra R	75	0.216	0.13	0.494	2.13	-	-	-	-	-	-	-	-	-	-	-	-
Subgenual frontal cortex L	76	-0.010	0.08	0.236	**3.09**	-	-	-	-	-	-	-	-	-	-	-	-
Subgenual frontal cortex R	77	-0.047	0.05	0.119	**3.49**	0.062	2.30	-	-	-	-	-	-	-	-	-	-
Subcallosal area L	78	0.142	0.12	0.395	2.05	-	-	0.467	2.63	-	-	-	-	-	-	-	-
Subcallosal area R	79	0.114	0.08	0.306	2.35	0.342	2.79	-	-	-	-	-	-	-	-	-	-
Presubgenual frontal cortex L	80	0.112	0.09	0.322	2.29	-	-	-	-	-	-	-	-	-	-	-	-
Presubgenual frontal cortex R	81	0.023	0.07	0.190	2.24	0.254	3.10	-	-	-	-	-	-	-	-	-	-
Superior temporal gyrus anterior part L	82	0.082	0.08	0.379	**3.72**	-	-	-	-	-	-	0.391	**3.87**	-	-	-	-

Chapter 6 | Prognostic imaging markers of cognitive decline in frontotemporal dementia

Preface: A team of researchers and clinicians at the University of Cambridge have contributed to data collection, including Dr. Richard Bevan-Jones, Dr. Thomas E Cope, Dr. Karalyn Patterson, and Dr. Luca Passamonti. Simon Jones, Dr. Tim Fryer and Dr. Young Hong helped with MRI and PET pre-processing. I performed all data analyses and wrote the main text. A related manuscript is in preparation.

Abstract: In this chapter, I assess the predictive value of *in vivo* neuroimaging measures of grey-matter atrophy (structural MRI) and microglial activation ([^{11}C]PK11195 PET), and apathy severity at baseline, on the annual rate of cognitive decline in the clinical frontotemporal dementia spectrum. Baseline grey-matter volume loss across all brain regions, and specifically in the frontal lobe bilaterally, and high levels of neuroinflammation in left frontal regions were associated with a steep decrease in cognitive performance over time. These imaging markers, together with the evaluation of apathy severity at baseline, may be useful tools to evaluate and stratify patients to improve cohort selection in clinical trials and the interpretation and prognostication of clinical outcomes.

6.1. Introduction

Despite the recent extensive application of PET tracers designed to bind microglial activation in Alzheimer's disease research, so far only few studies have been conducted in frontotemporal dementia. PET imaging using TSPO ligands to index activated microglia has shown increased neuroinflammation in frontotemporal regions in patients with sporadic and genetic frontotemporal dementia (Cagnin *et al.,* 2004; Kim *et al.,* 2019; Bevan-Jones *et al.,* 2020). For example, using [^{11}C]PK11195 PET, Cagnin et al. (2004) found increased tracer binding in left dorsolateral prefrontal cortex and the right hippocampus and parahippocampus of 5 patients with nfvFTD or bvFTD, compared to healthy controls (Cagnin *et al.,* 2004).

With the same tracer, Bevan-Jones at al. (2020) demonstrated that *in vivo* PET scans of frontotemporal dementia cases are characterised by elevated neuroinflammation, which is regionally co-localised with protein aggregation in each clinical syndrome. They included patients with all three main clinical syndromes (9 with bvFTD, 9 with nfvPPA and 10 with svPPA), and identified distinct group-related neuroinflammation patterns: in bvFTD mainly involving the superior and inferior frontal gyri and the left orbital gyrus; in svPPA the left insula, bilateral superior and inferior temporal gyri, the right superior parietal gyrus, and the inferior lateral anterior temporal lobe; while in nfvPPA the peak uptake was in the left inferior frontal gyrus. The distinct spatial neuroinflammation patterns accurately distinguished the three frontotemporal syndromes from controls and from each other.

Using *post mortem* brain tissue from patients with frontotemporal dementia, Venneti et al. found that [^{11}C]PK11195 binds specifically to activated microglia and correlates with microglial activation identified by immunohistochemistry (Venneti *et al.,* 2008). In another *post mortem* study, elevated microglial activation was found in the frontal and temporal lobes of 78 patients with frontotemporal lobar degeneration (Lant *et al.,* 2014). Overall, these studies combine with previous evidence from genetic associations (Ferrari *et al.,* 2014; Broce *et al.,* 2018; Pottier *et al.,* 2019), CSF studies (Sjögren *et al.,* 2004; Woollacott *et al.,* 2018) and animal models (Yoshiyama *et al.,* 2007; Bhaskar *et al.,* 2010), to suggest a key role of neuroinflammation in frontotemporal dementia-associated pathology, especially in frontotemporal brain regions – and that microglial activation may present at early stages of this disease.

In contrast to the limited literature on PET imaging of inflammation, structural MRI has been widely used in frontotemporal dementia to measure structural brain changes, mostly in cross-sectional studies but also longitudinally (see (Staffaroni *et al.*, 2017; Whitwell, 2019) for a review). In frontotemporal dementia patients, atrophy patterns have been found to correlate more with clinical manifestations than with the associated neuropathology (Gorno-Tempini *et al.*, 2004; Hornberger *et al.*, 2011, 2014; Piguet *et al.*, 2011). This evidence supports the hypothesis that clinical symptoms reflect localised brain damage, and have poor predictive power for the underlying neuropathology across the frontotemporal dementia spectrum. Longitudinal volumetric MRI measures have also become validated biomarkers of disease progression in different clinical frontotemporal phenotypes (Rohrer *et al.*, 2008, 2012; Knopman *et al.*, 2009; Gordon *et al.*, 2010; Brambati *et al.*, 2015; Binney *et al.*, 2017; Staffaroni *et al.*, 2019), suggesting that rates of atrophy may be useful in monitoring and evaluating future therapies. Whereas the value of volumetric MRI measures for the assessment of frontotemporal dementia is therefore well established, the potential value of PET tracers for neuroinflammation to track clinical progression remains unexplored. In particular, there are no reports in the literature of investigations on the predictive value of PET markers for neuroinflammation for the clinical and cognitive changes in the frontotemporal dementia spectrum.

In this chapter, I assess whether *in vivo* measures of brain atrophy, derived from structural MRI, and microglial activation, as measured by [^{11}C]PK11195 PET predict the annual rate of cognitive decline in the clinical frontotemporal dementia spectrum. Taking into account the evidence from Chapter 5, and by previous studies on the variable affinity of [^{18}F]AV-1451 for different tau isoforms and TDP-43 pathology, in this study I focus on imaging markers for atrophy and inflammation, not including [^{18}F]AV-1451 PET in my analyses (see "*Chapter 9 - General Discussion*" for further comments).

Considering convergent evidence reported in the literature and from the two previous experimental chapters of this thesis (Chapter 4 and 5), I expected to find a significant association between baseline measures of both atrophy and neuroinflammation with annual rate of cognitive decline in these patients. Specifically, the hypotheses associations were between lower grey-matter volumes and higher inflammation levels with a faster decline in cognition. Furthermore, I also test the prognostic value of baseline apathy for the annual rate of cognitive decline in post-symptomatic patients. Given previous evidence and findings reported in Chapter

4 on apathy as a major symptom across all frontotemporal syndromes and its predictive value for cognitive decline in the pre-symptomatic phase, a detrimental effect of high apathy levels on worse cognitive performance over time was also hypothesised.

6.2. Methods

6.2.1. Participants

Thirty patients with frontotemporal dementia were recruited as part of the NIMROD study (Bevan-Jones *et al.*, 2017) from the Cambridge University Centre for Frontotemporal Dementia specialist NHS clinics. Ten patients met diagnostic criteria for bvFTD (Rascovsky *et al.*, 2011), 10 cases for nfvPPA and 10 for svPPA (Gorno-Tempini *et al.*, 2011). At the baseline, patients underwent a research protocol 3T MRI and [^{11}C]PK11195 PET, and a standard battery of cognitive tests, which includes the revised Addenbrooke's Cognitive Examination (ACE-R), and the revised Cambridge Behavioural Inventory (CBI-R). Clinical and cognitive assessment were severity repeated on an average of 6-months (mean ± standard deviation (SD)=6.33 ± 0.49 months) intervals up to 5 years.

Written informed consent was obtained from the participants. The NIMROD protocol was approved by the National Research Ethic Service's East of England Cambridge Central Committee and the UK Administration of Radioactive Substances Advisory Committee.

6.2.2. Imaging data acquisition and pre-processing

Structural MRI and [^{11}C]PK11195 PET data were acquired and processed using previously described methods (Bevan-Jones *et al.*, 2017, 2020). Briefly, patients underwent first a 3T MRI scan, and then a dynamic [^{11}C]PK11195 PET scan for 75 minutes. MRI used Siemens Magnetom Tim Trio and Verio scanners (Siemens Healthineers, Erlangen, Germany) with a MP-RAGE T1-weighted sequence, while PET used a GE Advance and GE Discovery 690 (GE Healthcare, Waukesha, USA) PET/CT scanners. Median (mean and standard deviation) of the time interval between the baseline clinical assessment and the imaging scans were: 1.5 (1.70 ± 1.76) months for MRI, and 4.0 (4.37 ± 3.03) months for [^{11}C]PK11195 PET.

Each T1 image was non-rigidly registered to the ICBM2009a template brain using ANTS (http://www.picsl.upenn.edu/ANTS/) and the inverse transform was applied to the Hammers atlas (resliced from MNI152 to ICBM2009a space) to bring the regions of interest to subject MRI space. The T1-weighted images were segmented into grey matter, white matter and cerebrospinal fluid (CSF) with SPM12 and used to determine regional grey matter, white matter and CSF volumes, and to calculate the total intracranial volume (grey matter + white matter + CSF) in each participant. For each subject, the aligned dynamic PET image series for each scan was rigidly co-registered to the T1-weighted MRI image.

Grey matter volumes and BP_{ND} for each tracer were calculated in 83 cortical and subcortical ROIs using a modified version of the Hammers atlas (Hammers *et al.*, 2003; Gousias *et al.*, 2008), which includes parcellation of the brainstem and cerebellar dentate nucleus. Prior to kinetic modelling, regional PET data were corrected for partial volume effects from CSF. For [^{11}C]PK11195, supervised cluster analysis was used to determine the reference tissue time-activity curve and BP_{ND} values were calculated in each ROI using a simplified reference tissue model with vascular binding correction (Yaqub *et al.*, 2012). Modality-specific regional values were combined across the whole brain to obtain a global value for grey-matter volume, corrected for total intracranial volume, and a global volume-weighted mean value for [^{11}C]PK11195 BP_{ND}. Left and right for frontal and temporal lobes were also calculated for each imaging modality (**Figure 19**).

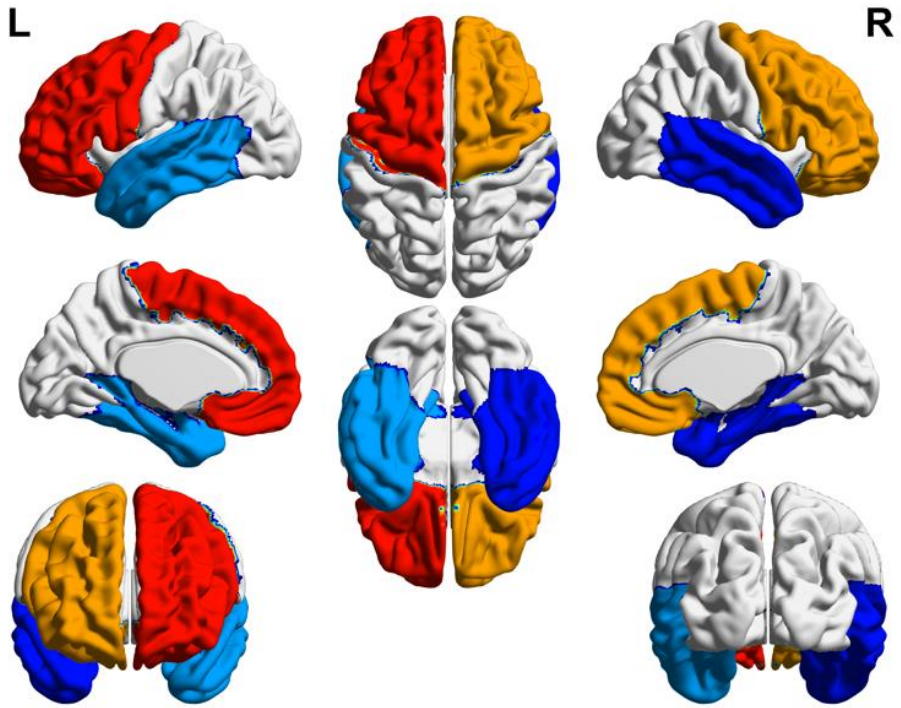

Figure 19. *Four macro-regions considered for the analyses: left frontal lobe (red), right frontal lobe (orange), left temporal lobe (light blue) and right temporal lobe (blue). Lobar values of grey-matter volumes were obtained by adding regional values, corrected for total intracranial volume, while [^{11}C]PK11195 BP_{ND} lobar values were calculated by averaging volume-weighted regional values.*

6.2.3. Statistical analyses

To investigate cognitive changes over time, I considered ACE-R total scores as global measure of cognitive performance, which was undertook at every clinical follow-up visit. At the baseline only, I considered apathy subscale of CBI-R as measure of apathy severity. This scale assesses patients' grade of loss of enthusiasm in personal interests, the reduced interest in new things and in maintaining social relationships, the indifference to family members and reduced affection.

Although Latent Growth Curve model approach was considered to analyse changes over time (see Chapter 3 and 4), in this cohort I decided to apply a linear mixed effects model. This decision was driven by the limited size of the sample and the unstructured nature of the longitudinal data, which were collected at a much more irregular time intervals than other cohorts. Thus, a linear mixed effects model was applied to the longitudinal ACE-R scores

collected from the first research visit to estimate the annual rate of cognitive decline (slope) across all patients. The model included the estimation of a random intercept and slope, with time (in years) as independent variable and the longitudinal cognitive scores as dependent variable. From this model, individual estimate intercept and slope for cognitive performance were extracted for each patient. P-values were obtained with the lmerTest package and via likelihood ratio tests of the model with the time effect against the null model without the time effect. The linear mixed effects analysis was performed using R (R Core Team, 2012) and lme4 (Bates, Maechler & Bolker, 2012).

To test where whole-brain values for grey matter atrophy and microglial activation predict cognitive decline in patients, linear regression models were applied with the estimated rate of cognitive change (slope) as dependent variable, and each modality-specific global value as predictor. Next, to explore the topographical distribution of the tested associations between cognition and brain imaging markers, analogous models were applied with modality-specific left and right frontal and temporal lobar values. I focused solely on frontal and temporal lobes because of the extensive literature about the central involvement of these two brain areas in the three clinical frontotemporal variants (Staffaroni *et al.*, 2017; Whitwell, 2019), and post mortem evidence for activated microglia in these regions (Lant *et al.*, 2014; Woollacott *et al.*, 2020). Age, education and sex were included as nuisance covariates. The association between whole-brain atrophy and neuroinflammation was tested including imaging global and lobar values in inter-modality Pearson correlations.

Univariate models were also applied to test the association between cognitive slope values (dependent variable) and cognitive performance at the baseline, assessed with ACE-R. To test the hypothesised detrimental effect of apathy on disease progression, I applied Pearson correlations on baseline apathy severity scores with baseline ACE-R scores and the annual rate of cognitive change. Age, education and sex were included as nuisance covariates.

6.3. Results

6.3.1. Descriptive statistics

The demographics, clinical and cognitive variables of our sample are summarized in **Table 16**. Age, years of education, baseline cognitive and clinical scores were compared between patient groups with independent-samples t-tests, while sex was compared with the Chi-square test.

***Table 16**. Demographic and clinical characteristics for patients and controls groups (*=significant ANOVA test between subgroups).*

Group	N	Sex (F/M)	Age (mean ± SD)	Education (mean ± SD)	ACE-R (mean ± SD)	Apathy (mean ± SD)
Total	30	14/16	66.10±8.7	13.0±2.9	66.8±17.6	7.5±6.5
bvFTD	10	5/5	60.0±8.6	12.4±2.8	55.8±16.7	12.6±6.3
nfvPPA	10	7/3	71.1±8.8	11.5±2.0	65.9±12.6	3.7±3.9
svPPA	10	2/8	67.2 ±4.7	13.0±2.9	66.8±17.6	6.1±6.0
Diff test		X^2=5.09 p=0.079	F=5.49 p=0.010*	F=6.19 p=0.006*	F=5.62 p=0.009*	F=7.00 p=0.004*
Post-hoc comparisons (Bonferroni)			bvFTD < nfvPPA	nfvPPA < svPPA	bvFTD < nfvPPA	nfvPPA & svPPA < bvFTD

Abbreviations: PT=patient; bvFTD=behavioural variant frontotemporal dementia; nfvPPA=non-fluent variant primary progressive aphasia; svPPA=semantic variant primary progressive aphasia F=Female; M=Male; ACE-R= Addenbrooke's Cognitive Examination Revised; SD=standard deviation

6.3.2. Linear mixed effects model on longitudinal cognitive scores

The linear mixed effects models on longitudinal ACE-R scores indicated a significant effect of time on cognitive performance, with a drop of 15.8 points per year on ACE-R total score. The model comparison against the null model confirmed the significant fixed effect of time (at group level) on ACE-R scores ($\Delta\chi2 = 50.22$, $\Delta df=2$, $p<0.0001$), with a significant between-subject variability (random slope - $\Delta\chi2 = 25.72$, $\Delta df=2$, $p<0.0001$) (**Figure 20**). The study was conducted in parallel with clinics and home visits, thus all available ACE-R scores were included in linear mixed effects models, either from clinical appointments or NIMROD-specific research visits. Although this may introduce some test-retest effects for a few sub-tasks of ACE-R, overall all patients showed a fast decline since the first cognitive assessments.

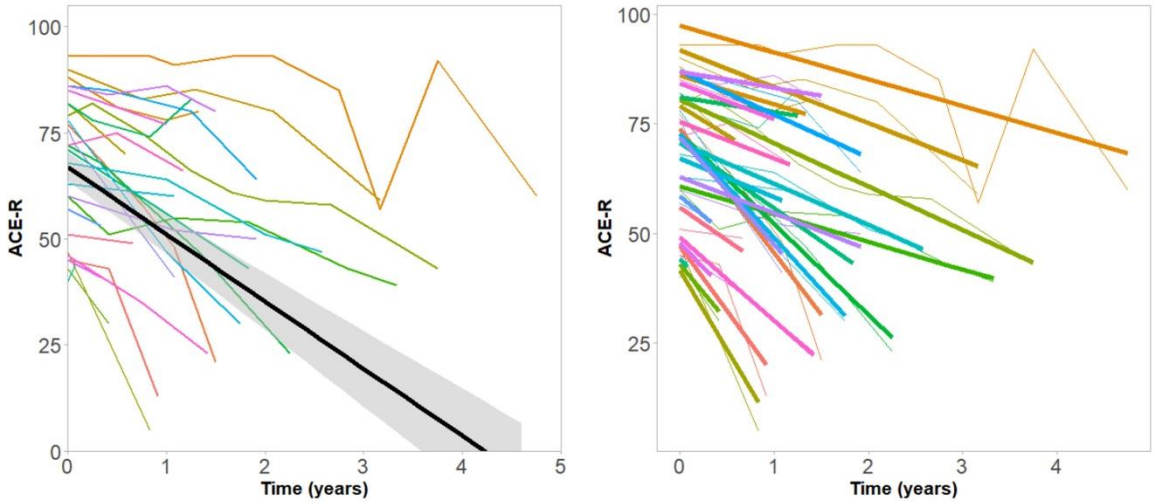

Figure 20. *Longitudinal cognitive scores (ACE-R - y axis) over time (x axis). Left panel represent the raw individual trajectory over time (coloured lines), and the linear average change at group level (black line). Right panel represent the linear change in cognition over time for each patient (coloured straight lines).*

6.3.3. Predictive value of grey-matter volumes and neuroinflammation levels

Across all patients, univariate models with individual slope scores as dependent variable and imaging predictors, identified a significant effect of global grey-matter volume (Std. Beta=0.588, p=0.003), but not of the average inflammation across all brain regions (Std. Beta=-0.047, p=0.827). Models with lobar values, indicated a significant association of cognitive slope with left and right frontal grey-matter volumes (Left: Std. Beta=0.773, p<0.001; Right: Std. Beta=0.596, p=0.004), and left frontal neuroinflammation levels (Std. Beta=-0.509, p=0.033) (**Figure 21**). I then applied a linear model to test whether the interaction between [^{11}C]PK11195 and MRI measures in left frontal regions predicts cognitive changes. The interaction term was not significant (p=0.515). Either grey-matter volumes or inflammation in temporal regions were not associated with cognitive decline.

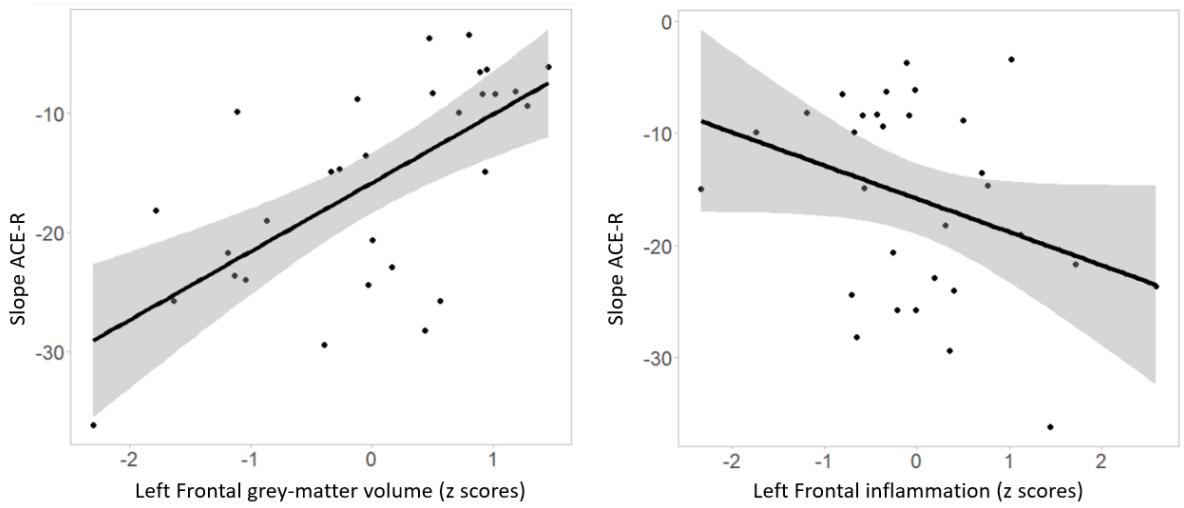

Figure 21. *Significant regression analyses of annual decline in cognition (slope in ACE-R scores, y axis) with baseline grey matter volume scores (x axis, left panel) and inflammation levels in left frontal lobe (x axis, right panel). For imaging values, Z scores are reported to make the two graphs comparable.*

6.3.4. Inter-modality imaging correlations

Inter-modality Pearson correlations between global and lobar values for grey-matter volumes and neuroinflammation levels indicated significant associations in the left and right frontal lobe (Left: R=-0.492, p=0.006; Right: R=-0.365, p=0.047), and in the left and right temporal lobe (Left: R=-0.590, p=0.001; Right: R=-0.372, p=0.043), but not between the global brain values (R=0.012, p=0.950).

6.3.5. Predictive value of baseline cognition and apathy

Univariate models with individual slope scores as dependent variable and baseline cognitive/clinical measures, indicated a significant association with baseline ACE-R scores (Std. Beta=0.649, p<0.0001 – **Figure 22**, left panel) and apathy severity (Std. Beta=-0.503, p=0.010 – **Figure 22**, right panel). Baseline ACE-R and apathy scores were not significantly correlated (R=-0.248, p=0.212), thus I included these two predictors as independent variables in a multivariable linear regression, to test their combined effect on cognitive decline, correcting for individual differences in age, education and sex. The model indicated a significant effect of both predictors in the model (ACE-R: Std. Beta=0.561, p=0.001; apathy: Std. Beta=-0.361,

p=0.024), over and above demographic variables (age: Std. Beta=-0.050, p=0.729 ; education: Std. Beta=0.064, p=0.659; sex: Std. Beta=0.071, p=0.639).

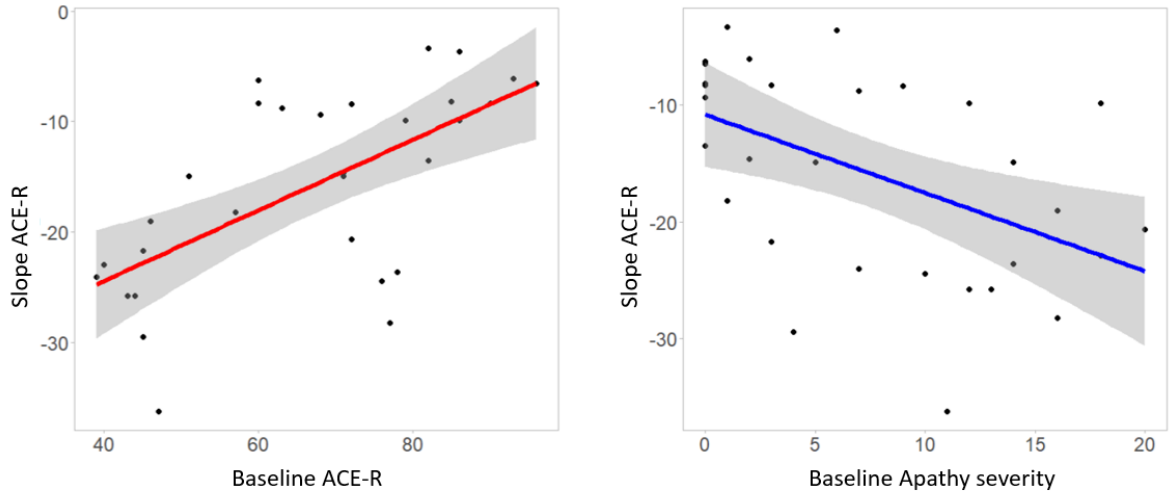

Figure 22. *Significant regression analyses of annual decline in cognition (slope in ACE-R scores, y axis) with baseline ACE-R scores (x axis, left panel) and apathy severity (x axis, right panel).*

6.4. Discussion

This study demonstrates the independent value of neuroimaging markers for brain atrophy (structural MRI), and brain neuroinflammation ([^{11}C]PK11195 PET) in predicting longitudinal cognitive decline in the frontotemporal dementia spectrum. Baseline grey-matter volume loss across all brain regions, and specifically in the frontal lobe bilaterally, is associated with a decrease in cognitive performance over time. Higher levels of neuroinflammation are also related to steeper cognitive decline, however this association is limited to the left frontal cortex.

In this study, PET imaging for microglial activation showed a limited predictive effect on longitudinal cognitive decline in frontotemporal dementia, as compared to atrophy markers. This result may be explained by the advanced stage of disease progression in the patients, during which neuroinflammatory processes may reach a plateau. Other TSPO studies have reported evidence that neuroinflammation may start early in frontotemporal dementia, preceding the development of the full syndrome in pre-symptomatic carriers of MAPT mutations (Miyoshi *et al.*, 2010; Bevan-Jones *et al.*, 2019). In particular, elevated levels of microglial activation were found in frontotemporal regions of a pre-symptomatic MAPT mutation carrier, compared to

controls, despite a lack of protein aggregation and only marginal grey-matter atrophy, limited to the amygdala region (Bevan-Jones *et al.,* 2019). Levels of [^{11}C]PK11195 binding in this pre-symptomatic carrier were comparable to those in a symptomatic patient with the same monogenetic mutation, who however was also characterised by elevated [^{18}F]AV-1451 binding (as index of tau pathology) (Bevan-Jones *et al.,* 2019). Although longitudinal PET studies are needed to clarify the role of microglial activation, as a promoter of junk protein accumulation or an early protective reaction, these results in pre-symptomatic frontotemporal dementia support the hypothesis that microglial activation may precede not only clinical symptom onset in frontotemporal dementia patients, but also the associated protein aggregation and neuronal loss.

In post-symptomatic frontotemporal cases, elevated microglial activation has been described in frontotemporal regions across all clinical variants by previous PET studies with TSPO ligands (Cagnin *et al.,* 2004; Kim *et al.,* 2019; Bevan-Jones *et al.,* 2020). However, none of these studies has investigated the association between frontotemporal inflammation intensity and cognitive impairment. Here, I report the significant association between *in vivo* neuroinflammation levels in the left frontal cortex and the following cognitive decline in patients with a clinical diagnosis of frontotemporal dementia. In this brain area, atrophy severity also showed a significant association with longitudinal cognitive decline and was related to inflammation levels in the same regions. The co-localisation of these associations in frontal regions may reflect the detrimental effect of high levels of neuroinflammation on different cognitive domains whose impairment characterises the three main clinical variants of the frontotemporal dementia spectrum. Tracking cognition in frontotemporal dementia is complicated by the variability of neuropsychological changes between different clinical variants, such as relative episodic memory impairments in bvFTD (Rascovsky *et al.,* 2011), and language deficits in primary progressive aphasia (Gorno-Tempini *et al.,* 2011). However, severe deficits in executive function have been reported across all three clinical syndromes, and in the pre-symptomatic phase of genetic frontotemporal dementia (Geschwind *et al.,* 2001; Rohrer *et al.,* 2015; Staffaroni *et al.,* 2020), and are closely related to frontal regions' functionality. For this reason, further investigation on decline in frontotemporal dementia spectrum should focus on indices for executive dysfunction, or other common features across all syndromes, such as social cognition deficits. This may also reduce the risk of test-retest effects in re-using the same tests

at follow-ups to assess domains that are not impaired in these patients, such as some parts of the ACE-R with visuospatial tasks that contribute to the global score of the assessment.

Moreover, faster decline in cognition was associated with baseline atrophy not only in frontal cortex but also a global index of whole-brain atrophy, calculated as grey-matter volume values across all brain regions. This result was expected in the light of previous MRI evidence that reported wide and profound atrophy patterns across all clinical frontotemporal variants (see (Staffaroni *et al.,* 2017; Whitwell, 2019) for a review). Indeed, the visual evaluation of MRI scans for evident and marked structural abnormalities associated with frontotemporal dementia is widely used during the diagnostic process of these patients, especially for bvFTD (Rascovsky *et al.,* 2011). In my study, the strong association between the whole-brain index for atrophy at baseline and the rate of cognitive decline in the following years of follow-up suggests that this index may be a useful marker to stratify frontotemporal dementia patients into slow or fast decline, which is particular important for the purpose of identifying and characterising the right cohorts for clinical trials.

Finally, the finding of the prognostic value of apathy severity at baseline for longitudinal cognitive decline aligns with previous evidence on the association of apathy severity and negative outcomes in frontotemporal dementia, such as cognitive and functional decline, decreased quality of life and survival rate (Zamboni *et al.,* 2008; Eslinger *et al.,* 2012; Perri *et al.,* 2014; Lansdall *et al.,* 2019, Murley *et al.,* 2020*b*). Together with our findings about the role of apathy as an early clinical manifestation in pre-symptomatic frontotemporal demenita, as reported in Chapter 4, this result in post-symptomatic patients supports the hypothesis that apathy has an early occurrence in the disease progression, preceding and predicting the subsequent decline in cognitive functions in these patients. Baseline cognitive performance was also associated with the annual rate of cognitive decline, but not with baseline apathy severity. In addition, when including both baseline apathy and cognition indices as predictors in the same regression model on cognitive slope over time, both measures showed significant effects. This suggests that apathy severity, as assessed by the apathy CBI-R subscale, explains a part of variability in cognitive decline of these patients that is not explained by the cognitive impairment itself. The lack of association between apathy and cognitive performance scores at baseline also implies that apathy may be an independent symptom that contributes to worsening cognitive deficits, rather than a consequence of cognitive deterioration in these patients.

Our cohort included patients with three different frontotemporal dementia syndromes, that are likely underpinned by different pathologies, involving different brain regions. This represent a limitation in pooling together all participants in the analyses, which is necessary because of the small sample sizes of each variant-specific sub-group. Because of high variability of neural correlates for each syndrome, also the analysis of the involvement of inflammation and atrophy in small regions for the prediction of cognitive decline was limited. For this reason, in this study I focused on macro-area that includes brain regions mainly involved across all three variants, but further studies with larger sample sizes should focus on each variant-specific brain areas. In particular, associations between cognitive decline and inflammation PET showed relatively low significance and need to be confirmed on larger datasets.

6.5. Conclusions

These results support the relevance of *in vivo* atrophy and neuroinflammation markers in frontal regions to predict clinical progression in patients across the frontotemporal dementia spectrum. The combination of structural MRI and [^{11}C]PK11195 PET to evaluate and stratify patients at baseline may be a valuable tool for clinical trials in frontotemporal dementia, to improve cohort selection and the interpretation and prognostication of clinical outcomes. Together with these imaging markers, the evaluation of apathy severity in these patients may equally be useful for patients' stratification, and to develop new symptomatic treatments to decelerate the clinical decline associated with this disease.

Chapter 7 | Neuroinflammation and tau co-localise *in vivo* in progressive supranuclear palsy

Preface: The contents of this chapter has been reported in a research article, which has been published in Malpetti et al. Neuroinflammation and tau co-localize in vivo in progressive supranuclear palsy. *Ann Neurol* 2020: 1–11 - doi: 10.1002/ana.25911

A team of researchers and clinicians at the University of Cambridge have contributed to data collection, including Dr. Luca Passamonti, Dr. Timothy Rittman, Dr. Patricia Vasquez-Rodriguez, and Dr. William Richard Bevan-Jones. I performed all data analyses and drafted the text, with textual revision input from all co-authors. Dr. Tim Fryer and Dr. Young Hong helped with PET pre-processing.

Abstract: In this chapter, I examine the relationship between tau pathology and microglial activation using [^{18}F]AV-1451 (indexing tau burden) and [^{11}C]PK11195 (microglial activation) PET in patients with PSP-Richardson's syndrome. [^{18}F]AV-1451 and [^{11}C]PK11195 binding were positively related across all ROIs, and specifically in sub-cortical (i.e. brainstem and cerebellum) and cortical macro-areas (i.e. supramarginal gyrus and insula). Tau burden and neuroinflammation in sub-cortical areas also related to disease severity. These results suggest that tau pathology and neuroinflammation co-localise in PSP, and that individual differences in subcortical tau pathology and neuroinflammation are linked to clinical severity.

7.1. Introduction

Progressive supranuclear palsy (PSP) is a devastating neurodegenerative disorder caused by the neuro-glial aggregation of tau protein, particularly in the basal ganglia, diencephalon, and brainstem (Dickson *et al.*, 2007; Kovacs *et al.*, 2020). The classical clinical phenotype of PSP is Richardson's syndrome, with vertical supranuclear gaze palsy, akinetic-rigidity, falls, and cognitive decline (Williams *et al.*, 2005; Höglinger *et al.*, 2017). The aggregation of misfolded and hyper-phosphorylated 4R tau, in oligomers and successively into fibrillary tangles, is central to PSP pathology (Dickson *et al.*, 2007; Kovacs *et al.*, 2020). However, neuroinflammation also occurs in PSP, with microglial activation (Ishizawa and Dickson, 2001; Fernández-Botrán *et al.*, 2011), with a proposed toxic alliance between tau-mediated neurodegeneration and neuroinflammation. In the related condition of frontotemporal dementia, tau burden and microglial activation are macroscopically co-localised (Bevan-Jones *et al.*, 2020).

Previous positron emission tomography (PET) has indicated changes in PSP using ligands targeting tau (Kepe *et al.*, 2013; Cho *et al.*, 2017; Hammes *et al.*, 2017; Ishiki *et al.*, 2017; Passamonti *et al.*, 2017; Schonhaut *et al.*, 2017; Smith *et al.*, 2017, Whitwell *et al.*, 2017*b*; Brendel *et al.*, 2018) and microglial activation (Gerhard *et al.*, 2006, Passamonti *et al.*, 2018*b*). However, previous work has not addressed whether *in vivo* tau pathology and microglial activation are related in PSP. Answering this question would shed new lights in the pathophysiological mechanisms underlying PSP and may facilitate the development of therapeutic strategies that synergistically target neuroinflammation and tau pathology in PSP.

I used [^{11}C]PK11195 PET to measure of microglial activation and [^{18}F]AV-1451 PET as an index of tau burden (see discussion regarding limitations of these ligands and their mitigation (Boche *et al.*, 2019; Leuzy *et al.*, 2019)). The latter binds to aggregated tau in Alzheimer's disease and, with lower affinity, to non-Alzheimer's tauopathies (Hall *et al.*, 2017). It also does not distinguish tau- from TDP-43-patholologies. However, this lack of specificity does not undermine its utility to test my hypotheses because: 1) the clinical-pathological correlation in PSP-Richardson's syndrome is very high (Gazzina *et al.*, 2019); 2) significant TDP-43 pathology is exceedingly rare in PSP, and 3) [^{18}F]AV-1451 displays a specific anatomical pattern of binding that clearly distinguishes PSP from Alzheimer's disease (Passamonti *et al.*, 2017). Moreover, to test my hypothesis, it is the distribution, not the relative affinity of binding,

that is critical. [^{11}C]PK11195 is widely used as a marker of microglial activation in neurodegenerative diseases (Stefaniak and O'Brien, 2015), including PSP (Gerhard *et al.*, 2006, Passamonti *et al.*, 2018*b*). It binds the translocator protein (TSPO) on mitochondrial membranes in activated microglia. Although its sensitivity may be affected by its relatively low signal-to-noise ratio and low brain penetration, [^{11}C]PK11195 is not significantly influenced by common genetic polymorphisms that affect second generation TSPO ligands.

I test the hypothesis that neuroinflammation and tau protein aggregation co-localise, and correlate with clinical severity in PSP. I assessed the topography of this relationship with [^{11}C]PK11195 PET and [^{18}F]AV-1451 PET using: (a) binding regional values from 83 brain regions to study correlations across the whole brain; and (b) a set of spatial patterns data-driven determined by principal component analysis (PCA).

7.2. Methods

7.2.1. Participants

As part of the Neuroimaging of Inflammation in Memory and Related Other Disorders (NIMROD) study (Bevan-Jones *et al.*, 2017), we recruited 17 patients with a clinical diagnosis of probable PSP according to Movement Disorder Society (MDS) NINDS-SPSP 1996 criteria. All patients also met the later MDS-PSP 2017 criteria for PSP-Richardson's syndrome (Höglinger *et al.*, 2017). Patients underwent PET scanning with both [^{11}C]PK11195 and [^{18}F]AV-1451, to respectively assess neuroinflammation and tau pathology. To minimise radiation exposure in healthy people, two groups of control participants were enrolled: n=16 underwent [^{11}C]PK11195 PET and n=15 underwent [^{18}F]AV-1451 PET. At the first visit, demographic and cognitive measures (i.e. the revised Addenbrooke's Cognitive Examination - ACE-R) were collected in all participants. Disease severity of patients was measured at the baseline visit and follow-up visits, using the PSP rating scale (PSP-RS) (Golbe and Ohman-Strickland, 2007).

Participants had mental capacity to take part in the study and provided written informed consent. The protocol was approved by the National Research Ethic Service East of England Cambridge Central Committee and the UK Administration of Radioactive Substances Advisory Committee.

7.2.2. Imaging data acquisition and pre-processing

Patients underwent 3T MRI together with [^{11}C]PK11195 and [^{18}F]AV-1451 PET, using dynamic imaging for 75 and 90 minutes respectively. MRI used Siemens Magnetom Tim Trio and Verio scanners (Siemens Healthineers, Erlangen, Germany), while PET used a GE Advance and GE Discovery 690 (GE Healthcare, Waukesha, USA). The use of identical emission data acquisition protocols and image reconstruction algorithms on the two scanners meant that the differences were effectively limited to the attenuation correction method (rotating rod ^{68}Ge/^{68}Ga transmission scan vs. a low dose CT scan) and the axial spatial resolution (6.8 mm FWHM vs. 5.1 mm FWHM). Regarding the attenuation correction, the CT (Hounsfield unit) to 511 keV linear attenuation coefficient transformation used on GE PET/CT systems is that of Burger et al (Burger *et al.*, 2002), which was determined from data acquired with a GE Discovery LS PET/CT, the PET part of which is identical to the GE Advance, thereby enhancing the correspondence between GE PET and PET/CT systems. With respect to differences in spatial resolution, the primary data given in the paper are for large regions of interest. This will limit the impact of any spatial resolution differences, which for brain imaging on the scanners used mainly occur in the axial dimension. Furthermore, patient motion, together with resolution losses in image processing steps, such as realignment of dynamic image series and co-registration to MR, will reduce these differences. The interval between [^{11}C]PK11195 and [^{18}F]AV-1451 PET scans had mean and standard deviation (SD) of 1.18 ± 1.67 months. Eleven patients underwent [^{11}C]PK11195 and [^{18}F]AV-1451 PET scans using a GE Discovery scanner, while 6 patients were scanned using a GE Advance scanner. These two groups did not differ in demographic or clinical characteristics ($p>0.05$).

For each subject, the aligned dynamic PET image series for each scan was rigidly co-registered to the T1-weighted MRI image. BP_{ND} was calculated in 83 cortical and subcortical ROIs using a modified version of the Hammers atlas (www.brain-development.org), which includes brainstem parcellation and the cerebellar dentate nucleus. Prior to kinetic modelling, regional PET data were corrected for partial volume effects from cerebrospinal fluid by dividing by the mean regional grey-matter plus white-matter fraction determined from SPM segmentation. For [^{11}C]PK11195, supervised cluster analysis was used to determine the reference tissue time-activity curve and BP_{ND} values were calculated in each ROI using a simplified reference tissue model with vascular binding correction (Yaqub *et al.*, 2012). For [^{18}F]AV-1451, BP_{ND} values

were quantified in each ROI using a basis function implementation of the simplified reference tissue model, with superior cerebellar cortex grey matter as the reference region. This cerebellar region was selected as reference region given *post mortem* evidence showing only sporadic tau in PSP (Jellinger, 2010; Passamonti *et al.*, 2017). The cerebellar reference region was carefully drawn to exclude cerebellar dentate nucleus and white matter, that have been reported as affected by tau pathology in PSP (Dickson *et al.*, 2007; Kovacs *et al.*, 2020). The same data acquisition and analysis approach was applied for the two control groups. In control groups, 10 individuals were scanned using the GE Discovery scanner (N=3 with [^{11}C]PK11195 and N=7 [^{18}F]AV-1451), and 21 were scanned using the GE Advance (N=13 with [^{11}C]PK11195 and N=8 [^{18}F]AV-1451).

7.2.3. Statistical Analyses

Age, years of education, ACE-R total and fluency scores were compared between patients and controls with independent-samples t-tests, while sex was compared with the Chi-square test. Statistical analysis proceeded in four steps.

First, to test whether microglial activation and tau pathology co-localised across the whole brain, I estimated the Pearson correlation of corresponding [^{11}C]PK11195 and [^{18}F]AV-1451 BP_{ND} group-average values across all 83 ROIs. I also applied a linear mixed effects model that takes into account the variability between subjects in both intercept and slope of the relation between the two tracers' regional binding. I compared three models: (i) an initial model with only a random intercept term for patients, (ii) a model with also the fixed effect of regional [11C]PK11195 PET values (x variable) on regional [18F]AV-1451 PET (y variable), and (iii) a model with uncorrelated random intercept and random slope terms. The R function permlmer() was used to perform permutation tests on the terms of interest in each model comparison.

Second, the number of ROIs was reduced from 83 to 43, averaging left and right regional BP_{ND} values, as in previous studies (Passamonti *et al.*, 2017, 2018*b*). This step reduces the degrees of freedom, increasing power, and is justified in PSP in which the motor syndrome is essentially symmetric. Differences between PSP and controls in the ROIs were tested for each ligand with independent t-tests and false discovery rate (Benjamini-Hochberg FDR) correction for multiple comparisons.

Third, in PSP patients, BP_{ND} values in the 43 bilateral ROIs were included in separate PCAs for [^{11}C]PK11195 and [^{18}F]AV-1451. This reduces the data dimensionality further, identifying a small set of components that best explain the data variance. The resulting component reveal anatomical patterns covary in terms of neuroinflammation or tau pathology. The orthogonal varimax rotation was applied on the single PCA, separately for each ligand. This rotation serves to maximise the dispersion of loadings within components and to facilitate their interpretability (i.e., anatomical patterns of neuroinflammation and tau pathology). We selected components with eigenvalues >1, up to a cumulative total of >80% of variance explained. PET components were visualised with BrainNet Viewer (Xia *et al.*, 2013*b*).

Finally, to test for co-localisation of microglial activation and tau pathology in specific neuroanatomical patterns of ligand binding, I performed Pearson correlations between individual scores of each ligand-specific component extracted. Bonferroni's method was used to correct for multiple comparisons. I also report the analyses adjusted for age, education and sex, or for variability in the time interval between PET scans, included as covariates of no interest. For each ligand, I tested for significant associations between regionally specific inter-modality correlating PCA clusters (i.e., anatomical patterns of neuroinflammation and tau pathology) and disease severity. For clinical severity, I imputed PSP-RS scores for the time of each scan, using multivariate imputation by chain equations (*mice* function in R software 4.0.0 - R Core Team, 2012). Patient id number, months from baseline to each follow-up visit, and all available PSP-RS scores were included in the multiple imputation. From this, 100 sets of PSP-RS scores were imputed for each PET scan, with N=50 iterations to generate each estimated dataset. The average value per participant across all 100 ligand-specific estimated PSP-RS scores (**Figure 23**, blue and red dots), was retained for correlation analyses with imaging components. These correlation analyses were repeated using a single raw PSP-RS score as clinical severity index, identified as the closest clinical assessment to both PET scans.

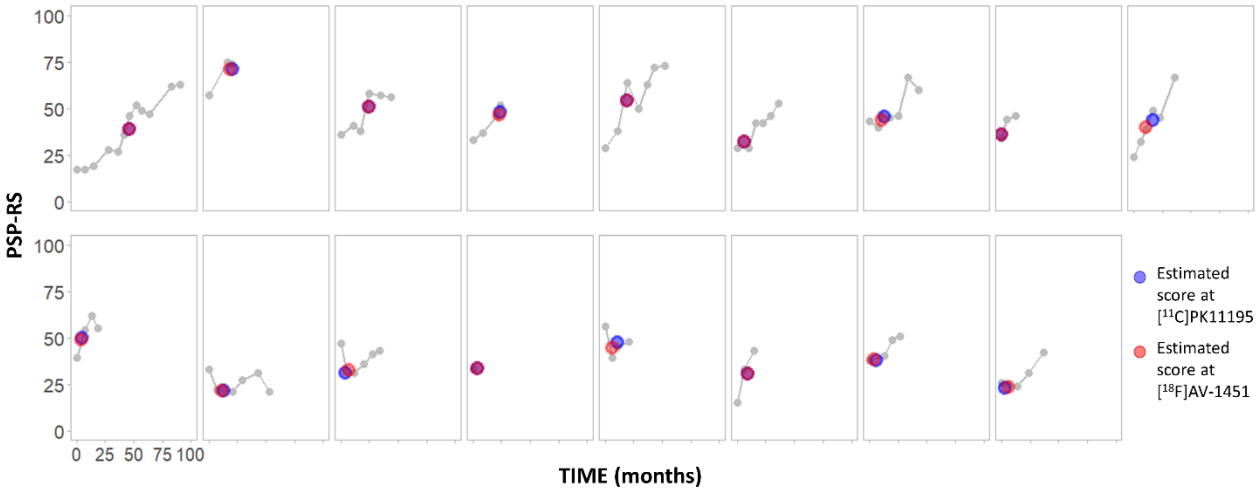

Figure 23. *Longitudinal PSP-RS scores for each patient (grey), and estimated PSP-RS scores at the time of [11C]PK11195 (blue) and [18F]AV-1451 PET (red).*

7.3. Results

7.3.1. Descriptive statistics

Demographics, clinical and cognitive variables are summarized in **Table 17**. There were no group differences in age ($t(46)=0.14$, $p=0.892$) or sex ($X^2(1)=0.230$, $p=0.632$). Differences between PSP and control groups were found in the ACE-R total scores ($t(46)=4.53$, $p<0.001$), fluency ACE-R sub-scores ($t(46)=6.11$, $p<0.001$), and years of education ($t(46)=3.64$, $p=0.001$). Mean and SD of estimated PSP-RS scores at the time of PET are also included in **Table 17**.

Table 17. *Demographic and clinical characteristics for patients and controls groups (*=significant t-test between groups). Raw PSP rating scale (PSP-RS) score refers to the closest assessment to the PET scan, while estimated PSP-RS using multiple imputation refers to the adjusted value to the time midway between the two PET scans.*

	PSP patients	**Controls**	**Difference**
N	17	31	
Sex (F/M)	7/10	15/16	X^2=0.23, p=0.632
Age (mean ± SD)	68.3±5.7	68.6±7.1	t(46)=0.14, p=0.892
Education (mean ± SD)	12.1±1.9	14.8±2.6	t(46)=3.73, p=0.001*
ACE-R (mean ± SD)	82.7±10.5	94.6±4.0	t(18.5)=4.53, p<0.001*
Fluency (mean ± SD)	7.0±3.2	12.1±1.7	t(21.1)=6.11, p<0.001*
Raw PSP-RS at PET scans (mean ± SD)	41.9±14.0	-	
Imputed PSP-RS at PET scans (mean ± SD)	40.5±12.2	-	

Abbreviations: ACE-R= Addenbrooke's Cognitive Examination Revised; PSP-RS= Progressive Supranuclear Palsy Rating Scale; SD= standard deviation; p= p-value; t()= t-test; X^2=Pearson's Chi-square test; F/M=Female/Male

7.3.2. Regional [^{11}C]PK11195 and [^{18}F]AV-1451 BP_{ND} in PSP

Regional group mean [^{11}C]PK11195 BP_{ND} correlated with the corresponding [^{18}F]AV-1451 BP_{ND} across the whole brain (R=0.577, p<0.0001) (**Figure 24**A). At the group level, patients with PSP had high [^{11}C]PK11195 BP_{ND} in the brainstem, cerebellum, thalamus, and occipital and cingulate cortex, with pons and medulla having the highest values (pons: 0.19 ± 0.08; medulla: 0.23 ± 0.13). High [^{18}F]AV-1451 BP_{ND} was found in the basal ganglia, midbrain and thalamus (**Figure 24**A), with the basal ganglia having the highest value (mean=0.33; SD =0.10). The model comparisons on linear mixed effects models identified as optimal model the one with a fixed term for the effect of [^{11}C]PK11195 on [^{18}F]AV-1451 regional, and uncorrelated intercept and slope terms ($\Delta\chi^2$ (1) = 21.28, p = 3.972e-06, perm-p= 0.001). In this model, the

effect of [^{11}C]PK11195 on [^{18}F]AV-1451 regional values at group level (fixed effect) was significant (Estimate=0.685, SD=0.053, Std Beta=0.550, p = 2.2e-16, perm-p= 0.001) (**Figure 24**B). From the graphs (**Figure 24**), the basal ganglia macro-region did not appear to display a significant correlation, thus I repeated an analogous linear mixed effects model on regional binding potential values in basal ganglia only. Comparing this model with the one without the fixed effect of [^{11}C]PK11195 PET, the model comparison indicated a significant effect of [^{11}C]PK11195 on [^{18}F]AV-1451 values in these regions (Estimate=0.426, SD=0.133, Std Beta=0.280; $\Delta\chi^2$ (1) = 8.82, p = 0.003, perm-p= 0.007).

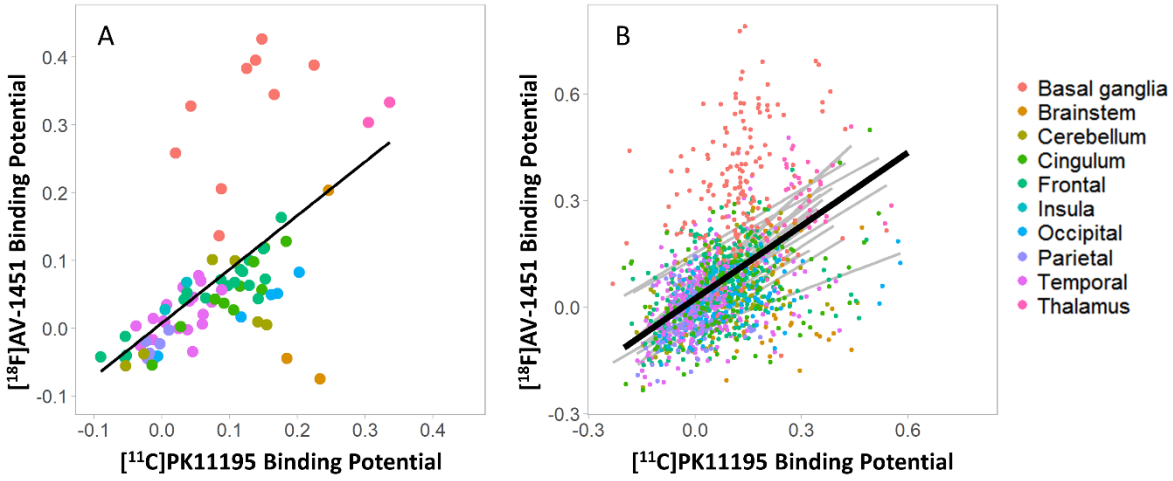

Figure 24. *Whole brain correlation between regional mean non-displaceable binding potential (BP_{ND}) of [^{11}C]PK11195 and [^{18}F]AV-1451 in the PSP group. Panels A: each point represents the average value across all patients for a specific brain region, while. Panel B: dots represent individual regional values for each patient, the black line represents the association between the two tracers at group level, while grey lines are individual correlations, within each patient. In both panels, colours indicate brain macro-areas reported on the right.*

[^{11}C]PK11195 binding values were higher in PSP patients than in controls in the putamen (t(31)=4.08, p<0.001 uncorrected, p=0.013 FDR correction), and pallidum (t(31)=3.72, p<0.001 uncorrected, p=0.017 FDR correction). Likewise, [^{18}F]AV-1451 binding was significantly increased in PSP, than controls, in the putamen (t(30)=3.66, p<0.001 uncorrected, p=0.008 FDR correction), pallidum (t(30)=5.69, p<0.001 uncorrected, p=0.0001 FDR correction), thalamus (t(30)=3.74, p<0.001 uncorrected, p=0.008 FDR correction), midbrain

(t(30)=3.84, p<0.001 uncorrected, p=0.008 FDR correction), and dentate nucleus (t(30)=3.87, p<0.001 uncorrected, p=0.008 FDR correction), confirming our previous findings (Passamonti *et al.*, 2017, 2018*b*). I report only those comparisons that survived FDR correction at p<0.05. I repeated the group comparisons applying multiple regression analyses with group as predictor of region-specific tracer binding and age, education and sex as covariates. Including covariates, [^{11}C]PK11195 binding values were higher in PSP patients than in controls in the putamen (t(31)=3.68, p<0.001 uncorrected, p=0.022 FDR correction), and pallidum (t(31)=3.95, p<0.001 uncorrected, p=0.021 FDR correction). [^{18}F]AV-1451 binding values were higher in PSP patients than controls in pallidum (t(31)=3.81, p<0.001 uncorrected, p=0.032 FDR correction), but also in thalamus, midbrain and dentate cerebellum gyrus when considering uncorrected p-values <0.05. I do not further discuss this group comparison as the principal aim of this study was to study the co-localisation of [^{11}C]PK11195 and [^{18}F]AV-1451 binding in PSP.

7.3.3. Principal component analysis

For [^{11}C]PK11195 BP_{ND}, four components were identified which collectively explained 81.4% of the data variance (**Figure 25**, left panel; Supplementary Table 6). Component 1 reflected [^{11}C]PK11195 binding in posterior cortical regions, the orbitofrontal cortex and cerebellar grey-matter (62.9% of the total variance). Component 2 grouped together medial and superior regions of the temporal lobe including the amygdala, hippocampus and para-hippocampal gyrus, as well as other cortical areas such as the insula and temporo-parietal junction (9.2% variance). Component 3 was weighted to brainstem regions (i.e. midbrain and pons), the dentate nucleus, and the cerebellar white-matter (5.1% variance). Component 4 comprised superior and medial frontal regions (4.3% variance).

Likewise, four components were found for [^{18}F]AV-1451 BP_{ND} which explained together 81.8% of the data variance (**Figure 25**, right panel; Supplementary Table 7). Component 1 reflected global [^{18}F]AV-1451 cortical binding, especially in frontal cortical regions (61.3% of the total variance). Component 2 reflected [^{18}F]AV-1451 BP_{ND} binding in the insula and medial temporal lobe regions (e.g. amygdala, hippocampus) (8.6% variance). Component 3 loaded onto the anterior superior temporal gyrus and frontal subgenual cortex (7.0% variance). Component 4 was weighted towards subcortical areas including the midbrain, pons, substantia nigra, thalamus, dentate nucleus and cerebellar white matter (5.0% variance).

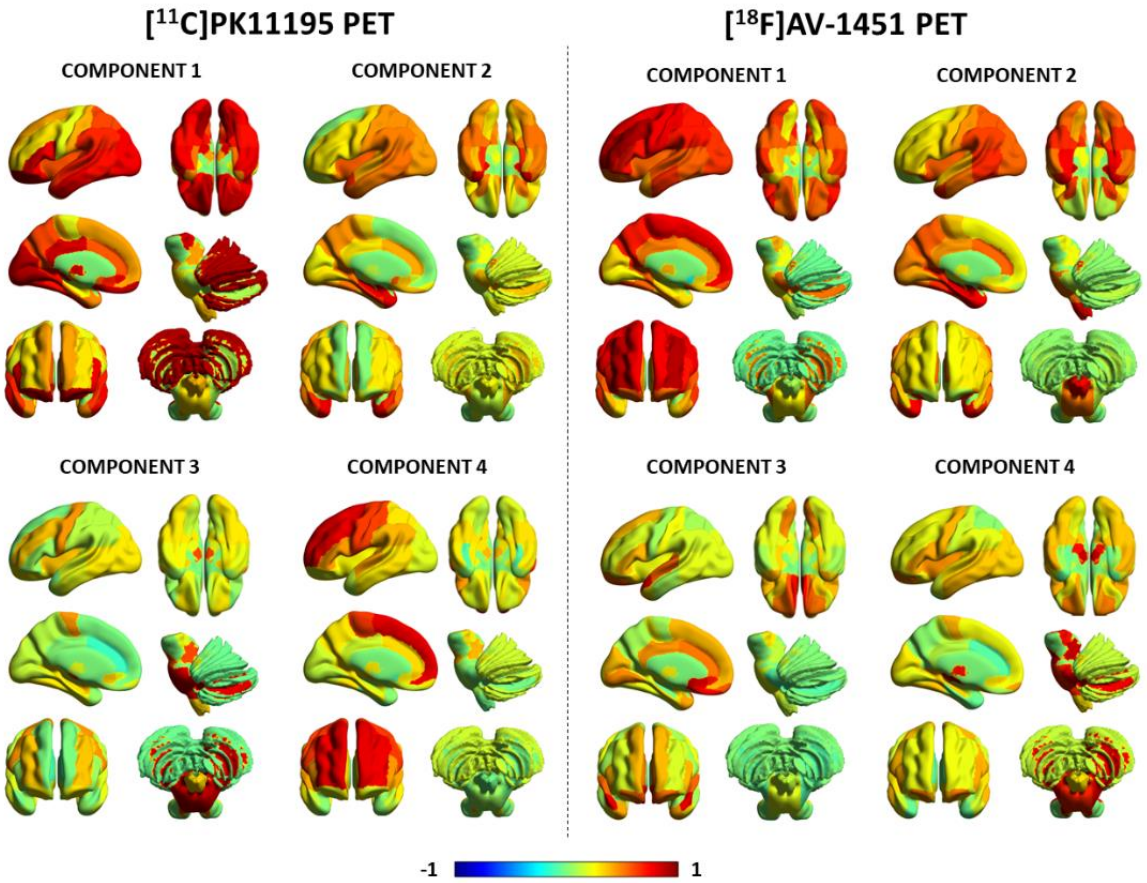

Figure 25. *First four principal components for [11C]PK11195 non-displaceable binding potential (BPND) and [18F]AV-1451 BPND in PSP. The colours represent the rotated weights of all brain regions for each component.*

7.3.4. Inter-modality correlations

After adjusting for Bonferroni correction (p=0.05/16 correlations between [^{18}F]AV-1451 and [^{11}C]PK11195 components), Pearson correlations between individual loading scores for the four [^{11}C]PK11195 components and the four [^{18}F]AV-1451 components showed two significant results (**Figure 26**): 1) [^{11}C]PK11195 component #2 positively correlated with [^{18}F]AV-1451 component #2 (R=0.836, p<0.001), and 2) [^{11}C]PK11195 component #3 positively correlated with [^{18}F]AV-1451 component #4 (R=0.769, p<0.001). Importantly, these correlations remained significant after correcting for age, education and sex ([^{11}C]PK11195 #2 - [^{18}F]AV-1451 #2: R=0.781, p<0.001; [^{11}C]PK11195 #3 - [^{18}F]AV-1451 #4: R=0.742, p=0.002), or for the variability in the time interval between PET scans ([^{11}C]PK11195 #2 - [^{18}F]AV-1451 #2: R=0.804, p<0.001; [^{11}C]PK11195 #3 - [^{18}F]AV-1451 #4: R=0.792, p<0.001). The correlations also remained significant when PET scanner type (GE Advance/GE Discovery) was included as covariate ([^{11}C]PK11195 #2 - [^{18}F]AV-1451 #2: R=0.796, p<0.001; [^{11}C]PK11195 #3 - [^{18}F]AV-1451 #4: R=0.776, p<0.001).

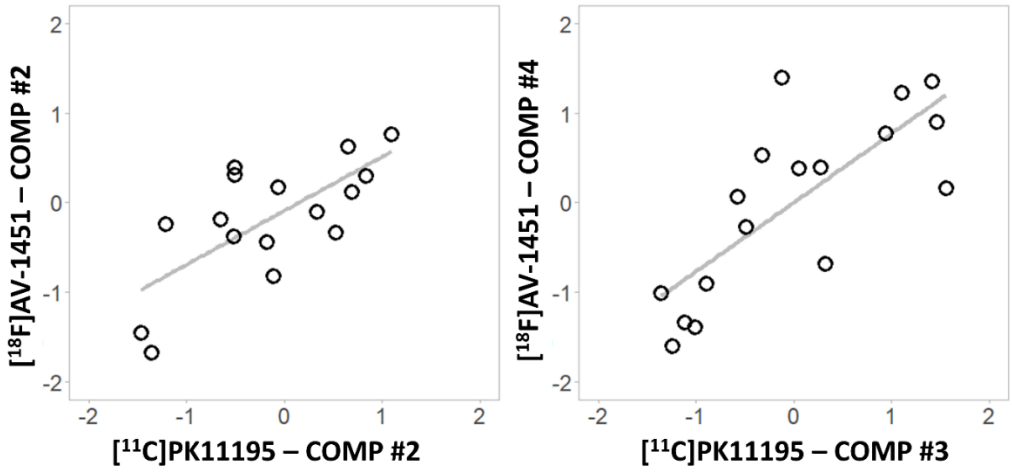

Figure 26. *Significant correlations between [11C]PK11195 and [18F]AV-1451 individual principal component (comp) scores.*

The individual PCA-derived scores for ligand-specific subcortical components separately correlated with disease severity (PSP-RS) (**Figure 27**). The imputed PSP-RS scores for the time of PET correlated highly with the nearest actual PSP-RS assessment ([^{11}C]PK11195, R=0.948, 95% CI= 0.858 to 0.981, p<0.0001; and [^{18}F]AV-1451, R=0.965, 95% CI= 0.902 to 0.987,

p<0.0001). Considering the imputed PSP-RS at the time of the PET scans, both [^{11}C]PK11195 component #3 (R=0.788, 95% CI= 0.496 to 0.920, p<0.001) and [^{18}F]AV-1451 component #4 (R=0.667, 95% CI= 0.275 to 0.869, p=0.003) positively correlated with disease severity (**Figure 27**). These correlations remained significant after correcting for age, education and sex ([^{11}C]PK11195 #3: R=0.773, 95% CI= 0.464 to 0.914, p=0.001; [^{18}F]AV-1451 #4: R=0.671, 95% CI= 0.280 to 0.871, p=0.009). We then applied a linear model to test whether the interaction between [^{11}C]PK11195 component #3 and [^{18}F]AV-1451 component #4 predicts PSP-RS. The interaction term was not significant in the model with the estimated PSP-RS score, adjusted to the time midway between the PET scans (p=0.883). Similar results were obtained using the closest raw PSP-RS to the PET scans as clinical severity measure.

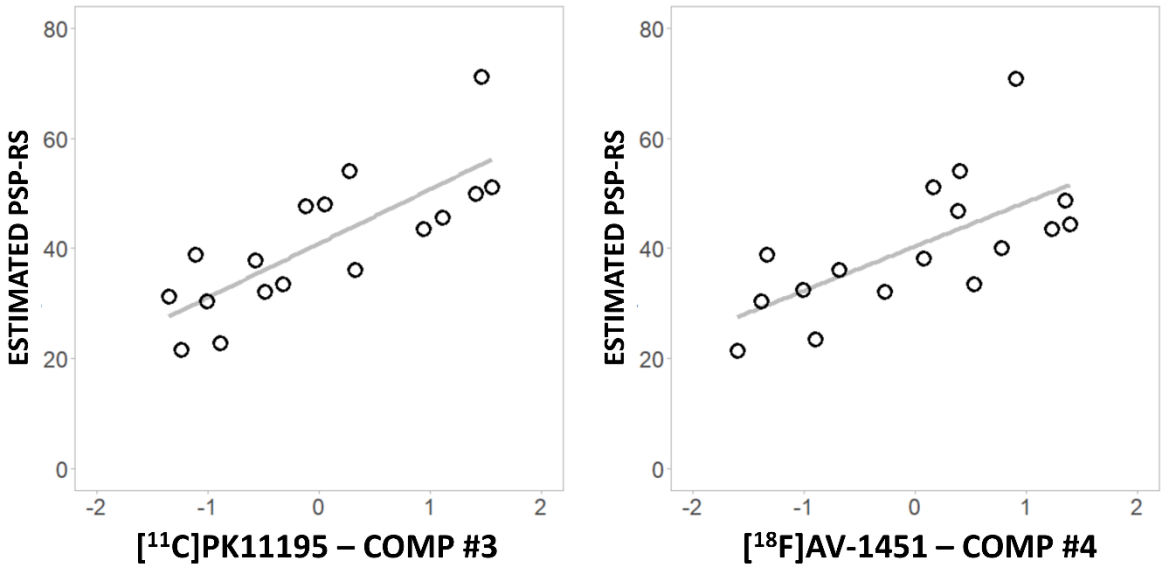

Figure 27. *Significant correlations between subcortical [^{11}C]PK11195 (left) and [^{18}F]AV-1451 (right) component (comp) scores and estimated PSP-RS at the time of each PET scan.*

7.4. Discussion

This study suggests that microglial activation and tau protein aggregation are co-localised in PSP, at least macroscopically at the level of brain regions. The relationship between neuroinflammation and tau pathology is observed across widespread brain regions, although it is most evident in a subset of cortical regions (i.e. insula and temporo-parietal junction) and subcortical structures (i.e. brainstem and cerebellum). This co-localisation resembles that observed between protein aggregation and microglial activation in both Tau- and TDP-43-associated forms of frontotemporal lobar degeneration observed by *post mortem* immunohistochemistry and *in vivo* with the ligands used in this PET study (Bevan-Jones *et al.*, 2020). The *in vivo* measures of neuroinflammation and tau burden in the brainstem and cerebellum were both associated with disease severity.

Before considering the implications of our findings for the pathogenesis of PSP, I discuss the caveats associated with the PET ligands. Although [^{18}F]AV-1451 shows strong *in vivo* and *post mortem* binding to tau pathology in Alzheimer's disease, it displays variable affinity in healthy aging and non-Alzheimer's tauopathies (Marquié *et al.*, 2015; Lowe *et al.*, 2016; Sander *et al.*, 2016). The tracer also binds to non-tau proteinopathies (i.e. is positive in TDP-43 pathology with C9orf72 mutations and semantic dementia (Bevan-Jones *et al.*, 2018*b*, *a*)), and other targets such as neuromelanin (Marquié *et al.*, 2015), choroid plexus (Lowe *et al.*, 2016) and monoamine oxidase (MAO) (Vermeiren *et al.*, 2018). However, off-target binding can neither fully account for [^{18}F]AV-1451 signal in striatum or cortex – as previous *post mortem* analyses reveal that no neuromelanin accumulates there (Hansen *et al.*, 2016; Passamonti *et al.*, 2017) – nor in choroid plexus as histological analysis revealed tangle-like inclusions in its epithelial cells (Ikonomovic *et al.*, 2016). The [^{18}F]AV-1451 off-target binding to MAO (Vermeiren *et al.*, 2018) expressed on reactive astrocytes and activated microglia (Saura *et al.*, 1994; Vermeiren *et al.*, 2018), could in principle contribute to correlated binding of the two ligands. However, a previous report of a carrier of a MAPT genetic mutation described high [^{11}C]PK11195 binding in the absence of significant [^{18}F]AV-1451 binding (Bevan-Jones *et al.*, 2019), which suggests that despite the potential for a common target, the two ligands are not equivalent in their binding. Furthermore, affinity of [^{18}F]AV-1451 for monoamine oxidase is weak and the use of MAO-inhibitors does not significantly displace [^{18}F]AV-1451 binding in patients with tauopathies (Hansen *et al.*, 2018). Nevertheless, I acknowledge that the affinity of [^{18}F]AV-1451 to the 4R tau in non-Alzheimer's tauopathies as PSP is lower than its affinity to

3/4-repeat Alzheimer's related tau pathology (Marquié *et al.*, 2015; Sander *et al.*, 2016). In PSP, higher [^{18}F]AV-1451 binding has been found in sub-cortical rather than cortical regions (the reverse for Alzheimer's disease), consistent with the well-established cortical versus sub-cortical distribution of PSP-Richardson's syndrome (Cho *et al.*, 2017; Hammes *et al.*, 2017; Passamonti *et al.*, 2017; Schonhaut *et al.*, 2017; Smith *et al.*, 2017, Whitwell *et al.*, 2017*b*). This supports the use of [^{18}F]AV-1451 PET to quantify and localise tau pathology in different tauopathies with clear and known pathologic substrates, such as PSP.

The [^{11}C]PK11195 ligand is selective for activated microglia over quiescent microglia or reactive astrocytes (Banati, 2002), but, it has been criticised for its relatively low signal-to-noise ratio and low brain penetration which may affect its sensitivity to activated microglia. Nevertheless, this would reduce effect sizes and increase type II errors, rather than leading to false positive findings. Second-generation PET radioligands for TSPO are characterised by higher signal-noise ratio than [^{11}C]PK11195 but their binding is markedly affected by single nucleotide polymorphisms (rs6971) which cause heterogeneity in PET data and require genetic screening. [^{11}C]PK11195 binding is less affected by this polymorphism, and has well established methods of kinetic analysis (Turkheimer *et al.*, 2007). Hence, [^{11}C]PK11195 PET was the ligand of choice for this study of PSP (Gerhard *et al.*, 2006, Passamonti *et al.*, 2018*b*).

With these caveats in mind, I turn to our principal results. To study the *in vivo* co-localisation between microglial activation and tau pathology in PSP, I applied correlation analyses between binding of the two ligands 1) across all brain regions, and 2) between principal components of a set of bilateral brain regions, extracted to reduce complexity of the imaging data. With the first approach, I found a positive correlation at group level between [^{11}C]PK11195 and [^{18}F]AV-1451 binding across the whole brain (**Figure 24**A), which remained significant also after accounting for the variability between patients (**Figure 24**B). This indicates a close association between microglial activation and tau pathology in PSP that extensively involves subcortical and cortical regions. This finding aligns with *in vivo* correlation between neuroinflammation and tau aggregation in Alzheimer's disease and frontotemporal dementia (Dani *et al.*, 2018; Bevan-Jones *et al.*, 2020). Collectively, these multi-tracer PET studies support previous *in vitro* evidence of the association between microglial activation and tau aggregation in different tauopathies (Vogels *et al.*, 2019). The spatial distribution of this *in vivo* association between microglial activation and tau pathology in PSP mirrors previous findings showing that tau

pathology affects not only subcortical but also cortical regions in PSP Richardson's syndrome (Dickson *et al.,* 2010; Schofield *et al.,* 2011).

When assessing the ligand-specific components from PCA, I found a positive correlation between [^{11}C]PK11195 and [^{18}F]AV-1451 binding in brainstem and cerebellar regions, loaded into anatomically overlapping components of both ligands (**Figure 26**, right panel). This association occurs in motor-related regions that are involved in the neuropathology and symptomatology of PSP (i.e. functional deficits, postural instability, and supranuclear gaze palsy) associated with PSP Richardson's syndrome (Williams and Lees, 2009). Of note, both tau pathology and microglial activation in the brainstem-cerebellar component correlated with disease severity, using either the imputed PSP-RS scores for time of PET scans (**Figure 27**) or the score of the closest PSP-RS assessment to PET scans. This finding adds relevant information to the literature as only a few previous studies have explored how [^{11}C]PK11195 and [^{18}F]AV-1451 binding relate to disease severity in PSP (Cho *et al.,* 2017; Passamonti *et al.,* 2017, 2018*b*; Schonhaut *et al.,* 2017; Smith *et al.,* 2017, Whitwell *et al.,* 2017*b*). In our sample, although the two components individually correlate with clinical severity, they did not interact in their association with PSP-RS. This suggests an additive and partially independent effect of the two pathological processes on clinical progression rather than a synergistic effect, although larger sample sizes and longitudinal designs will need to explore this relationship further.

[^{11}C]PK11195 and [^{18}F]AV-1451 binding were also correlated in a cortical component (**Figure 26**, left panel), which for both ligands was weighted towards regions of the medial temporal lobe, insula and temporo-parietal junction. Previous studies have implicated the medial temporal lobe and limbic structures in basic emotional recognition, which is in turn found to be impaired in PSP, alongside theory of mind and social cognition (Ghosh *et al.,* 2009, 2012). While recognition of happiness was reported to be preserved in patients with PSP, their recognition of negative emotions (i.e. anger, disgust, surprise, fear and sadness) has been reported as affected (Ghosh *et al.,* 2009). Basal ganglia, insula and amygdala have been reported to be implicated in the recognition of predominately negative emotions, and these neuropsychological function is abnormal in PSP (Schofield *et al.,* 2011; Ghosh *et al.,* 2012). the association between microglial activation and tau pathology I found in limbic regions may complement biological explanations of emotion-related and social deficits in PSP. However,

longitudinal studies are needed to clarify the timing of these interacting effects on pathological and clinical disease progression.

Our finding of tau and neuroinflammation co-localisation in the cortex of patients with PSP Richardson's syndrome is in keeping with previous *post mortem* evidence showing tau pathology and atrophy not only in subcortical and limbic regions, but also in the parietal lobe (Schofield *et al.,* 2011). Specifically, the supramarginal gyrus has been described as the most affected brain region in two independent pathological cohorts of patients with PSP Richardson's syndrome (Schofield *et al.,* 2011). The absence of *in vivo* evidence about supramarginal atrophy in the literature may enhance the importance of the demonstrated association between neuroinflammation and tau accumulation in this region as an early biomarker of later-stage neuronal loss.

This study has limitations. First, I acknowledge the limited power of the analyses related to the relatively small size of our sample. Although our cohort is larger than many previous multi-tracer PET studies on rare neurodegenerative diseases like PSP, larger and independent replication samples would be helpful. Second, the recruitment was based on clinical diagnosis, which was confirmed at each follow-up visit; however, *post mortem* pathological confirmation was available only in 8 patients. However, all 8 had PSP, and over 95% of patients with a clinical diagnosis of PSP-Richardson's syndrome have PSP pathology or related 4R-tuaopathy. Third, our results are based on a cross-sectional design, which cannot be used to infer causal relationship between tau and microglial activation. A longitudinal assessment of tau burden, microglial activation and clinical progression alongside mediation analyses are necessary next steps to clarify the interplay between the two pathological processes and their effect on disease severity across time.

7.5. Conclusions

My results confirm the relevance of neuroinflammation to PSP-Richardson's syndrome and a close association with tau pathology. Our findings indicate a macroscopic anatomical relationship between neuroinflammation and tau pathology. Although we cannot infer the causal direction in the relationship between pathological mechanisms, I speculate that microglial activation may be activated by an initial tau misfolding and contribute to tau pathology and propagation. The latter, in turn, may lead to further neuroinflammation, as previously suggested in Alzheimer's disease (see review (Vogels *et al.*, 2019)). Pre-clinical research suggests that microglial activation may precede the formation of tangles (Yoshiyama *et al.*, 2007) and then promote the spreading of pathological tau (Asai *et al.*, 2015). Our findings suggest that the co-localisation of neuroinflammation and tau pathology is an important pathogenetic mechanism in PSP, and both processes may be involved in defining PSP clinical severity. A better understanding of the interaction between the pathological substrates in PSP and its effects on disease progression may crucially contribute to improving patients' stratification and clinical trials. Specifically, our results encourage the application of [^{11}C]PK11195 and [^{18}F]AV-1451 PET as markers of co-localised pathological mechanisms in PSP to develop new targeting therapies and empower clinical trials.

7.6. Supplementary materials of Chapter 7

Supplementary Table 6. Rotated regional weights of four significant [^{11}C]PK11195 PET principal components (PC) identified by principal component analysis on non-displaceable binding potential regional values.

Regions	PC 1	PC 2	PC 3	PC 4
Lingual_gyrus	0.903	0.297	0.145	0.127
Cerebellum_gm	0.900	0.173	-0.034	0.156
Anterior_orbital_gyrus	0.897	0.104	0.288	0.184
Cuneus	0.892	0.232	0.132	0.157
Medial_orbital_gyrus	0.869	0.233	0.196	0.269
Straight_gyrus	0.861	0.370	0.066	0.169
Lateral_orbital_gyrus	0.827	0.351	0.019	0.295
Thalamus	0.820	0.124	0.203	0.294
Gyrus_cinguli_posterior_part	0.816	0.299	0.017	0.165
Caudate_nucleus	0.814	0.086	0.069	-0.002
Presubgenual_frontal_cortex	0.786	0.161	0.211	0.355
Inferior_frontal_gyrus	0.779	0.273	0.059	0.447
Middle_and_inferior_temporal_gyrus	0.774	0.495	0.206	0.277
Lateral_remainder_of_occipital_lobe	0.762	0.437	0.287	0.190
Fusiform_gyrus	0.758	0.371	0.260	-0.076
Anterior_temporal_lobe_lateral_part	0.745	0.547	0.147	0.126
Posterior_orbital_gyrus	0.740	0.490	0.223	0.205
Posterior_temporal_lobe	0.723	0.522	0.287	0.304
Subgenual_frontal_cortex	0.691	0.363	0.350	0.279
Superior_temporal_gyrus_posterior_part	0.687	0.398	0.187	0.423
Inferiolateral_remainder_of_parietal_lobe	0.674	0.499	0.117	0.391
Superior_parietal_gyrus	0.610	0.464	0.112	0.291
Insula	0.586	0.560	0.362	0.253
Cingulate_gyrus_anterior_part	0.579	0.413	-0.127	0.318
Subcallosal_area	0.567	0.555	-0.025	-0.086
Anterior_temporal_lobe_medial_part	0.475	0.798	0.051	0.025
Hippocampus	0.235	0.794	0.311	0.170
Amygdala	0.238	0.789	0.351	0.202
Superior_temporal_gyrus_anterior_part	0.645	0.670	-0.011	0.145
Parahippocampal_and_ambient_gyri	0.513	0.668	0.225	0.279
Nucleus_accumbens	0.443	0.567	-0.237	0.166
Brainstem_pon	0.304	0.129	0.876	0.061
Cerebellum_dentate	0.067	-0.030	0.847	0.198
Cerebellum_wm	0.089	0.365	0.797	-0.015
Brainstem_mid	0.436	0.233	0.608	0.390
Superior_frontal_gyrus	0.426	0.012	-0.004	0.792
Middle_frontal_gyrus	0.298	0.285	0.359	0.778
Precentral_gyrus	0.205	0.315	0.451	0.634
Postcentral_gyrus	0.402	0.455	0.115	0.622
Substantia_nigra	-0.051	0.113	0.074	0.026
Brainstem_med	0.386	0.234	0.331	-0.026
Putamen	0.620	0.099	0.008	0.043
Pallidum	-0.030	0.138	0.473	0.120
Cumulative % of Variance	**62.8**	**72.0**	**77.1**	**81.4**

Supplementary Table 7. Rotated regional weights of four significant [18F]AV-1451 PET principal components (PC) identified by principal component analysis on non-displaceable binding potential regional values.

Regions	PC 1	PC 2	PC 3	PC 4
Middle_frontal_gyrus	0.891	0.278	0.177	0.210
Postcentral_gyrus	0.791	0.465	0.231	0.159
Precentral_gyrus	0.769	0.355	0.073	0.392
Superior_frontal_gyrus	0.766	0.241	0.382	0.225
Lateral_orbital_gyrus	0.731	0.437	0.200	0.174
Inferior_frontal_gyrus	0.711	0.305	0.384	0.410
Inferiolateral_remainder_of_parietal_lobe	0.706	0.620	0.173	0.202
Superior_parietal_gyrus	0.704	0.567	0.077	0.029
Middlend_inferior_temporal_gyrus	0.656	0.511	0.078	0.388
Lateral_remainder_of_occipital_lobe	0.645	0.550	0.193	0.330
Medial_orbital_gyrus	0.584	0.107	0.572	0.415
Superior_temporal_gyrus_posterior_part	0.577	0.380	0.545	0.301
Anterior_orbital_gyrus	0.533	0.106	0.517	0.497
Amygdala	0.240	0.878	0.283	0.131
Hippocampus	0.281	0.825	-0.016	0.341
Parahippocampal_and_ambient_gyri	0.410	0.767	0.326	-0.038
Anterior_temporal_lobe_medial_part	0.307	0.758	0.422	-0.045
Fusiform_gyrus	0.355	0.752	0.178	0.064
Brainstem_med	0.086	0.736	0.133	0.299
Anterior_temporal_lobe_lateral_part	0.449	0.682	0.301	0.188
Posterior_temporal_lobe	0.559	0.668	0.200	0.358
Posterior_orbital_gyrus	0.565	0.636	0.344	0.269
Insula	0.540	0.554	0.225	0.457
Cingulate_gyrus_anterior_part	0.464	0.551	0.511	-0.074
Subcallosal_area	-0.206	0.189	0.840	-0.029
Superior_temporal_gyrus_anterior_part	0.396	0.334	0.794	0.164
Subgenual_frontal_cortex	0.313	0.236	0.785	0.289
Straight_gyrus	0.344	0.400	0.732	0.081
Presubgenual_frontal_cortex	0.418	0.086	0.700	0.318
Cerebellum_dentate	0.003	-0.007	0.193	0.907
Brainstem_mid	0.221	0.227	0.136	0.872
Cerebellum_wm	0.524	0.121	-0.081	0.770
Thalamus	0.395	0.229	0.285	0.726
Brainstem_pon	0.262	0.519	0.193	0.679
Substantia_nigra	0.457	0.274	0.099	0.547
Putamen	0.223	0.296	-0.011	0.296
Caudate_nucleus	0.084	0.061	0.553	0.301
Nucleusccumbens	0.389	0.402	0.255	0.066
Lingual_gyrus	0.246	0.419	0.477	0.210
Pallidum	0.274	0.133	0.227	0.473
Cuneus	0.321	0.482	0.376	0.279
Gyrus_cinguli_posterior_part	0.504	0.450	0.453	0.116
Cerebellum_gm	-0.038	0.032	0.009	0.135
Cumulative % of Variance	**61.3**	**69.9**	**76.9**	**81.8**

Chapter 8 | Prognostic markers of clinical decline in progressive supranuclear palsy

Preface: The content of this chapter is similar to a manuscript which is currently submitted and under peer review (Malpetti et al. "Neuroinflammation predicts disease progression in progressive supranuclear palsy"). The related manuscript has been deposited in medRxiv (https://www.medrxiv.org/ - doi: 10.1101/2020.05.19.20106393).
A team of researchers and clinicians at the University of Cambridge have contributed to data collection, including Dr. Luca Passamonti, Dr. Timothy Rittman, Dr. Patricia Vasquez-Rodriguez, and Dr. William Richard Bevan-Jones. I performed all data analyses and wrote the text, with input from all co-authors. Simon Jones, Dr. Tim Fryer and Dr. Young Hong helped with MRI and PET pre-processing.

Abstract: In this chapter, I test the hypothesis that baseline *in vivo* assessments of regional atrophy (measured by structural MRI), neuroinflammation ([^{11}C]PK11195 PET) and tau pathology ([^{18}F]AV-1451 PET) predict disease progression. Patients showed a 6.2-point change per year on the PSP-RS. Overall, the results suggest that *in vivo* PET markers of neuroinflammation and tau pathology in subcortical regions (i.e. brainstem and cerebellum) predict clinical progression in PSP. Conversely, MRI markers of brain atrophy did not significantly correlate with clinical progression.

8.1. Introduction

Neuroinflammation has been recognized as an common pathogenic process in Progressive Supranuclear Palsy (PSP) and other tauopathies such as Alzheimer's disease (Vogels *et al.*, 2019), with genetic, epidemiological, and imaging associations. For example, activated microglia are found in the neighbourhood of neurofibrillary tangles, even during early stages of disease (Ishizawa and Dickson, 2001; Fernández-Botrán *et al.*, 2011), and are directly synaptotoxic (Vogels *et al.*, 2019). Neuroinflammation, including microglial activation, interacts with tau pathology to promote cell dysfunction and death in preclinical models of tauopathy.

PET radioligands have been developed to assess neuroinflammation and tau pathology accumulation *in vivo* in clinical cohorts. [^{11}C]PK11195 is a widely used PET tracer, that binds primarily to activated microglia in PSP (Gerhard *et al.*, 2006, Passamonti *et al.*, 2018*b*) and other neurodegenerative disorders (Chandra *et al.*, 2019). The ligand [^{18}F]AV-1451 is widely to assess tau pathology in Alzheimer's disease, and can be informative about tau pathology in PSP (Cho *et al.*, 2017; Passamonti *et al.*, 2017; Schonhaut *et al.*, 2017; Smith *et al.*, 2017, Whitwell *et al.*, 2017*b*, 2019) despite lower sensitivity to the tau isoforms in PSP, and off target binding in some regions (Lowe *et al.*, 2016; Marquié *et al.*, 2017). However, it has not been shown whether either of these PET biomarkers of neuroinflammation and tau pathology predict longitudinal clinical progression in these patients.

My main hypothesis was that inflammation in the subcortical regions associated with PSP pathology promote disease progression. I therefore test whether baseline *in vivo* measures of neuroinflammation ([^{11}C]PK11195 PET) predict the annual rate of clinical progression in patients with PSP-Richardson's syndrome. I test secondary hypotheses regarding the predictive value of baseline inflammation elsewhere, tau pathology ([^{18}F]AV-1451 PET) and atrophy (structural MRI).

8.2. Methods

8.2.1. Participants

For this second study, I included the same 17 patients from the previous study, described in Chapter 7. As previously described, all participants underwent a baseline neuropsychological assessment, followed by an MRI scan and two PET scans with [^{11}C]PK11195 and [^{18}F]AV-1451, to respectively assess neuroinflammation and tau pathology. In this second study, disease severity was measured at the baseline visit an serially up to 4 years using the PSP-RS (Golbe and Ohman-Strickland, 2007). Assessments were at an average of 5-months intervals (standard deviation (SD) ± 2.3 months). *Post mortem* confirmation of PSP pathology was available in 8 patients, and for all 17 participants the clinical diagnosis was reviewed and confirmed at follow-up.

8.2.2. Imaging data acquisition and pre-processing

Full details of the imaging protocols have been published elsewhere (Passamonti *et al.*, 2017, 2018*b*). In brief, patients underwent 3T MRI, together with dynamic PET imaging of [^{11}C]PK11195 and [^{18}F]AV-1451 for 75 and 90 minutes, respectively. MP-RAGE T1-weighted MRI was acquired on Siemens Magnetom Tim Trio and Verio scanners (Siemens Healthineers, Erlangen, Germany), while PET scans were performed on a GE Advance and a GE Discovery 690 PET/CT (GE Healthcare, Waukesha, USA). Median (mean and standard deviation) of the time interval between the baseline clinical assessment and the imaging scans were: 0.0 (1.1 ± 1.5) months for MRI, 2.0 (2.7±2.0) months for [^{11}C]PK11195 PET, and 1.0 (1.9±1.8) months for [^{18}F]AV-1451 PET.

For each subject, the aligned dynamic PET image series for each scan was rigidly co-registered to the T1-weighted MRI image. Grey matter volumes and non-displaceable binding potential (BP_{ND}) values for each tracer were calculated in 83 cortical and subcortical ROIs using a modified version of the Hammersmith atlas (www.brain-development.org), which includes parcellation of the brainstem and cerebellar dentate nucleus. Each T1 image was spatially normalised using ANTS (http://www.picsl.upenn.edu/ANTS/) and the inverse transform was applied to a version of the Hammersmith atlas to bring the regions of interest to native T1 space. The T1-weighted images were segmented into grey matter, white matter and CSF with SPM12

(www.fil.ion.ucl.ac.uk) and used to determine regional grey matter, white matter and CSF volumes, and to calculate the total intracranial volume (grey matter + white matter + CSF) in each participant. Prior to kinetic modelling, regional PET data were corrected for partial volume effects from cerebrospinal fluid by dividing by the mean regional grey-matter plus white-matter fraction determined from SPM segments smoothed to PET spatial resolution. For [^{11}C]PK11195, supervised cluster analysis was used to determine the reference tissue time-activity curve and BP_{ND} values were calculated in each ROI using a simplified reference tissue model with vascular binding correction (Yaqub *et al.,* 2012). For [^{18}F]AV-1451, BP_{ND} values were quantified in each ROI using a basis function implementation of the simplified reference tissue model (Gunn *et al.,* 1997), with superior cerebellar cortex grey matter as the reference region. This cerebellar region was selected as reference region given *post mortem* evidence showing minimal tau pathology in PSP (see pathology data in Supplementary material in Passamonti et al. (Passamonti *et al.,* 2017)).

8.2.3. Statistical Analyses

Grey matter volumes and BP_{ND} values for each ligand were combined across the two hemispheres to derive 43 bilateral whole-brain regions of interest (ROIs) (Passamonti *et al.*, 2017, 2018*b*), which were next included in separate PCAs for each imaging modality. Varimax rotation was applied in all PCAs to maximize interpretability and specificity of the resulting components. The components with eigenvalues > 1 were retained, explaining >80% of the cumulative variance.

A linear mixed effects model was applied to the longitudinal PSP-RS scores collected from the first research visit to estimate the clinical annual rate of change at group level, and then extract a patient-specific estimate of disease progression. The model included the estimation of a random intercept and slope, with time (in years) as independent variable and PSP-RS scores as dependent variable. The effect of time on clinical changes has been also tested via likelihood ratio tests of the model described above against the null model without the time effect. The linear mixed effects analysis was performed using R and lme4 package (R Core Team, 2012).

To test whether specific neuroanatomical patterns of grey matter atrophy, microglial activation and tau pathology predict clinical progression, linear regression models were applied with the estimated rate of change (slope) as dependent variable, and each method specific PCA

component as predictor. First, I tested for significant linear regressions on slope with each modality-specific subcortical component as predictor, accordingly with my main hypothesis. Then, I explored the predictive value of cortical components running separate linear regression analyses for each imaging method and component. Age, education and sex were included as covariates of no interest. I tested the correlations between rate of change of clinical scores, the disease duration and the first raw PSP-RS score at the baseline research visit.

Analogous linear regression models were then estimated with the intercept of the clinical severity as dependent variable. This identifies a cross-sectional association between imaging markers and clinical severity at baseline, which was robustly estimated at individual level from the linear mixed effects model on longitudinal PSP-RS scores. For cross-sectional analyses, I expected to find significant associations with subcortical imaging components (Smith *et al.*, 2017, Whitwell *et al.*, 2017*b*).

Lastly, the modality-specific subcortical components were included in cross-modality Pearson correlations to test for associations between the strength of regional atrophy, neuroinflammation and tau pathology.

8.3. Results

8.3.1. Descriptive statistics

The demographics, clinical and cognitive variables of our sample are summarized in **Table 18**. Fifteen out of 17 patients died within 5 years from the baseline assessment (median = 2.5 years; mean ± SD = 2.2 ± 1.0 years from baseline visit). In **Table 18**, I report demographic, clinical characteristics and group comparisons for two subgroups of patients, identified dividing the total group on the median of the time interval between study baseline and death in years. Age, years of education, baseline PSP-RS, and annual rate of change in PSP-RS were compared with independent-samples t-tests; sex was compared with the Chi-square test.

Table 18. *Demographic and clinical characteristics for the total patient group, and for sub-groups split based on patient survival from study baseline relative to the median time interval between study baseline and death (median = 2.5 years; mean ± SD = 2.2 ± 1.0).*

	Total group patients	**Patient survival ≤ 2.5 years**	**Patient survival > 2.5 years**	**Difference**
N	17	8	9	
Sex (F/M)	7/10	3/5	4/5	X^2=0.08, p=0.772
Age (mean ± SD)	68.3±5.7	68.8±7.5	67.9±3.8	t(15)=0.30, p=0.776
Education (mean ± SD)	12.1±1.9	11.9±1.9	12.3±2.0	t(15)=-0.48, p=0.635
Disease Duration (mean ± SD)	4.7±1.8	5.0±1.7	4.8±1.4	t(15)=-0.18, p=0.859
PSP-RS baseline (mean ± SD)	41.2±14.5	46.0±15.6	37.0±12.8	t(15)=1.31, p=0.211
Clinical progression – PSP-RS points/year (mean ± SD)	6.2±1.5	6.4±0.8	5.9±1.9	t(15)= 0.73, p=0.478

Abbreviations: PSP-RS=Progressive Supranuclear Palsy – Rating Scale; SD=standard deviation; t()=t-test; p=p-value

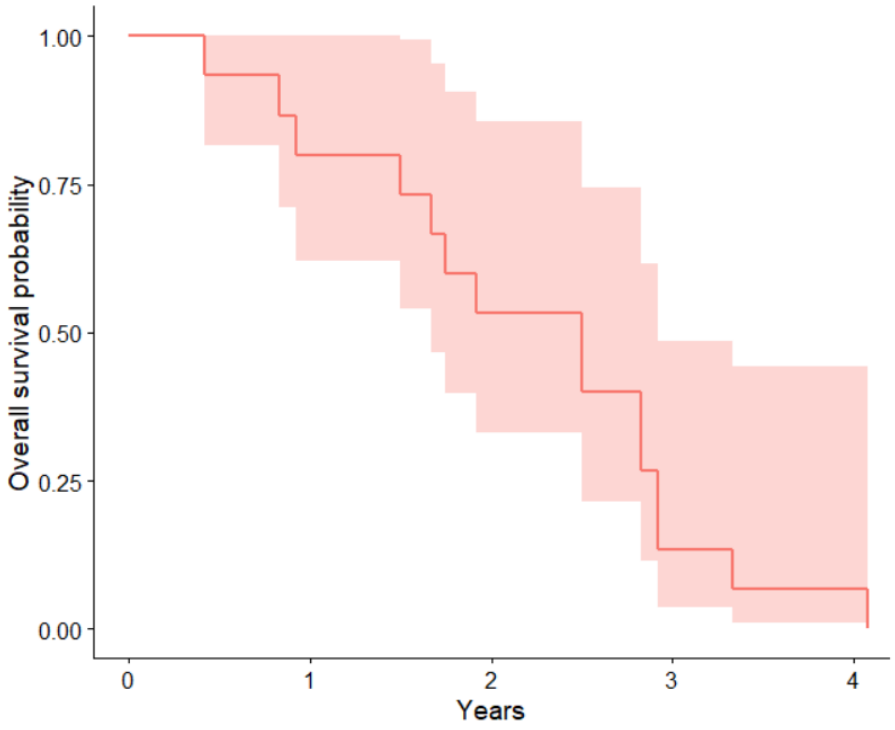

Figure 28. Survival probability plot over time from baseline assessment.

8.3.2. Principal component analysis

For grey matter volumes, seven components were identified, which explained 80.3% of the total data variance. See **Figure 29** (left panel) for a pictorial representation of the first four components and Supplementary Table 8 for more details on regional weights in all seven components. Component 1 was widely distributed, including medial frontal cortex, and thalamus, occipito-parietal regions, posterior cingulate cortex, and post-central cortex, (32.0% of the total variance). Component 2 (11.8% variance) was weighted to the midbrain, substantia nigra and pons in the brainstem, nucleus accumbens and putamen in the striatum as well as to the amygdala, hippocampus and pre-central cortex, cerebellar grey-matter and dentate gyrus. Component 3 (10.0% variance) loaded onto orbitofrontal cortex, anterior temporal lobe and lingual gyrus. Component 4 (7.9% variance) encompassed the superior temporal gyrus, fusiform gyrus, middle inferior temporal lobe, and insula.

For [^{11}C]PK11195 BP_{ND} and [^{18}F]AV-1451 BP_{ND}, each PCA identified four components, which collectively and respectively explained 81.4% and 81.8% of the data variance, as reported in the previous study (Chapter 7). For [^{11}C]PK11195 (**Figure 29**, middle panel), component 1 loaded onto posterior cortical regions, the orbitofrontal cortex and cerebellar grey-matter; component 2 grouped together medial and superior regions of the temporal lobe, insula and temporo-parietal junction; component 3 was weighted to brainstem regions (i.e. midbrain and pons), the dentate nucleus, and cerebellar white-matter; while component 4 included the superior and medial frontal regions. For [^{18}F]AV-1451 (**Figure 29**, right panel), component 1 reflected global cortical binding; component 2 grouped insula and medial temporal lobe regions; component 3 loaded onto the anterior superior temporal gyrus and frontal subgenual cortex; component 4 was weighted towards subcortical areas including the midbrain, pons, substantia nigra, thalamus, dentate nucleus, and cerebellar white matter.

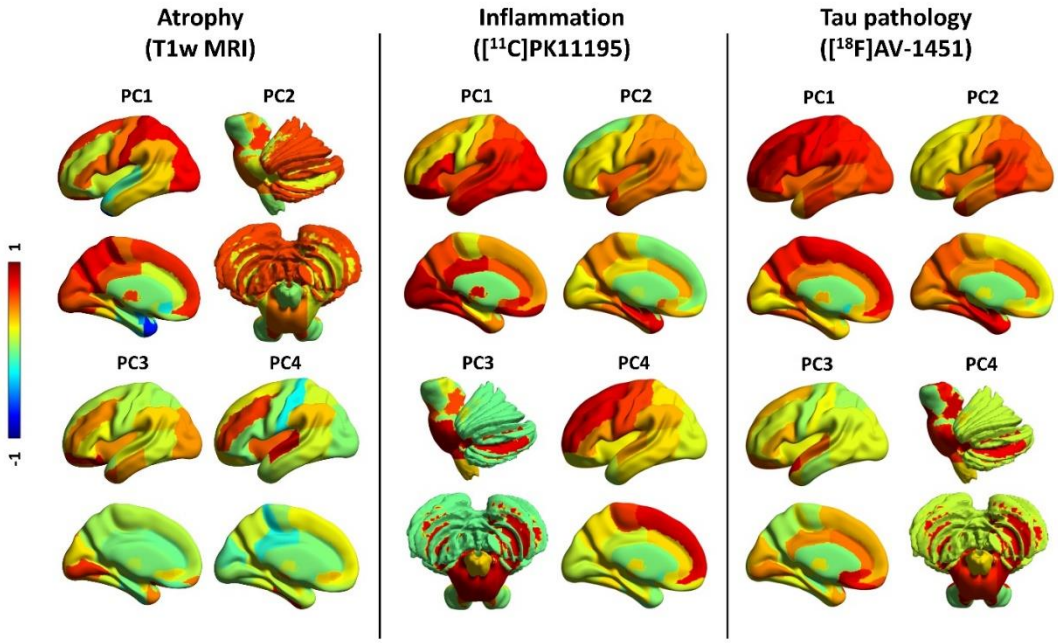

***Figure 29**. First four principal components (PC) for grey matter volumes (left panel), [11C]PK11195 non-displaceable binding potential (BP_{ND} – middle panel), and [18F]AV-1451 BPND (right panel). The colours represent the rotated weights (range: from -1 to 1) of all brain regions for each component.*

8.3.3. Linear mixed effects model on longitudinal PSP-RS

The linear mixed effects model on longitudinal PSP-RS scores, considering the first research visit as baseline score, indicated a significant effect of time (Mean=6.15 points/year, SD=1.06, **Figure 30**). The model comparison against the null model confirmed the significant effect of time ($\Delta\chi2 = 42.61$, $\Delta df=3$, $p<0.0001$). I also applied an analogous model that included all PSP-RS scores available from patients' initial clinical diagnosis visit to their latest clinical visit, confirming a similar annual rate of change in PSP-RS (Mean=7.20 points/year; SD=1.18).

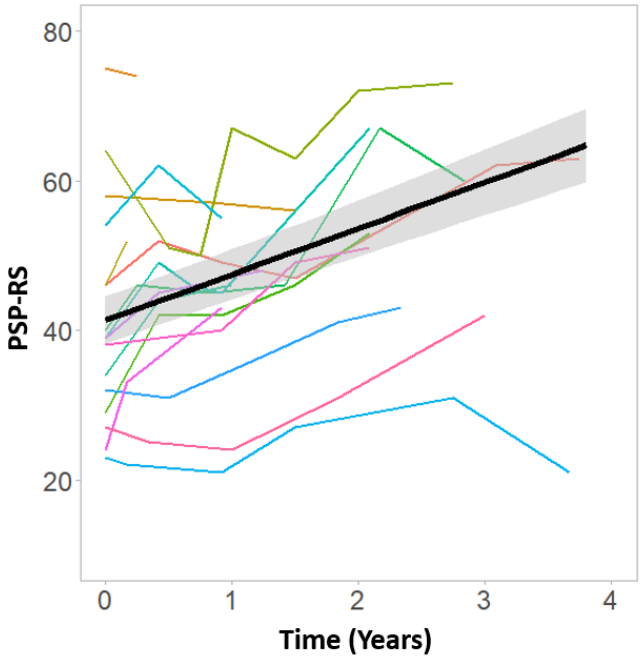

***Figure 30**. Longitudinal change in clinical severity (y axis), as measured by Progressive Supranuclear Palsy Rating Scale (PSP-RS), over time (x axis). Coloured lines represent PSP-RS in each patient at consecutive visits. Black line represents the linear fit at group level, which show an annual rate of change of 6.15 (p<0.0001) points in PSP-RS.*

8.3.4. Single-modality linear regressions

I tested whether imaging markers in subcortical components predicted longitudinal PSP-RS progression, applying a linear regression model for each of the three modality-specific subcortical components (MRI components #2, [^{11}C]PK11195 component #3 and [^{18}F]AV-1451 component #4). Correcting for age, education and sex, the annual rate of clinical progression was related positively with: 1) the [^{11}C]PK11195 subcortical component #3 (Std Beta=0.624, p=0.023 and 2) the [^{18}F]AV-1451 subcortical component #4 (Std Beta=0.840, p=0.003) (**Figure**

31, top row). Applying univariate regression models on slope with single cortical components, age, education and sex as predictors, no other components had significant correlations with the annual rate of clinical progression ($p>0.05$ after FDR correction for multiple comparisons). For MRI, no component showed an association with clinical rate of change ($p>0.05$ after FDR correction for multiple comparisons). The regression models on clinical progression were not significant for disease duration (Std Beta=-0.06, p=0.826 uncorrected), or the baseline PSP-RS score (Std Beta=0.33, p=0.196) as single regressors.

I tested whether imaging markers in subcortical components were related to baseline variation in disease severity. Across the three modality-specific subcortical components, linear regression models with individual PSP-RS *intercept* scores as the dependent variable, correcting for age, education and sex, indicated significant associations with the [^{11}C]PK11195 subcortical component #3 (Std Beta=0.755, p=0.002), and for [^{18}F]AV-1451 subcortical component #4 (Std Beta=0.673, p=0.019) (**Figure 31**, bottom row). However, there was no significant association between intercept and any of the grey-matter components or cortical PET components (all $p>0.05$ after FDR correction for multiple comparisons). The regression model on clinical intercept scores with disease duration (Std Beta=0.41, p=0.107) was not significant.

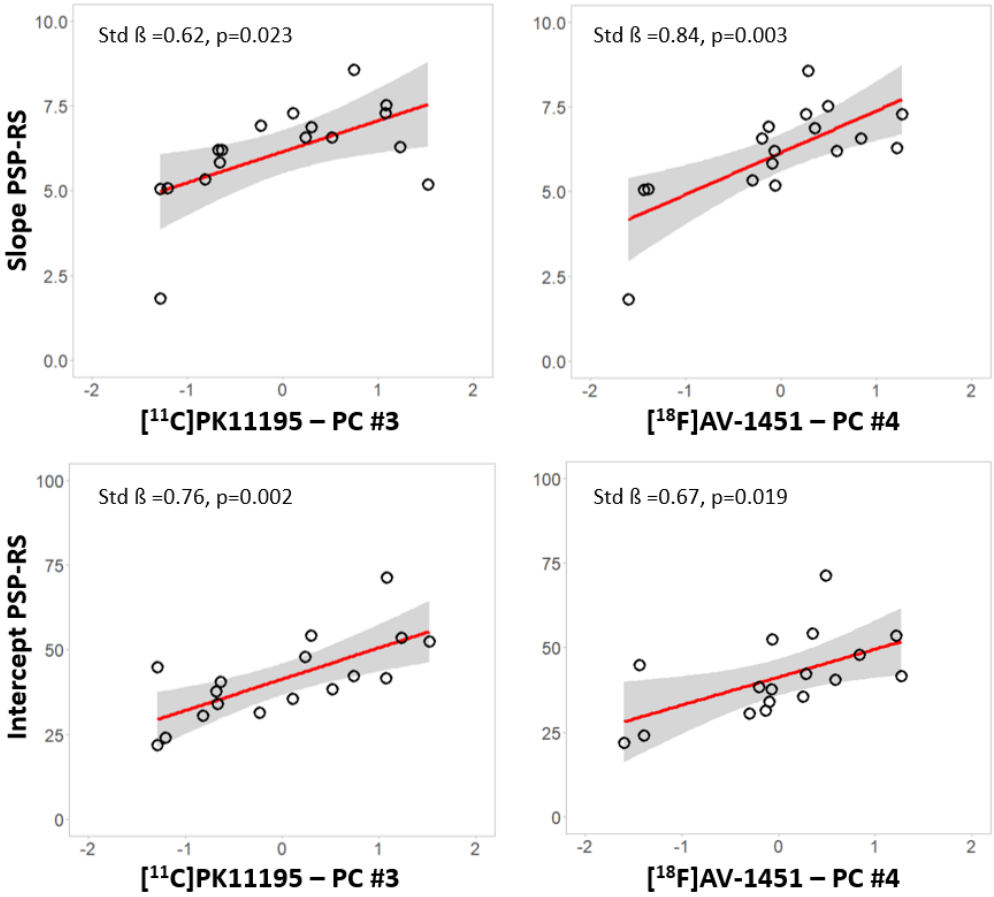

Figure 31. *Significant regression analyses of annual change in Progressive Supranuclear Palsy Rating Scale (PSP-RS) scores (top row) and intercept PSP-RS scores (bottom row) against baseline scores for each modality-specific principal component (x axis – residual component values corrected for covariates): [^{11}C]PK11195 PET (left panel), and [^{18}F]AV-1451 PET (right panel). Estimated parameters are reported for each model with age, education and sex as covariates.*

8.3.5. Inter-modality correlations between predictive imaging components

Simple correlations across subjects between MRI and PET subcortical components of clinical slope were significant for MRI component #2 with [^{11}C]PK11195 component #3 (R=-0.584, p=0.014 uncorrected, p=0.014 FDR correction), and [^{18}F]AV-1451 component #4 (R=-0.626, p=0.007 uncorrected, p=0.011 FDR correction). The correlation between [^{11}C]PK11195 component #3 and [^{18}F]AV-1451 component #4 was also significant (R=0.769, p<0.0001 uncorrected, p<0.0001 FDR correction) (see Chapter 7).

8.4. Discussion

The main finding of this study is that subcortical neuroinflammation is associated with clinical severity at baseline and faster future clinical progression of PSP. A similar effect is seen for the estimated subcortical tau pathology, with the caveats related to interpreting [^{18}F]AV-1451 binding in PSP. The PET markers were correlated with each other and with structural MRI measures for atrophy in the same regions. However, subcortical grey matter atrophy was not correlated with subsequent clinical progression and was not significantly related to clinical severity at the baseline. Similarly, clinical severity at baseline was not predictive of clinical progression in the following years, suggesting that the annual rate of clinical changes is approximately constant throughout different stages of disease.

Several studies have explored the association between changes in clinical severity and *in vivo* neuroimaging markers for microglial activation (Gerhard *et al.,* 2006), tau pathology (Cho *et al.,* 2017; Passamonti *et al.,* 2017; Schonhaut *et al.,* 2017; Smith *et al.,* 2017, Whitwell *et al.,* 2017*b*) and atrophy (Whitwell *et al.,* 2012*b*; Dutt *et al.,* 2016; Tsai *et al.,* 2016; Höglinger *et al.,* 2017). This study however focuses on the prognostic (or predictive) potential of baseline multimodal imaging markers. The baseline uptake of both [^{11}C]PK11195 and [^{18}F]AV-1451 in PSP-related subcortical regions were correlated with the subsequent annual rate of change in severity, as measured by the PSP-RS. Note that I am not testing whether the progression of PET markers compares with progression of disease severity. The progression of [^{18}F]AV-1451 uptake has been compared with the progression of MRI measured of atrophy (Whitwell *et al.,* 2019), with greater changes in atrophy than changes in PET signals over time. But, for prognostic value, I found that grey matter volumetric measures were weaker predictors than the PET markers, despite the correlation of subcortical grey matter volumes with [^{11}C]PK11195 and [^{18}F]AV-1451 binding. The latter correlation suggests a close relationship between not only microglial activation and tau pathology (Ishizawa and Dickson, 2001) (see Chapter 7), but also with neurodegeneration in the subcortical regions most often associated with the pathological hallmarks of PSP (Sintini *et al.,* 2019). Our findings align with studies of another tauopathy, Alzheimer's disease, in which the baseline *in vivo* PET markers of tau pathology and microglial activation predicted clinical progression (Pontecorvo *et al.,* 2019), which also outperformed structural MRI predictors (see Chapter 3).

The correlation of *in vivo* PET measures with baseline disease severity has been reported in previous studies (Smith *et al.*, 2017, Whitwell *et al.*, 2017*b*). Using [^{11}C]PK11195 PET to assess neuroinflammation, a positive association was observed between clinical severity, assessed with PSP-RS, and ligand binding in the pallidum, midbrain and pons (Passamonti *et al.*, 2018*b*). There was a strong association between [^{11}C]PK11195 binding and [^{18}F]AV-1451 in these subcortical regions, although inconsistent findings are reported in studies using [^{18}F]AV-1451in PSP (Cho *et al.*, 2017; Passamonti *et al.*, 2017; Schonhaut *et al.*, 2017; Smith *et al.*, 2017, Whitwell *et al.*, 2017*b*). The sometimes lack of significant correlates of [^{18}F]AV-1451 in PSP is often tribute to the low affinity of the ligand for 4R tau pathology, but in relatively small studies, the sessional variance of clinical rating scales may also reduce power. Therefore, our estimate of baseline clinical severity used the intercept extracted from the linear mixed effects model of longitudinal PSP-RS scores rather than single baseline assessment.

The null result for structural MRI predictors might be surprising given previous reports on the utility of visual and volumetric assessments of atrophy in midbrain and other subcortical regions, including caudate nucleus, putamen, globus pallidus, subthalamus and thalamus, as *in vivo* biomarker in patients with PSP (Whitwell *et al.*, 2017*a*). Indeed, structural MRI has provided the most studied and validated diagnostic biomarkers in PSP. However, a biomarker's properties for diagnostics (i.e. presence of PSP (Whitwell *et al.*, 2017*a*; Correia *et al.*, 2020)) or correlates of severity (i.e. at baseline) do not imply the property of prognostication. In our PSP cohort, only measures for inflammation and tau were associated with disease progression. The null result for structural MRI measures may be interpreted in two ways. First, this could indicate that measures of grey-matter atrophy is less sensitive than molecular imaging in small cohorts, which may also suggest a preferable applicability of PET imaging on individualised prognosis and clinical trials. Second, for my study I focus on grey-matter regional volumes, but other MRI-related measures may be more informative on clinical progression in PSP patients, such as the quantification of structural connectivity and white-matter changes. Further studies with larger cohorts and multiple MRI-derived variables may confirm or clarify this null result.

Overall, our findings on the *in vivo* association between imaging markers of different pathological processes and their prognostic relevance accord with *post mortem* data (Ishizawa and Dickson, 2001; Fernández-Botrán *et al.*, 2011), and suggest a key role for early microglial activation and tau burden on neurodegeneration, and consequent clinical progression. A

growing literature supports a role for neuroinflammation in driving tau spreading and neurodegeneration in tauopathies (Yoshiyama *et al.*, 2007; Asai *et al.*, 2015; Maphis *et al.*, 2015). Furthermore, genome wide association studies implicate inflammatory pathways in the etiology of tauopathies (Broce *et al.*, 2018, Jabbari *et al.*, 2020*b*). For example, Jabbari et al. reported an association between a common variation at the leucine-rich repeat kinase 2 (LRRK2) locus and survival from symptom onset to death in patients with PSP (Jabbari *et al.*, 2020*b*). This relationship may be mediated by the effect of increased LRRK2 expression on microglia proinflammatory responses (Moehle *et al.*, 2012), promoting spread and accumulation of misfolded tau protein, analogous to Alzheimer's disease (Maphis *et al.*, 2015; Perea *et al.*, 2018). This hypothesis is supported by the association between dysregulation in expression of the microglial-related gene CXCR4, regional accumulation of neurofibrillary tangles and increased risk of PSP (Bonham *et al.*, 2018). The role of early neuroinflammation in tauopathies is supported by PET evidence that microglial activation is observed before the PET evidence of aggregated tau and symptoms in carriers of MAPT mutations (Miyoshi *et al.*, 2010; Bevan-Jones *et al.*, 2019). A preliminary study of longitudinal changes in microglial activation in two PSP patients showed stable microglial activation across a 6-10 months (Gerhard *et al.*, 2006), but may have lacked power.

There are several limitations to this study. We recruited according to clinical diagnostic criteria, and although clinicopathological correlations of PSP-Richardson's syndrome are very high, including 8 of 8 cases in our study with *post mortem* pathology, they are not perfect. Moreover, the average rate of change in severity was 6-7 points per year on the PSP-RS, which is lower than several previous observational studies (Golbe and Ohman-Strickland, 2007; Litvan and Kong, 2014) and clinical trials (Boxer *et al.*, 2014; Tolosa *et al.*, 2014; Bang *et al.*, 2016; Nuebling *et al.*, 2016). This difference may be partially explained by the selection criteria, favouring patients robust enough to undergo three brain scans at baseline. However, our cases were otherwise typical, and 15 out of 17 died within 5 years from baseline (mean 2.2 years ± 1.2). The modest size of our cohort prevented the application of complex models for the direct comparison between MRI and PET predictors, such as multiple linear regression or linear mixed models with several independent variables. The replication of these findings with larger and multicentre clinical cohorts will be an important next step to establish the generalizability of our results. Other limitations relate to the PET tracers used. [^{11}C]PK11195 binds to the 18-kDa translocator protein which is overexpressed in activated microglia but also in other cell types,

like astrocytes and vascular smooth muscle cells (Gui *et al.*, 2020), although [^{11}C]PK11195 has been found selective for activated microglia over reactive astrocytes (Banati, 2002). There are also caveats for [^{18}F]AV-1451, with its off-target binding (monoamine oxidase, choroid plexus, neuromelanin) and lower affinity for PSP tau compared with Alzheimer related tau. Nonetheless, the topological distribution of [^{18}F]-AV-1451 binding and correlations with severity maintain utility for this ligand even in PSP (Cho *et al.*, 2017; Passamonti *et al.*, 2017; Schonhaut *et al.*, 2017; Smith *et al.*, 2017, Whitwell *et al.*, 2017*b*).

8.5. Conclusions

My results support the relevance of neuroinflammation to progression of PSP-Richardson's syndrome. I suggest that [^{11}C]PK11195 may be a valuable biomarker for clinical trials in PSP, complementary to structural MRI. The PET markers may be useful for stratification of patients based on prognosis, and the evaluation of therapeutic response, supporting the development immunomodulatory strategies for disease-modifying treatments in PSP alone or in conjunction with treatments directed against tau and other pathogenic pathways.

8.6. Supplementary materials of Chapter 8

Supplementary Table 8. Rotated regional weights of seven significant MRI principal components (PC) identified by principal component analysis on grey-matter regional volumes.

Regions	PC1	PC2	PC3	PC4	PC5	PC6	PC7
Postcentral_gyrus	0.871	0.101	0.115	-0.227	0.151	0.132	-0.003
Superior_parietal_gyrus	0.769	0.082	0.077	0.167	0.037	-0.038	0.290
Lateral_remainder_of_occipital_lobe	0.742	-0.085	0.449	0.020	0.111	0.140	0.135
Anterior_temporal_lobe_medial_part	-0.710	0.118	0.488	0.128	0.177	-0.127	-0.100
Medial_orbital_gyrus	0.693	0.208	0.499	0.148	0.294	-0.175	0.202
Superior_frontal_gyrus	0.672	0.039	0.114	0.234	0.616	0.226	0.018
Thalamus	0.646	0.391	0.116	0.165	-0.309	0.140	-0.377
Cuneus	0.633	-0.037	0.294	-0.072	0.268	-0.296	-0.054
Gyrus_cinguli_posterior_part	0.598	0.254	0.004	-0.164	-0.076	-0.126	0.358
Caudate_nucleus	0.588	0.293	0.256	-0.100	0.214	0.383	0.004
Inferior_frontal_gyrus	0.546	0.434	0.225	0.017	0.041	0.254	0.536
Cerebellum_dentate	0.205	0.894	-0.037	-0.071	0.080	-0.054	-0.020
Nucleus_accumbens	0.029	0.814	0.075	0.016	0.181	0.032	0.000
Amygdala	-0.421	0.790	0.262	0.261	0.051	-0.037	-0.029
Brainstem_mid	0.104	0.656	0.082	0.491	-0.052	0.203	0.099
Substantia_nigra	0.311	0.653	0.003	0.505	-0.151	-0.034	0.114
Putamen	0.513	0.638	0.062	0.053	-0.078	0.382	0.043
Hippocampus	-0.002	0.610	-0.004	0.149	0.503	0.482	-0.088
Precentral_gyrus	0.526	0.608	0.110	0.051	0.238	-0.162	0.223
Cerebellum_gm	0.319	0.607	0.288	0.071	0.249	0.217	-0.015
Posterior_orbital_gyrus	0.075	0.152	0.872	0.033	-0.052	0.100	0.324
Anterior_orbital_gyrus	0.289	0.300	0.710	0.305	0.392	0.144	-0.037
Lingual_gyrus	0.574	-0.048	0.660	0.048	0.020	0.176	0.022
Anterior_temporal_lobe_lateral_part	0.124	0.063	0.605	0.062	-0.029	0.233	-0.063
Brainstem_pon	-0.255	0.505	-0.573	-0.204	0.045	0.163	0.329
Superior_temporal_gyrus_posterior_part	-0.084	0.272	0.207	0.802	0.221	0.107	-0.027
Fusiform_gyrus	-0.279	-0.055	-0.136	0.783	-0.056	-0.225	0.088
Middle_and_inferior_temporal_gyrus	0.155	0.112	0.460	0.628	0.253	0.139	-0.027
Insula	0.174	0.120	0.450	0.558	0.046	-0.075	0.269
Parahippocampal_and_ambient_gyri	0.065	0.099	-0.008	0.098	0.960	-0.050	-0.052
Subcallosal_area	0.132	0.204	0.209	-0.026	0.761	0.079	0.070
Brainstem_med	0.140	0.034	-0.102	-0.037	-0.013	0.939	0.107
Lateral_orbital_gyrus	0.057	0.118	0.334	-0.024	0.055	0.757	-0.049
Presubgenual_frontal_cortex	0.124	-0.041	0.256	0.368	0.125	0.545	0.470
Superior_temporal_gyrus_anterior_part	-0.201	-0.002	0.062	0.097	0.061	0.005	-0.839
Subgenual_frontal_cortex	-0.231	-0.051	0.301	0.316	0.072	0.301	0.671
Inferiolateral_remainder_of_parietal_lobe	0.401	0.042	0.323	0.350	-0.149	-0.171	0.616
Cerebellum_wm	0.078	0.197	0.072	-0.148	0.234	0.061	-0.142
Cingulate_gyrus_anterior_part	0.164	0.291	-0.031	0.004	-0.279	0.124	0.250
Straight_gyrus	0.085	-0.062	-0.065	0.080	0.101	-0.039	0.085
Middle_frontal_gyrus	0.319	0.338	0.427	0.122	0.176	-0.278	0.142
Pallidum	-0.030	0.374	-0.149	-0.034	0.216	0.031	0.170
Posterior_temporal_lobe	0.324	0.151	0.166	0.175	0.077	0.121	0.397
Cumulative % of Variance	**32.0**	**43.8**	**53.8**	**61.6**	**68.8**	**75.2**	**80.8**

Chapter 9 | General discussion

9.1. Summary of the results

In this thesis, I investigated the prognostic value of *in vivo* markers for inflammation, tau pathology and atrophy, and behavioural measures, in predicting the clinical progression and cognitive decline in three clinical syndromes associated with tau pathology. Alzheimer's disease represented a good model with which to address my research question for two main reasons: (i) its consistency of molecular pathology as compared with frontotemporal dementia, and (ii) the higher affinity of tau PET ligands for Alzheimer's type tau pathology. Then, I moved to investigate multimodal imaging markers and behavioural measures in frontotemporal dementia. This spectrum is characterised by a more complex clinicopathological framework, with molecular heterogeneity and molecular uncertainty in sporadic forms. Finally, I addressed my research question in the primary tauopathy PSP, which is rarely associated with a genetic aetiology but for which clinicopathological correlations of PSP-Richardson's syndrome are very high.

I focused on grey matter atrophy from structural MRI, as an index of neurodegeneration, and [^{11}C]PK11195 PET and [^{18}F]AV-1451 PET as markers of microglial activation and tau (and/or TDP-43) pathology, respectively. In frontotemporal dementia, I investigated pre-symptomatic gene carriers and symptomatic patients, including the role of apathy as an early marker of cognitive deterioration.

In patients with Alzheimer's disease (Alzheimer's dementia and amyloid positive MCI), I showed that microglial activation and tau burden in temporo-parietal cortical regions at baseline are the most predictive measures of cognitive decline, over and above the effect of atrophy and demographics. Second, in pre-symptomatic carriers of a genetic mutation associated with frontotemporal dementia (i.e. in MAPT, GRN, or C9orf72 gene), compared to non-carrier relatives, I found that apathy occurs early in disease progression and worsens over time, reflecting early brain changes in frontal and cingulate cortex, and predicting a subsequent sub-clinical deterioration of cognitive performance. Third, in a case series of post-symptomatic familial frontotemporal dementia with both [^{11}C]PK11195 PET and [^{18}F]AV-1451 PET, I found that across all genetic mutations, these patients are consistently associated with neuroinflammation in frontotemporal regions, and that the distribution of microglial activation reflected clinical symptoms in each patient. Fourth, in a larger group of genetic and sporadic frontotemporal dementia post-symptomatic cases, I found that atrophy and neuroinflammation

markers in frontal regions, and apathy severity, at baseline predict clinical progression. Finally, in patients with PSP-Richardson's syndrome I found that pathological tau accumulation and neuroinflammation are co-localised in subcortical and cortical regions, previously described as affected by PSP-related neuropathology. In these subcortical regions, baseline PET markers for microglial activation and tau pathology, but not atrophy measures, were related to clinical severity and clinical progression over time.

9.2. Neuroinflammation and prognosis

My results in Alzheimer's disease, frontotemporal dementia and PSP suggest that neuroinflammation is not just present as a pathological bystander, but that it may actively participate in the cascade of events that defines the individual clinical severity and prognosis in these patients. My results indicate that *in vivo* measures and evaluation of activated microglia in patients with clinical syndromes associated with Alzheimer's and non-Alzheimer's tau pathology may be valuable to predict their future clinical progression, and to classify them into fast or slow cognitive and functional decline.

My results align with previous evidence supporting a role of neuroinflammation and immune-mediated dysfunction in the pathogenesis of tauopathies. In particular, epidemiological studies of Alzheimer's disease reported a reduced risk in individuals with long term use of anti-inflammatory treatments (McGeer *et al.*, 1996; McGeer and McGeer, 2013). In frontotemporal dementia, there is epidemiological evidence of increased prevalence of autoimmune diseases in patients with frontotemporal dementia due to TDP-43 pathology (Miller *et al.*, 2013) or C9orf72 gene mutation (Miller *et al.*, 2016). Accordingly, genetic studies have identified several immune loci as risk variants for these diseases, indicating a link between inflammatory pathways and Alzheimer's disease (Verheijen and Sleegers, 2018; McQuade and Blurton-Jones, 2019), frontotemporal dementia (Broce *et al.*, 2018), and PSP (Höglinger *et al.*, 2011; Respondek *et al.*, 2018).

Post mortem and preclinical evidence in tauopathies has shown activated microglia surrounding tau inclusions in syndrome-specific brain regions. However, in these conditions, it is still underdetermined whether altered and chronic microglial activation is a cause, an active contributor or a consequence to tau pathology. This may be a bidirectional relationship: inflammatory factors can initialise neuronal tau aggregation and contribute to tau spreading and

tau-induced synapse dysfunction (Maphis *et al.,* 2015; Perea *et al.,* 2018; Vogels *et al.,* 2019); on the other hand, the initial tau aggregation can lead to over-activation of microglia and proinflammatory cytokine release (Vogels *et al.,* 2019). The close relationship between microglial activation and tau pathology has been supported by studies with mouse models of neuronal tauopathies that showed how removing senescent microglia or using anti-inflammatory drugs contributes to tau pathology reduction and cognitive performance improvement (Yoshiyama *et al.*, 2007; Asai *et al.*, 2015; Bussian *et al.*, 2018). The contribution of tau inclusions to microglial activation has also been supported by in vitro studies showing that the presence of tau monomers, oligomers, and fibrils leads to changes in microglial morphology and activation (Morales et al., 2013). In humans, multimodal imaging in vivo studies, employing a longitudinal design and mediation analyses, may be helpful to clarify the directionality of the relationship between inflammation and tau pathology. Longitudinal studies in pre-symptomatic gene carriers may be particularly informative on the timeline and progression of these two processes approaching dementia onset. Previous PET studies with TSPO tracers in pre-symptomatic carriers of MAPT mutations have reported evidence that neuroinflammation may precede the development of the full syndrome but also associated protein aggregation and atrophy (Miyoshi et al., 2010; Bevan-Jones et al., 2019). Evidence from previous animals studies also converged with these findings. For example, in a longitudinal study on P301S tau transgenic mice with PET imaging, it has been shown that longitudinal increases in TSPO expression predict future greater tau accumulation and lower performance (Eckenweber et al., 2020).

However, to determine whether inflammation is causal, intervention studies are also required. Previous animal studies showed how inhibition of specific inflammatory cytokines signalling (i.e. IL-1 β) can provide disease-modifying benefits in tauopathy models, attenuating cognitive deficits and tau burden (Kitazawa et al., 2011). Inhibition of colony-stimulating factor 1 receptor (CSF1R) signalling in 5xfAD mice also resulted in chronic microglial elimination, neuronal loss prevention and memory performance improvements (Spangenberg et al., 2016). In mouse models of tauopathy, microglial activation has also been shown to precede tau pathology (Yoshiyama et al., 2007), and immunosuppressant drug administration in these mice not only attenuates inflammation and decrease tau pathology but also extends their life span (Yoshiyama *et al.*, 2007; Garwood *et al.*, 2010). These findings converge with previous studies with the hTau mouse model of tauopathy, which showed that chemically or genetically

enhancing microglial activation leads to an acceleration in tau pathology accumulation and spreading, and cognitive dysfunction (Bhaskar et al., 2010; Maphis et al., 2015).

Although there is growing evidence about the importance of inflammation in neurodegenerative disease and its relationship with junk proteins' aggregation, its impact on patients' prognosis and the utility of PET markers for microglial activation to predict cognitive and clinical changes are under-investigated. Overall, my results with [11C]PK11195 PET as a prognostic tool in different tauopathies suggest that in vivo measures of microglial activation may be useful to define individual trajectories of clinical and disease progression. The in vivo quantification of activated microglia with PET imaging in these patients resulted to be important not just in terms of neuroinflammation levels, but also considering the differential topography of its distribution in the brain across different diseases. Interestingly, across all three tauopathies included in my thesis, inflammation emerged as particularly important in those regions that are involved in the early stage of disease-specific pathological progression. In patients with Alzheimer's disease, inflammation PET binding in the anterior temporal lobe was predictive for cognitive decline over 3 years, while in patients with frontotemporal dementia, the key region was the left frontal lobe. In contrast, in PSP, inflammation levels were predictive of clinical progression when subcortical regions were considered. Anterior and medial temporal regions for Alzheimer's disease (Braak et al., 2011) as well as frontal regions for frontotemporal dementia (Broe et al., 2003; Kril and Halliday, 2011), and central structures, brainstem and dentate cerebellum for PSP (Williams et al., 2007; Kovacs et al., 2020), are involved in the early stage of each disease-specific progression. This may suggest an early and differential involvement of regional inflammation in distinct diseases. Recently, a regional variation in densities of microglia and its gene expression patters has been demonstrated, as well as regional differences in microglial responses to pathological triggers and in clearance capacity of dysfunctional synapses and neurons (De Biase and Bonci, 2019; Vogels et al., 2019). Regional differences in terms of microglia phenotypes may underline and contribute to differential regional vulnerability across tauopathies, and chronic microglial activation may influence disease-specific processes interacting differently with distinct junk proteins or other pathological contributors. This may then contribute to differential neurodegeneration and dementia progression in patients with tauopathies. In this complex framework, although my results indicate inflammation may play an important role in disease and clinical progression in tauopathies, different clinical syndromes present distinct decline trajectories. In addition to regional differences in microglia phenotypes, clinical syndromes can be underlined by different pathological processes that can contribute to

differential clinical manifestations and progression. For example, tauopathy can present with different tau isoforms (i.e. tau 4R and 3R isoforms) and conformation (i.e. straight vs. paired helical filaments), and co-occur with other proteinopathies. Tau and non-tau pathology, and its interaction with inflammation and other features (i.e. vascular disease), their distribution and progression are all aspects that may need to be taken into account to explain differences in disease progression observed between tau-related clinical syndromes.

Overall, my results also indicate that both visual evaluation of [^{11}C]PK11195 PET maps and the quantification of its binding in different brain regions may be a better approach than considering a global value across all brain regions to quantify inflammation levels in each patient.

9.3. Tau pathology markers: ongoing challenges

Similarly to the *in vivo* assessment of microglial activation with [^{11}C]PK11195 PET, also [^{18}F]AV-1451 PET showed good utility as a prognostic marker in patients with Alzheimer's disease and PSP. This tracer has been widely used in Alzheimer's disease to measure mixed 3R/4R tau pathology and to evaluate its distribution at group and individual level in patients with different clinical phenotypes and at different stages of the disease. Although the tracer has also been successfully used in non-Alzheimer's tauopathies, the interpretation of its binding in these diseases needs more caution than in Alzheimer's tau pathology. As described in the introduction (Chapter 1, section: "*1.5.1. PET imaging for tau pathology: [^{18}F]AV-1451 PET*"), [^{18}F]AV-1451 tracer was originally developed to bind Alzheimer's type tau (paired helical filament), for which it shows strong *in vivo* and *post mortem* binding correlation, however, it is characterised by a lower affinity for non-Alzheimer's tau aggregates (Marquié *et al.*, 2015; Lowe *et al.*, 2016; Sander *et al.*, 2016; Smith *et al.*, 2016; Lowe *et al.*, 2020; Smith *et al.*, 2020; Soleimani-Meigooni *et al.*, 2020).

Despite the caveats related to [^{18}F]AV-1451, this tracer shows higher binding in sub-cortical regions of PSP patients with Richardson's syndrome as compared to subcortical binding found in controls (Cho *et al.*, 2017; Hammes *et al.*, 2017; Passamonti *et al.*, 2017; Schonhaut *et al.*, 2017; Smith *et al.*, 2017, Whitwell *et al.*, 2017*b*). Despite potential off-target binding, like MAO in striatum and neuromelanin in brainstem, this overall suggests that [^{18}F]AV-1451 binding in PSP-related regions is reflecting pathological changes. In PSP patients, the

subcortical binding is higher than in cortical regions, as opposed to patients with Alzheimer's disease, which thus requires specific considerations in the interpretation of the results. Cortical binding in these patients is generally weaker than in subcortical regions, but at the same time also less likely to be influenced by off-target sites. My findings, combined with the previous evidence, support the use of [^{18}F]AV-1451 PET to quantify and localise tau pathology in PSP, and to predict clinical progression in these patients. However, more work is needed to clarify what contributes to its off-target binding and the low correlation between *in vivo* and *post mortem* uptake in non-Alzheimer's tauopathies.

Similar to [^{18}F]AV-1451 PET usage in PSP, the evaluation of this tracer's utility in frontotemporal dementia also requires specific considerations. In particular, in frontotemporal dementia studies with [^{18}F]AV-1451, the low specificity of this tracer and uncertainty over the target of its binding in non-Alzheimer's pathologies needs to be taken into account; as well as the underlying pathological heterogeneity that characterises these patients. In this context, [^{18}F]AV-1451 PET can be used to quantify and localise pathological molecules in conditions with known pathology, but critically cannot differentiate the specific type of pathological molecules involved (i.e. tau or TDP-43). Accordingly, for my project on prognostic tools in frontotemporal dementia (Chapter 6), I decided to focus on imaging markers for atrophy and inflammation only, although most of the patients included in the NIMROD study also underwent [^{18}F]AV-1451 PET. This choice was motivated by previous evidence on the variability in affinity of [^{18}F]AV-1451 for different tau isoforms and TDP-43 pathology in different diseases, but also on the pathological heterogeneity underlying the clinical syndromes of frontotemporal dementia. Previous cross-sectional studies in sporadic and familial frontotemporal dementia have reported elevated *in vivo* [^{18}F]AV-1451 binding in cases characterised by tau and TDP-43 pathology – however with lower binding affinity than in Alzheimer's disease. This tracer indeed reveals the distribution of tau pathology in cases due to MAPT mutations (Bevan Jones *et al.,* 2016; Smith *et al.,* 2016; Spina *et al.,* 2017), but equally shows characteristic binding in TDP-43-related diseases, such as bvFTD due to C9orf72 mutation (Bevan-Jones *et al.,* 2018*a*; Tsai *et al.,* 2019) and svPPA (Bevan-Jones *et al.,* 2018*b*; Josephs *et al.,* 2018; Makaretz *et al.,* 2018, Cho *et al.,* 2019*b*; Tsai *et al.,* 2019). Together, these observations suggest that the [^{18}F]AV-1451 ligand is not specific for tau pathology, but also has variable sensitivity to the presence of TDP-43 pathology, despite not binding TDP-43 itself. Therefore, the molecular interpretation of increased [^{18}F]AV-1451 binding in frontotemporal

dementia is not clarified yet (Marquié *et al.,* 2015; Sander *et al.,* 2016). In addition, in seven cases with genetic frontotemporal dementia (Chapter 5), comparing [^{11}C]PK11195 and [^{18}F]AV-1451 patterns across patients with different genetic mutations associated with this disease, [^{11}C]PK11195 emerged as more informative than [^{18}F]AV-1451 on single subject clinical manifestations. In these cases, the visual evaluation of voxel-wise [^{18}F]AV-1451 maps indicated that only in MAPT cases the tracer was consistently informative about the distribution of the underlying pathology, while in GRN and C9orf72 cases the results were more variable. Overall these findings in frontotemporal dementia support the use of [^{18}F]AV-1451 only to assess relative topographical binding distribution within each individual, rather than the absolute quantification of its binding and its correlation with clinical outcomes across patients with different clinical and pathological sub-types which lead to variable tracer affinity.

Although [^{18}F]AV-1451 is still the most widely used tracer for tau in neurodegenerative diseases, new tracers are under evaluation to improve tau imaging in non-Alzheimer's tauopathies. For example, the novel tau-PET tracer [^{18}F]PI-2620 has shown good sensitivity and affinity to 3/4R tau in Alzheimer's disease (Kroth *et al.,* 2019; Mormino *et al.,* 2020; Mueller *et al.,* 2020), and less off-target binding to MAO (Kroth *et al.,* 2019). Initial findings also suggest that this tracer has good affinity for 4R tau PSP pathology (Kroth *et al.,* 2019; Brendel *et al.,* 2020), which is supported by pre-clinical data showing that [^{18}F]PI-2620 binds to tau aggregates/aggregate folds in PSP *in vitro* tissues (Kroth *et al.,* 2019). These promising results, and their further corroboration, may be worthy considerations for future tau imaging studies in non-Alzheimer's tauopathies.

9.4. Structural MRI vs. PET imaging in predicting tauopathies' clinical progression

In contrast to [^{11}C]PK11195 PET, structural MRI emerged as less informative for prognosis than molecular imaging in Alzheimer's disease and PSP. However, in frontotemporal dementia, structural MRI measures for atrophy in frontal regions were predictive of apathy and clinical progression in pre-symptomatic gene mutation carriers and post-symptomatic patients, respectively. This difference may be due to several reasons. Frontotemporal dementia clinical phenotypes are underlined by heterogenous and variable pathologies (Bang *et al.,* 2015; Olney *et al.,* 2017), which makes the diagnosis difficult and the identification of appropriate biomarkers to be used across the spectrum and to stratify patients challenging. Structural MRI

for atrophy in frontotemporal dementia may lack sensitivity in the early stage of the disease, but in post-symptomatic cases it is a well-established useful biomarker in patients' evaluation and diagnostic process (Gorno-Tempini *et al.,* 2011; Rascovsky *et al.,* 2011). However, even in the pre-symptomatic phase of this disease, early brain changes have been identified with structural MRI, assessing individuals carrying a genetic mutation years before the dementia onset (Rohrer *et al.,* 2015; Cash *et al.,* 2018). Similarly, also in individuals at higher genetic risk for Alzheimer's disease, structural MRI evidence suggests an early occurrence of regional brain volume reductions (Caselli and Reiman, 2012). Comparing these two diseases, patients with frontotemporal dementia are characterised by a faster clinical progression to death than patients with Alzheimer's disease (Rascovsky *et al.,* 2005; Roberson *et al.,* 2005), despite some variations across different clinical syndromes. In previous longitudinal MRI studies, patients with frontotemporal dementia also showed more marked grey matter changes and greater atrophy rates than patients with Alzheimer's disease (Chan *et al.,* 2001; Whitwell *et al.,* 2006; Krueger *et al.,* 2010; Frings *et al.,* 2014). In addition, patients with frontotemporal dementia also show greater progression of atrophy than those observed in patients with PSP, whose rate of whole brain atrophy is similar to those with Alzheimer's disease (Whitwell *et al.,* 2006). Although I did not compare the prognostic value of MRI and PET imaging directly between the three diagnostic groups, in light of the previous evidence, my results suggest that structural MRI may be more useful as a prognostic tool in degenerative diseases with a fast atrophy progression (i.e. frontotemporal dementia). As such, it may be less informative in those diseases where the volumetric changes occur slower and maybe at a later stage of the progression.

On the other hand, PET imaging for tau pathology and microglial activation may be a better prognostic tool in patients with Alzheimer's disease or PSP than in those with frontotemporal dementia for several reasons. First, both Alzheimer's disease and PSP are characterised by less heterogenous clinicopathological correlations than frontotemporal dementia. As reported in the literature and in Chapter 1, Alzheimer's disease is mainly associated with 3/4R-tau pathology and β-amyloid, while PSP by 4R-tau pathology. In contrast, frontotemporal dementia is a large spectrum and can be associated with several pathologies, mainly 3R- or 4R-tau, several TDP-43 types, and FUS. Second, [^{11}C]PK11195 and [^{18}F]AV-1451 PET tracers have been developed in the context of Alzheimer's disease, and especially the latter has been showing higher affinity for Alzheimer's tau pathology than non-Alzheimer's diseases tau. Finally, the fast rate of neuronal and glia loss that characterises frontotemporal dementia may challenge the ability of

these tracers to bind to intraneuronal junk protein inclusions and neuroinflammation markers. The lack of binding may be brought about by the lack of targets due to a severe and extensive atrophy and cell death.

9.5. Utility of *in vivo* neuroimaging measures for cognitive prognosis

In Alzheimer's disease (Chapter 3), frontotemporal dementia (Chapter 6) and PSP (Chapter 8), I tested the independent prognostic value of structural MRI and PET imaging on longitudinal clinical/cognitive decline, running univariable regression models with each modality as single predictor. Then, I tested their predictive value in combination, including different imaging-modality predictors in the same multivariable model on annual rate of clinical/cognitive change. The univariable models were useful to test the utility of single imaging measures in predicting clinical progression, and evaluating the association of individual differences in brain markers at baseline with annual rate of change in clinical/cognitive measures over time across patients. Similarly, models that include multiple imaging predictors can give more information about individual modalities' predictive value in interaction or after excluding the effect of all other predictors. However, the results obtained by these regression models do not only give indications on the prognostic utility of a specific biomarker, but they can also be interpreted in terms of the role that a specific pathological process plays in defining, influencing and contributing to clinical progression in patients.

Cross-sectional studies are useful for evaluating the association between brain changes and clinical severity at a given time point, while longitudinal correlational studies can be informative about their relationship over time. In contrast, my projects with baseline imaging measures and longitudinal clinical assessments aimed to identify which pathological processes in disease-specific brain regions are important to define or contribute to clinical progression in the years following imaging acquisition. Once it is established which the most important pathological hallmarks are for clinical prognosis in different tauopathies, the practical consequences to be considered for further studies and future clinical trials are mainly two. First, the results can indicate which pathological targets may be considered in developing new disease-modifying treatments. In all three tauopathies that I included in my thesis, neuroinflammation emerged as consistently present and particularly important to define patients' prognosis, either alone or in combination with junk protein aggregation. This supports the development of immunomodulatory strategies for disease-modifying treatments alone or in

conjunction with treatments targeting other pathogenic processes. Second, my results also support the use of structural MRI and PET imaging of tau pathology and microglial activation for clinical prognostication and patients' stratification in clinical trials.

9.6. Apathy as early marker in frontotemporal dementia

In frontotemporal dementia, in addition to "positive" behavioural symptoms, such as disinhibition and stereotypical behaviours, apathy is also widely present across all frontotemporal lobar degeneration clinical syndromes (Mendez *et al.*, 2008; Rohrer and Warren, 2010; Coyle-Gilchrist *et al.*, 2016; Lansdall *et al.*, 2017, Murley *et al.*, 2020*a*). Despite its common incidence in these patients, apathy has been under-investigated as compared to clinical positive symptoms and cognitive impairments. Recently, the research interest for this key clinical feature has been increasing, however, the understanding of its complexity and relationship with other aspects of frontotemporal dementia progression remain incomplete. Few studies investigated longitudinal apathy changes in symptomatic patients with frontotemporal dementia, reporting a worsening trend in apathy severity over time and associations between apathy and increased functional disability (O'Connor *et al.*, 2016*b*, *a*). Apathy has also been reported to have a detrimental effect on survival rate and functional independence loss in patients on the frontotemporal dementia spectrum (Lansdall *et al.*, 2019, Murley *et al.*, 2020*b*). Accordingly, in our cohort of frontotemporal dementia patients, I found that in addition to atrophy and microglial activation, also apathy severity at baseline was predictive of annual rate of cognitive decline across all clinical syndromes (Chapter 6). The aim of this exploratory analysis was investigating the prognostic value of apathy across the frontotemporal dementia clinical spectrum, independently from the specific clinical diagnosis, adopting a cross-diagnostical approach which is finding more and more approval in the literature (Piguet, 2020). If the focus was exploring the prognostic value of baseline apathy within each clinical variant of frontotemporal dementia, a larger sample size than NIMROD cohort (N=30) would have been advisable. In contrast to previous studies, I sought to test the value of apathy as an early prognostic marker in frontotemporal dementia without the confound of the consequences of symptomatic disease, including treatment or changes in functional roles. I therefore focused on pre-symptomatic carriers of a gene mutation associated with frontotemporal dementia. Even in the pre-symptomatic phase, I confirmed a detrimental influence of apathy on the rate of future cognitive decline, and not an influence of cognitive impairment on the future progression of apathy. Apathy and executive impairment were present even in the at-risk population who had

not converted to symptomatic stages. In other words, the study including those approaching dementia onset, but without dementia.

Considering apathy severity as an outcome, rather than a predictor, the frontal and cingulate grey matter volumes at baseline were associated with progression of apathy. This evidence from longitudinal data suggests a temporal directionality from brain differences at baseline to apathy progression, and from apathy severity to cognitive decline (Figure 32). My results support the hypothesis that apathy progression reflects early brain changes in genetic frontotemporal dementia, years before the dementia onset. A corollary is that apathy assessment may be a useful biomarker to identify patients with a more aggressive form of the disease with more rapid cognitive decline. However, whether apathy is a direct cause of decline, or a mere correlative marker, remains unresolved until interventional trials are applied that treat apathy.

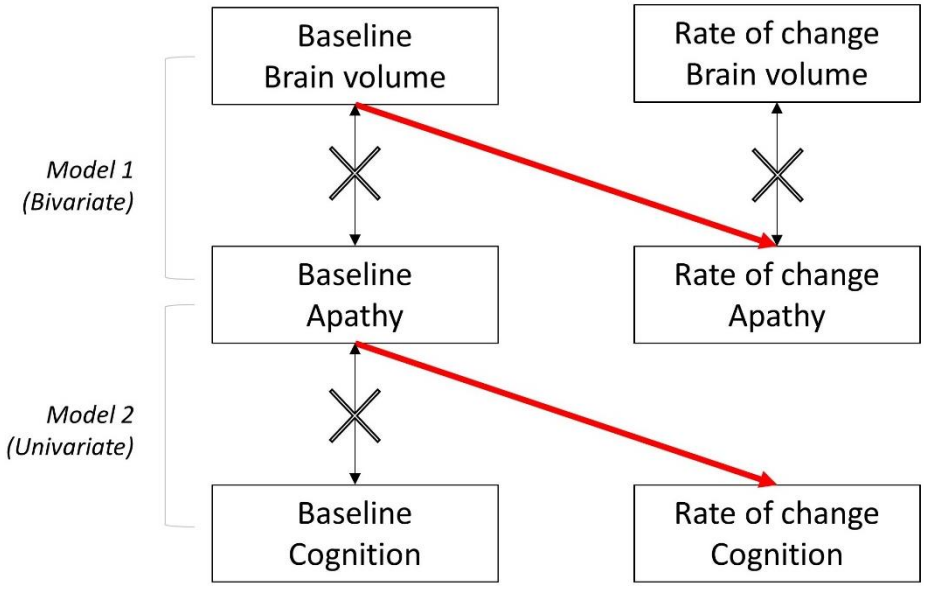

Figure 32. *Temporal directionality between structural brain, apathy and cognitive changes in pre-symptomatic frontotemporal dementia. From the longitudinal study on pre-symptomatic gene carriers on GENFI data (Chapter 4), two main conclusions are drawn: (i) apathy progression (annual rate of change) reflects brain differences (baseline) approaching the dementia onset, and not vice versa; (ii) apathy severity (baseline) predicts cognitive decline (annual rate of change) approaching the dementia onset, and not vice versa.*

9.7. Disease-specific biomarkers for differential therapy and stratification

This work supports immune-mediated strategies to modify the course of disease in all three tau-related conditions investigated, Alzheimer's dementia, frontotemporal dementia and PSP. These might benefit from better stratification or treatment individualisation based on clinical and imaging assessment at baseline.

Disease-modifying treatments for these three tauopathies are yet to be discovered. Experimental medicine studies for these diseases may benefit from improved approaches of patient stratification, balancing the risk and benefit to recruit certain patients in clinical trials. These should take into account different aspects of their clinicopathological complexity, such as (i) the individual clinical severity and/or prognosis, (ii) the stage of the disease progression, (iii) the genetic variants associated with each disease, and/or (iv) the degree of inflammation and other pathological processes. In particular, the absence of effective prognostic markers in living patients contributes to the failure of experimental treatments and leads the current drug studies to base their hypotheses on animal models. Disease-specific optimal prognostic markers should be considered to improve clinical trials and management. Indeed, defining which the most predictive imaging and behavioural markers are in each disease is important in clinical practice and experimental medicine studies. *In vivo* imaging PET and MRI are able to inform us on the underpinning pathological processes that have long term impact on the clinical progression associated with a specific disease. In addition, clinical markers can elucidate whether specific symptoms and their severity can be predictive of patients' progression. These tools and the comparison of their prognostic value can guide the selection of disease-specific modifying and targeting treatments. For example, my results in Alzheimer's disease and PSP suggest that both tau pathology and inflammation should be considered as targets for future treatments, and acting on these two processes in combination may be more efficient than considering them in isolation. On the other hand, my results in frontotemporal dementia indicate that future disease-modifying treatment strategies may be enhanced by immunomodulation, and that apathy may also be a modifiable factor by pharmacological or non-pharmacological interventions.

Identifying disease-specific optimal prognostic tools is also important to predict the clinical progression of a single patient. This can result particularly important for clinical practice and the management of individual patients, but also to guide the selection of single patients for specific treatments and research studies. An accurate stratification of patients based on relevant

imaging and behavioural prognostic markers may improve the efficacy of disease-specific treatments, and the results' interpretation in experimental medicine studies. Stratifying the participants into slow vs. fast decliner or into early vs. advance disease stage may be informative to identify which window we should consider and intervene on for more efficient treatments. For example, in frontotemporal dementia, apathy assessment as well as inflammation markers could be combined in patients' evaluation to predict their clinical progression. My results in frontotemporal dementia also support the combination between interventions at different levels, such as behavioural symptom management and immune-mediated treatments.

9.8. General limitations

There are limitations to this study that I considered during the conduct of each single project and tried to mitigate, as described in each experimental chapter, and more generally here.

9.8.1. Modest sample size

For projects conducted on NIMROD data (Chapters 3, 5-8), the main limitation is the relatively modest sample size of each single cohort, which reduces the power of the statistical analyses and the applicability of complex models. Indeed, models like LGCM need a certain number of subjects to converge in stable solutions (i.e. 5-10 participants for each estimated parameters). Simpler analyses can converge with small sample sizes, but caution is needed in the interpretation of results. This is particularly the case for our PSP cohort (N=17), although it is larger than many previous multi-tracer PET studies on neurodegenerative diseases of such rarity. The modest size of this cohort did not permit the application of multivariable models for the direct comparison between MRI and PET predictors, after correcting for multiple covariates, such as age, education and sex. Similarly, in the Alzheimer's disease cohort, the relatively small sample size limited the applicability of the one-step prediction procedure with multiple predictors, which may lead to a more precise prediction than the two-step procedures. Indeed, for univariable models with single-modality predictors, I ran the analyses across the whole population, but for the multivariable regression models the sample size dropped to N=26 due to the exclusion of controls (who underwent [^{18}F]AV-1451 or [^{11}C]PK11195 PET, but not both, to limit radiation exposure). To mitigate this and validate my results, I compared different statistical approaches, such as the frequentist and Bayesian multivariable regressions and model

selection, in addition to the one-step prediction LGCM procedure. These all converge on the same conclusion and most parsimonious model. Finally, in the frontotemporal dementia NIMROD cohort, because of the relatively small sample size, I decided to combine genetic and sporadic patients with distinct clinical diagnoses (bvFTD, nfvPPA and svPPA) in order to investigate the prognostic value of MRI and [^{11}C]PK11195 PET. With a larger and longitudinal sample however, it would be interesting to try to replicate the results differentiating patients by genes and clinical phenotypes. In the case series of familial frontotemporal dementia, the sample size of N=7 patients, made statistically-sound correlational analysis between imaging and clinical severity by genetic subgroups unadvisable. Nevertheless, as small sample sizes can be informative about typicality of a feature in a population, I decided to highlight some associations that are particularly striking or relevant to the literature on gene-specific or phenotype-specific anatomical associations.

Considering the limited sample size, I approached each cohort and all analyses with specific pathology-related *a priori* hypotheses based on previous literature, rather than choosing an exploratory approach. Furthermore, I focused my main discussion only on those results that survived multiple comparisons correction. However, only the replication of my findings with larger cohorts will enable the verification and generalizability of these results.

9.8.2. Longitudinal data collection

In addition to the modest sample size, longitudinal studies in cohorts of patients with PSP and frontotemporal dementia are particularly challenging because of the aggressiveness of these diseases. Indeed, these patients are characterised by a faster decline and a shorter survival rate than those with Alzheimer's disease (Rascovsky *et al.,* 2005; Roberson *et al.,* 2005). This factor can contribute to dropouts and practical difficulties for data collection at follow-ups. Although the complexity of the NIMROD design may have introduced a bias in patient selection criteria - favouring the recruitment of participants that were robust enough to undergo three brain scans at baseline and be followed up for a few years - in our patients with PSP and frontotemporal dementia we still only managed to collect less data at follow-ups than in patients with Alzheimer's disease. For example, eight out of 17 PSP patients died within 2.5 years from the beginning of the study, and another seven within 5 years of follow-up. As a result, in both the NIMROD cohorts of PSP and frontotemporal dementia patients, it was not possible to apply LGCM, because of the limited size of the two samples, as well as due to the inconsistency of

the time intervals between cognitive/clinical assessments over time. In these patients, instead, I used the linear mixed effects approach, to estimate a slope for clinical progression at group and individual levels. The limitations related to sample size and unstructured longitudinal assessments are not the case in the GENFI database. However, the data collection for this project is still ongoing, which implies that the most recently recruited participants still have incomplete longitudinal data. For this reason, I included only the first three waves of assessment in my analyses, following the minimum requirement in LGCM guidelines (Newsom, 2015). In the next few years, it will be possible to replicate these analyses with more data, either for a larger sample size or longer follow-ups.

9.8.3. *Post mortem* pathological confirmation

Another limitation of my study is associated with the recruitment for NIMROD cohorts that was based on clinical diagnosis**,** without *post mortem* confirmation in most cases. This could contribute to increase the heterogeneity of our sample by including patients with similar clinical phenotype but different underpinning pathologies. However the following steps were taken to decrease this potential confound: (i) the clinical diagnosis for all patients included in this study was confirmed at each follow-up visit; (ii) only amnestic cases with Alzheimer's dementia were included; (iii) only MCI who resulted amyloid positive at PIB PET were included, reducing the probability to recruit MCI due to non-Alzheimer's pathologies; (iv) in the PSP cohort, *post mortem* pathological confirmation was available in 8 patients, whose diagnosis was confirmed for PSP pathology. In addition, it has been observed that over 95% of patients with a clinical diagnosis of PSP-Richardson's syndrome have PSP pathology or related 4R-tauopathy. For patients with frontotemporal dementia in NIMROD and for pre-symptomatic mutation carriers in GENFI we did not have *post mortem* examinations either. However, previous studies reported a clear relationship between each monogenetic mutation and the pathological accumulation of abnormal tau or TDP-43 protein (Bang *et al.*, 2015; Greaves and Rohrer, 2019). This enables the inference of the underlying pathology from a genetic test, associated with a clinical evaluation, before *post mortem* examination. Accordingly, I assessed the association of clinical symptoms with neuroinflammation distribution, as measured by [^{11}C]PK11195 binding, and abnormal tau/TDP-43 aggregation, as indexed by [^{18}F]AV-1451 PET, in a case series of patients with frontotemporal dementia and related monogenetic mutations (Chapter 5).

Multimodal imaging studies in larger samples of patients with familial frontotemporal dementia and pre-symptomatic genetic mutation carriers will be needed to confirm the *in vivo* clinico-pathology association on the spectrum of frontotemporal dementia.

9.8.4. PET methodological limitations

Other limitations of my studies are associated with the PET tracers used, as extensively described in the introduction (Chapter 1) and in each experimental chapter (Chapters 3, 5-8). Briefly, [^{11}C]PK11195 binds to TSPO, whose expression in the neuroinflammation cascade is complex. It has been found not only in activated microglia but also in other cell types, like astrocytes and vascular smooth muscle cells (Gui *et al.*, 2020). However, previous studies encourage the use of this tracer because of its selectivity for activated microglia over and above quiescent microglia and astrocytes (Banati, 2002) and the robust methods that have been developed for its non-invasive kinetic analysis (Turkheimer *et al.*, 2007; Yaqub *et al.*, 2012). Despite its lower signal-noise ratio as compared to second-generation TSPO PET radioligands (e.g. [^{11}C]PBR28 and [^{18}F]DPA-714), [^{11}C]PK11195 is less affected by genetic polymorphisms that affect the second-generation radioligands' binding, especially in high and mixed affinity binders (Guo *et al.*, 2012; Kobayashi *et al.*, 2018) that represent ~90% of the Caucasian population (Owen *et al.*, 2012). There are also limitations related to the use of [^{18}F]AV-1451, related to its off-target binding (monoamine oxidase, choroid plexus, neuromelanin) and lower affinity for non-Alzheimer's tau pathology, as described in each project-related experimental chapter (Chapters 5, 7-8) and in the introduction (Chapter 1). Another limitation associated with [^{18}F]AV-1451 PET is the relatively arbitrary choice across different studies of the reference region to model the PET tracer's binding potential. In all projects with NIMROD data, we decided to use the superior cerebellar cortex as the reference region for [^{18}F]AV-1451. We opted for this region for several reasons. First, evidence of the impact of potential off-target binding in this region is not widespread for all neurodegenerative diseases, and *post mortem* evidence showed minimal tau pathology in PSP (see pathology data in supplementary material in Passamonti et al. (Passamonti *et al.*, 2017)). Second, the scanners used in this study have PET axial fields of view of 15.2 cm (GE Advance) and 15.7 cm (GE Discovery 690). For male subjects, in particular, this limited field of view can result in the inferior cerebellum being very near to the axial edge of the field of view, where statistical quality is poor, or partially outside the axial field of view. This problem was exacerbated on the PET-only GE Advance where positioning was based on a short transmission scan rather than a much higher quality CT scout.

Furthermore, on systems with a limited axial field of view, motion during the scan can alter the coverage of the inferior cerebellum over time, leading to perturbations of the reference tissue time-activity curve. Given that chronologically, the PET-only data (2014-15) preceded the PET/CT data (2015-19), with the study transferring to the GE Discovery 690 when the GE Advance was replaced by a GE SIGNA PET/MR, the use of the superior cerebellum for GE Advance data was also performed for the GE Discovery 690 data. Finally, our use of the superior cerebellar grey matter (defined using a 90% lower limit on the SPM grey matter probability map smoothed to the PET spatial resolution) is consistent with the widespread use of "cerebellar grey matter" for reference tissue analysis of [^{18}F]AV-1451 data.

9.9. Future directions

This thesis provides *in vivo* evidence for (i) the occurrence of inflammation in disease-related brain regions of patients with Alzheimer's disease, frontotemporal dementia and PSP; (ii) the prognostic value of PET markers for inflammation (i.e. [^{11}C]PK11195) and junk protein aggregation (i.e. [^{18}F]AV-1451) to predict clinical and cognitive progression over time in these patients; (iii) and, specifically for frontotemporal dementia, the predictive value of apathy and structural brain changes on decline in pre- and post-symptomatic patients. These findings provide the basis for future studies in several directions

First, my results on *in vivo* imaging of inflammation in these patients could be confirmed and expanded by alternative ligands for other aspects of the inflammatory cascade. [^{11}C]PK11195 PET has been widely used as a marker of microglial activation by binding TSPO, however this protein's overexpression is only one phenomenon among many underpinning neuroinflammation in dementia and related disorders. Despite the well-established applicability of TSPO tracers for *in vivo* imaging of activated microglia, these tools are not able to distinguish pro-inflammatory M1 and anti-inflammatory M2 phenotypes (Shen *et al.*, 2018; Ghadery *et al.*, 2019). Recently, new non-TSPO tracers have been developed to visualise and measure microglial activation levels, such as ligands for CB2R, expressed by immune cells like monocytes and macrophages, and P2X7, an ATP-gated ion channel expressed on activated microglia (Boche *et al.*, 2019). Among the most promising novel non-TSPO tracers are those that target purinergic receptors such as P2X7, which is selective for the M1 phenotype. This protein is selectively expressed on microglia and related to neurodegeneration-inducing pro-inflammatory cascades. Much effort has also been invested into the development of alternative

tracers for astrocyte-related responses (Boche et al., 2019). The best-known one is [^{11}C]DED, an irreversible MAO-B inhibitor that has been used as an astrocytosis marker in Alzheimer's disease and amyotrophic lateral sclerosis. The replication of my study with alternative neuroinflammation tracers would produce a more comprehensive reference frame for the prognostic role of distinct inflammatory events in neurodegenerative diseases.

Similarly, novel tau imaging methods may clarify the contribution of tau pathology to clinical progression in tauopathies. Although [^{18}F]AV-1451 is still the most validated tracer to visualise and measure tau burden in dementia, future studies may benefit from the limited off-target binding and high affinity for non-Alzheimer's tau which second-generation tau-PET tracers, such as [^{18}F]PI-2620, have shown in preliminary reports (Kroth *et al.,* 2019; Brendel *et al.,* 2020).

Second, despite the innovative statistical approaches applied in this project to investigate the relationship between baseline markers and longitudinal clinical progression, the cross-sectional nature of our imaging assessment does not enable inferences on the direction of causality between pathological processes. Multimodal and longitudinal imaging studies are needed to clarify the temporal sequence of different pathological processes and their interaction, to fully understand the impact of the different disease paths on individual clinical progression. This would be made possible by longitudinal studies with multiple pathology and clinical markers that allow the application of mediation analysis. Longitudinal studies will be also needed to confirm the prognostic value of these imaging markers and to evaluate newly-developed disease-modifying treatments' effect on patient clinical progression. Larger and longer longitudinal studies should further clarify whether these diseases progress through polyphasic stages, and thus differentiate the potential prognostic utility of various markers accordingly.

Third, particularly important will also be (i) the replication of these results with longer follow-up; and (ii) the evaluation of molecular markers in pre-symptomatic disease stages, such as through multi-tracer PET imaging in carriers of gene mutations associated with Alzheimer's disease or frontotemporal dementia. In the latter, it would be interesting to test whether apathy severity is predictive of the clinical conversion from pre- to post-symptomatic condition, as well as whether there are differences between patients carrying distinct gene mutations. This may be possible in a few years, with open longitudinal studies like GENFI that will have

complete longitudinal data. GENFI, or similar studies, will equally provide data to assess the rate of conversion from pre-symptomatic status to dementia in gene carriers. This rate is now represented by too few cases, and does not allow us to explore and identify sensitive predictive measures. In this context, it will also be necessary to identify better models to estimate the years from symptom onset in pre-symptomatic gene carriers, as the average age of onset within families is not always accurate, especially in GRN and C9orf72 mutations more than in MAPT families (Moore *et al.*, 2020).

Fourth, PET imaging has been, and still is, an essential tool to uncover many of the *in vivo* pathology processes associated with neurodegeneration, and to investigate *ante mortem* molecular changes in human brains and their association with clinical phenotypes/symptoms. Although my results align with previous evidence supporting the utility of PET imaging as a diagnostic and prognostic marker in neurodegenerative diseases, the costs associated with this technique may limit its applicability in small centres and clinics. For this, many research studies have been focusing on potential alternative biomarkers for widescale prediction in populations, with lower costs and broader accessibility. For example, fluid markers may represent more scalable and widely usable tools because of their reduced cost and invasiveness as compared to PET imaging. Most previous studies have investigated cerebrospinal fluid markers of inflammation and proteinopathies, reporting promising results in Alzheimer's disease (Ray et al., 2007; Shen et al., 2019; Park et al., 2020), but also in PSP (Hall et al., 2012; Magdalinou et al., 2015; Starhof et al., 2018), and frontotemporal dementia cases (Sjögren et al., 2004; Woollacott et al., 2018). However, cerebrospinal fluid markers require a lumbar puncture which can be perceived as invasive. More recently, particular attention has been directed to new blood markers for tau, inflammation and other pathological processes in patients with dementia (Bright *et al.*, 2019; Inci *et al.*, 2020; Karikari *et al.*, 2020; Swift *et al.*, 2020). Blood markers may be preferred in clinical trials and practice for their lower costs and invasiveness relative to PET imaging and lumbar puncture. In particular serum neurofilament light (NfL), phospho-Tau181 (p-Tau181) and assays that target the threonine 217 phosphorylation site (p-Tau217) are promising prognostic markers in Alzheimer's disease and frontotemporal lobar degeneration spectrums (see for review (Ashton *et al.*, 2020; Gaetani *et al.*, 2020; Swift *et al.*, 2020; Zetterberg and Bendlin, 2020)). However, blood markers, as well as other fluid markers, are not informative on the spatial *in vivo* distribution of pathological processes, that can be visualised with PET imaging in human brains. Further studies combining PET imaging and

blood markers for these processes are needed to compare their diagnostic and prognostic value, and their ability to track disease progression in neurodegenerative conditions.

In addition to alternative PET imaging markers and additional fluid markers, what remains under-investigated by my study - and in the wider literature - is the association of microglial activation and tau pathology with other dementia-related processes, that can be assessed by other imaging techniques. Across all tauopathies, it will be particularly important to investigate the relationship between inflammatory processes and (i) network dysfunction, as Passamonti et al. did in Alzheimer's disease (Passamonti *et al.*, 2019); (ii) synapse loss, now measurable *in vivo* with synaptic PET tracers, as shown in our recent study on [11C]UCB-J in PSP (Holland *et al.*, 2020); and (iii) vascular lesions, that one of my colleagues in the NIMROD study is investigating (see (Low *et al.*, 2019) for a review).

Finally, the replication of my findings with multimodal imaging techniques and alternative biomarkers in larger multicentre clinical cohorts will be needed to establish the replicability and generalizability of these results; and to validate the specifically chosen analysis methods and tests. Larger samples will also enable a better characterisation of clinical progression and distinct phenotypes, by investigating the prognostic value of different biomarkers on specific cognitive domains and clinical features rather than global measures over time.

9.10. Conclusions

Together these studies indicate a role of neuroinflammation for clinical manifestations and progression in multiple degenerative tauopathies (i.e. Alzheimer's disease, frontotemporal lobar degeneration and PSP). In these three diseases, activated microglia as measured by [^{11}C]PK11195 PET in pathology-related regions can predict cognitive decline and clinical progression over time. In Alzheimer's disease and PSP, inflammation and tau pathology as measured by *in vivo* PET imaging have proved informative regarding patients' future clinical progression, over and above atrophy measures. In these diseases, the regional distribution of PET markers for inflammation and tau pathology indicated an additive and partially independent effect of these two pathological processes on clinical progression rather than a synergistic effect. In frontotemporal dementia, apathy and structural brain changes were also predictive of clinical changes in pre- and post-symptomatic patients.

Overall, this work supports immune-mediated strategies to modify the course of disease, in isolation or in combination with treatments targeting other pathological processes (i.e. tau pathology) or specific clinical symptoms (i.e. apathy). This might be coupled with improved stratification or individualised treatment approaches based on cognitive and imaging assessment at baseline.

References

Adachi M, Kawanami T, Ohshima H, Sugai Y, Hosoya T. Morning glory sign: a particular MR finding in progressive supranuclear palsy. Magn Reson Med Sci 2004; 3: 125–32.

Agosta F, Galantucci S, Filippi M. Advanced magnetic resonance imaging of neurodegenerative diseases. Neurol Sci 2017; 38: 41–51.

Albert MS, DeKosky ST, Dickson D, Dubois B, Feldman HH, Fox NC, et al. The diagnosis of mild cognitive impairment due to Alzheimer's disease: Recommendations from the National Institute on Aging-Alzheimer's Association workgroups on. Alzheimer's Dement 2011; 7: 270–279.

Alexander SK, Rittman T, Xuereb JH, Bak TH, Hodges JR, Rowe JB. Validation of the new consensus criteria for the diagnosis of corticobasal degeneration. J Neurol Neurosurg Psychiatry 2014; 85: 923–927.

Alzheimer A. Uber eine eigenartige Erkrankung der Hirnrinde. Zentralbl Nervenh Psych 1907; 18: 177–179.

Arendt T, Brückner MK, Morawski M, Jäger C, Gertz HJ. Early neurone loss in Alzheimer's disease: cortical or subcortical? Acta Neuropathol Commun 2015; 3: 10.

Asai H, Ikezu S, Tsunoda S, Medalla M, Luebke J, Haydar T, et al. Depletion of microglia and inhibition of exosome synthesis halt tau propagation. Nat Neurosci 2015; 18: 1584–1593.

Aschenbrenner AJ, Gordon BA, Benzinger TLS, Morris JC, Hassenstab JJ. Influence of tau PET, amyloid PET, and hippocampal volume on cognition in Alzheimer disease. Neurology 2018; 91: e859–e866.

Ashton NJ, Hye A, Rajkumar AP, Leuzy A, Snowden S, Suárez-Calvet M, et al. An update on blood-based biomarkers for non-Alzheimer neurodegenerative disorders. Nat Rev Neurol 2020; 16: 265–284.

Banati RB. Visualising microglial activation in vivo. Glia 2002; 40: 206–217.

Bang J, Lobach I V, Lang AE, Grossman M, Knopman DS, Miller BL, et al. Predicting disease progression in progressive supranuclear palsy in multicenter clinical trials. Paskinsonism Relat Disord 2016; July: 41–48.

Bang J, Spina S, Miller BL. Frontotemporal dementia. Lancet 2015; 386: 1672–1682.

Bateman RJ, Xiong C, Benzinger TLS, Fagan AM, Goate A, Fox NC, et al. Clinical and Biomarker Changes in Dominantly Inherited Alzheimer's Disease. N Engl J Med 2012; 367: 795–804.

Bates D, Mächler M, Bolker BM, Walker SC. Fitting linear mixed-effects models using lme4. J Stat Softw 2015; 67

Bejanin A, Schonhaut DR, La Joie R, Kramer JH, Baker SL, Sosa N, et al. Tau pathology and neurodegeneration contribute to cognitive impairment in Alzheimer's disease. Brain 2017; 140: 3286–3300.

Bensimon G, Ludolph A, Agid Y, Vidailhet M, Payan C, Leigh PN. Riluzole treatment, survival and diagnostic criteria in Parkinson plus disorders: The NNIPPS Study. Brain 2009; 132: 156–171.

Bentler PM, Chou CP. Practical Issues in Structural Modeling. Sociol Methods Res 1987; 16: 78–117.

Le Ber I, Camuzat A, Hannequin D, Pasquier F, Guedj E, Rovelet-Lecrux A, et al. Phenotype variability in progranulin mutation carriers: a clinical, neuropsychological, imaging and genetic study. Brain 2008; 131: 732–746.

Bevan-Jones RW, Cope TE, Jones SP, Passamonti L, Hong YT, Fryer T, et al. [18 F]AV-1451 binding is increased in frontotemporal dementia due to C9orf72 expansion. Ann Clin Transl Neurol 2018; 5: 1292–1296.

Bevan-Jones WR, Cope TE, Jones PS, Kaalund SS, Passamonti L, Allinson K, et al. Neuroinflammation and protein aggregation co-localize across the frontotemporal dementia spectrum. Brain 2020; 143: 1010–1026.

Bevan-Jones WR, Cope TE, Jones PS, Passamonti L, Hong YT, Fryer T, et al. In vivo evidence for pre-symptomatic neuroinflammation in a MAPT mutation carrier. Ann Clin Transl Neurol 2019; 6: 373–378.

Bevan-Jones WR, Cope TE, Jones PS, Passamonti L, Hong YT, Fryer TD, et al. [18F]AV-1451 binding in vivo mirrors the expected distribution of TDP-43 pathology in the semantic variant of primary progressive aphasia. J Neurol Neurosurg Psychiatry 2018; 89: 1032–1037.

Bevan-Jones WR, Surendranathan A, Passamonti L, Vázquez Rodríguez P, Arnold R, Mak E, et al. Neuroimaging of Inflammation in Memory and Related Other Disorders (NIMROD)

study protocol: a deep phenotyping cohort study of the role of brain inflammation in dementia, depression and other neurological illnesses. BMJ Open 2017; 7: e013187.

Bevan Jones WR, Cope TE, Passamonti L, Fryer TD, Hong YT, Aigbirhio F, et al. [^{18} F]AV-1451 PET in behavioral variant frontotemporal dementia due to MAPT mutation. Ann Clin Transl Neurol 2016; 3: 940–947.

Bhaskar K, Konerth M, Kokiko-Cochran ON, Cardona A, Ransohoff RM, Lamb BT. Regulation of tau pathology by the microglial fractalkine receptor. Neuron 2010; 68: 19–31.

De Biase LM, Bonci A. Region-Specific Phenotypes of Microglia: The Role of Local Regulatory Cues. Neuroscientist 2019; 25: 314–333.

Binney RJ, Pankov A, Marx G, He X, McKenna F, Staffaroni AM, et al. Data-driven regions of interest for longitudinal change in three variants of frontotemporal lobar degeneration. Brain Behav 2017; 7: 1–11.

Bischof GN, Jessen F, Fliessbach K, Dronse J, Hammes J, Neumaier B, et al. Impact of tau and amyloid burden on glucose metabolism in Alzheimer's disease. Ann Clin Transl Neurol 2016; 3: 934–939.

Boche D, Gerhard A, Rodriguez-Vieitez E. Prospects and challenges of imaging neuroinflammation beyond TSPO in Alzheimer's disease. Eur J Nucl Med Mol Imaging 2019; 46: 2831–2847.

Bolker BM, Brooks ME, Clark CJ, Geange SW, Poulsen JR, Stevens MHH, et al. Generalized linear mixed models : a practical guide for ecology and evolution. 2008: 127–135.

Bonham LW, Karch CM, Fan CC, Tan C, Geier EG, Wang Y, et al. CXCR4 involvement in neurodegenerative diseases. Transl Psychiatry 2018; 8

Boxer AL, Lang AE, Grossman M, Knopman DS, Miller BL, Schneider LS, et al. Davunetide in patients with progressive supranuclear palsy: A randomised, double-blind, placebo-controlled phase 2/3 trial. Lancet Neurol 2014; 13: 676–685.

Boxer AL, Yu J, Golbe LI, Litvan I, Lang AE, Höglinger GU. Advances in progressive supranuclear palsy: new diagnostic criteria, biomarkers, and therapeutic approaches. Lancet Neurol 2017; 16: 552–563.

Braak H, Braak E. Neuropathological stageing of Alzheimer-related changes. Acta Neuropathol 1991; 82: 239–59.

Braak H, Thal DR, Ghebremedhin E, Del Tredici K. Stages of the pathologic process in alzheimer disease: Age categories from 1 to 100 years. J Neuropathol Exp Neurol 2011; 70: 960–969.

Brambati SM, Amici S, Racine CA, Neuhaus J, Miller Z, Ogar J, et al. Longitudinal gray matter contraction in three variants of primary progressive aphasia: A tenser-based morphometry study. NeuroImage Clin 2015; 8: 345–355.

Brendel M, Barthel H, Van Eimeren T, Marek K, Beyer L, Song M, et al. Assessment of 18F-PI-2620 as a Biomarker in Progressive Supranuclear Palsy. JAMA Neurol 2020: 1–12.

Brendel M, Schönecker S, Höglinger G, Lindner S, Havla J, Blautzik J, et al. [18F]-THK5351 PET Correlates with Topology and Symptom Severity in Progressive Supranuclear Palsy. Front Aging Neurosci 2018; 9: 1–12.

Brenneis C, Seppi K, Schocke M, Benke T, Wenning GK, Poewe W. Voxel based morphometry reveals a distinct pattern of frontal atrophy in progressive supranuclear palsy. J Neurol Neurosurg Psychiatry 2004; 75: 246–9.

Brier MR, Gordon B, Friedrichsen K, McCarthy J, Stern A, Christensen J, et al. Tau and Aβ imaging, CSF measures, and cognition in Alzheimer's disease. Sci Transl Med 2016; 8: 338ra66-338ra66.

Bright F, Werry EL, Dobson-Stone C, Piguet O, Ittner LM, Halliday GM, et al. Neuroinflammation in frontotemporal dementia. Nat Rev Neurol 2019; 15: 540–555.

Broce I, Karch CM, Wen N, Fan CC, Wang Y, Hong Tan C, et al. Immune-related genetic enrichment in frontotemporal dementia: An analysis of genome-wide association studies. PLoS Med 2018; 15: 1–20.

Broe M, Hodges JR, Schofield E, Shepherd CE, Kril JJ, Halliday GM. Staging disease severity in pathologically confirmed cases of frontotemporal dementia. Neurology 2003; 60: 1005–1011.

Burger C, Goerres G, Schoenes S, Buck A, Lonn A, Von Schulthess G. PET attenuation coefficients from CT images: Experimental evaluation of the transformation of CT into PET 511-keV attenuation coefficients. Eur J Nucl Med 2002; 29: 922–927.

Burrell JR, Hodges JR, Rowe JB. Cognition in corticobasal syndrome and progressive supranuclear palsy: A review. Mov Disord 2014; 29: 684–693.

Bussian TJ, Aziz A, Meyer CF, Swenson BL, van Deursen JM, Baker DJ. Clearance of senescent glial cells prevents tau-dependent pathology and cognitive decline. Nature 2018; 562: 578–582.

Cagnin A, Rossor M, Sampson EL, MacKinnon T, Banati RB. In vivo detection of microglial activation in frontotemporal dementia. Ann Neurol 2004; 56: 894–897.

Calsolaro V, Edison P. Neuroinflammation in Alzheimer's disease: Current evidence and future directions. Alzheimer's Dement 2016; 12: 719–732.

Caselli RJ, Reiman EM. Characterizing the Preclinical Stages of Alzheimer's Disease and the Prospect of Presymptomatic Intervention. J Alzheimer's Dis 2012; 33: S405–S416.

Cash DM, Bocchetta M, Thomas DL, Dick KM, van Swieten JC, Borroni B, et al. Patterns of gray matter atrophy in genetic frontotemporal dementia: results from the GENFI study. Neurobiol Aging 2018; 62: 191–196.

Chan D, Fox NC, Jenkins R, Scahill RI, Crum WR, Rossor MN. Rates of global and regional cerebral atrophy in AD and frontotemporal dementia. Neurology 2001; 57: 1756–1763.

Chandra A, Gennaro PV, Oliver P. Applications of amyloid , tau , and neuroinflammation PET imaging to Alzheimer ' s disease and mild cognitive impairment. 2019: 1–19.

Chare L, Hodges JR, Leyton CE, McGinley C, Tan RH, Kril JJ, et al. New criteria for frontotemporal dementia syndromes: Clinical and pathological diagnostic implications. J Neurol Neurosurg Psychiatry 2014; 85: 866–871.

Chen Z, Chen JA, Shatunov A, Jones AR, Kravitz SN, Huang AY, et al. Genome-wide survey of copy number variants finds MAPT duplications in progressive supranuclear palsy. Mov Disord 2019; 34: 1049–1059.

Chi H, Chang HY, Sang TK. Neuronal cell death mechanisms in major neurodegenerative diseases. Int J Mol Sci 2018; 19

Chiotis K, Saint-Aubert L, Rodriguez-Vieitez E, Leuzy A, Almkvist O, Savitcheva I, et al. Longitudinal changes of tau PET imaging in relation to hypometabolism in prodromal and Alzheimer's disease dementia. Mol Psychiatry 2018; 23: 1666–1673.

Cho H, Choi JY, Hwang MS, Kim YJ, Lee HM, Lee HS, et al. In vivo cortical spreading pattern of tau and amyloid in the Alzheimer disease spectrum. Ann Neurol 2016; 80: 247–258.

Cho H, Choi JY, Hwang MS, Lee SH, Ryu YH, Lee MS, et al. Subcortical ^{18} F-AV-1451 binding patterns in progressive supranuclear palsy. Mov Disord 2017; 32: 134–140.

Cho H, Choi JY, Hwang MSBSN, Lee JH, Kim YJ, Lee HM, et al. Tau PET in Alzheimer disease and mild cognitive impairment. Neurology 2016; 87: 375–383.

Cho H, Choi JY, Lee HS, Lee J-H, Ryu YH, Lee MS, et al. Progressive tau accumulation in Alzheimer's disease: two-year follow-up study. J Nucl Med 2019: jnumed.118.221697.

Cho H, Kim HJ, Choi JY, Ryu YH, Lee MS, Na DL, et al. 18F-flortaucipir uptake patterns in clinical subtypes of primary progressive aphasia. Neurobiol Aging 2019; 75: 187–197.

Chou Y-Y, Leporé N, Avedissian C, Madsen SK, Parikshak N, Hua X, et al. Mapping correlations between ventricular expansion and CSF amyloid and tau biomarkers in 240 subjects with Alzheimer's disease, mild cognitive impairment and elderly controls. Neuroimage 2009; 46: 394–410.

Chow TW, Binns MA, Cummings JL, Lam I, Black SE, Miller BL, et al. Apathy symptom profile and behavioral associations in frontotemporal dementia vs dementia of Alzheimer type. Arch Neurol 2009; 66: 888–893.

Clavaguera F, Hench J, Goedert M, Tolnay M. Invited review: Prion-like transmission and spreading of tau pathology. Neuropathol Appl Neurobiol 2015; 41: 47–58.

Cordato NJ, Pantelis C, Halliday GM, Velakoulis D, Wood SJ, Stuart GW, et al. Frontal atrophy correlates with behavioural changes in progressive supranuclear palsy. Brain 2002; 125: 789–800.

Correia MM, Rittman T, Barnes CL, Coyle-Gilchrist IT, Ghosh B, Hughes LE, et al. Towards accurate and unbiased imaging-based differentiation of Parkinson's disease, progressive supranuclear palsy and corticobasal syndrome. Brain Commun 2020; 2: fcaa051.

Coughlin D, Irwin DJ. Emerging Diagnostic and Therapeutic Strategies for Tauopathies. Curr Neurol Neurosci Rep 2017; 17

Coyle-Gilchrist ITS, Dick KM, Patterson K, Vázquez Rodríquez P, Wehmann E, Wilcox A, et al. Prevalence, characteristics, and survival of frontotemporal lobar degeneration syndromes. Neurology 2016; 86: 1736–1743.

Crawford JR, Garthwaite PH. Comparison of a single case to a control or normative sample in neuropsychology: Development of a Bayesian approach. Cogn Neuropsychol 2007; 24: 343–

372.

Curran PJ, Obeidat K, Losardo D. Twelve frequently asked questions about growth curve modeling. J Cogn Dev 2010; 11: 121–136.

Dani M, Wood M, Mizoguchi R, Fan Z, Walker Z, Morgan R, et al. Microglial activation correlates in vivo with both tau and amyloid in Alzheimer ' s disease. 2018: 1–15.

Daniel SE, De Bruin VMS, Lees AJ. The clinical and pathological spectrum of steele-Richardson-Olszewski syndrome (progressive supranuclear palsy): A reappraisal. Brain 1995; 118: 759–770.

Desikan RS, Ségonne F, Fischl B, Quinn BT, Dickerson BC, Blacker D, et al. An automated labeling system for subdividing the human cerebral cortex on MRI scans into gyral based regions of interest. Neuroimage 2006; 31: 968–980.

Dickerson BC, Bakkour A, Salat DH, Feczko E, Pacheco J, Greve DN, et al. The cortical signature of Alzheimer's disease: Regionally specific cortical thinning relates to symptom severity in very mild to mild AD dementia and is detectable in asymptomatic amyloid-positive individuals. Cereb Cortex 2009; 19: 497–510.

Dickson DW, Ahmed Z, Algom AA, Tsuboi Y, Josephs KA. Neuropathology of variants of progressive supranuclear palsy. Curr Opin Neurol 2010; 23: 394–400.

Dickson DW, Rademakers R, Hutton ML. Progressive supranuclear palsy: Pathology and genetics. Brain Pathol 2007; 17: 74–82.

Ducharme S, Price BH, Dickerson BC. Apathy: A neurocircuitry model based on frontotemporal dementia. J Neurol Neurosurg Psychiatry 2018; 89: 389–396.

Dugger BN, Davis K, Malek-Ahmadi M, Hentz JG, Sandhu S, Beach TG, et al. Neuropathological comparisons of amnestic and nonamnestic mild cognitive impairment. BMC Neurol 2015; 15: 1–8.

Dugger BN, Hentz JG, Adler CH, Sabbagh MN, Shill HA, Jacobson S, et al. Clinicopathological outcomes of prospectively followed normal elderly brain bank volunteers. J Neuropathol Exp Neurol 2014; 73: 244–252.

Dujardin S, Colin M, Buée L. Invited review: Animal models of tauopathies and their implications for research/translation into the clinic. Neuropathol Appl Neurobiol 2015; 41: 59–80.

Duncan TE, Duncan SC. The ABC's of LGM: An Introductory Guide to Latent Variable Growth Curve Modeling. Soc Personal Psychol Compass 2009; 3: 979–991.

Dupont A-C, Largeau B, Santiago Ribeiro M, Guilloteau D, Tronel C, Arlicot N. Translocator Protein-18 kDa (TSPO) Positron Emission Tomography (PET) Imaging and Its Clinical Impact in Neurodegenerative Diseases. Int J Mol Sci 2017; 18: 785.

Dutt S, Binney RJ, Heuer HW, Luong P, Attygalle S, Bhatt P, et al. Progression of brain atrophy in PSP and CBS over 6 months and 1 year. Neurology 2016; 87: 2016–2025.

Eckenweber F, Medina-Luque J, Blume T, Sacher C, Biechele G, Wind K, et al. Longitudinal TSPO expression in tau transgenic P301S mice predicts increased tau accumulation and deteriorated spatial learning. J Neuroinflammation 2020; 17: 1–12.

Edison P, Archer H a., Gerhard A, Hinz R, Pavese N, Turkheimer FE, et al. Microglia, amyloid, and cognition in Alzheimer's disease: An [11C](R)PK11195-PET and [11C]PIB-PET study. Neurobiol Dis 2008; 32: 412–419.

Eslinger PJ, Moore P, Antani S, Anderson C, Grossman M. Apathy in frontotemporal dementia: Behavioral and neuroimaging correlates. Behav Neurol 2012; 25: 127–136.

Fan Z, Aman Y, Ahmed I, Chetelat G, Landeau B, Ray Chaudhuri K, et al. Influence of microglial activation on neuronal function in Alzheimer's and Parkinson's disease dementia. Alzheimer's Dement 2015; 11: 608-621.e7.

Fan Z, Brooks DJ, Okello A, Edison P. An early and late peak in microglial activation in Alzheimer's disease trajectory. Brain 2017; 140: 792–803.

Fan Z, Okello A a., Brooks DJ, Edison P. Longitudinal influence of microglial activation and amyloid on neuronal function in Alzheimer's disease. Brain 2015; 138: 3685–3698.

Femminella GD, Ninan S, Atkinson R, Fan Z, Brooks DJ, Edison P. Does microglial activation influence hippocampal volume and neuronal function in Alzheimer's disease and Parkinson's disease dementia? J Alzheimer's Dis 2016; 51: 1275–1289.

Femminella GD, Thayanandan T, Calsolaro V, Komici K, Rengo G, Corbi G, et al. Imaging and molecular mechanisms of Alzheimer's disease: A review. Int J Mol Sci 2018; 19

Ferman TJ, Smith GE, Kantarci K, Boeve BF, Pankratz VS, Dickson DW, et al. Nonamnestic mild cognitive impairment progresses to dementia with Lewy bodies. Neurology 2013; 81: 2032–2038.

Fernández-Botrán R, Ahmed Z, Crespo FA, Gatenbee C, Gonzalez J, Dickson DW, et al. Cytokine expression and microglial activation in progressive supranuclear palsy. Park Relat Disord 2011; 17: 683–688.

Fernández M, Gobartt AL, Balañá M. Behavioural symptoms in patients with Alzheimer's disease and their association with cognitive impairment. BMC Neurol 2010; 10

Ferrari R, Hernandez DG, Nalls MA, Rohrer JD, Ramasamy A, Kwok JBJ, et al. Frontotemporal dementia and its subtypes: A genome-wide association study. Lancet Neurol 2014; 13: 686–699.

Forrest SL, Kril JJ, Stevens CH, Kwok JB, Hallupp M, Kim WS, et al. Retiring the term FTDP-17 as MAPT mutations are genetic forms of sporadic frontotemporal tauopathies. Brain 2018; 141: 521–534.

Frings L, Yew B, Flanagan E, Lam BYK, Hüll M, Huppertz HJ, et al. Longitudinal grey and white matter changes in frontotemporal dementia and Alzheimer's disease. PLoS One 2014; 9: 1–8.

Frisoni GB, Fox NC, Jack CR, Scheltens P, Thompson PM. The clinical use of structural MRI in Alzheimer disease. Nat Rev Neurol 2010; 6: 67–77.

Friston KJ, Holmes AP, Worsley KJ. Comments and controversies: How many subjects constitute a study? Neuroimage 1999; 10: 1–5.

Fujita M, Kobayashi M, Ikawa M, Gunn RN, Rabiner EA, Owen DR, et al. Comparison of four 11C-labeled PET ligands to quantify translocator protein 18 kDa (TSPO) in human brain: (R)-PK11195, PBR28, DPA-713, and ER176—based on recent publications that measured specific-to-non-displaceable ratios. EJNMMI Res 2017; 7

Gaetani L, Paolini Paoletti F, Bellomo G, Mancini A, Simoni S, Di Filippo M, et al. CSF and Blood Biomarkers in Neuroinflammatory and Neurodegenerative Diseases: Implications for Treatment. Trends Pharmacol Sci 2020; 41: 1023–1037.

Ganguli M, Snitz BE, Saxton JA, Chang CCH, Lee CW, Vander Bilt J, et al. Outcomes of mild cognitive impairment by definition: A population study. Arch Neurol 2011; 68: 761–767.

Garibotto V, Herholz K, Boccardi M, Picco A, Varrone A, Nordberg A, et al. Clinical validity of brain fluorodeoxyglucose positron emission tomography as a biomarker for Alzheimer's

disease in the context of a structured 5-phase development framework. Neurobiol Aging 2017; 52: 183–195.

Garwood CJ, Cooper JD, Hanger DP, Noble W. Anti-Inflammatory Impact of Minocycline in a Mouse Model of Tauopathy [Internet]. Front Psychiatry 2010; 1Available from: http://journal.frontiersin.org/article/10.3389/fpsyt.2010.00136/abstract

Gazzina S, Respondek G, Compta Y, Allinson KS, Spillantini MG, Molina-Porcel L, et al. Neuropathological validation of the MDS-PSP criteria with PSP and other frontotemporal lobar degeneration. bioRxiv 2019: 520510.

Gerhard A, Trender-Gerhard I, Turkheimer F, Quinn NP, Bhatia KP, Brooks DJ. In vivo imaging of microglial activation with [11C]-PK11195 PET progresive supranuclear palsy. Mov Disord 2006; 21: 89–93.

Gerhard A, Watts J, Trender-Gerhard I, Turkheimer F, Banati RB, Bhatia K, et al. In vivo imaging of microglial activation with [11C](R -PK11195 PET in corticobasal degeneration. Mov Disord 2004; 19: 1221–1226.

Gerstenecker A, Duff K, Mast B, Litvan I. Behavioral abnormalities in progressive supranuclear palsy. Psychiatry Res 2013; 210: 1205–1210.

Geschwind DH, Robidoux J, Alarcón M, Miller BL, Wilhelmsen KC, Cummings JL, et al. Dementia and neurodevelopmental predisposition: Cognitive dysfunction in presymptomatic subjects precedes dementia by decades in frontotemporal dementia. Ann Neurol 2001; 50: 741–746.

Ghadery C, Best LA, Pavese N, Tai YF, Strafella AP. PET Evaluation of Microglial Activation in Non-neurodegenerative Brain Diseases [Internet]. Curr Neurol Neurosci Rep 2019; 19Available from: http://dx.doi.org/10.1007/s11910-019-0951-x

Ghetti B, Oblak AL, Boeve BF, Johnson KA, Dickerson BC, Goedert M. Invited review: Frontotemporal dementia caused by microtubule-associated protein tau gene (MAPT) mutations: A chameleon for neuropathology and neuroimaging. Neuropathol Appl Neurobiol 2015; 41: 24–46.

Ghosh BCP, Calder AJ, Peers P V., Lawrence AD, Acosta-Cabronero J, Pereira JM, et al. Social cognitive deficits and their neural correlates in progressive supranuclear palsy. Brain 2012; 135: 2089–2102.

Ghosh BCP, Rowe JB, Calder AJ, Hodges JR, Bak TH. Emotion recognition in progressive supranuclear palsy. J Neurol Neurosurg Psychiatry 2009; 80: 1143–1145.

Glass CK, Saijo K, Winner B, Marchetto MC, Gage FH. Mechanisms Underlying Inflammation in Neurodegeneration. Cell 2010; 140: 918–934.

Goedert M, Spillantini MG. A Century of Alzheimer's Disease. Science (80-) 2006; 314: 777–781.

Goedert M, Spillantini MG, Jakes R, Rutherford D, Crowther RA. Multiple isoforms of human microtubule-associated protein tau: sequences and localization in neurofibrillary tangles of Alzheimer's disease. Neuron 1989; 3: 519–526.

Golbe LI, Ohman-Strickland PA. A clinical rating scale for progressive supranuclear palsy. Brain 2007; 130: 1552–1565.

González H, Elgueta D, Montoya A, Pacheco R. Neuroimmune regulation of microglial activity involved in neuroinflammation and neurodegenerative diseases. J Neuroimmunol 2014; 274: 1–13.

Gordon E, Rohrer JD, Fox NC. Advances in neuroimaging in frontotemporal dementia. J Neurochem 2016; 138: 193–210.

Gordon E, Rohrer JD, Kim LG, Omar R, Rossor MN, Fox NC, et al. Measuring disease progression in frontotemporal lobar degeneration: A clinical and MRI study. Neurology 2010; 74: 666–673.

Gorno-Tempini M, Dronkers NF, Rankin KP, Ogar JM, Phengrasamy L, Rosen HJ, et al. Cognition and anatomy in three variants of primary progressive aphasia. Ann Neurol 2004; 55: 335–346.

Gorno-Tempini ML, Hillis AE, Weintraub S, Kertesz A, Mendez M, Cappa SF, et al. Classification of primary progressive aphasia and its variants. Neurology 2011; 76: 1006–1014.

Gousias IS, Rueckert D, Heckemann RA, Dyet LE, Boardman JP, Edwards AD, et al. Automatic segmentation of brain MRIs of 2-year-olds into 83 regions of interest. Neuroimage 2008; 40: 672–684.

Greaves C V., Rohrer JD. An update on genetic frontotemporal dementia. J Neurol 2019; 266: 2075–2086.

Guarino A, Favieri F, Boncompagni I, Agostini F, Cantone M, Casagrande M. Executive functions in Alzheimer disease: A systematic review. Front Aging Neurosci 2019; 10

Gui Y, Marks JD, Das S, Hyman BT, Serrano-Pozo A. Characterization of the 18 kDa translocator protein (TSPO) expression in post-mortem normal and Alzheimer's disease brains. Brain Pathol 2020; 30: 151–164.

Gunn RN, Lammertsma AA, Hume SP, Cunningham VJ. Parametric imaging of ligand-receptor binding in PET using a simplified reference region model. Neuroimage 1997; 6: 279–287.

Guo Q, Owen DR, Rabiner EA, Turkheimer FE, Gunn RN. Identifying improved TSPO PET imaging probes through biomathematics: The impact of multiple TSPO binding sites in vivo. Neuroimage 2012; 60: 902–910.

Hall B, Mak E, Cervenka S, Aigbirhio FI, Rowe JB, O'Brien JT. In vivo tau PET imaging in dementia: Pathophysiology, radiotracer quantification, and a systematic review of clinical findings. Ageing Res Rev 2017; 36: 50–63.

Hall S, Öhrfelt A, Constantinescu R, Andreasson U, Surova Y, Bostrom F, et al. Accuracy of a panel of 5 cerebrospinal fluid biomarkers in the differential diagnosis of patients with dementia and/or Parkinsonian disorders. Arch Neurol 2012; 69: 1445–1452.

Hamelin L, Lagarde J, Dorothée G, Potier MC, Corlier F, Kuhnast B, et al. Distinct dynamic profiles of microglial activation are associated with progression of Alzheimer's disease. Brain 2018; 141: 1855–1870.

Hammers A, Allom R, Koepp MJ, Free SL, Myers R, Lemieux L, et al. Three-dimensional maximum probability atlas of the human brain, with particular reference to the temporal lobe. Hum Brain Mapp 2003; 19: 224–247.

Hammes J, Bischof GN, Giehl K, Faber J, Drzezga A, Klockgether T, et al. Elevated in vivo [18F]-AV-1451 uptake in a patient with progressive supranuclear palsy. Mov Disord 2017; 32: 170–171.

Hansen AK, Brooks DJ, Borghammer P. MAO-B Inhibitors Do Not Block In Vivo Flortaucipir([18F]-AV-1451) Binding. Mol Imaging Biol 2018; 20: 356–360.

Hansen AK, Knudsen K, Lillethorup TP, Landau AM, Parbo P, Fedorova T, et al. In vivo imaging of neuromelanin in Parkinson's disease using 18F-AV-1451 PET. Brain 2016; 139:

2039–2049.

Hardy CJD, Buckley AH, Downey LE, Lehmann M, Zimmerer VC, Varley RA, et al. The language profile of behavioral variant frontotemporal dementia. J Alzheimer's Dis 2015; 50: 359–371.

Harper L, Fumagalli GG, Barkhof F, Scheltens P, O'Brien JT, Bouwman F, et al. MRI visual rating scales in the diagnosis of dementia: Evaluation in 184 post-mortem confirmed cases. Brain 2016; 139: 1211–1225.

Harrison XA, Donaldson L, Correa-cano ME, Evans J, Fisher DN, Goodwin CED, et al. A brief introduction to mixed effects modelling and multi-model inference in ecology. 2018: 1–32.

Hauw JJ, Daniel SE, Dickson D, Horoupian DS, Jellinger K, Lantos PL, et al. Preliminary NINDS neuropathologic criteria for Steele-Richardson-Olszewski syndrome (progressive supranuclear palsy). Neurology 1994; 44: 2015–9.

Hebert LE, Scherr PA, Bienias JL, Bennett DA, Evans DA. Alzheimer disease in the US population: prevalence estimates using the 2000 census. Arch Neurol 2003; 60: 1119–22.

Heneka MT, Carson MJ, Khoury J El, Landreth GE, Brosseron F, Feinstein DL, et al. Neuroinflammation in Alzheimer's disease. Lancet Neurol 2015; 14: 388–405.

Hirtz D, Thurman DJ, Gwinn-Hardy K, Mohamed M, Chaudhuri AR, Zalutsky R. How common are the 'common' neurologic disorders? Neurology 2007; 68: 326–337.

Höglinger GU, Melhem NM, Dickson DW, Sleiman PMA, Wang LS, Klei L, et al. Identification of common variants influencing risk of the tauopathy progressive supranuclear palsy. Nat Genet 2011; 43: 699–705.

Höglinger GU, Respondek G, Stamelou M, Kurz C, Josephs K a., Lang AE, et al. Clinical diagnosis of progressive supranuclear palsy: The movement disorder society criteria. Mov Disord 2017; 32: 853–864.

Holland N, Jones PS, Savulich G, Wiggins JK, Hong YT, Fryer TD, et al. Synaptic Loss in Primary Tauopathies Revealed by [<scp> ^{11} C </scp>] <scp>UCB-J</scp> Positron Emission Tomography. Mov Disord 2020: mds.28188.

Hollocks MJ, Lawrence AJ, Brookes RL, Barrick TR, Morris RG, Husain M, et al. Differential relationships between apathy and depression with white matter microstructural

changes and functional outcomes. Brain 2015; 138: 3803–3815.

Hong M, Zhukareva V, Vogelsberg-Ragaglia V, Wszolek Z, Reed L, Miller BI, et al. Mutation-specific functional impairments in distinct tau isoforms of hereditary FTDP-17. Science (80-) 1998; 282: 1914–1917.

Hornberger M, Geng J, Hodges JR. Convergent grey and white matter evidence of orbitofrontal cortex changes related to disinhibition in behavioural variant frontotemporal dementia. Brain 2011; 134: 2502–2512.

Hornberger M, Piguet O. Episodic memory in frontotemporal dementia: A critical review. Brain 2012; 135: 678–692.

Hornberger M, Piguet O, Kipps C, Hodges JR. Executive function in progressive and nonprogressive behavioral variant frontotemporal dementia. Neurology 2008; 71: 1481–1488.

Hornberger M, Yew B, Gilardoni S, Mioshi E, Gleichgerrcht E, Manes F, et al. Ventromedial-frontopolar prefrontal cortex atrophy correlates with insight loss in frontotemporal dementia and Alzheimer's disease. Hum Brain Mapp 2014; 35: 616–626.

Husain M. Transdiagnostic neurology: neuropsychiatric symptoms in neurodegenerative diseases. Brain 2017; 140: 1535–1536.

Iaccarino L, La Joie R, Edwards L, Strom A, Schonhaut DR, Ossenkoppele R, et al. Spatial Relationships between Molecular Pathology and Neurodegeneration in the Alzheimer's Disease Continuum. Cereb Cortex 2020: 1–14.

Iaccarino L, Tammewar G, Ayakta N, Baker SL, Bejanin A, Boxer AL, et al. Local and distant relationships between amyloid, tau and neurodegeneration in Alzheimer's Disease. NeuroImage Clin 2018; 17: 452–464.

Ikonomovic MD, Abrahamson EE, Price JC, Mathis CA, Klunk WE. [F-18]AV-1451 positron emission tomography retention in choroid plexus: More than "off-target" binding. Ann Neurol 2016; 80: 307–308.

Inci I, Kusbeci OY, Eskut N. The neutrophil-to-lymphocyte ratio as a marker of peripheral inflammation in progressive supranuclear palsy: a retrospective study. Neurol Sci 2020; 41: 1233–1237.

Iqbal K, Del C. Alonso A, Chen S, Chohan MO, El-Akkad E, Gong CX, et al. Tau pathology in Alzheimer disease and other tauopathies. Biochim Biophys Acta - Mol Basis Dis 2005;

1739: 198–210.

Irwin DJ. Tauopathies as clinicopathological entities. Park Relat Disord 2016; 22: S29–S33.

Irwin DJ, Brettschneider J, McMillan CT, Cooper F, Olm C, Arnold SE, et al. Deep clinical and neuropathological phenotyping of Pick disease. Ann Neurol 2016; 79: 272–287.

Ishiki a., Harada R, Okamura N, Tomita N, Rowe CC, Villemagne VL, et al. Tau imaging with [18F]THK-5351 in progressive supranuclear palsy. Eur J Neurol 2017; 24: 130–136.

Ishizawa K, Dickson DW. Microglial activation parallels system degeneration in progressive supranuclear palsy and corticobasal degeneration. J Neuropathol Exp Neurol 2001; 60: 647–57.

Jabbari E, Holland N, Chelban V, Jones PS, Lamb R, Rawlinson C, et al. Diagnosis Across the Spectrum of Progressive Supranuclear Palsy and Corticobasal Syndrome. JAMA Neurol 2020; 77: 377–387.

Jabbari E, Tan MMX, Reynolds RH, Mok KY, Ferrari R, Murphy DP, et al. Common variation at the LRRK2 locus is associated with survival in the primary tauopathy progressive supranuclear palsy. bioRxiv 2020: 2020.02.04.932335.

Jack CR, Barnes J, Bernstein MA, Borowski BJ, Brewer J, Clegg S, et al. Magnetic resonance imaging in Alzheimer's Disease Neuroimaging Initiative 2. Alzheimer's Dement 2015; 11: 740–756.

Jack CR, Holtzman DM. Biomarker modeling of alzheimer's disease. Neuron 2013; 80: 1347–1358.

Jack CR, Knopman DS, Jagust WJ, Petersen RC, Weiner MW, Aisen PS, et al. Tracking pathophysiological processes in Alzheimer's disease: an updated hypothetical model of dynamic biomarkers. Lancet Neurol 2013; 12: 207–16.

Jack CR, Lowe VJ, Senjem ML, Weigand SD, Kemp BJ, Shiung MM, et al. 11C PiB and structural MRI provide complementary information in imaging of Alzheimer's disease and amnestic mild cognitive impairment. Brain 2008; 131: 665–680.

Jack CR, Wiste HJ, Schwarz CG, Lowe VJ, Senjem ML, Vemuri P, et al. Longitudinal tau PET in ageing and Alzheimer's disease. Brain 2018; 141: 1517–1528.

Jaeger J. Digit Symbol Substitution Test. J Clin Psychopharmacol 2018; 38: 513–519.

Jagust W. Imaging the evolution and pathophysiology of Alzheimer disease. Nat Rev

Neurosci 2018; 19: 687–700.

Jellinger K. Cerebellar involvement in progressive supranuclear palsy. Mov Disord 2010; 25: 1104–1105.

Jellinger K a., Attems J. Prevalence and impact of vascular and Alzheimer pathologies in Lewy body disease. Acta Neuropathol 2008; 115: 427–436.

Jellinger KA. Neuropathological assessment of the Alzheimer spectrum. J Neural Transm 2020; 127: 1229–1256.

Jellinger KA, Attems J. Prevalence of dementia disorders in the oldest-old: An autopsy study. Acta Neuropathol 2010; 119: 421–433.

Jiskoot LC, Bocchetta M, Nicholas JM, Cash DM, Thomas D, Modat M, et al. Presymptomatic white matter integrity loss in familial frontotemporal dementia in the GENFI cohort: A cross-sectional diffusion tensor imaging study. Ann Clin Transl Neurol 2018; 5: 1025–1036.

Jiskoot LC, Dopper EGP, Heijer T Den, Timman R, Van Minkelen R, Van Swieten JC, et al. Presymptomatic cognitive decline in familial frontotemporal dementia: A longitudinal study. Neurology 2016; 87: 384–391.

Jiskoot LC, Panman JL, Asseldonk L Van, Franzen S, Meeter LHH. Longitudinal cognitive biomarkers predicting symptom onset in presymptomatic frontotemporal dementia. J Neurol 2018; 265: 1381–1392.

Jiskoot LC, Panman JL, Meeter LH, Dopper EGP, Donker Kaat L, Franzen S, et al. Longitudinal multimodal MRI as prognostic and diagnostic biomarker in presymptomatic familial frontotemporal dementia. Brain 2019; 142: 193–208.

Johnson E, Kumfor F. Overcoming apathy in frontotemporal dementia: challenges and future directions. Curr Opin Behav Sci 2018; 22: 82–89.

Johnson K a., Schultz A, Betensky R a., Becker JA, Sepulcre J, Rentz D, et al. Tau positron emission tomographic imaging in aging and early Alzheimer disease. Ann Neurol 2016; 79: 110–119.

Joie R La, Visani A V., Baker SL, Brown JA, Bourakova V, Cha J, et al. Prospective longitudinal atrophy in Alzheimer's disease correlates with the intensity and topography of baseline tau-PET. Sci Transl Med 2020; 12: 1–13.

Josephs KA. Current Understanding of Neurodegenerative Diseases Associated With the Protein Tau. Mayo Clin Proc 2017; 92: 1291–1303.

Josephs KA, Hodges JR, Snowden JS, MacKenzie IR, Neumann M, Mann DM, et al. Neuropathological background of phenotypical variability in frontotemporal dementia. Acta Neuropathol 2011; 122: 137–153.

Josephs KA, Martin PR, Botha H, Schwarz CG, Duffy JR, Clark HM, et al. [18 F]AV-1451 tau-PET and primary progressive aphasia. Ann Neurol 2018; 83: 599–611.

Josephs KA, Whitwell JL, Weigand SD, Senjem ML, Boeve BF, Knopman DS, et al. Predicting functional decline in behavioural variant frontotemporal dementia. Brain 2011; 134: 432–448.

Jovicich J, Czanner S, Greve D, Haley E, Van Der Kouwe A, Gollub R, et al. Reliability in multi-site structural MRI studies: Effects of gradient non-linearity correction on phantom and human data. Neuroimage 2006; 30: 436–443.

Jucker M, Walker LC. Self-propagation of pathogenic protein aggregates in neurodegenerative diseases. Nature 2013; 501: 45–51.

Kaalund SS, Passamonti L, Allinson KSJ, Murley AG, Robbins TW, Spillantini MG, et al. Locus coeruleus pathology in progressive supranuclear palsy, and its relation to disease severity. Acta Neuropathol Commun 2020; 8: 11.

Kaat LD, Boon AJW, Kamphorst W, Ravid R, Duivenvoorden HJ, Van Swieten JC. Frontal presentation in progressive supranuclear palsy. Neurology 2007; 69: 723–729.

Kantarci K, Jack CR. Quantitative Magnetic Resonance Techniques as Surrogate Markers of Alzheimer's Disease. NeuroRx 2004; 1: 196–205.

Karikari TK, Pascoal TA, Ashton NJ, Janelidze S, Benedet AL, Rodriguez JL, et al. Blood phosphorylated tau 181 as a biomarker for Alzheimer's disease: a diagnostic performance and prediction modelling study using data from four prospective cohorts. Lancet Neurol 2020; 19: 422–433.

Kepe V, Bordelon Y, Boxer A, Huang S-C, Liu J, Thiede FC, et al. PET imaging of neuropathology in tauopathies: progressive supranuclear palsy. J Alzheimers Dis 2013; 36: 145–53.

Kersaitis C, Halliday GM, Kril JJ. Regional and cellular pathology in frontotemporal

dementia: Relationship to stage of disease in cases with and without Pick bodies. Acta Neuropathol 2004; 108: 515–523.

Kim M-J, McGwier M, Jenko KJ, Snow J, Morse C, Zoghbi SS, et al. Neuroinflammation in frontotemporal lobar degeneration revealed by 11 C-PBR28 PET . Ann Clin Transl Neurol 2019: 1327–1331.

Kim SL, Lee MJ, Lee MS. Cognitive dysfunction associated with falls in progressive supranuclear palsy. Gait Posture 2014; 40: 605–609.

Kinahan PE, Rogers JG. Analytic 3D image reconstruction using all detected events. IEEE Trans Nucl Sci 1989; 36: 964–968.

Kipps CM, Mioshi E, Hodges JR. Emotion, social functioning and activities of daily living in frontotemporal dementia. Neurocase 2009; 15: 182–189.

Kitazawa M, Cheng D, Tsukamoto MR, Koike MA, Wes PD, Vasilevko V, et al. Blocking IL-1 Signaling Rescues Cognition, Attenuates Tau Pathology, and Restores Neuronal β-Catenin Pathway Function in an Alzheimer's Disease Model. J Immunol 2011; 187: 6539–6549.

Klunk WE, Engler H, Nordberg A, Wang Y, Blomqvist G, Holt DP, et al. Imaging brain amyloid in Alzheimer's disease with Pittsburgh Compound-B. Ann Neurol 2004; 55: 306–319.

Knopman DS, Jack CR, Kramer JH, Boeve BF, Caselli RJ, Graff-Radford NR, et al. Brain and ventricular volumetric changes in frontotemporal lobar degeneration over 1 year. Neurology 2009; 72: 1843–1849.

Knopman DS, Petersen RC. Mild cognitive impairment and mild dementia: A clinical perspective. Mayo Clin Proc 2014; 89: 1452–1459.

Kobayashi M, Jiang T, Telu S, Zoghbi SS, Gunn RN, Rabiner EA, et al. 11 C-DPA-713 has much greater specific binding to translocator protein 18 kDa (TSPO) in human brain than 11 C-(R)-PK11195. J Cereb Blood Flow Metab 2018; 38: 393–403.

Kobylecki C, Jones M, Thompson JC, Richardson AM, Neary D, Mann DMA, et al. Cognitive–behavioural features of progressive supranuclear palsy syndrome overlap with frontotemporal dementia. J Neurol 2015; 262: 916–922.

Koikkalainen J, Rhodius-Meester H, Tolonen A, Barkhof F, Tijms B, Lemstra AW, et al.

Differential diagnosis of neurodegenerative diseases using structural MRI data. NeuroImage Clin 2016; 11: 435–449.

Kovacs GG. Invited review: Neuropathology of tauopathies: Principles and practice. Neuropathol Appl Neurobiol 2015; 41: 3–23.

Kovacs GG, Botond G, Budka H. Protein coding of neurodegenerative dementias: The neuropathological basis of biomarker diagnostics. Acta Neuropathol 2010; 119: 389–408.

Kovacs GG, Lukic MJ, Irwin DJ, Arzberger T, Respondek G, Lee EB, et al. Distribution patterns of tau pathology in progressive supranuclear palsy. Acta Neuropathol 2020; 140: 99–119.

Kovacs GG, Milenkovic I, Wöhrer A, Höftberger R, Gelpi E, Haberler C, et al. Non-Alzheimer neurodegenerative pathologies and their combinations are more frequent than commonly believed in the elderly brain: A community-based autopsy series. Acta Neuropathol 2013; 126: 365–384.

Koychev I, Gunn RN, Firouzian A, Lawson J, Zamboni G, Ridha B, et al. PET Tau and Amyloid-β Burden in Mild Alzheimer's Disease: Divergent Relationship with Age, Cognition, and Cerebrospinal Fluid Biomarkers. J Alzheimer's Dis 2017; 60: 283–293.

Kreisl WC, Lyoo CH, Liow J-S, Wei M, Snow J, Page E, et al. 11C-PBR28 binding to translocator protein increases with progression of Alzheimer's disease. Neurobiol Aging 2016; 44: 53–61.

Kril JJ, Halliday GM. Pathological staging of frontotemporal lobar degeneration. J Mol Neurosci 2011; 45: 379–383.

Kroth H, Oden F, Molette J, Schieferstein H, Capotosti F, Mueller A, et al. Discovery and preclinical characterization of [18F]PI-2620, a next-generation tau PET tracer for the assessment of tau pathology in Alzheimer's disease and other tauopathies. Eur J Nucl Med Mol Imaging 2019; 46: 2178–2189.

Krueger CE, Dean DL, Rosen HJ, Halabi C, Miller BL, Kramer JH. Logitudinal Rates of Lobar Atrophy in Frontotemporal Dementia, Semantic Dementia and Alzheimer's Disease. Alzheimer Dis Assoc Disord 2010; 24: 43–48.

Laforce R, Soucy JP, Sellami L, Dallaire-Théroux C, Brunet F, Bergeron D, et al. Molecular imaging in dementia: Past, present, and future. Alzheimer's Dement 2018; 14: 1522–1552.

Van Langenhove T, Leyton CE, Piguet O, Hodges JR. Comparing Longitudinal Behavior Changes in the Primary Progressive Aphasias. J Alzheimer's Dis 2016; 53: 1033–1042.

Lansdall CJ, Coyle-Gilchrist ITS, Jones PS, Rodríguez PV, Wilcox A, Wehmann E, et al. Apathy and impulsivity in frontotemporal lobar degeneration syndromes. Brain 2017; 140: 1792–1807.

Lansdall CJ, Coyle-Gilchrist ITS, Simon Jones P, Rodríguez PV, Wilcox A, Wehmann E, et al. White matter change with apathy and impulsivity in frontotemporal lobar degeneration syndromes. Neurology 2018; 90: e1066–e1076.

Lansdall CJ, Coyle-Gilchrist ITS, Vázquez Rodríguez P, Wilcox A, Wehmann E, Robbins TW, et al. Prognostic importance of apathy in syndromes associated with frontotemporal lobar degeneration. Neurology 2019; 92: e1547–e1557.

Lant SB, Robinson AC, Thompson JC, Rollinson S, Pickering-Brown S, Snowden JS, et al. Patterns of microglial cell activation in frontotemporal lobar degeneration. Neuropathol Appl Neurobiol 2014; 40: 686–696.

Lee VMY, Brunden KR, Hutton M, Trojanowski JQ. Developing Therapeutic Approaches to Tau, Selected Kinases, and Related Neuronal Protein Targets. Cold Spring Harb Perspect Med 2011; 1: a006437–a006437.

Leung KK, Bartlett JW, Barnes J, Manning EN, Ourselin S, Fox NC. Cerebral atrophy in mild cognitive impairment and Alzheimer disease: Rates and acceleration. Neurology 2013; 80: 648–654.

Leuzy A, Chiotis K, Lemoine L, Gillberg PG, Almkvist O, Rodriguez-Vieitez E, et al. Tau PET imaging in neurodegenerative tauopathies—still a challenge. Mol Psychiatry 2019

Levy ML, Cummings JL, Fairbanks LA, Ph D, Masterman D, Miller BL, et al. Apathy Is Not Depression. 1998; 10: 314–319.

Levy R, Dubois B. Apathy and the functional anatomy of the prefrontal cortex-basal ganglia circuits. Cereb Cortex 2006; 16: 916–928.

Litvan I, Agid Y, Calne D, Campbell G, Dubois B, Duvoisin RC, et al. Clinical research criteria for the diagnosis of progressive supranuclear palsy (Steele-Richardson-Olszewski syndrome): report of the NINDS-SPSP international workshop. [Review] [88 refs]. Neurology 1996; 47: 1–9.

Litvan I, Bhatia KP, Burn DJ, Goetz CG, Lang AE, Mckeith I, et al. SIC Task Force Appraisal of Clinical Diagnostic Criteria for Parkinsonian Disorders. 2003; 18: 467–486.

Litvan I, Kong M. Rate of decline in progressive supranuclear palsy. Mov Disord 2014; 29: 463–468.

Livingston G, Sommerlad A, Orgeta V, Costafreda SG, Huntley J, Ames D, et al. Dementia prevention, intervention, and care. Lancet 2017; 390: 2673–2734.

Low A, Mak E, Rowe JB, Markus HS, O'Brien JT. Inflammation and cerebral small vessel disease: A systematic review. Ageing Res Rev 2019; 53: 100916.

Lowe VJ, Curran G, Fang P, Liesinger AM, Josephs K a., Parisi JE, et al. An autoradiographic evaluation of AV-1451 Tau PET in dementia. Acta Neuropathol Commun 2016; 4: 1–19.

Lowe VJ, Lundt ES, Albertson SM, Min HK, Fang P, Przybelski SA, et al. Tau-positron emission tomography correlates with neuropathology findings. Alzheimer's Dement 2020; 16: 561–571.

Lyketsos CG, Lopez O, Jones B, Fitzpatrick AL, Breitner J, DeKosky S. Prevalence of neuropsychiatric symptoms in dementia and mild cognitive impairment: results from the cardiovascular health study. JAMA 2002; 288: 1475–83.

Maass A, Lockhart SN, Harrison TM, Bell RK, Mellinger T, Swinnerton K, et al. Entorhinal Tau Pathology, Episodic Memory Decline, and Neurodegeneration in Aging. J Neurosci 2018; 38: 530–543.

Magdalinou NK, Paterson RW, Schott JM, Fox NC, Mummery C, Blennow K, et al. A panel of nine cerebrospinal fluid biomarkers may identify patients with atypical parkinsonian syndromes. J Neurol Neurosurg Psychiatry 2015; 86: 1240–1247.

Mahoney CJ, Beck J, Rohrer JD, Lashley T, Mok K, Shakespeare T, et al. Frontotemporal dementia with the C9ORF72 hexanucleotide repeat expansion: Clinical, neuroanatomical and neuropathological features. Brain 2012; 135: 736–750.

Makaretz SJ, Quimby M, Collins J, Makris N, McGinnis S, Schultz A, et al. Flortaucipir tau PET imaging in semantic variant primary progressive aphasia. J Neurol Neurosurg Psychiatry 2018; 89: 1024–1031.

Maphis N, Xu G, Kokiko-Cochran ON, Jiang S, Cardona A, Ransohoff RM, et al. Reactive

microglia drive tau pathology and contribute to the spreading of pathological tau in the brain. Brain 2015; 138: 1738–1755.

Marquié M, Normandin MD, Meltzer AC, Tick MS, Andrea N V, Antón-fernández A, et al. Pathologic correlations of [F-18]-AV-1451 imaging in non- Alzheimer tauopathies. Ann Neurol 2017; 81: 117–128.

Marquié M, Normandin MD, Vanderburg CR, Costantino IM, Bien EA, Rycyna LG, et al. Validating novel tau positron emission tomography tracer [F-18]-AV-1451 (T807) on postmortem brain tissue. Ann Neurol 2015; 78: 787–800.

Massey L a., Micallef C, Paviour DC, O'Sullivan SS, Ling H, Williams DR, et al. Conventional magnetic resonance imaging in confirmed progressive supranuclear palsy and multiple system atrophy. Mov Disord 2012; 27: 1754–1762.

Matarazzo JD, Herman DO. Base rate data for the WAIS-R : Test-Retest stability and VIQ-PIQ differences Base Rate Data for the WAIS-R : Test-Retest Stability. 2008; 0475

Mattsson N, Insel PS, Donohue M, Jögi J, Ossenkoppele R, Olsson T, et al. Predicting diagnosis and cognition with 18 F-AV-1451 tau PET and structural MRI in Alzheimer's disease. Alzheimer's Dement 2019; 15: 570–580.

McGeer PL, McGeer EG. The amyloid cascade-inflammatory hypothesis of Alzheimer disease: Implications for therapy. Acta Neuropathol 2013; 126: 479–497.

McGeer PL, Schulzer M, McGeer EG. Arthritis and anti-inflammatory agents as possible protective factors for Alzheimer's disease: A review of 17 epidemiologic studies. Neurology 1996; 47: 425–432.

McKhann GM, Knopman DS, Chertkow H, Hyman BT, Jack CR, Kawas CH, et al. The diagnosis of dementia due to Alzheimer's disease: Recommendations from the National Institute on Aging-Alzheimer's Association workgroups on diagnostic guidelines for Alzheimer's disease. Alzheimer's Dement 2011; 7: 263–269.

McNeish D, Matta T. Differentiating between mixed-effects and latent-curve approaches to growth modeling. Behav Res Methods 2018; 50: 1398–1414.

McQuade A, Blurton-Jones M. Microglia in Alzheimer's Disease: Exploring How Genetics and Phenotype Influence Risk. J Mol Biol 2019; 431: 1805–1817.

Melis RJF, Haaksma ML, Muniz-Terrera G. Understanding and predicting the longitudinal

course of dementia. Curr Opin Psychiatry 2019; 32: 123–129.

Mendez MF, Lauterbach EC, Sampson SM. An Evidence-Based Review of the Psychopathology of Frontotemporal Dementia: A Report of the ANPA Committee on Research. J Neuropsychiatry Clin Neurosci 2008; 20: 130–149.

Mhatre SD, Tsai CA, Rubin AJ, James ML, Andreasson KI. Microglial Malfunction: The Third Rail in the Development of Alzheimer's Disease. Trends Neurosci 2015; 38: 621–636.

Miller ZA, Rankin KP, Graff-Radford NR, Takada LT, Sturm VE, Cleveland CM, et al. TDP-43 frontotemporal lobar degeneration and autoimmune disease. J Neurol Neurosurg Psychiatry 2013; 84: 956–962.

Miller ZA, Sturm VE, Camsari GB, Karydas A, Yokoyama JS, Grinberg LT, et al. Increased prevalence of autoimmune disease within C9 and FTD/MND cohorts Completing the picture. Neurol Neuroimmunol NeuroInflammation 2016; 3: 1–8.

Mioshi E, Dawson K, Mitchell J, Arnold R, Hodges JR. The Addenbrooke's Cognitive Examination Revised (ACE-R): a brief cognitive test battery for dementia screening. Int J Geriatr Psychiatry 2006; 21: 1078–1085.

Miyoshi M, Shinotoh H, Wszolek ZK, Strongosky AJ, Shimada H, Arakawa R, et al. In vivo detection of neuropathologic changes in presymptomatic MAPT mutation carriers: A PET and MRI study. Parkinsonism Relat Disord 2010; 16: 404–408.

Moehle MS, Webber PJ, Tse T, Sukar N, Standaert DG, Desilva TM, et al. LRRK2 inhibition attenuates microglial inflammatory responses. J Neurosci 2012; 32: 1602–1611.

Moore KM, Nicholas J, Grossman M, McMillan CT, Irwin DJ, Massimo L, et al. Age at symptom onset and death and disease duration in genetic frontotemporal dementia: an international retrospective cohort study. Lancet Neurol 2020; 19: 145–156.

Morales I, Jiménez JM, Mancilla M, Maccioni RB. Tau oligomers and fibrils induce activation of microglial cells. J Alzheimer's Dis 2013; 37: 849–856.

Mormino EC, Toueg TN, Azevedo C, Castillo JB, Guo W, Nadiadwala A, et al. Tau PET imaging with 18F-PI-2620 in aging and neurodegenerative diseases. Eur J Nucl Med Mol Imaging 2020

Mueller A, Bullich S, Barret O, Madonia J, Berndt M, Papin C, et al. Tau PET imaging with 18F-PI-2620 in Patients with Alzheimer Disease and Healthy Controls: A First-in-Humans

Study. J Nucl Med 2020; 61: 911–919.

Mueller C, Hussl A, Krismer F, Heim B, Mahlknecht P, Nocker M, et al. The diagnostic accuracy of the hummingbird and morning glory sign in patients with neurodegenerative parkinsonism. Park Relat Disord 2018; 54: 90–94.

Murley AG, Coyle-Gilchrist I, Rouse MA, Jones PS, Li W, Wiggins J, et al. Redefining the multidimensional clinical phenotypes of frontotemporal lobar degeneration syndromes. Brain 2020; 143: 1555–1571.

Murley AG, Rouse MA, Coyle-Gilchrist I, Simon P, Li W, Wiggins J, et al. Predicting loss of independence and mortality in frontotemporal lobar degeneration syndromes. 2020

Murray ME, Kouri N, Lin W-L, Jack CR, Dickson DW, Vemuri P. Clinicopathologic assessment and imaging of tauopathies in neurodegenerative dementias. Alzheimers Res Ther 2014; 6: 1.

Nelson PT, Alafuzoff I, Bigio EH, Bouras C, Braak H, Cairns NJ, et al. Correlation of Alzheimer Disease Neuropathologic Changes With Cognitive Status: A Review of the Literature. J Neuropathol Exp Neurol 2012; 71: 362–381.

Nestor SM, Rupsingh R, Borrie M, Smith M, Accomazzi V, Wells JL, et al. Ventricular enlargement as a possible measure of Alzheimer's disease progression validated using the Alzheimer's disease neuroimaging initiative database. Brain 2008; 131: 2443–2454.

Newsom JT. Longitudinal structural equation modeling: A comprehensive introduction. Routledge; 2015

Nobis L, Husain M. Apathy in Alzheimer's disease. Curr Opin Behav Sci 2018; 22: 7–13.

Nuebling G, Hensler M, Paul S, Zwergal A, Crispin A, Lorenzl S. PROSPERA: a randomized, controlled trial evaluating rasagiline in progressive supranuclear palsy. J Neurol 2016; 263: 1565–1574.

O'Callaghan C, Hodges JR, Hornberger M. Inhibitory Dysfunction in Frontotemporal Dementia. Alzheimer Dis Assoc Disord 2013; 27: 102–108.

O'Connor C, Landin-Romero R, Clemson L, Kaizik C, Daveson N, Hodges J, et al. Behavioral-variant frontotemporal dementia: Distinct phenotypes with unique functional profiles. Neurology 2017; 0

O'Connor CM, Clemson L, Flanagan E, Kaizik C, Brodaty H, Hodges JR, et al. The

Relationship between Behavioural Changes, Cognitive Symptoms, and Functional Disability in Primary Progressive Aphasia: A Longitudinal Study. Dement Geriatr Cogn Disord 2016; 42: 215–226.

O'Connor CM, Clemson L, Hornberger M, Leyton CE, Hodges JR, Piguet O, et al. Longitudinal change in everyday function and behavioral symptoms in frontotemporal dementia. Neurol Clin Pract 2016; 6: 419–428.

O'Keeffe FM, Murray B, Coen RF, Dockree PM, Bellgrove MA, Garavan H, et al. Loss of insight in frontotemporal dementia, corticobasal degeneration and progressive supranuclear palsy. Brain 2007; 130: 753–764.

Okello A, Edison P, Archer H a., Turkheimer FE, Kennedy J, Bullock R, et al. Microglial activation and amyloid deposition in mild cognitive impairment: A PET study. Neurology 2009; 72: 56–62.

Okello A, Koivunen J, Edison P, Archer HA, Turkheimer FE, Någren K, et al. Conversion of amyloid positive and negative mci to ad over 3 years: An c-pib pet study symbol. Neurology 2009; 73: 754–760.

Olney NT, Ong E, Goh SM, Bajorek L, Dever R, Staffaroni AM, et al. Clinical and volumetric changes with increasing functional impairment in familial frontotemporal lobar degeneration. Alzheimer's Dement 2019: 1–10.

Olney NT, Spina S, Miller BL. Frontotemporal Dementia. Neurol Clin 2017; 35: 339–374.

Ossenkoppele R, Schonhaut DR, Schöll M, Lockhart SN, Ayakta N, Baker SL, et al. Tau PET patterns mirror clinical and neuroanatomical variability in Alzheimer's disease. Brain 2016; 139: 1551–1567.

Ossenkoppele R, Smith R, Ohlsson T, Strandberg O, Mattsson N, Insel PS, et al. Associations between tau, Aβ, and cortical thickness with cognition in Alzheimer disease. Neurology 2019; 92: e601–e612.

Owen DR, Yeo AJ, Gunn RN, Song K, Wadsworth G, Lewis A, et al. An 18-kDa Translocator Protein (TSPO) Polymorphism Explains Differences in Binding Affinity of the PET Radioligand PBR28. J Cereb Blood Flow Metab 2012; 32: 1–5.

Padala PR, Padala KP, Lensing SY, Ramirez D, Monga V, Bopp MM, et al. Methylphenidate for apathy in community-dwelling older veterans with mild Alzheimer's disease: A double-

blind, randomized, placebo-controlled trial. Am J Psychiatry 2018; 175: 159–168.

Pan P, Song W, Yang J, Huang R, Chen K, Gong QY, et al. Gray Matter Atrophy in Behavioral Variant Frontotemporal Dementia: A Meta-Analysis of Voxel-Based Morphometry Studies. Dement Geriatr Cogn Disord 2012; 33: 141–148.

Panman JL, Jiskoot LC, Bouts MJRJ, Meeter LHH, van der Ende EL, Poos JM, et al. Gray and white matter changes in presymptomatic genetic frontotemporal dementia: a longitudinal MRI study. Neurobiol Aging 2019; 76: 115–124.

Parbo P, Ismail R, Sommerauer M, Stokholm MG, Hansen AK, Hansen K V., et al. Does inflammation precede tau aggregation in early Alzheimer's disease? A PET study. Neurobiol Dis 2018; 117: 211–216.

Park SA, Han SM, Kim CE. New fluid biomarkers tracking non-amyloid-β and non-tau pathology in Alzheimer's disease. Exp Mol Med 2020; 52: 556–568.

Pasqualetti G, Brooks DJ, Edison P. The Role of Neuroinflammation in Dementias. Curr Neurol Neurosci Rep 2015; 15: 17.

Passamonti L, Lansdall CJ, Rowe JB. The neuroanatomical and neurochemical basis of apathy and impulsivity in frontotemporal lobar degeneration. Curr Opin Behav Sci 2018; 22: 14–20.

Passamonti L, Rodríguez PV, Hong YT, Allinson KSJ, Bevan-Jones WR, Williamson D, et al. [11C]PK11195 binding in Alzheimer disease and progressive supranuclear palsy. Neurology 2018; 90: e1989–e1996.

Passamonti L, Tsvetanov KA, Jones PS, Bevan-Jones WR, Arnold R, Borchert RJ, et al. Neuroinflammation and Functional Connectivity in Alzheimer's Disease: Interactive Influences on Cognitive Performance. J Neurosci 2019; 39: 7218–7226.

Passamonti L, Vázquez Rodríguez P, Hong YT, Allinson KSJ, Williamson D, Borchert RJ, et al. ^{18} F-AV-1451 positron emission tomography in Alzheimer's disease and progressive supranuclear palsy. Brain 2017: aww340.

Perea JR, Llorens-Martín M, Ávila J, Bolós M. The Role of Microglia in the Spread of Tau: Relevance for Tauopathies. Front Cell Neurosci 2018; 12: 1–8.

Perri R, Monaco M, Fadda L, Caltagirone C, Carlesimo GA. Neuropsychological correlates of behavioral symptoms in alzheimer's disease, frontal variant of frontotemporal, subcortical

vascular, and lewy body dementias: A comparative study. J Alzheimer's Dis 2014; 39: 669–677.

Peters F, Villeneuve S, Belleville S. Predicting progression to dementia in elderly subjects with mild cognitive impairment using both cognitive and neuroimaging predictors. J Alzheimer's Dis 2014; 38: 307–318.

Petersen RC, Negash S. Mild cognitive impairment: An overview. CNS Spectr 2008; 13: 45–53.

Petersen RC, Roberts RO, Knopman DS, Boeve BF, Geda YE, Ivnik RJ, et al. Mild Cognitive Impairment. Arch Neurol 2009; 66: 464–467.

Peterson KA, Patterson K, Rowe JB. Language impairment in progressive supranuclear palsy and corticobasal syndrome [Internet]. J Neurol 2019Available from: https://doi.org/10.1007/s00415-019-09463-1

Piguet O. Neither white nor black: embracing clinical variability in dementia diagnosis. Brain 2020; 143: 1291–1293.

Piguet O, Brooks WS, Halliday GM, Schofield PR, Stanford PM, Kwok JBJ, et al. Similar early clinical presentations in familial and non-familial frontotemporal dementia. J Neurol Neurosurg Psychiatry 2004; 75: 1743–1745.

Piguet O, Hornberger M, Mioshi E, Hodges JR. Behavioural-variant frontotemporal dementia: diagnosis, clinical staging, and management. Lancet Neurol 2011; 10: 162–172.

Pontecorvo MJ, Devous MD, Kennedy I, Navitsky M, Lu M, Galante N, et al. A multicentre longitudinal study of flortaucipir (18F) in normal ageing, mild cognitive impairment and Alzheimer's disease dementia. Brain 2019: 1–13.

Pontecorvo MJ, Devous MD, Navitsky M, Lu M, Salloway S, Schaerf FW, et al. Relationships between flortaucipir PET tau binding and amyloid burden, clinical diagnosis, age and cognition. Brain 2017; 140: 748–763.

Pottier C, Ren Y, Perkerson RB, Baker M, Jenkins GD, van Blitterswijk M, et al. Genome-wide analyses as part of the international FTLD-TDP whole-genome sequencing consortium reveals novel disease risk factors and increases support for immune dysfunction in FTLD. Acta Neuropathol 2019; 137: 879–899.

Del Prete M, Spaccavento S, Craca A, Fiore P, Angelelli P. Neuropsychiatric symptoms and

the APOE genotype in Alzheimer's disease. Neurol Sci 2009; 30: 367–373.

Querfurth HW, LaFerla FM. Alzheimer's disease care. N Engl J Med 2010: 329–344.

Quigley H, Colloby SJ, O'Brien JT. PET imaging of brain amyloid in dementia: A review. Int J Geriatr Psychiatry 2011; 26: 991–999.

Ransohoff RM. How neuroinflammation contributes to neurodegeneration. Science (80-) 2016; 353: 777–783.

Rascovsky K, Hodges JR, Knopman D, Mendez MF, Kramer JH, Neuhaus J, et al. Sensitivity of revised diagnostic criteria for the behavioural variant of frontotemporal dementia. Brain 2011; 134: 2456–2477.

Rascovsky K, Salmon DP, Lipton AM, Leverenz JB, DeCarli C, Jagust WJ, et al. Rate of progression differs in frontotemporal dementia and Alzheimer disease. Neurology 2005; 65: 397–403.

Ray S, Britschgi M, Herbert C, Takeda-Uchimura Y, Boxer A, Blennow K, et al. Classification and prediction of clinical Alzheimer's diagnosis based on plasma signaling proteins. Nat Med 2007; 13: 1359–1362.

Raz N, Lindenberger U, Rodrigue KM, Kennedy KM, Head D, Williamson A, et al. Regional brain changes in aging healthy adults: General trends, individual differences and modifiers. Cereb Cortex 2005; 15: 1676–1689.

Respondek G, Levin J, Höglinger GU. Progressive supranuclear palsy and multiple system atrophy: Clinicopathological concepts and therapeutic challenges. Curr Opin Neurol 2018; 31: 448–454.

De Reuck JL, Deramecourt V, Cordonnier C, Leys D, Pasquier F, Maurage CA. Cerebrovascular lesions in patients with frontotemporal lobar degeneration: A neuropathological study. Neurodegener Dis 2012; 9: 170–175.

Reuter M, Schmansky NJ, Rosas HD, Fischl B. Within-subject template estimation for unbiased longitudinal image analysis. Neuroimage 2012; 61: 1402–1418.

Ringman JM, Liang LJ, Zhou Y, Vangala S, Teng E, Kremen S, et al. Early behavioural changes in familial Alzheimer's disease in the Dominantly Inherited Alzheimer Network. Brain 2015; 138: 1036–1045.

Rittman T, Borchert R, Jones S, van Swieten J, Borroni B, Galimberti D, et al. Functional

network resilience to pathology in presymptomatic genetic frontotemporal dementia. Neurobiol Aging 2019; 77: 169–177.

Rittman T, Coyle-Gilchrist IT, Rowe JB. Managing cognition in progressive supranuclear palsy. Neurodegener Dis Manag 2016; 6: 499–508.

Roberson ED, Hesse JH, Rose KD, Slama H, Johnson JK, Yaffe K, et al. Frontotemporal dementia progresses to death faster than Alzheimer disease. Neurology 2005; 65: 719–725.

Rogalski E, Cobia D, Harrison TM, Wieneke C, Weintraub S, Mesulam MM. Progression of language decline and cortical atrophy in subtypes of primary progressive aphasia. Neurology 2011; 76: 1804–1810.

Rohrer JD, Clarkson MJ, Kittus R, Rossor MN, Ourselin S, Warren JD, et al. Rates of hemispheric and lobar atrophy in the language variants of frontotemporal lobar degeneration. J Alzheimer's Dis 2012; 30: 407–411.

Rohrer JD, Guerreiro R, Vandrovcova J, Uphill J, Reiman D, Beck J, et al. The heritability and genetics of frontotemporal lobar degeneration. Neurology 2009; 73: 1451–1456.

Rohrer JD, McNaught E, Foster J, Clegg SL, Barnes J, Omar R, et al. Tracking progression in frontotemporal lobar degeneration. Neurology 2008; 71: 1445–1451.

Rohrer JD, Nicholas JM, Cash DM, van Swieten J, Dopper E, Jiskoot L, et al. Presymptomatic cognitive and neuroanatomical changes in genetic frontotemporal dementia in the Genetic Frontotemporal dementia Initiative (GENFI) study: A cross-sectional analysis. Lancet Neurol 2015; 14: 253–262.

Rohrer JD, Ridgway GR, Modat M, Ourselin S, Mead S, Fox NC, et al. Distinct profiles of brain atrophy in frontotemporal lobar degeneration caused by progranulin and tau mutations. Neuroimage 2010; 53: 1070–1076.

Rohrer JD, Warren JD. Phenomenology and anatomy of abnormal behaviours in primary progressive aphasia. J Neurol Sci 2010; 293: 35–38.

Rohrer JD, Warren JD, Modat M, Ridgway GR, Douiri A, Rossor MN, et al. Patterns of cortical thinning in the language variants of frontotemporal lobar degeneration. Neurology 2009; 72: 1562–1569.

Rosen HJ, Allison SC, Schauer GF, Gorno-Tempini ML, Weiner MW, Miller BL. Neuroanatomical correlates of behavioural disorders in dementia. Brain 2005; 128: 2612–

2625.

Rosen HJ, Gorno-Tempini ML, Goldman WP, Perry RJ, Schuff N, Weiner M, et al. Patterns of brain atrophy in frontotemporal dementia and semantic dementia. Neurology 2002; 58: 198–208.

Rosseel Y. lavaan : An R Package for Structural Equation Modeling. J Stat Softw 2012; 48

Rowe JB. Parkinsonism in frontotemporal dementias. 2019. p. 249–275

Saint-Aubert L, Lemoine L, Chiotis K, Leuzy A, Rodriguez-Vieitez E, Nordberg A. Tau PET imaging: present and future directions. Mol Neurodegener 2017; 12: 1–21.

Sakae N, Roemer SF, Bieniek KF, Murray ME, Baker MC, Kasanuki K, et al. Microglia in frontotemporal lobar degeneration with progranulin or C9ORF72 mutations. Ann Clin Transl Neurol 2019; 6: 1782–1796.

Sander K, Lashley T, Gami P, Gendron T, Lythgoe MF, Rohrer JD, et al. Characterization of tau positron emission tomography tracer [18F]AV-1451 binding to postmortem tissue in Alzheimer's disease, primary tauopathies, and other dementias. Alzheimer's Dement 2016; 12: 1116–1124.

Saura J, Luque JM, Cesura AM, Da Prada M, Chan-Palay V, Huber G, et al. Increased monoamine oxidase B activity in plaque-associated astrocytes of Alzheimer brains revealed by quantitative enzyme radioautography. Neuroscience 1994; 62: 15–30.

Scarf AM, Kassiou M. The Translocator Protein. J Nucl Med 2011; 52: 677–680.

Schain M, Kreisl WC. Neuroinflammation in Neurodegenerative Disorders—a Review. Curr Neurol Neurosci Rep 2017; 17

Schermelleh-Engel K, Moosbrugger H, Müller H. Evaluating the Fit of Structural Equation Models : Tests of Significance and Descriptive Goodness-of-Fit Measures. Methods Psychol Res online 2003

Schofield E, Kersaitis C, Shepherd CE, Kril JJ, Halliday GM. Severity of gliosis in Pick's disease and frontotemporal lobar degeneration: Tau-positive glia differentiate these disorders. Brain 2003; 126: 827–840.

Schofield EC, Hodges JR, Macdonald V, Cordato NJ, Kril JJ, Halliday GM. Cortical atrophy differentiates Richardson's syndrome from the parkinsonian form of progressive supranuclear palsy. Mov Disord 2011; 26: 256–263.

Schöll M, Lockhart SN, Schonhaut DR, O'Neil JP, Janabi M, Ossenkoppele R, et al. PET Imaging of Tau Deposition in the Aging Human Brain. Neuron 2016; 89: 971–982.

Schöll M, Maass A, Mattsson N, Ashton NJ, Blennow K, Zetterberg H, et al. Biomarkers for tau pathology. Mol Cell Neurosci 2018: 0–1.

Schonhaut DR, McMillan CT, Spina S, Dickerson BC, Siderowf A, Devous MD, et al. 18F-flortaucipir tau positron emission tomography distinguishes established progressive supranuclear palsy from controls and Parkinson disease: A multicenter study. Ann Neurol 2017; 82: 622–634.

Schroeter ML, Raczka K, Neumann J, Yves von Cramon D. Towards a nosology for frontotemporal lobar degenerations-A meta-analysis involving 267 subjects. Neuroimage 2007; 36: 497–510.

Schuster C, Elamin M, Hardiman O, Bede P. Presymptomatic and longitudinal neuroimaging in neurodegeneration - From snapshots to motion picture: A systematic review. J Neurol Neurosurg Psychiatry 2015; 86: 1089–1096.

Schwartz RS, Halliday GM, Cordato DJ, Kril JJ. Small-vessel disease in patients with Parkinson's disease: A clinicopathological study. Mov Disord 2012; 27: 1506–1512.

Schwarz AJ, Yu P, Miller BB, Shcherbinin S, Dickson J, Navitsky M, et al. Regional profiles of the candidate tau PET ligand18F-AV-1451 recapitulate key features of Braak histopathological stages. Brain 2016; 139: 1539–1550.

Seelaar H, Rohrer JD, Pijnenburg YAL, Fox NC, Van Swieten JC. Clinical, genetic and pathological heterogeneity of frontotemporal dementia: A review. J Neurol Neurosurg Psychiatry 2011; 82: 476–486.

Seeley WW. Selective functional, regional, and neuronal vulnerability in frontotemporal dementia. Curr Opin Neurol 2008; 21: 701–707.

Seeley WW, Carlin DA, Allman JM, Macedo MN, Bush C, Miller BL, et al. Early frontotemporal dementia targets neurons unique to apes and humans. Ann Neurol 2006; 60: 660–667.

Seeley WW, Crawford R, Rascovsky K, Kramer JH, Weiner M, Miller BL, et al. Frontal paralimbic network atrophy in very mild behavioral variant frontotemporal dementia. Arch Neurol 2008; 65: 249–255.

Serrano-Pozo A, Frosch MP, Masliah E, Hyman BT. Neuropathological alterations in Alzheimer disease. Cold Spring Harb Perspect Med 2011; 1: 1–23.

Shen XN, Niu LD, Wang YJ, Cao XP, Liu Q, Tan L, et al. Inflammatory markers in Alzheimer's disease and mild cognitive impairment: A meta-analysis and systematic review of 170 studies. J Neurol Neurosurg Psychiatry 2019; 90: 590–598.

Shen Z, Bao X, Wang R. Clinical PET imaging of microglial activation: Implications for microglial therapeutics in Alzheimer's disease. Front Aging Neurosci 2018; 10: 1–10.

Shimizu S, Hirose D, Hatanaka H, Takenoshita N, Kaneko Y, Ogawa Y, et al. Role of Neuroimaging as a Biomarker for Neurodegenerative Diseases. Front Neurol 2018; 9: 265.

Singh V, Chertkow H, Lerch JP, Evans AC, Dorr AE, Kabani NJ. Spatial patterns of cortical thinning in mild cognitive impairment and Alzheimer's disease. Brain 2006; 129: 2885–2893.

Sintini I, Schwarz CG, Senjem ML, Reid RI, Botha H, Ali F, et al. Multimodal neuroimaging relationships in progressive supranuclear palsy. Park Relat Disord 2019; 66: 56–61.

Sjögren M, Folkesson S, Blennow K, Tarkowski E. Increased intrathecal inflammatory activity in frontotemporal dementia: Pathophysiological implications. J Neurol Neurosurg Psychiatry 2004; 75: 1107–1111.

Smith R, Pawlik D, Nilsson CF, Englund E, Hansson O. [18F]Flortaucipir distinguishes Alzheimer's disease from progressive supranuclear palsy pathology in a mixed-pathology case. Acta Neuropathol 2020; 139: 411–413.

Smith R, Puschmann A, Schöll M, Ohlsson T, Van Swieten J, Honer M, et al. 18F-AV-1451 tau PET imaging correlates strongly with tau neuropathology in MAPT mutation carriers. Brain 2016; 139: 2372–2379.

Smith R, Santillo AF, Waldö ML, Strandberg O, Berron D, Vestberg S, et al. 18 F-Flortaucipir in TDP-43 associated frontotemporal dementia. Sci Rep 2019; 9: 1–10.

Smith R, Schain M, Nilsson C, Strandberg O, Olsson T, Hägerström D, et al. Increased basal ganglia binding of 18F-AV-1451 in patients with progressive supranuclear palsy. Mov Disord 2017; 32: 108–114.

Smith R, Wibom M, Pawlik D, Englund E, Hansson O. Correlation of In Vivo [18 F]Flortaucipir With Postmortem Alzheimer Disease Tau Pathology. JAMA Neurol 2019; 76: 310.

Snowden JS, Adams J, Harris J, Thompson JC, Rollinson S, Richardson A, et al. Distinct clinical and pathological phenotypes in frontotemporal dementia associated with MAPT, PGRN and C9orf72 mutations. Amyotroph Lateral Scler Front Degener 2015; 16: 497–505.

Snowden JS, Rollinson S, Thompson JC, Harris JM, Stopford CL, Richardson AMT, et al. Distinct clinical and pathological characteristics of frontotemporal dementia associated with C9ORF72 mutations. Brain 2012; 135: 693–708.

Soleimani-Meigooni DN, Iaccarino L, La Joie R, Baker S, Bourakova V, Boxer AL, et al. 18F-flortaucipir PET to autopsy comparisons in Alzheimer's disease and other neurodegenerative diseases. Brain 2020

Southekal S, Devous MD, Kennedy I, Navitsky M, Lu M, Joshi AD, et al. Flortaucipir F 18 Quantitation Using Parametric Estimation of Reference Signal Intensity. J Nucl Med 2018; 59: 944–951.

Spangenberg EE, Lee RJ, Najafi AR, Rice RA, Elmore MRP, Blurton-Jones M, et al. Eliminating microglia in Alzheimer's mice prevents neuronal loss without modulating amyloid-β pathology. Brain 2016; 139: 1265–1281.

Spina S, Schonhaut DR, Boeve BF, Seeley WW, Ossenkoppele R, O'Neil JP, et al. Frontotemporal dementia with the V337M MAPT mutation. Neurology 2017; 88: 758–766.

Spires-Jones TL, Hyman BT. The Intersection of Amyloid Beta and Tau at Synapses in Alzheimer's Disease. Neuron 2014; 82: 756–771.

Staffaroni A, Elahi F, McDermott D, Marton K, Karageorgiou E, Sacco S, et al. Neuroimaging in Dementia. Semin Neurol 2017; 37: 510–537.

Staffaroni AM, Bajorek L, Casaletto KB, Cobigo Y, Goh SM, Wolf A, et al. Assessment of executive function declines in presymptomatic and mildly symptomatic familial frontotemporal dementia: NIH-EXAMINER as a potential clinical trial endpoint. Alzheimer's Dement 2020; 16: 11–21.

Staffaroni AM, Ljubenkov PA, Kornak J, Cobigo Y, Datta S, Marx G, et al. Longitudinal multimodal imaging and clinical endpoints for frontotemporal dementia clinical trials. Brain 2019; 142: 443–459.

Stamelou M, Diehl-Schmid J, Hapfelmeier A, Kontaxopoulou D, Stefanis L, Oertel WH, et al. The frontal assessment battery is not useful to discriminate progressive supranuclear palsy

from frontotemporal dementias. Park Relat Disord 2015; 21: 1264–1268.

Starhof C, Winge K, Heegaard NHH, Skogstrand K, Friis S, Hejl A. Cerebrospinal fluid pro-inflammatory cytokines differentiate parkinsonian syndromes. J Neuroinflammation 2018; 15: 1–7.

Starkstein SE, Ingram L, Garau ML, Mizrahi R. On the overlap between apathy and depression in dementia. 2005: 1070–1074.

Steele JC, Richardson JC, Olszewski J. Progressive Supranuclear Palsy: A Heterogeneous Degeneration Involving the Brain Stem, Basal Ganglia and Cerebellum With Vertical Gaze and Pseudobulbar Palsy, Nuchal Dystonia and Dementia. Arch Neurol 1964; 10: 333–359.

Stefaniak J, O'Brien J. Imaging of neuroinflammation in dementia: a review. J Neurol Neurosurg Psychiatry 2015; 87: jnnp-2015-311336.

Stopford CL, Thompson JC, Neary D, Richardson AMT, Snowden JS. Working memory, attention, and executive function in Alzheimer's disease and frontotemporal dementia. Cortex 2012; 48: 429–446.

Swift IJ, Sogorb-Esteve A, Heller C, Synofzik M, Otto M, Graff C, et al. Fluid biomarkers in frontotemporal dementia: past, present and future. J Neurol Neurosurg Psychiatry 2020: jnnp-2020-323520.

Takada LT, Sha SJ. Neuropsychiatric features of C9orf72-associated behavioral variant frontotemporal dementia and frontotemporal dementia with motor neuron disease. Alzheimers Res Ther 2012; 4: 38.

Taler V, Phillips NA. Language performance in Alzheimer's disease and mild cognitive impairment: A comparative review. J Clin Exp Neuropsychol 2008; 30: 501–556.

Tan CC, Yu JT, Tan L. Biomarkers for preclinical alzheimer's disease. J Alzheimer's Dis 2014; 42: 1051–1069.

Tavares TP, Mitchell DGV, Coleman KKL, Coleman BL, Shoesmith CL, Butler CR, et al. Early symptoms in symptomatic and preclinical genetic frontotemporal lobar degeneration. J Neurol Neurosurg Psychiatry 2020; 91: 975–984.

Taylor JP, Hardy J, Fischbeck KH. Toxic proteins in neurodegenerative disease. Science (80-) 2002; 296: 1991–1995.

Terada T, Yokokura M, Obi T, Bunai T, Yoshikawa E, Ando I, et al. In vivo direct relation of

tau pathology with neuroinflammation in early Alzheimer's disease [Internet]. J Neurol 2019Available from: http://link.springer.com/10.1007/s00415-019-09400-2

Timmers T, Ossenkoppele R, Wolters EE, Verfaillie SCJ, Visser D, Golla SS V., et al. Associations between quantitative [18F]flortaucipir tau PET and atrophy across the Alzheimer's disease spectrum. Alzheimers Res Ther 2019; 11: 60.

Toledo JB, Arnold SE, Raible K, Brettschneider J, Xie SX, Grossman M, et al. Contribution of cerebrovascular disease in autopsy confirmed neurodegenerative disease cases in the National Alzheimer's Coordinating Centre. Brain 2013; 136: 2697–2706.

Tolosa E, Litvan I, Höglinger GU, Burn DJ, Lees A, Andrés M V., et al. A phase 2 trial of the GSK-3 inhibitor tideglusib in progressive supranuclear palsy. Mov Disord 2014; 29: 470–478.

Tsai RM, Bejanin A, Lesman-segev O, Lajoie R, Visani A, Bourakova V, et al. F-flortaucipir (AV-1451) tau PET in frontotemporal dementia syndromes. 2019; 7: 1–18.

Tsai RM, Lobach I, Bang J, Whitwell JL, Senjem ML, Jack CR, et al. Clinical correlates of longitudinal brain atrophy in progressive supranuclear palsy. Park Relat Disord 2016; 28: 29–35.

Tsuboi Y, Slowinski J, Josephs KA, Honer WG, Wszolek ZK, Dickson DW. Atrophy of superior cerebellar peduncle in progressive supranuclear palsy. Neurology 2003; 60: 1766–1769.

Turkheimer FE, Edison P, Pavese N, Roncaroli F, Anderson AN, Hammers A, et al. Reference and target region modeling of [11C]-(R)-PK11195 brain studies. J Nucl Med 2007; 48: 158–167.

Utianski RL, Whitwell JL, Schwarz CG, Duffy JR, Botha H, Clark HM, et al. Tau uptake in agrammatic primary progressive aphasia with and without apraxia of speech. Eur J Neurol 2018; 25: 1352–1357.

Utianski RL, Whitwell JL, Schwarz CG, Senjem ML, Tosakulwong N, Duffy JR, et al. Tau-PET imaging with [18F]AV-1451 in primary progressive apraxia of speech. Cortex 2018; 99: 358–374.

Venneti S, Wang G, Nguyen J, Wiley CA. The positron emission tomography ligand DAA1106 binds with high affinity to activated microglia in human neurological disorders. J Neuropathol Exp Neurol 2008; 67: 1001–10.

Ventura J, Subotnik KL, Gretchen-Doorly D, Casaus L, Boucher M, Medalia A, et al. Cognitive remediation can improve negative symptoms and social functioning in first-episode schizophrenia: A randomized controlled trial. Schizophr Res 2019; 203: 24–31.

Verheijen J, Sleegers K. Understanding Alzheimer Disease at the Interface between Genetics and Transcriptomics. Trends Genet 2018; 34: 434–447.

Vermeiren C, Motte P, Viot D, Mairet-Coello G, Courade JP, Citron M, et al. The tau positron-emission tomography tracer AV-1451 binds with similar affinities to tau fibrils and monoamine oxidases. Mov Disord 2018; 33: 273–281.

Vicini Chilovi B, Conti M, Zanetti M, Mazzù I, Rozzini L, Padovani A. Differential Impact of Apathy and Depression in the Development of Dementia in Mild Cognitive Impairment Patients. Dement Geriatr Cogn Disord 2009; 27: 390–398.

Villemagne VL, Burnham S, Bourgeat P, Brown B, Ellis KA, Salvado O, et al. Amyloid β deposition, neurodegeneration, and cognitive decline in sporadic Alzheimer's disease: A prospective cohort study. Lancet Neurol 2013; 12: 357–367.

Villemagne VL, Okamura N. Tau imaging in the study of ageing, Alzheimer's disease, and other neurodegenerative conditions. Curr Opin Neurobiol 2016; 36: 43–51.

Villemagne VL, Pike KE, Chételat G, Ellis KA, Mulligan RS, Bourgeat P, et al. Longitudinal assessment of Aβ and cognition in aging and Alzheimer disease. Ann Neurol 2011; 69: 181–192.

Vivash L, OBrien TJ. Imaging Microglial Activation with TSPO PET: Lighting Up Neurologic Diseases? J Nucl Med 2016; 57: 165–168.

Vogels T, Murgoci AN, Hromádka T. Intersection of pathological tau and microglia at the synapse. Acta Neuropathol Commun 2019; 7: 109.

Walhovd KB, Westlye LT, Amlien I, Espeseth T, Reinvang I, Raz N, et al. Consistent neuroanatomical age-related volume differences across multiple samples. Neurobiol Aging 2011; 32: 916–932.

Wear HJ, Wedderburn CJ, Mioshi E, Williams-Gray CH, Mason SL, Barker RA, et al. The Cambridge Behavioural Inventory revised. Dement Neuropsychol 2008; 2: 102–107.

Whitwell JL. Alzheimer ' s disease neuroimaging. 2018; 31: 396–404.

Whitwell JL. FTD spectrum: Neuroimaging across the FTD spectrum. In: Physiology &

behavior. 2019. p. 187–223

Whitwell JL, Höglinger GU, Antonini A, Bordelon Y, Boxer AL, Colosimo C, et al. Radiological biomarkers for diagnosis in PSP: Where are we and where do we need to be? Mov Disord 2017; 32: 955–971.

Whitwell JL, Jack CR, Parisi JE, Knopman DS, Boeve BF, Petersen RC, et al. Rates of cerebral atrophy differ in different degenerative pathologies. Brain 2006; 130: 1148–1158.

Whitwell JL, Jack CR, Senjem ML, Parisi JE, Boeve BF, Knopman DS, et al. MRI correlates of protein deposition and disease severity in postmortem frontotemporal lobar degeneration. Neurodegener Dis 2009; 6: 106–117.

Whitwell JL, Josephs KA, Murray ME, Kantarci K, Przybelski SA, Weigand SD, et al. MRI correlates of neurofibrillary tangle pathology at autopsy: A voxel-based morphometry study. Neurology 2008; 71: 743–749.

Whitwell JL, Lowe VJ, Tosakulwong N, Weigand SD, Senjem ML, Schwarz CG, et al. [18F]AV-1451 tau positron emission tomography in progressive supranuclear palsy. Mov Disord 2017; 32: 124–133.

Whitwell JL, Tosakulwong N, Schwarz CG, Botha H, Senjem ML, Spychalla AJ, et al. MRI Outperforms [18F]AV-1451 PET as a Longitudinal Biomarker in Progressive Supranuclear Palsy. Mov Disord 2019; 34: 105–113.

Whitwell JL, Weigand SD, Boeve BF, Senjem ML, Gunter JL, Dejesus-Hernandez M, et al. Neuroimaging signatures of frontotemporal dementia genetics: C9ORF72, tau, progranulin and sporadics. Brain 2012; 135: 794–806.

Whitwell JL, Xu J, Mandrekar JN, Gunter JL, Jack CR, Josephs K a. Rates of brain atrophy and clinical decline over 6 and 12-month intervals in PSP: Determining sample size for treatment trials. Park Relat Disord 2012; 18: 252–256.

Williams DR, Holton JL, Strand C, Pittman A, De Silva R, Lees AJ, et al. Pathological tau burden and distribution distinguishes progressive supranuclear palsy-parkinsonism from Richardson's syndrome. Brain 2007; 130: 1566–1576.

Williams DR, Lees AJ. Progressive supranuclear palsy: clinicopathological concepts and diagnostic challenges. Lancet Neurol 2009; 8: 270–279.

Williams DR, De Silva R, Paviour DC, Pittman A, Watt HC, Kilford L, et al. Characteristics

of two distinct clinical phenotypes in pathologically proven progressive supranuclear palsy: Richardson's syndrome and PSP-parkinsonism. Brain 2005; 128: 1247–1258.

Woollacott IOC, Nicholas JM, Heslegrave A, Heller C, Foiani MS, Dick KM, et al. Cerebrospinal fluid soluble TREM2 levels in frontotemporal dementia differ by genetic and pathological subgroup. Alzheimer's Res Ther 2018; 10: 1–14.

Woollacott IOC, Rohrer JD. The clinical spectrum of sporadic and familial forms of frontotemporal dementia. J Neurochem 2016; 138: 6–31.

Woollacott IOC, Toomey CE, Strand C, Courtney R, Benson BC, Rohrer JD, et al. Microglial burden, activation and dystrophy patterns in frontotemporal lobar degeneration. J Neuroinflammation 2020; 17: 1–27.

Xia CF, Arteaga J, Chen G, Gangadharmath U, Gomez LF, Kasi D, et al. [18F]T807, a novel tau positron emission tomography imaging agent for Alzheimer's disease. Alzheimer's Dement 2013; 9: 666–676.

Xia M, Wang J, He Y. BrainNet Viewer: a network visualization tool for human brain connectomics. PLoS One 2013; 8: e68910.

Yaqub M, Van Berckel BNM, Schuitemaker A, Hinz R, Turkheimer FE, Tomasi G, et al. Optimization of supervised cluster analysis for extracting reference tissue input curves in (R)-[11C]PK11195 brain PET studies. J Cereb Blood Flow Metab 2012; 32: 1600–1608.

Yin F, Banerjee R, Thomas B, Zhou P, Qian L, Jia T, et al. Exaggerated inflammation, impaired host defense, and neuropathology in progranulin-deficient mice. J Exp Med 2010; 207: 117–128.

Yokokura M, Mori N, Yagi S, Yoshikawa E, Kikuchi M, Yoshihara Y, et al. In vivo changes in microglial activation and amyloid deposits in brain regions with hypometabolism in Alzheimer's disease. Eur J Nucl Med Mol Imaging 2011; 38: 343–351.

Yoshiyama Y, Higuchi M, Zhang B, Huang SM, Iwata N, Saido TCC, et al. Synapse Loss and Microglial Activation Precede Tangles in a P301S Tauopathy Mouse Model. Neuron 2007; 53: 337–351.

Yoshiyama Y, Lee VMY, Trojanowski JQ. Therapeutic strategies for tau mediated neurodegeneration. J Neurol Neurosurg Psychiatry 2013; 84: 784–795.

Zamboni G, Huey ED, Krueger F, Nichelli PF, Grafman J. Apathy and disinhibition in

frontotemporal dementia: Insights into their neural correlates. Neurology 2008; 71: 736–742.

Zetterberg H, Bendlin BB. Biomarkers for Alzheimer's disease—preparing for a new era of disease-modifying therapies. Mol Psychiatry 2020

Zhao QF, Tan L, Wang HF, Jiang T, Tan MS, Tan L, et al. The prevalence of neuropsychiatric symptoms in Alzheimer's disease: Systematic review and meta-analysis. J Affect Disord 2016; 190: 264–271.

Zou J, Tao S, Johnson A, Tomljanovic Z, Polly K, Klein J, et al. Microglial activation, but not tau pathology, is independently associated with amyloid positivity and memory impairment. Neurobiol Aging 2020; 85: 11–21.

List of tables

Table 1. Neuroimaging methods applied in each group of patients with mild cognitive impairment (MCI), Alzheimer's dementia (AD), frontotemporal dementia (FTD), or progressive supranuclear palsy (PSP), and controls. 33

Table 2. Demographic and clinical characteristics for the patient and control groups. 60

Table 3. Demographic and clinical characteristics for the subsample of control and patient groups. 61

Table 4. Regional weights of the structural MRI component (left), and rotated regional weights of [18F]AV-1451 components (middle) and the [11C]PK11195 components (right). 63

Table 5. Results for the univariable regression models on slope across all population. 67

Table 6. Results for the univariable regression models on cognitive slope in patients. 67

Table 7. Results for the univariable regression models on slope (left) and intercept (right) across all population with age, sex and education as covariates. 69

Table 8. Results for the multiple regression model in patients with Alzheimer's dementia and Mild Cognitive Impairment. For each of the three multiple regression models applied and described in the methods' section, the estimated coefficients are reported for the full/initial model and the final model, indicated by the stepwise backward elimination. 71

Table 9. Results of the multivariable regression models on the regression slope in patients. For both frequentist (top) and Bayesian (bottom) the estimated coefficients for variables included in the final ("best") models are reported. 74

Table 10. Model comparison on the Bayesian multiple regression with cognitive slope as the dependent variable and brain imaging components and demographic variables as predictors. The models are ordered by the higher Bayes Factor (BF10) to the lowest. The table shows the ten most likely models, the null model, and the least likely model at the bottom. The Bayes Factor has been calculated for each model to the null model with respect to the null model. By convention, a BF>3 indicates positive evidence in favour of the alternate model, BF>10 strong evidence and BF>100 very strong evidence. The top three ranked models are therefore

significantly ‘better’ prognostic models than any other model, including any model with MRI. 75

Table 11. Demographic and clinical characteristics at the baseline for pre-symptomatic gene carriers and non-carrier subjects. P values are the result of t-test or $\chi 2$ tests as appropriate. .. 90

Table 12. Model fit indices and estimated slopes of Latent Growth Curve Models on longitudinal brain volumes in non-carriers (Non-Car) and in pre-symptomatic carriers (Pres-Car)..... 94

Table 13. Model fit indices and estimated slopes of Latent Growth Curve Models on longitudinal brain in pre-symptomatic carriers by gene groups. 95

Table 14. Model fit indices and estimated covariance parameters of Bivariate Latent Growth Curve Models on longitudinal apathy scores (Ap) and longitudinal brain volumes (Br)..... 96

Table 15. Demographics, genetic and clinical features for each patient. 107

Table 16. Demographic and clinical characteristics for patients and controls groups (*=significant ANOVA test between subgroups). 130

Table 17. Demographic and clinical characteristics for patients and controls groups (*=significant t-test between groups). Raw PSP rating scale (PSP-RS) score refers to the closest assessment to the PET scan, while estimated PSP-RS using multiple imputation refers to the adjusted value to the time midway between the two PET scans. 144

Table 18. Demographic and clinical characteristics for the total patient group, and for sub-groups split based on patient survival from study baseline relative to the median time interval between study baseline and death (median = 2.5 years; mean ± SD = 2.2 ± 1.0). 162

List of figures

Figure 1. Representation of the association between clinical syndromes (top) and neuropathology (bottom boxes) in tauopathies included in my thesis. Thick solid lines represent the predominant clinicopathological correlation for each disease, while slim dashed lines represent less common clinicopathological associations. Abbreviations: FTD=frontotemporal dementia; PPA= primary progressive aphasia; PSP=progressive supranuclear palsy; FTLD=frontotemporal lobar degeneration; TDP-43= transactive response DNA binding protein of 43 kD; CBD=corticobasal degeneration; FTDP-17=Frontotemporal dementia with parkinsonism-17; AGD=Argyrophilic grain disease; GGT=Globular glial tauopathy. 4

Figure 2. NIMROD study design from Bevan-Jones et al. (2017).....32

Figure 3. Classification and general characteristics of participants recruited in the GENFI study. 36

Figure 4. Representation of four possible scenarios that can be identified by LGCM on variable Y measured over time (x axis): (A) positive average slope with significant between-subject variance, and negative covariance between intercept and slope; (B) positive average slope with significant between-subject variance, and positive covariance between intercept and slope; (C) positive average slope with significant between-subject variance, but non-significant intercept variance; (D) positive average slope but non-significant variance.....41

Figure 5. Graphical representation of a standard univariate linear latent growth curve model and the estimated parameters.....42

Figure 6. Schematic representation of statistical analyses for one-step and two-step prediction procedures. Abbreviation: ACE-R: Addenbrooke's Cognitive Examination – Revised; i: intercept; s: slope; PC: principal component; AV: [18F]AV-1451; PK: [11C]PK11195; Bas: baseline; y: years. 59

Figure 7. Longitudinal cognitive changes in patients and controls, as measured by revised Addenbrooke's Cognitive Examination (ACE-R). Points represent annualised ACE-R scores at baseline, 1-year, 2-years and 3-years follow-up for each subject in control (blue) and patient (red) groups.....61

Figure 8. Regional weights of the structural MRI component (left), and rotated regional weights of [^{18}F]AV-1451 components (middle) and the [^{11}C]PK11195 components (right). Components were identified applying three independent principal component analyses on 15 temporo-parietal regions. For structural MRI, regional grey matter (GM) volumes were included in the analysis, while for each PET tracer, the binding potential values in those regions were considered, separately for each modality. The colours represent the region-specific weights (range: from -1 to 1) on each component (**Table 4**). 62

Figure 9. Latent growth curve model to test the initial values (intercept – "i") and longitudinal changes (slope – "s") in scores of revised Addenbrooke's Cognitive Examination (ACE-R) across all sample. Circles indicate latent variables, rectangles indicate observed variables, and triangles denote intercepts (1= population means on the parameters). Thick single-headed arrows indicate regressions while thick double-headed arrows indicate variance and covariance (grey for intercept and black for slope). Values in Roman are standardized parameter estimates, and values in italics are unstandardized parameter estimates (with standard errors in parentheses). The annual rate of change was positively associated with performance at baseline (lower initial cognitive scores were associated with a higher annual rate of cognitive changes). 64

Figure 10. Regression analyses with annual change in scores of revised Addenbrooke's Cognitive Examination (Slope ACE-R, y axis) and individual baseline scores for each modality-specific principal component (x axis): structural MRI (left panel), [18F]AV-1451 PET (middle panel), and [11C]PK11195 PET (right panel). Different colours represent different diagnostic groups (patients with Alzheimer's disease = red circles, patients with amyloid-positive mild cognitive impairment = red squares, controls = blue triangles). Abbreviations: Std=standard; p=p-value. 66

Figure 11. Results of the multiple linear regression in patients, with cognitive slope (annual cognitive change) extracted by the Latent Growth Curve Model as dependent variable, and brain components' scores, age and education as independent variables. Solid arrows indicate significant coefficients of brain imaging measures indicated by the stepwise backward elimination, while dashed arrows indicate variables excluded by the final model. Values in Roman are standardized estimates, and values in italics are unstandardized beta estimates (standard errors in parentheses). 72

Figure 12. Longitudinal increase in apathy scores over 2-year period in pre-symptomatic carriers (red) and non-carriers (blue). On the left, the latent growth curve model applied to test longitudinal changes in apathy levels, as assessed by the apathy sub-scale of the revised Cambridge Behavioural Inventory (CBI) over two years of follow-up, including the estimated years from onset (EYO) as covariate. Estimated regression values in pre-symptomatic group are reported in italics (est=estimate; SE=standard error; z=z-value). The graph on the right represents the raw data at group level for apathy scores (y axis) over 2-year follow-up visits (x axis). Individuals' data are not plotted, to protect anonymity. 91

Figure 13. Cross-sectional and longitudinal changes in apathy and executive function in pre-symptomatic carriers (red) and non-carriers (blue). Panel A: graphs represent the relationships of the estimated initial scores ("intercept" – left graph) and the annual rate of change ("slope" – right graph) in apathy scores with the estimated years from onset (EYO). Panel B: graphs represent the relationships of the estimated intercept (left graph) and slope (right graph) in executive function with estimated years to onset (EYO). Individuals' data are not plotted, to protect anonymity. 92

Figure 14. Effect of baseline apathy on annual rate of change in executive function. On the left, the latent growth curve model applied to test the predictive value of baseline apathy levels, as assessed by the apathy sub-scale of the revised Cambridge Behavioural Inventory (CBI), for longitudinal cognitive decline, estimated from Digit Symbol (Digit Symb) test scores over two years of follow-up. The estimated years from onset (EYO) was included as covariate in the model. Estimated regression values in pre-symptomatic group are reported in italics (est=estimate; SE=standard error; z=z-value). The graph on the right represents the relationship between the estimated annual rate of change in executive function (y axis) and the baseline apathy scores (x axis). Individuals' data are not plotted, to protect anonymity. .. 93

Figure 15. Bivariate latent growth curve model. On the left, the bivariate latent growth curve model (LGCM) applied to test the relationship between longitudinal changes in apathy, as assessed by the apathy-subscale of the revised Cambridge Behavioural Inventory (CBI), and in grey-matter (GM) volumes over two years of follow-up. The graphs on the right represent the significant regressions identified by the bivariate LGCMs: annual rate of change in apathy scores (slope – y axis) was associated with baseline grey-matter volumes in frontal lobe (x axis – top graph) and cingulate cortex (x axis – bottom graph). Estimated regression values in pre-symptomatic group are reported in italics (est=estimate; SE=standard error; z=z-value). Individuals' data are not plotted, to protect anonymity. 97

Figure 16. Axial slices of the [^{11}C]PK11195 (left panel) and [^{18}F]AV-1451 (right panel) binding potential (BP_{ND}) maps for each patient (A-G). The last row represents the average BP_{ND} images across 15 controls. Patients A and B are MAPT mutation carriers; cases C and D are patients with GRN mutations; and patients E, F and G are C9orf72 mutation carriers. BP_{ND} scale bar runs along the bottom side of the figure and applies to both PET tracers. The maps were spatially normalised to MNI space and smoothed (6mm full width at half maximum), and the slices are reported in the neurological display convention (left on the left). 111

Figure 17. Z-maps for [^{11}C]PK11195 (left panel) and [^{18}F]AV-1451 (right panel) binding potential (BP_{ND}) for each patient (A-G) as compared to 15 controls. Patients A and B are MAPT mutation carriers; cases C and D are patients with GRN mutations; and patients E, F and G are C9orf72 mutation carriers. Z-scale bar runs along the bottom side of the figure and applies to both PET tracers ($z > 1.645$ which corresponds to $p<0.05$ are reported in red). The slices are reported in the neurological display convention (left on the left) and aligned in MNI space. 112

Figure 18. Correlation matrices and linkage dendrogram obtained with [^{11}C]PK11195 binding potential regional values. Top-left panel: Spearman correlation matrix between all individuals ($p < 0.05$ FDR); the first 15 rows and columns represent controls while the other 7 rows and columns represent patients. Top-right panel: Spearman correlation matrix between patients, the numbers represents the strength of correlation (rho, $p < 0.05$ FDR). Bottom panel: the dendrogram produced by hierarchical cluster analysis. Patients with MAPT mutation are highlighted in red, patients with GRN mutation in blue and those with C9orf72 mutation in yellow. 113

Figure 19. Four macro-regions considered for the analyses: left frontal lobe (red), right frontal lobe (orange), left temporal lobe (light blue) and right temporal lobe (blue). Lobar values of grey-matter volumes were obtained by adding regional values, corrected for total intracranial volume, while [^{11}C]PK11195 BP_{ND} lobar values were calculated by averaging volume-weighted regional values. 128

Figure 20. Longitudinal cognitive scores (ACE-R - y axis) over time (x axis). Left panel represent the raw individual trajectory over time (coloured lines), and the linear average change at group level (black line). Right panel represent the linear change in cognition over time for each patient (coloured straight lines). 131

Figure 21. Significant regression analyses of annual decline in cognition (slope in ACE-R scores, y axis) with baseline grey matter volume scores (x axis, left panel) and inflammation levels in left frontal lobe (x axis, right panel). For imaging values, Z scores are reported to make the two graphs comparable. 132

Figure 22. Significant regression analyses of annual decline in cognition (slope in ACE-R scores, y axis) with baseline ACE-R scores (x axis, left panel) and apathy severity (x axis, right panel)..... 133

Figure 23. Longitudinal PSP-RS scores for each patient (grey), and estimated PSP-RS scores at the time of [11C]PK11195 (blue) and [18F]AV-1451 PET (red). 143

Figure 24. Whole brain correlation between regional mean non-displaceable binding potential (BP_{ND}) of [^{11}C]PK11195 and [^{18}F]AV-1451 in the PSP group. Panels A: each point represents the average value across all patients for a specific brain region, while. Panel B: dots represent individual regional values for each patient, the black line represents the association between the two tracers at group level, while grey lines are individual correlations, within each patient. In both panels, colours indicate brain macro-areas reported on the right..... 145

Figure 25. First four principal components for [11C]PK11195 non-displaceable binding potential (BPND) and [18F]AV-1451 BPND in PSP. The colours represent the rotated weights of all brain regions for each component..... 147

Figure 26. Significant correlations between [11C]PK11195 and [18F]AV-1451 individual principal component (comp) scores..... 148

Figure 27. Significant correlations between subcortical [^{11}C]PK11195 (left) and [^{18}F]AV-1451 (right) component (comp) scores and estimated PSP-RS at the time of each PET scan. 149

Figure 28. Survival probability plot over time from baseline assessment..... 162

Figure 29. First four principal components (PC) for grey matter volumes (left panel), [11C]PK11195 non-displaceable binding potential (BP_{ND} – middle panel), and [18F]AV-1451 BPND (right panel). The colours represent the rotated weights (range: from -1 to 1) of all brain regions for each component. 164

Figure 30. Longitudinal change in clinical severity (y axis), as measured by Progressive Supranuclear Palsy Rating Scale (PSP-RS), over time (x axis). Coloured lines represent PSP-

RS in each patient at consecutive visits. Black line represents the linear fit at group level, which show an annual rate of change of 6.15 ($p<0.0001$) points in PSP-RS. 165

Figure 31. Significant regression analyses of annual change in Progressive Supranuclear Palsy Rating Scale (PSP-RS) scores (top row) and intercept PSP-RS scores (bottom row) against baseline scores for each modality-specific principal component (x axis – residual component values corrected for covariates): [^{11}C]PK11195 PET (left panel), and [^{18}F]AV-1451 PET (right panel). Estimated parameters are reported for each model with age, education and sex as covariates. 167

Figure 32. Temporal directionality between structural brain, apathy and cognitive changes in pre-symptomatic frontotemporal dementia. From the longitudinal study on pre-symptomatic gene carriers on GENFI data (Chapter 4), two main conclusions are drawn: (i) apathy progression (annual rate of change) reflects brain differences (baseline) approaching the dementia onset, and not vice versa; (ii) apathy severity (baseline) predicts cognitive decline (annual rate of change) approaching the dementia onset, and not vice versa. 184